Composition and impact of wildfire-enriched aerosols on estuarine microbial communities: The 2019-20 Australian Black Summer

By Raissa Louise Gill

Thesis submitted in fulfilment of the requirements for the degree of Doctor of Philosophy at the University of Technology Sydney under the supervision of Professor Martina Doblin and Associate Professor Fraser Torpy.

This work is a compilation of published and unpublished works where I am first author.

University of Technology Sydney,
Faculty of Science, School of Life Sciences, Climate Change Cluster
Productive Coasts & Plants and Environmental Quality Research Group

Submitted: 30 June 2025

Revised: 13 March 2026

Certificate of original authorship

I, Raissa Gill, declare that this thesis, is submitted in fulfilment of the requirements for the award of Doctor of Philosophy, in the School of Life Sciences at the University of Technology Sydney.

This thesis is wholly my own work unless otherwise referenced or acknowledged. In addition, I certify that all information sources and literature used are indicated in the thesis.

This document has not been submitted for qualifications at any other academic institution.

This research was supported by an Australian Government Research Training Program (RTP) Scholarship doi.org/10.82133/C42F-K220.

Signature:

Production Note:
Signature removed prior to publication.

Date: 30 June 2025

Acknowledgements

I would like to express my gratitude to my primary supervisor, **Prof. Martina Doblin**, for her unwavering support, thoughtful guidance, and patience. Your mentorship and encouragement continually motivated me throughout this journey and were instrumental in shaping both my research and development as a scholar. I am also very grateful to my co-supervisor, **Assoc. Prof. Fraser Torpy**, for his thoughtful guidance and support throughout this journey - thank you for always encouraging me to remember and focus on my physical health throughout the demands of my PhD. I would like to thank both **Martina** and **Fraser** for the opportunity to undertake this PhD and for trusting me to pursue this research in the direction I felt was most meaningful. Your support in providing resources and access to professional networks has been invaluable to my growth as a researcher. I am especially grateful for the inclusive and supportive environment you helped foster – being part of two research groups could have easily felt disjointed, but I've always felt like I had a university family looking out for me.

Thank you to everyone in **COAST Lab** and **PEQR** for creating such a friendly and encouraging research community. In COAST, I extend my sincere appreciation to **Dr Michaela Larsson** for her support and guidance since my early days as a volunteer, to **Dr Phoebe Argyle** for her generosity, willingness to help, and motivating baked treats, and to **Giselle Firme** for her well-timed check-ins and encouraging words. I am also grateful for the camaraderie of **Callum Muir** and **Aaron Wright**, whose company during field sampling made collecting estuarine water far more enjoyable than it had any right to be. In PEQR, I'd like to thank to **Dr Peter Irga** for trusting me with valuable teaching opportunities and for encouraging my growth as an educator. I am also grateful to **Ky Chau** for making lab-based particle extractions both productive and fun, to **Loraine Lyu** for her generosity and excellent food recommendations, and to **Gabrielle Duani** for the friendly check-ins at strange hours of the day. I would like to thank **Stephen Matheson** for his joyous approach to statistical analysis, for nerding out over R with me, and for the productive evenings spent discussing "research strategies" at Fortress.

Lastly, thank you to everyone who made my project possible, from support staff, research collaborators, government bodies, and friends and family. Special thanks to my **Dad** and **Marina** for their constant support, games of phone tennis, and daily check ins on me and Charlie after

her many surgeries during the COVID lockdowns. Doing a PhD is stressful enough, let alone when someone you love is seriously injured, I couldn't have made it through without you. I'd also like to thank my **Mum** and **Paddy** for housing me after my scholarship ended, which allowed me to focus on my health and my PhD thesis. Finally, a big thank you to my fiancé **Bobby** for being my biggest advocate - celebrating my strengths, working with me on my weaknesses, and reminding me to prioritise myself. I'm deeply grateful for your encouragement, perspective, and all the moments of discovery and laughter along the way. Thank you for your immense support in the final stages of my candidature which allowed me to finish my PhD thesis – I couldn't have done this without you.

Format of thesis

This thesis is submitted as a thesis by compilation and comprises six chapters, two of which are original works written for the sole purposes of this thesis, and four of which present individual studies containing published or publishable research as part of this thesis. Each chapter has been formatted as a standalone section, with independent figure and table numbering and their own supplementary material at the end of the thesis where applicable. A single reference list is provided for the entire thesis. The format of each of these chapters is outlined below.

Chapter 1 – *Introduction and literature review* – is an original work that introduces the research area, reviews relevant literature, identifies key knowledge gaps, and outlines the rationale and aims of the thesis.

Chapter 2 – *Fine particle pollution during megafires contains potentially toxic elements* – is a peer-reviewed article presented in its published form with minor formatting adjustments for consistency with the overall thesis structure.

Chapter 3 – *Nutrient profile and sources of aerosols collected during intense wildfires in the Southern Hemisphere* – is an article currently under peer review and is presented as the version submitted for publication with minor formatting modifications.

Chapter 4 – *Acute exposure to wildfire-enriched aerosols elicits divergent microbial responses across multiple Australian estuaries* – is under preparation for submission to a peer-reviewed journal and is presented as a draft manuscript.

Chapter 5 – *Aerosols generated by extreme wildfires elicit dose- and time-dependent changes in estuarine microbial communities* – is under preparation for submission to a peer-reviewed journal and is presented as a draft manuscript.

Chapter 6 – *Summary and significance* – is an original work that summarises the thesis findings, discusses their contribution to the research field and broader significance, and outlines recommendations for future research before concluding the thesis.

Publications included in thesis

Chapter 2:

Gill. R, Fleck. R, Chau. K, Westerhausen. M. T, Lockwood. T. E, Violi. J. P, Irga. P. J, Doblin. M. A, Torpy. F. R, 2024. Fine particle pollution during megafires contains potentially toxic elements. *Environmental Pollution*. pp. 123306. Published.

Chapter 3:

Gill. R, Fleck. R, Chau. K, Westerhausen. M. T, Lockwood. T. E, Violi. J. P, Irga. P. J, Torpy. F. R, Doblin. M. A, 2025. Nutrient profile and sources of aerosols collected during intense wildfires in the Southern Hemisphere. *Environmental Pollution*. Under review.

Contribution of authors

The contributions of each author to the publications included in this thesis are described in the "CRediT authorship contribution statement" found at the end of the relevant data chapters. All authors have provided their signatures below to confirm their respective contributions.

Author name	Signature	Date signed
Raissa Gill (myself, first author)	Production Note: Signature removed prior to publication.	30 April 2025
Prof. Martina Doblin (primary supervisor and co-author)	Production Note: Signature removed prior to publication.	1 May 2025
Assoc. Prof. Fraser Torpy (co-supervisor and co-author)	Production Note: Signature removed prior to publication.	30 April 2025
Dr. Robert Fleck	Production Note: Signature removed prior to publication.	30 April 2025
Ky Chau	Production Note: Signature removed prior to publication.	6 May 2025
Dr. Mika Westerhausen	Production Note: Signature removed prior to publication.	6 May 2025
Dr. Thomas Lockwood	Production Note: Signature removed prior to publication.	1 May 2025
Dr. Jake Violi	Production Note: Signature removed prior to publication.	30 April 2025
Dr. Peter Irga	Production Note: Signature removed prior to publication.	30 April 2025

Table of Contents

Composition and impact of wildfire-enriched aerosols on estuarine microbial communities: The 2019-20 Australian Black Summer i
Certificate of original authorship ii
Acknowledgements iii
Format of thesis v
Publications included in thesis vi
Contribution of authors vii
Table of Contents viii
Table of Figures xii
Table of Tables xix
Abstract xx
1. Introduction and literature review 1
1.1 Overview of aerosols 1
1.2 Fertilising effect of aerosols on the biosphere 4
1.3 Toxic effects of aerosols on the biosphere 6
1.4 Australia's aerosol emissions 8
1.5 Properties of wildfire aerosols 11
1.6 Wildfires and aquatic microbes 13
1.7 The 2019-20 Black Summer wildfires 15
1.8 Research aims and objectives 17
2. Fine particle pollution during megafires contains potentially toxic elements 21
Highlights 21
Abstract 22
Graphical abstract 23
2.1 Introduction 24
2.2 Material and methods 26
2.2.1 Study site 26
2.2.2 Sample collection 26
2.2.3 Sample extraction 27
2.2.4 Sample processing 28
2.2.5 Airborne concentration and source analyses 29
2.2.6 Particle size and morphology 30

2.2.7 Potentially toxic elements 30
2.2.8 Data analysis 31
2.3 Results and discussion 33
2.3.1 Particle pollution in Sydney's CBD during the Black Summer Wildfires 33
2.3.2 Impact of wildfires on particle size and morphology 35
2.3.3 Potentially toxic elements: chemical composition and solubility 38
2.4 Conclusions 44
Funding 45
CRediT authorship contribution statement 45
Declaration of competing interest 45
Acknowledgements 46
3. Nutrient profile and sources of aerosols collected during intense wildfires in the Southern Hemisphere 47
Highlights 47
Abstract 48
3.1 Introduction 49
3.2 Material and methods 51
3.2.1 Aerosol capture and extraction 51
3.2.2 Chemical analyses 51
3.2.3 Source apportionment 54
3.2.4 Data analysis 56
3.3 Results 57
3.3.1 Macronutrients 57
3.3.2 Micronutrients 58
3.3.3 Aerosol sources 60
3.4 Discussion 63
Funding 67
CRediT authorship contribution statement 68
Declaration of competing interest 68
Acknowledgements 68
4. Acute exposure to wildfire-enriched aerosols elicits divergent microbial responses across multiple Australian estuaries 69
Highlights 69
Abstract 70
Graphical abstract 71
4.1 Introduction 73

4.2 Material and methods 75
4.2.1 Study region 75
4.2.2 Wildfire-enriched PM sampling 77
4.2.3 Estimating dry deposition flux of PM_{10} 77
4.2.4 Wildfire deposition scenarios 78
4.2.5 Estuary field sampling 78
4.2.6 Experimental bottle incubations 79
4.2.7 Photophysiological traits 81
4.2.8 Cellular abundance and functional traits 83
4.2.9 Statistical analysis 86
4.3 Results and discussion 87
4.3.1 Estuary characteristics during sampling 87
4.3.2 Assessment of wildfire aerosol inputs 89
4.3.3 Overview of multivariate impacts of wildfire-enriched aerosols 91
4.3.4 Divergent heterotrophic response to average wildfire conditions 93
4.3.5 Divergent autotrophic response to average wildfire conditions 96
4.3.6 Convergent heterotrophic responses to extreme wildfire conditions 98
4.3.7 Potential drivers of wildfire responses 99
4.3.8 Significance and conclusions 102
Funding 103
CRediT authorship contribution statement 103
Declaration of competing interest 103
Acknowledgements 103
5. Aerosols generated by extreme wildfires elicit dose- and time-dependent changes in estuarine microbial communities 104
Highlights 104
Abstract 105
5.1 Introduction 107
5.2 Material and methods 110
5.2.1 Estuary field sampling 110
5.2.2 Wildfire-enriched particulate matter 111
5.2.3 Experimental design 111
5.2.4 Experimental setup and sampling 112
5.2.5 PAM fluorometry 113
5.2.6 Flow cytometry 114
5.2.7 eDNA analysis 115

5.2.8 Physical water parameters 116
5.2.9 Statistical analysis 116
5.3 Results and discussion 117
5.3.1 Dose response curves 117
5.3.2 Temporal dynamics 120
5.3.3 Overview of community composition 124
5.3.4 Bacterial community 127
5.3.5 Eukaryotic community 129
5.3.6 Physical water parameters 131
5.4 Summary and conclusions 132
Funding 132
CRediT authorship contribution statement 133
Declaration of competing interest 133
Acknowledgements 133
6. Summary and significance 134
Prelude 134
6.1 Summary of major thesis findings 134
6.2 Research methodology and considerations 136
6.3 Conceptual contributions to the field 137
6.4 Broader significance of research 138
6.5 Future research directions 142
6.6 Concluding remarks 144
Chapter 2: Supplementary Material 146
Supplementary Figures 146
Supplementary Tables 148
Supplementary Text 151
Supplementary References 153
Chapter 4: Supplementary Material 154
Supplementary Tables 154
Supplementary Figures 157
Chapter 5: Supplementary Material 161
Supplementary Figures 161
References 162

Table of Figures

Figure 1.1 Schematic depicting size of aerosols relative to a strand of human hair, taken from Environmental Protection Agency (2020). 2

Figure 1.2. Schematic illustrating the pathway and fate of aerosols in the ocean, taken from Mahowald et al., (2018). 5

Figure 1.3 Schematic depicting the three major dust aerosol pathways across Australia (brown arrows), taken from Perron et al. (2020a). 9

Figure 1.4 Monthly burned forested area in Australia between 1987 and 2019 inclusive, taken from Canadell et al. (2021). 10

Figure 1.5 Schematic of the various stages of particle capture and extraction using the filter forensics approach. From left to right: HVAC filter room at particle capture site (University of Technology Sydney, Australia); unprocessed HVAC filters from different time points and the sample extraction process; subset of sample collected and major physical and chemical analyses for downstream processing to be conducted for Chapters 2 and 3. 18

Figure 1.6 Series of images demonstrating the estuary sampling procedure employed for sample collection in Chapters 4 and 5 ("A") and map depicting locations of estuaries sampled in Chapter 4 (coloured diamonds) as well as location of PM sampling and air quality monitoring (black diamonds). 19

Figure 1.7 Schematic depicting an overview of the setup and procedure for incubation experiments in Chapter 4. From left to right: filtration of estuary water and filling of bottles; bottles dosed with PM enriched by Black Summer fire emissions in two deposition scenarios and secured; 24-hour incubation initiated in temperature- and light-controlled bath; initial samples taken and stored for measurement and downstream processing. This process was repeated for each estuary in Chapter 4. 19

Figure 1.8 Series of images depicting the overall set up of incubation experiments in Chapter 5, including two continuous deposition scenarios running for 10-days in bottles (top-left image) and ten continuous scenarios running for 5-days in flasks (top-right image). Bottom image depicts the concentration gradient of PM enriched by Black Summer fire emissions added to vessels. 20

Figure 2.1 Airborne concentration and source analysis of PM pollution in Sydney's CBD during the 2019-2020 Black Summer Wildfires and 2020-2021 Reference period. A) depicts location of HVAC sampling relative to confirmed fire cases (orange points as single fires or perimeters of burnt zones); B) polar plots for the two study periods (Wildfire and Reference) by pollutant (PM_{10} and $PM_{2.5}$), where colour denotes the probability of exceeding hourly concentrations of 50 μg m^3 PM_{10} and 25 μg m^3 $PM_{2.5}$ by wind direction and wind speed; C) regional back-trajectory analysis of Wildfire period depicting origin of air-masses associated with exceeding 50 μg m^3 PM_{10} and 25 μg m^3 $PM_{2.5}$ (red/blue regions indicate highest/lowest probabilities); D) daily mean concentration of PM_{10} (black) and $PM_{2.5}$ (blue); E) daily mean (solid line) and hourly maximum (point) concentrations. Dashed lines on D) and E) depict periods of Wildfire (orange) and Reference (black) HVAC sampling (n = 120 days). 34

Figure 2.2 Particle number size distributions of Wildfire (n = 21) and Reference (n = 12) PM. Individual solid lines depict replicates, where dashed lines denote the mean count median diameters for the Wildfire (orange) and Reference (black) periods. SEM images show the size and morphology of PM sample composites. Overall size distributions differed significantly between study periods (two-sample z-test: p = 0.001). Wildfire filters collected from the two buildings did not differ (two-sample z-test: p = 0.240). 36

Figure 2.3 Principal Components Analysis (PCA) biplot depicting differences in the potentially toxic fingerprint of Wildfire (orange, n = 12) and Reference (black, n = 9) PM. Points closer together have more similar mass composition and vice versa. Blue vectors represent the direction and magnitude of elements driving the greatest differences amongst samples. Study periods differed significantly in both the centre (PERMANOVA: p = 0.001) and spread (PERMDISP: p = 0.026) of PCA clusters. Wildfire filters collected from the two buildings (closed/open circles) did not differ (PERMANOVA: p = 0.227; PERMDISP: p = 0.821). 39

Figure 3.1 Macronutrient content of aerosols sampled in Sydney, Australia during the 2019-20 Black Summer wildfires (n = 12) and ambient urban conditions (2020-21, n = 9). Solubilities for non-ionic analytes (right-side of vertical dashed line) are denoted by blue points and the second y-axis, where values closer to 100% indicate that the element is primarily in the dissolved fraction. All data are shown as medians and upper/lower quartiles on a natural log scale, and statistical significance of wildfire-enriched versus urban comparisons are shown below the x-axis. 57

Figure 3.2 Micronutrient content of Black Summer wildfire (2019-20, n = 12) and ambient urban aerosols (2020-21, n = 9). Solubilities of trace elements (right of dashed line) are indicated by blue points and the second axis. All values are displayed as medians and upper/lower quartiles on a natural log scale, and statistical significance of wildfire-enriched versus urban comparisons are shown below the x-axis. 59

Figure 3.3 PMF-resolved source profiles (A: left subplots) and sample contributions (B: right subplots) for aerosols captured in Sydney, Australia during Black Summer wildfire (2019-20, n = 11) and ambient urban conditions (2020-21, n = 9). Factors 1-6 (F1-F6) are displayed by row and labelled according to its deduced source (see Results). For left subplots (A), analytes are shown along the x-axis, with the y-axis indicating average contributions (%) to each factor's mass (bars) or to total analyte mass as measured across all factors (points). Analytes used as chemical tracers in this study are coloured according to its source classification. Right subplots (B) show each factor's contribution (%) to wildfire-enriched (orange) and urban (grey) sample mass (%). All values are displayed on a natural log scale. 61

Figure 4.1 Site map of the five estuaries sampled near Batemans Bay on the South Coast of NSW, Australia (coloured diamonds). Also shown are the locations of particulate matter (PM) sampling in Sydney's CBD and air quality monitoring in Batemans Bay during the 2019-20 Black Summer wildfires (black diamonds). PM samples were collected at the University of Technology Sydney (UTS) Ultimo campus, and air quality data was obtained from the NSW Department of Climate Change, Energy, the Environment and Water (DCEEW). 76

Figure 4.2 Photograph of the incubation bath used to conduct 24-hour bottle incubation experiments. The bath was constructed using a 90 L plastic container insulated with rubber matting (A) and was heated with a heating immersion circulator (B) supplemented with an additional pump (C) for mixing. The interior corner was protected against the heating element using thermally resistant mounting tape (D). An LED light with a cool white spectral output was used to illuminate the bath (E). 80

Figure 4.3 Abundances (A) and functional traits (B) of microbial populations (x-axis) in five estuaries (colour) surrounding Batemans Bay at the time of sampling (n = 3 per estuary). Flow cytometry measurements are depicted as means ± standard deviations (bars), whereas boxplots display the more variable PAM fluorometry results. Estuaries include Lake Brou (BRO), Lake Tabourie (TAB), Clyde River (CLY), Moruya River (MOR) and Tuross River (TUR). Microbial subpopulations include phytoplankton (PHY), eukaryotes (EUK), synechococcus (SYN), bacteria

(BAC), high-DNA bacteria (HDNA), low-DNA bacteria (LDNA), virus-like particles (VLP). Functional traits include equivalent spherical diameter (ESD), side scatter (SSC), chlorophyll (CHL) and phycoerytherin (PE) autofluorescence, maximum (Fv/Fm) and effective (Fq'/Fm') quantum yields, and relative rate of photosynthesis onset (Alpha). All abbreviations are defined in the Abbreviations section at the start of this chapter..... 88

Figure 4.4 Atmospheric PM_{10} concentrations (μg m^{-3}) in Batemans Bay during the 2019-20 Australian Black Summer wildfires. The black line and diamonds represent the average daily PM_{10} concentration, with grey bars indicating the range (minimum to maximum) of hourly concentrations observed each day. The corresponding dry deposition flux of PM_{10} (g m^{-2} d^{-1}) is shown on the secondary y-axis (scaled equivalently), where black lines and diamonds denote the daily mean flux and grey bars represent the range. The blue line indicates the mean daily PM_{10} concentration (~12 μg m^{-3}) after local fires were extinguished on 9 February 2020, with an estimated flux of ~0.021 g m^{-2} d^{-1} (or ~21 mg)..... 90

Figure 4.5 Principal components analysis (PCA) biplots depicting microbial traits in estuaries (colour) after 24-hour incubations with wildfire-enriched particles (n = 6 per estuary). Data was normalised to the mean of the Control Incubation for each estuary. Points indicate treatments: empty circles = Control Incubations ("C"); small filled circles = Average Scenario ("A"); large filled circles = Extreme Scenario ("E"). All panels display the same PCA biplot with treatments and loadings added sequentially: (A) Control Incubations; (B) + Average Scenario; (C) + Extreme Scenario; (D) A + B + loadings; (E) A + B + C + loadings. Loadings are labelled with population and trait abbreviations, as defined in the Abbreviations section at the start of this chapter. Bold loadings indicate cell abundance or population ratios. Axis percentages show the variance explained by PC1 and PC2..... 91

Figure 4.6 Abundance of microbial populations in five estuaries following 24-hour incubations with wildfire-enriched particles (n = 6 per estuary). Populations are depicted across rows (A) to (G) with estuaries separated by facet and incubation treatment along the x-axis. Cell abundances are shown on a natural log scale. All abbreviations are defined in the Abbreviations section at the start of this chapter..... 94

Figure 4.7 Functional traits associated with divergent microbial responses to the Average or Extreme Scenario of wildfire-enriched particle deposition in five estuaries (n = 6 per estuary). Populations and traits are denoted by right facets, while estuaries are denoted by top facets. All abbreviations are defined in the Abbreviations section at the start of this chapter. 97

Figure 4.8 Heatmap depicting Pearson correlation coefficients (colour) between the horizontal trait axis (PC1) in Principal Components Analysis (PCA) (x-axis) and mean estuary characteristics at the time of sampling (t0) or in historical datasets (Hist.) (y-axis). Characteristics are grouped into four distinct facets, including (from left-right) water quality parameters, nutrients, microbial traits, and geomorphology. All abbreviations are defined in the Abbreviations section at the start of this chapter..... 99

Figure 5.1 Photograph of the experimental set up for the "Scenario" experiment (left) and "Dose response" experiment (right). 113

Figure 5.2 Dose response curves depicting cellular abundance (y-axis) relative to Control Incubations (dashed line) with increasing wildfire deposition flux (x-axis). Microbial populations are separated into individual facets, where duration of exposure is denoted by colour. Orange and dark red bars depict concentrations corresponding to average and maximum daily deposition during the 2019-20 Black Summer wildfires. Points and black error bars represent means and standard errors, respectively (n = 5). 119

Figure 5.3 Community traitscape of Clyde River microbes in Scenario experiment following 10-day incubations with wildfire-enriched particles, as indicated by Principal Component Analysis (PCA). Data was normalised to the mean control (no aerosol) incubation and includes flow cytometry-based measurements of eukaryotes ("EUK"), Synechococcus ("SYN"), heterotrophic bacteria ("HET"), chlorophyll-positive ("CHL+BAC") and phycoerytherin-positive ("PE+BAC") bacteria, and virus-like particles ("VLP"). Points represent replicate incubation vessels, coloured by day and shaped by treatment (C = control incubation; A = average scenario; M = maximum scenario). All biplots depict the same PCA, but are separated by treatment (A) or marked with PCA loadings (B). Loadings (black diamonds and text) indicate the contribution of each trait to community variation, with bolded labels representing those relating to cellular abundance. Percentages on axes indicate the total variation explained by the first two principal components (PC1 and PC2). 121

Figure 5.4 Time series displaying changes in cell abundance (y-axis) relative to Control Incubations (dashed lines) over 10 days of daily wildfire exposure in the Scenario experiment. Populations are separated into individual facets, where wildfire treatment is shown by colour: Orange and dark red points depict average and maximum daily deposition scenarios during the 2019-20 wildfires. Points and error bars indicate means and standard deviations, respectively. 122

Figure 5.5 Non-metric multidimensional (nMDS) ordinations of the composition of bacteria (A) and eukaryotes (B) in the Scenario experiment based on Bray-Curtis dissimilarities. Each point represents a replicate community (n = 5) after 10-day incubations under one of three treatments: Control (C, blue); Average wildfire (A, orange); Maximum wildfire (M, dark red). 125

Figure 5.6 Bacterial alpha diversity indices (A, B), species richness (C) and number of unique ranks identified across various levels of taxonomy (D) - from phylum to species. Note that total taxa counts are higher than species counts because they include all distinct groupings at each taxonomic rank (i.e. phylum x class x order x family x genus x species x taxa). Plots are coloured by incubation treatment in the Scenario experiment, including Control (”C”), Average (”A”) and Maximum (”M”), respectively. Asterisks in (A) to (C) represent significant treatment comparisons (PERMANOVA, $p_{adj} < 0.05$). 126

Figure 5.7 Eukaryote alpha diversity indices (A, B), species richness (C) and number of unique taxonomic ranks (D) from Phylum to Taxa. Plots are coloured by incubation treatment, including Control (”C”), Average (”A”) and Maximum (”M”), respectively. Asterisks in (A) to (C) represent significant treatment comparisons (PERMANOVA, $p_{adj} < 0.05$). 127

Figure 5.8 Bacterial community composition in incubation of Clyde River microbes with wildfire-enriched particles in Scenario experiment. Each bar on the x-axis represents an individual replicate bottle, while the y-axis shows the relative abundance of taxa. Bars are coloured by Phylum × Order, with individual taxa indicated by each segment. Facets represent 10-day incubation treatments. Legend labels in bold denote orders contributing >5 % to the observed dissimilarity between treatments (SIMPER), where letters listed after each taxa indicate the following treatment comparisons: Control × Average (”a”), Control × Maximum (”b”), Average × Maximum (”c”). 128

Figure 5.9 Eukaryotic community composition in incubations of Clyde River microbes with wildfire-enriched particles in Scenario experiment. Each bar on the x-axis represents an individual replicate bottle, while the y-axis shows the relative abundance of taxa. Bars are coloured by Phylum × Class, with individual taxa indicated by each segment. Facets represent 10-day incubation treatments. Legend labels in bold denote orders contributing >5 % to the observed dissimilarity between treatments (SIMPER), where letters listed after each taxa indicate the following treatment comparisons: Control × Average (”a”), Control × Maximum (”b”), Average × Maximum (”c”). 130

Figure 5.10 Physical water parameters of 10-day bottle incubations with wildfire-enriched particles in the Scenario experiment. Plots are coloured by incubation treatment, including Control (”C”), Average (”A”) and Maximum (”M”), respectively. Asterisks represent significant treatment comparisons (Tukey HSD, $p_{adj} < 0.05$). Facets are labelled with parameter as follows: C_µScm = conductivity; DO_mgL = dissolved oxygen; light_µmolm2s = light received in shaken vessel; pH = pH; Sal_ppt = salinity; Temp_C = temperature. 131

Figure 6.1 Proportion of valid ICOLLs and Rivers (n = 84) in each NSW LGA that displayed at least one significant shift in water quality during and/or after the 2019-20 Black Summer fires, relative to pre-fire conditions (PERMANOVA with Bray-Curtis distance and 999 permutations; $p < 0.05$). 140

Figure 6.2 Average contributions of water quality variables to the overall dissimilarity between fire phases (top facets) for all valid fire-impacted estuaries (SIMPER with Bray-curtis distance and 999 permutations). Estuaries are grouped by type (colour). 141

Table of Tables

Table 2.1 Particle size metrics of Wildfire (n = 21) and Reference (n = 12) PM (mean ± se). Significant PERMANOVA ($P_{(p\text{-}aov)}$) comparisons are denoted by stars (***p ≤ 0.001; **p ≤ 0.01; *p < 0.05), where ns indicates non-significant (p > 0.05). Bold values denote finer particle metrics. 37

Table 2.2 Potentially toxic ions (and Na^+) in Wildfire (n = 12) and Reference (n = 9) PM (median, q1-q3). Significant differences between periods (PERMANOVA ($P_{(p\text{-}aov)}$) are denoted by stars (***p ≤ 0.001; **p ≤ 0.01; *p < 0.05), where ns indicates non-significant (p > 0.05). Bold values denote higher median concentrations (mg/g or µg/g). LOD = limit of detection. 39

Table 2.3 Potentially toxic trace elements in Wildfire (n = 12) and Reference (n = 9) PM (median, q1-q3). Significant PERMANOVA ($P_{(p\text{-}aov)}$) and PERMDISP ($P_{(p\text{-}disp)}$) comparisons are denoted by stars (***p ≤ 0.001; **p ≤ 0.01; *p < 0.05), where ns indicates non-significant (p > 0.05). Bold values denote higher median concentrations (µg/g) / solubilities (%) and wider quartile ranges (solubility only). LOD = limit of detection. 41

Table 4.1 PCA loadings for microbial traits of estuaries following 24-hour incubations with wildfire-enriched particles (n = 6 per estuary). Columns under the “Average Scenario” (left-hand side) indicate divergent responses of estuaries observed along PC1, while the “Extreme Scenario” (right-hand side) depicts uniform responses of estuaries along PC2. Loadings are labelled with population and trait abbreviations, as defined in the Abbreviations section at the start of this chapter. 92

Table 5.1 Summary of water quality parameters across a three-point transect sampled in Clyde River in May 2022. Sites 1-3 reflect readings at each of the three points for water collection, while the Composite indicates the mean ± sd of values. 111

Abstract

The Australian Black Summer megafires of 2019-20 emitted record-breaking quantities of aerosols into the atmosphere, delivering bioactive particles to ecosystems proximal and downwind of the source. High volume, heating, ventilation and air conditioning (HVAC) filters sampled in Sydney revealed finer particles (0.9 vs 1.5 µm) enriched with potentially toxic (Cl^-, Co, F^-, Mn, NO_3^-, Sb, SO_4^{2-}) and nutritional (Ca^{2+}, Co, Fe, Mg^{2+}, Mn, NO_3^-, Si, SO_4^{2-}) elements. This finer, fire-enriched material displayed higher dissolution of mercury (12.1% vs 1.0%) and three nutrients (Ca, N, Si). Bottle incubations revealed dynamic responses of NSW estuarine microbes to wildfire-enriched particle additions. Under an average 24-hour scenario for dry deposition, responses varied by estuary, including heterotrophic, phototrophic, or no response. Under an extreme scenario, all estuaries veered towards heterotrophy, with an increase in metabolically active heterotrophs, and decrease in phytoplankton abundance and pigments. Five-day incubations with Clyde River microbes showed dose-dependent growth that varied temporally, with heterotrophic bacteria dominating in the first 24 hours (0.5-fold increase), and photosynthetic bacteria and eukaryotes thereafter (up to 125-fold increase). Additionally, the cyanobacterium *Synechococcus* was differentially inhibited (0.9-fold decrease). This thesis highlights the complexity of gauging estuarine responses to wildfire inputs, with implications for monitoring Australia's fire-prone future.

1. Introduction and literature review

1.1 Overview of aerosols

Aerosols are suspensions of liquid and/or solid particles in the atmosphere. These particles are commonly referred to as particulate matter (PM), particularly in air quality studies. Aerosols are well recognised for their adverse effects on human health, contributing to global disease burden and premature mortality (Cohen et al., 2017; Yu et al., 2024). They also influence the biosphere through the provision of toxicants and nutrients, altering local biogeochemical cycles and ecosystem productivity (Hamilton et al., 2022; Mahowald et al., 2018).

Particle size is a fundamental property influencing aerosol behaviour and is therefore widely used as the primary framework for describing atmospheric PM. It is commonly divided into a coarse fraction consisting of particles <10 μm in diameter (PM_{10}), and a fine fraction containing particles <2.5 μm ($PM_{2.5}$) that forms a subset of PM_{10} (Environmental Protection Agency, 2020) (Figure 1.1). Less commonly, particles between ~0.1 and 1 μm are further distinguished as the accumulation mode ($PM_{0.1\text{-}1}$), where removal mechanisms are relatively inefficient, allowing particles to accumulate in the atmosphere over time.

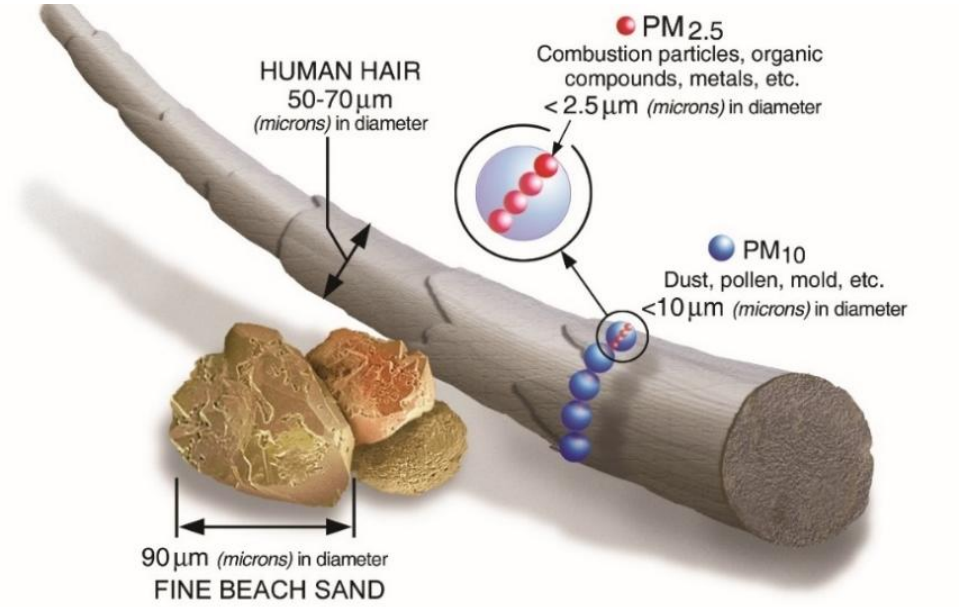


Figure 1.1 Schematic depicting size of aerosols relative to a strand of human hair, taken from Environmental Protection Agency (2020).

Besides size, atmospheric PM is also described according to its emission source. Primary particles are those emitted directly into the atmosphere, and they originate from a variety of sources including those of natural (mineral dust, volcanic eruptions, biomass burning, sea-spray) and anthropogenic (mining, shipping, manufacturing, vehicular traffic) origins (Hamilton et al., 2022). These are comprised of a diverse mixture of bioactive elements, including those with potentially toxic (e.g., copper) or fertilising (e.g., iron) effects on the biosphere (Mahowald et al., 2018). However, these can be broadly linked to their emission source(s), each of which impart a distinct chemical signature (Journet et al., 2008): Mineral dust is typically enriched in crustal trace elements such as aluminium (Al), iron (Fe), manganese (Mn), silica (Si), and titanium (Ti) (Hird et al., 2024; Radhi et al., 2011; Strzelec et al., 2020a); Volcanic eruptions are rich in carbon (C) and sulfur (S), with variable crustal elements (Andersson et al., 2013); Biomass burning emissions are dominated by organic carbon (OC), nitrogen-containing compounds (N), and inorganic ions including potassium (K^+), nitrate (NO_3^-), sulfate (SO_4^{2-}), oxalate ($C_2O_4^{2-}$) and calcium (Ca^{2+}) (Reid et al., 2005; Strzelec et al., 2020a); Sea-spray is composed mostly of sodium (Na^+) and chloride (Cl^-), with minor contributions of magnesium (Mg^{2+}) (Adachi and Buseck, 2015); Anthropogenic activities such as mining, shipping, manufacturing, and transportation emit significant quantities of toxic trace metals, including lead (Pb), mercury (Hg), nickel (Ni), copper (Cu) and zinc (Zn) (McNeill et al., 2020; Pacyna et al., 2006; Strzelec et al., 2020a).

Once airborne, these primary emissions quickly mix into the lower 1-3 km of the atmosphere, where particles can either remain near their emission source or are transported great distances via air currents (Mahowald et al., 2011). While primary particles are an important source of aerosols in the atmosphere, aerosols experience continuous physical and chemical transformation during transport - a process known as "atmospheric aging" (Spokes and Jickells, 1996). One of the major pathways through which aging alters particle size is coagulation, which occurs when individual particles collide with one another to form larger aggregates, especially in dense, highly-concentrated plumes (Seinfeld and Pandis, 2016). Aerosols also act as condensation nuclei for cloud and fog droplets, increasing in size as water vapor diffuses onto the surface of existing particles (Williams et al., 2002).

Beyond physical growth, aging drives substantial chemical transformations of both gas-phase and particle-bound species. Through oxidation of gaseous precursors, new particulate material is formed in the atmosphere – commonly referred to as secondary aerosols – including NO_3^- from nitrogen oxides (NO_x), SO_4^{2-} from sulfur dioxide (SO_2), and secondary organic aerosol (SOA) from volatile organic compounds (VOCs) (Hallquist et al., 2009; Riemer et al., 2019). These reactions are initiated by highly reactive, primary oxidants, such as hydroxyl (OH) and NO_3^- radicals, and ozone (O_3) (Hallquist et al., 2009; Kanakidou et al., 2005; Ng et al., 2017). Newly formed SOA can subsequently condense onto existing particles, promoting further particle growth and changes to chemical composition (Hallquist et al., 2009).

Simultaneously, multiphase reactions enhance the solubility of aerosol-bound elements. For example, sulfuric and nitric acids (H_2SO_4 and HNO_3) can coat insoluble dust particles containing Fe, liberating ionic, more bioavailable forms (Fe^{2+} or Fe^{3+}) by destabilising Fe-O bonds (Shi et al., 2011). Photochemical redox reactions further promote Fe mobilisation via (1) complexation with oxidation products such as oxalate ($C_2O_4^{2-}$), which act as organic ligands that form stable water-soluble Fe complexes, and (2) reduction of Fe^{3+} to Fe^{2+} through electron transfer following adsorption of Fe-$C_2O_4^{2-}$ complexes onto Fe-(oxyhydr)oxide surfaces (Johnson and Meskhidze, 2013). Besides mineral elements, these same processes also enhance the solubility of aeolian macronutrients like phosphorus (P) and N (Geng et al., 2009; Hamilton et al., 2022).

After transport and chemical transformation, aerosols are eventually removed from the atmosphere through deposition processes. Dry deposition occurs when PM settles by gravity or collides with terrestrial or aquatic surfaces (Kanakidou et al., 2005). This process is driven by atmospheric turbulence, which generates chaotic air movements that enhance the downward transport of aerosols towards terrestrial and aquatic surfaces (Cheng et al., 2022). Size is a key attribute influencing atmospheric residence time, which is typically <1 day for larger PM (>10 μm) and up to one week for PM_{10} (<10 μm) (Textor et al., 2006). This is due to the strong dependence between dry deposition velocity and particle diameter, where larger, heavier particles, such as wildfire ash (Bodí et al., 2014), settle faster from the atmosphere (Farmer et al., 2021; Nho-Kim, 2004). To a lesser extent, dry deposition rates are also influenced by air mass concentration, with denser plumes settling more rapidly from the atmosphere (Seinfeld and Pandis, 2016). Land use also plays a role, with more complex terrain such as forests enabling higher deposition rates compared to simpler surfaces like grasslands (Farmer et al., 2021). In contrast, wet deposition refers to the process by which PM becomes embedded in clouds or captured by falling rain or ice, leading to its removal from the atmosphere via precipitation (Seinfeld and Pandis, 1998). This mechanism can efficiently clear both fine and coarse particles from the atmosphere, and is strongly dependent on meteorological conditions such as cloud cover, humidity, and precipitation rates (Seinfeld and Pandis, 1998).

1.2 Fertilising effect of aerosols on the biosphere

Aerosols play a crucial role in shaping the Earth's biosphere, with atmospheric deposition serving as a key pathway for delivering nutrients and other bioactive materials to downwind ecosystems (Hamilton et al., 2022) (Figure 1.2). Among these nutrients, OC is essential to all energy flows on Earth, where ~50-70% of aeolian OC is deposited on land and ~30-50% in the oceans (Kanakidou et al., 2012; Nagata, 2000). In terrestrial environments, OC may be assimilated into biomass by soil bacteria, incorporated into underlying mineral soil by biological and physical mechanisms, and/or transported to waterways via groundwater and precipitation (Bodí et al., 2014). Critically, the OC content of soils is a principal indicator of fertility, where it supports plant growth by increasing the water-holding capacity of soil and providing nutrition (Banwart et al., 2019). For instance, *Cunninghamia lanceloata* seedlings have been shown to absorb wildfire smoke-derived carbon directly through their roots over 180 days, and assimilate it into root, branch and

leaf biomass (Zhan et al., 2025). Notably, this stimulatory effect was only observed at low concentrations, with high smoke exposure being inhibitory to growth (Zhan et al., 2025).

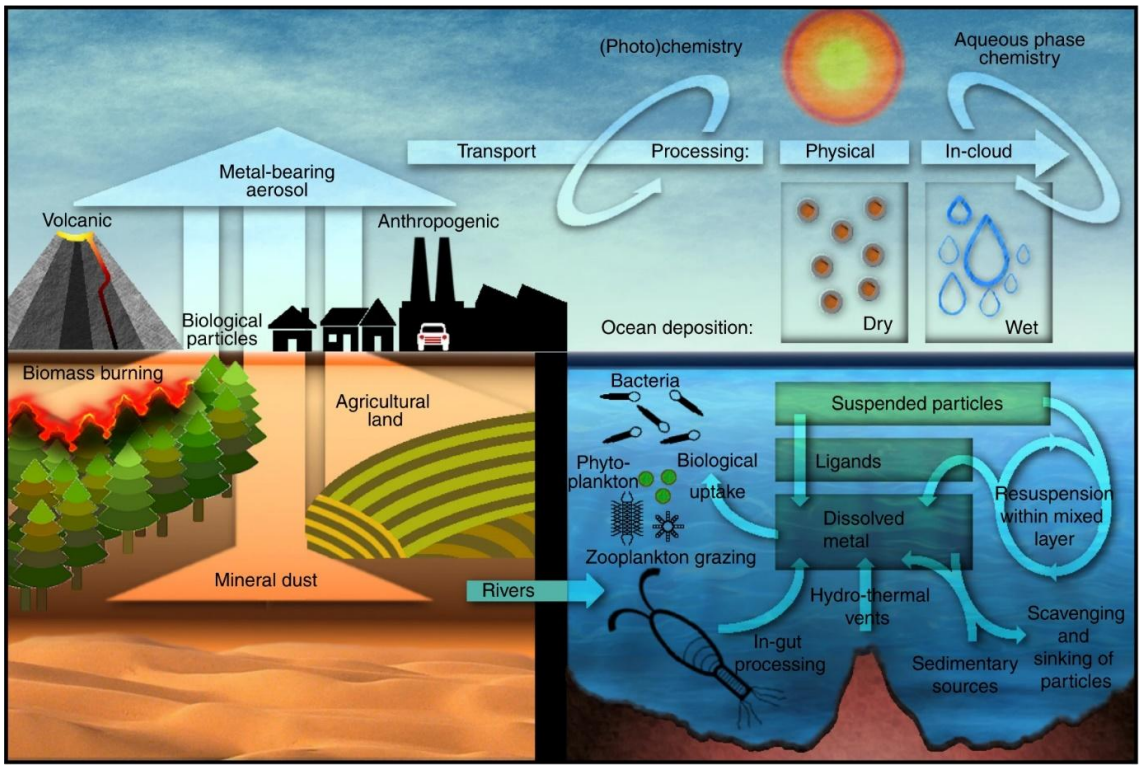


Figure 1.2. Schematic illustrating the pathway and fate of aerosols in the ocean, taken from Mahowald et al., (2018).

In aquatic systems, OC is converted into biomass by bacteria and fed through the microbial loop via grazing (Azam et al., 1983) or incorporated into sediments for long-term storage (Nellemann et al., 2009) (Figure 1.2). Dissolved forms of OC (DOC) are readily available to bacteria, stimulating their proliferation (Nagata, 2000). For example, experimental additions of Saharan dust aerosol to alpine lakes in Spain had a positive effect on bacterial abundance and growth in oligotrophic systems featuring severe P-limitation and low DOC (Reche et al., 2009). In contrast, particulate forms of OC (POC) must first be solubilised through processes such as photodegradation and bacterial exoenzyme cleavage (Nagata, 2000).

In addition to OC, atmospheric deposition of aerosols also delivers other critical nutrients that influence ecosystem productivity. N and P in particular, are the two major rate-limiting nutrients in most ecosystems around the world, where they support growth, metabolism, protein

synthesis and/or photosynthetic processes in a range of land-based and aquatic organisms (Chapin et al., 2011). On a global scale, ~43% of terrestrial ecosystems are P limited and 39% experience co-limitation of N and P (Du et al., 2020). For example, following a one-time addition of N or P to plant plots in Alaska and Peru, the succession of plants and soil microbes after six years indicated enhanced primary production for both nutrients, but with significantly greater effects in plots treated with P - indicating primary P-limitation and secondary N-limitation (Darcy et al., 2018). Other essential nutrients deposited on land include potassium (K), calcium (Ca), and S, which play important roles in plant growth, cell structure, and stress mitigation (Kopriva et al., 2019).

Freshwater and estuarine ecosystems tend to exhibit co-limitation of N and P, except for lake benthos where P-limitation is prevalent (Elser et al., 2007). In the ocean, experimental evidence has shown phytoplankton growth to be primarily limited by N (39%), Fe (32%), and N-Fe co-limitation (9%) (Browning and Moore, 2023). The deposition of micronutrients such as Fe, Mn, Si and Zn may stimulate phytoplankton growth and activity provided macronutrients aren't limiting (Boyd et al., 2017; Martin et al., 1991; Saito et al., 2008). Given these organisms are key photosynthesisers at the base of aquatic food webs, the addition of these elements can have beneficial effects on primary productivity and trophic flows (Meng et al., 2016; Tsagaraki et al., 2017; Zhang et al., 2019). For instance, mineral dust deposition to the Atlantic Ocean in 2003 triggered a seven-fold increase in phytoplankton biomass and ten-fold increase in production within four days, where the influx of Si drove a community shift from picocyanobacteria dominance to a diatom-dominated assemblage (Duarte et al., 2006). Similarly, deposition of iron-rich mineral dust has enriched surface waters of the Southern Ocean, supporting roughly one-third of annual phytoplankton productivity in this iron-limited region (Weis et al., 2024).

1.3 Toxic effects of aerosols on the biosphere

While the provision of nutrients is generally beneficial for ecosystem productivity, atmospheric deposition of aerosols can also have negative consequences for biota and biogeochemistry. In forests, excess or prolonged deposition of N may reduce the availability of P in soils, intensifying P-limitation in these ecosystems (Li et al., 2015). This imbalance can lead to depleted P supply in older plant stems, resulting in reduced growth and photosynthesis of mature leaves as well as

restricted P remobilisation (Netzer et al., 2018). N-driven deficiency has been documented across European needle forests between 1990 and 2006, where the level of P in *Pinus sylvestris* needles was negatively associated with level of atmospheric N deposition, especially in areas with favorable climatic conditions for growth (Sardans et al., 2016). Similarly, plant species richness across ~15,000 herbaceous sites in the United States increased at low levels of N deposition, and decreased at higher levels between 1985 and 2011 (Simkin et al., 2016). Critically, this study demonstrated that 24% of sites were susceptible to species loss induced by N-deposition, with higher vulnerability in open-canopy vegetation and more acidic soils (Simkin et al., 2016).

Acidic species such as NO_3^-, SO_4^{2-} and Cl^- can reduce the concentrations of Ca and DOC in soils with low buffering capacity by increasing the supply of co-deposited hydrogen ions (H^+) (Zhang et al., 2023). This occurs through two mechanisms: 1) H^+ displaces base cations like Ca^{2+} from exchange sites, mobilising and leaching them from soil; 2) elevated H+ concentrations alter the solubility and charge interactions of organic matter with soil particles, promoting DOC breakdown and leaching (Zhang et al., 2023). This ultimately reduces plant growth and increases mortality (Battles et al., 2014; Monteith et al., 2007). Similarly in aquatic ecosystems, if acidic ions within aerosol deposits predominate over base cations such as Ca^{2+}, Mg^{2+} and K^+, this may decrease the pH of receiving waterways (Brahney et al., 2013; Lydersen et al., 2014). Conversely, the deposition of base cations may raise pH levels (Brahney et al., 2013; Lydersen et al., 2014). Such changes may influence the bioavailability of metals by competing for sorption sites and increasing residence time in the water column (Du Laing et al., 2009). Moreover, acidification may promote the release of heavy metals from underlying sediments (Zhang et al., 2014). While aquatic bacteria often tolerate heavy metals due to diverse detoxification strategies and resistance, phytoplankton tend to exhibit low tolerance, with previous studies indicating reduced cell abundance, chlorophyll content, and primary production (Nayar et al., 2004). These impacts are significant for both terrestrial and aquatic ecosystems given that many aerosol sources co-emit potentially toxic elements, including cadmium (Cd), Pb, and Mn (Gao et al., 2023; Wang et al., 2017). For instance, mixed aerosol additions containing Cu suppressed phytoplankton growth in seawater mesocosms when added alone, but enhanced growth when accompanied by Fe-containing aerosols (Wang et al., 2017).

Excessive nutrient inputs, particularly N and P, may lead to eutrophication of waterways and the formation of nuisance blooms of toxic or non-toxic phytoplankton (Smith and Schindler, 2009). For example, sediment core analyses of a lake in the United States revealed that prescribed burning over ~90 years caused extensive cyanobacterial blooms (Waters et al., 2023). Besides increases in phytoplankton biomass, impacts can manifest as changes in water appearance (discoloration, surface scum or foam), accumulation of toxins in and surrounding the waterbody (including organisms like fish, humans, invertebrates and shellfish), and mass fish kills affecting both wild and aquacultural populations (Hallegraeff et al., 2021; Lim et al., 2023). The latter may result from direct toxicity or hypoxia which can occur after bloom cessation, when widespread cell death leads to a large increase in carbon loading and subsequent heterotrophic degradation, driving oxygen demand beyond available supply (Zhang et al., 2010). This process may be enhanced by increased virulence of aquatic pathogens following atmospheric deposition, due to greater replication and/or increased contact between hosts (Lafferty et al., 2004; Wilson et al., 1996).

1.4 Australia's aerosol emissions

Australia is a significant source of natural aerosols, contributing to ~6% of global mineral dust emissions (Tanaka and Chiba, 2006) and ~6-8% of biomass burning aerosols (Ito and Penner, 2004; Van Der Werf et al., 2006). Dust is mobilised from geological basins and sandy deserts across the arid central "outback" of Australia, where circulation follows three major pathways: 1) the north-west pathway, which flows towards the North West Shelf and the Indian Ocean; (2) the south-west pathway, which flows into the Great Australian Bight; and (3) the south-east pathway, which flows towards the Tasman Sea, Southern Ocean and South Pacific (Figure 1.3) (Baddock et al., 2015; Mackie et al., 2008; Perron et al., 2020a). Air that circulates in these pathways export ~41 Mt of mineral dust each year, of which half is deposited across the continent while the other half is exported offshore (Che et al., 2024). This is amplified by Australia's large, episodic dust storms (e.g. Attiya and Jones, 2022), which are driven by low rainfall and cold air masses during spring-summer, and by prolonged drought in summer-autumn (Sturman and Tapper, 1996).

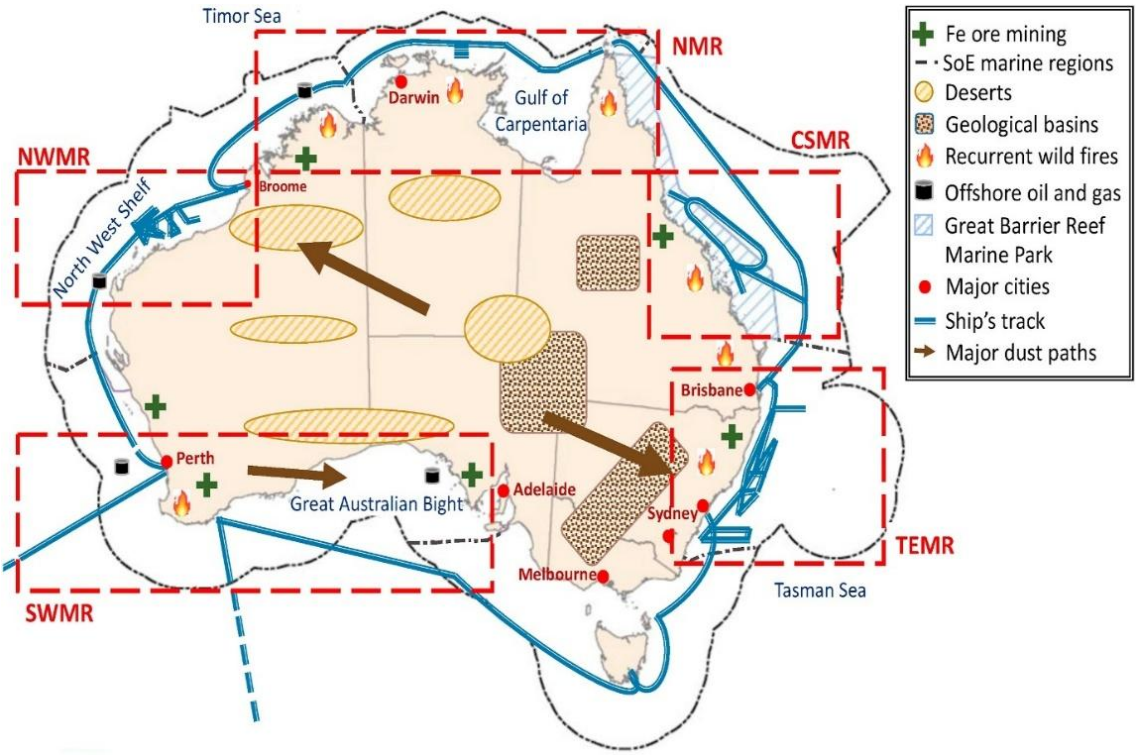


Figure 1.3 Schematic depicting the three major dust aerosol pathways across Australia (brown arrows), taken from Perron et al. (2020a).

Biomass burning emissions are mainly driven by wildfires (otherwise known as "bushfires" in Australia), which occur seasonally throughout the austral spring-summer (Figure 1.4) (Abram et al., 2021; Canadell et al., 2021). Australia is among the most fire-prone continents on Earth due to two key factors: (1) forested areas being dominated by eucalypts, which have high fuel loadings (Boer et al., 2020) – this creates continual stretches of biomass along the forest floor (from bark/leaf litter, dead wood, etc.), increasing fuel connectivity and enabling wildfire to spread easily and rapidly; (2) climatic conditions that favour dry fuels, increasing its flammability (Nolan et al., 2016) – conditions include high solar irradiance, low relative humidity, and prolonged drought. Together, these factors prime the landscape for large and frequent wildfires, which are easily ignited and spread during spells of hot, dry and windy weather (Abram et al., 2021). Across south-eastern Australia, most known fire ignitions result from anthropogenic activities – particularly arson and escaped fires from prescribed burns – whereas lightning strike constitutes a smaller proportion (Clarke et al., 2019).

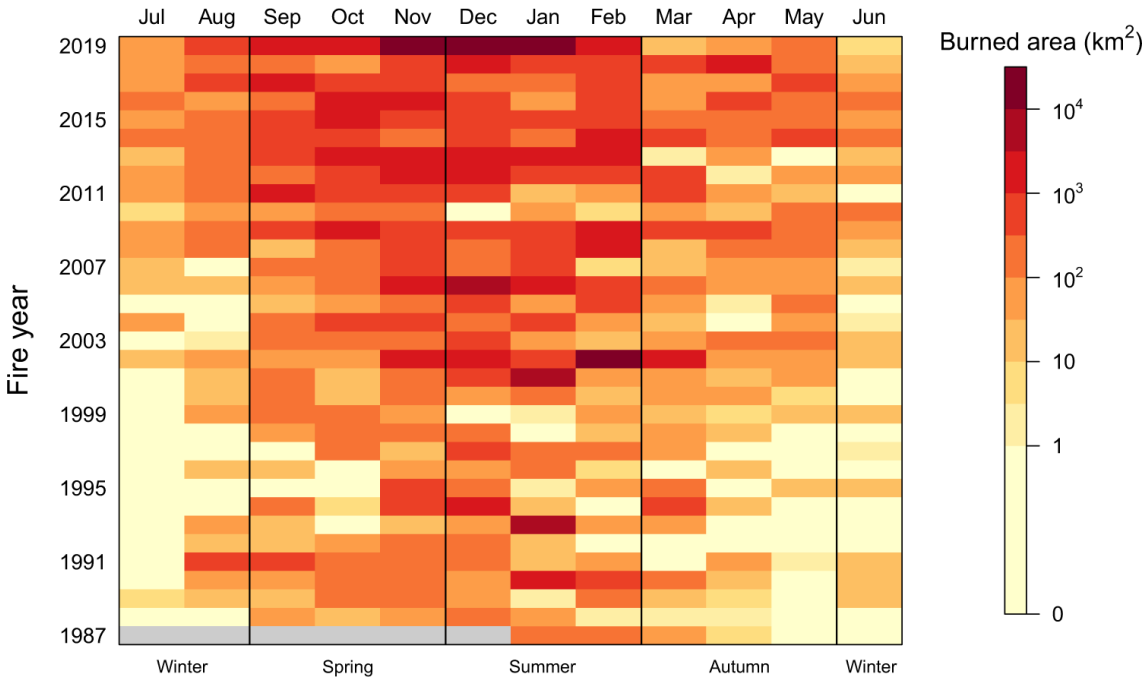


Figure 1.4 Monthly burned forested area in Australia between 1987 and 2019 inclusive, taken from Canadell et al. (2021).

While the sources, composition, and ecological impacts of mineral dust aerosols are relatively well-documented, wildfire aerosols remain comparatively understudied. This represents a critical knowledge gap given Australia's status as both a major emitter of biomass burning aerosols (Ito and Penner, 2004; Van Der Werf et al., 2006) and one of the most fire-prone continents on Earth (Boer et al., 2020; Nolan et al., 2016). As climate change intensifies, temperature and precipitation patterns will facilitate more fire-prone weather, increasing the scale, frequency and magnitude of wildfire smoke emissions (Aldersley et al., 2011; Canadell et al., 2021; Pechony and Shindell, 2010). Already, Australia has seen an increase in burnt forested area over the past ~30 years, especially during austral autumn and winter (Figure 1.4) (Canadell et al., 2021). Unlike dust, which originates from relatively consistent geomorphological processes, wildfire aerosols are chemically complex due to differences in factors like vegetation, land-use, combustion temperature and meteorological conditions (Hamilton et al., 2022; Reid et al., 2005). Understanding their properties is therefore essential for anticipating how future fire regimes will affect downwind ecosystems, especially aquatic environments where observations and incubation experiments remain scarce (Hamilton et al., 2022).

1.5 Properties of wildfire aerosols

Fresh wildfire emissions are comprised of a complex mixture of gases (chlorine (Cl_2), carbon monoxide (CO), carbon dioxide (CO_2), NO_x, O_3, SO_2, VOCs) and PM, the latter of which includes OC, N-containing species, K^+, SO_4^{2-}, $C_2O_4^{2-}$, and Ca^{2+} (Akagi et al., 2011; Benedict et al., 2017; Reid et al., 2005; Strzelec et al., 2020b). These are released as primary aerosols – derived directly from biomass combustion during fire propagation – and as secondary aerosols formed by the transformation of primary gases in the atmosphere (Li et al., 2003; Pósfai et al., 2003; Reid et al., 2005).

Fresh wildfire particles are predominantly found in the accumulation mode (0.1 – 1 μm) with a count median diameter (CMD) of 0.10 – 0.16 μm, however a variety of particle sizes are emitted up to ~1 mm in diameter (Reid et al., 2005). These particles exhibit diverse morphology, varying in their degree of sphericity and the number of particles comprising aggregates (Giordano et al., 2015). Both these properties are influenced by combustion phase, with flaming fires at higher temperatures (~1400 K) producing smaller particles with more complicated shapes than smouldering fires at lower temperatures (~800-1000 K) (Müller et al., 2007; Reid et al., 2005).

Combustion phase also influences chemical composition, where flaming fires proceed with higher efficiency, producing emissions enriched in CO_2, H_2O, NO_x, SO_2, and elemental carbon, and smouldering fires at lower efficiency with emissions dominated by CO, CH_4, NMOC and primary organic aerosol (Sinha et al., 2003). While the properties of fresh biomass smoke are relatively well understood, wildfire emissions are often more complex than burnt biomass alone, as fire activity can entrain material from the surrounding environment and undergo rapid atmospheric processing within the plume.

Besides primary combustion-derived aerosols, wildfire plumes often contain significant quantities of mineral dust elements, including Al, Fe, Mn, Si, and Ti (Hird et al., 2024; Radhi et al., 2011; Strzelec et al., 2020b). These elements typically exhibit very low fractional solubility and require extensive atmospheric processing to become bioavailable (Baker et al., 2006a; Mahowald et al., 2018). During wildfires, dust particles are uplifted from vegetation surfaces and

surrounding soils, becoming entrained within the smoke plumes (Wagner et al., 2018). This process also facilitates the remobilisation of legacy anthropogenic contaminants, including Hg (Howard et al., 2019) and Pb (Isley and Taylor, 2020; Wu et al., 2017). In large wildfire events, intense pyroconvective activity can enhance the uplift of larger particles (Peterson et al., 2021; Wagner et al., 2018). Due to their coarser particle size, dust tends to settle out from the atmosphere faster than smoke, depositing closer to its emission source (Li et al., 2021).

Exposure to freshly emitted, "young" plumes is generally limited to areas near active fires, however most exposures occur via "aged" plumes that have undergone atmospheric aging (section 1.1), particularly during large-scale fire events (Hirsch and Koren, 2021; Peterson et al., 2021). As wildfire plumes age in the atmosphere, the size of particles tends to increase by 0.03 – 0.08 μm due to processes such as hygroscopic growth, gas-to-particle conversion, condensation and coagulation (Reid et al., 2005). The latter is particularly prevalent in densely concentrated plumes emitted during high-temperature flaming combustion (Reid et al., 2005). Aged smoke particles also tend to exhibit more spherical morphologies due to processes such as condensation of secondary species and hygroscopic growth, which smooths particle edges and promotes physical rounding (Reid et al., 2005; Sparks and Wagner, 2021). These plumes are often enriched in secondary organic and inorganic aerosols, including $C_2O_4^{2-}$, Cl^-, NO_3^-, and SO_4^{2-}, formed through oxidation of primary gas-phase emissions including VOCs, Cl_2, NO_x, and SO_2 (Akagi et al., 2011; Benedict et al., 2017; Li et al., 2015; Pósfai et al., 2003). As this oxidative processing proceeds, photochemical redox reactions within the plume further modify composition and enhance the solubility of both combustion-derived and wind-entrained elements (Ito, 2015; Johnson and Meskhidze, 2013; Stockdale et al., 2016). In some cases, pyrocumulonimbus convection amplifies atmospheric processing by injecting smoke to greater altitudes, thereby extending plume residence times in the atmosphere and facilitating long-range transport (Peterson et al., 2021; Wagner et al., 2018).

Despite increasing recognition of the complex physical and chemical evolution of wildfire aerosols, significant uncertainty remains around the composition of wildfire emissions beyond fresh biomass smoke. Besides individual elements like Fe, the concentration and solubility of many elements in aged wildfire aerosols located downwind of its emission source remain poorly constrained. Additionally, other properties including particle size and the prevalence of entrained sources like mineral dust remain poorly documented. Logistical and temporal

challenges in sampling active wildfire events have resulted in a limited number of studies capturing the properties of aged wildfire aerosols globally (Sokolik et al., 2019). This scarcity of data hinders our ability to accurately predict the impact of wildfires on atmospheric loadings of bioactive particles and its deposition to receiving environments.

1.6 Wildfires and aquatic microbes

During wildfires, plumes of smoke and entrained dust can be deposited not only in estuarine waters adjacent to burn zones but can extend to downwind coastal waters and remote ocean locations (Peterson et al., 2021). On entry to the water column, soluble nutrients and toxins carried in these plumes becomes available to an array of aquatic organisms, including phytoplankton, bacteria and viruses (Bixby et al., 2015; Santín et al., 2015). These microbes play critical roles in aquatic ecosystems (Crump and Bowen, 2024), where they fuel the base of food webs through phytoplankton photosynthesis (Araujo-Lima et al., 1986) and drive nutrient cycling through bacterial metabolism (Azam et al., 1983), aided by viral lysis (Bratbak et al., 1994).

In marine systems, wildfire aerosols have shown variable effects on microbial growth and community composition. Incubation experiments using ash leachate collected from the 2017 Thomas Fires (USA) stimulated growth of a diversity of eukaryotic microbes over four days in coastal waters (Ladd et al., 2023). In offshore incubations, ash additions from the same fire had a neutral to negative effect on phytoplankton growth and reduced microzooplankton grazing within 24 hours, while simultaneously enhancing bacterial growth and DOM remineralisation over five days (Baetge et al., 2025). Incubations with ash from the 2017 Ria de Vigo Fires (Spain) over three days supported growth of coastal bacteria and phytoplankton under low-nutrient conditions, but had minimal effect when nutrients were abundant (Gutiérrez-Barral et al., 2024). Satellite observations following the 2020 Indo-China Peninsula Fires reported a distinct increase in chlorophyll-a – an indicator of phytoplankton biomass – in the western Pacific Ocean (Liu and Wang, 2025). While such events may boost primary productivity, harmful outcomes have also been documented: during the 1997 Indonesia Fires, phytoplankton blooms (red tides) led to widespread mortality of coral and fish on the Mentawai reef due to hypoxic conditions (Abram et al., 2003).

Estuarine and freshwater systems also exhibit diverse microbial responses to wildfire aerosol deposition. A 16-year study of ten Californian lakes (USA) found that overhead plumes of smoke had variable impacts on primary production and reduced respiration, particularly in cold, nutrient-poor systems (Smits et al., 2024). Another long-term dataset (14 years) identified a correlation between cyanobacterial growth and fire-derived $PM_{2.5}$ in western USA lakes, following a lag period of 2-7 days (Olson et al., 2023). Experiments with total suspended particles (TSP) from the 2007 Angora Fires (USA) supported the growth of filamentous cyanobacteria and smaller picoplankton in Lake Tahoe over three days, as opposed to larger nanophytoplankton (Mackey et al., 2013). A broader review of wildfire impacts on water quality found algal responses to be highly variable, with 28% of studies reporting positive effects, 24% negative, and 48% showing no detectable impact (Paul et al., 2022).

Investigating the impact of wildfire aerosols on aquatic microbes presents a unique set of challenges due to the hazards of sampling during active fires and the spatial and temporal variability of fire events. Insights to date have relied on field studies conducted at a safe distance (e.g. Scordo et al., 2021), post-fire monitoring (e.g. Cooper et al., 2015), paleolimnological records (e.g. Charette and Prepas, 2003), or studies of marine systems which can be sampled at a safe distance (Kramer et al., 2020) or make use of remote satellite techniques (Li et al., 2021). Observed microbial responses are highly variable, influenced by factors such as pre-existing nutrient limitation, light availability, and the source and atmospheric lifetime of deposited material (Cropp et al., 2013). This variability underscores the need for controlled experimental approaches to disentangle the mechanisms driving microbial responses to wildfire aerosols. Given the central role of microbes in primary production, nutrient cycling, and overall ecosystem health, understanding these responses is critical for anticipating how aquatic environments may be altered under a changing, more fire-prone climate.

Prior to the 2019-20 Black Summer fires, knowledge of fire-driven aerosol impacts in Australia remained limited, with most research concentrated in the United States. Australian studies had historically focused on other dimensions of wildfire impact, including air quality and smoke exposure (He et al., 2016), plume composition and emissions (Howard et al., 2019; Isley and Taylor, 2020; Kristensen et al., 2014; Surawski et al., 2016; Wu et al., 2017), fire behaviour and climate-fuel dynamics (Bradstock, 2010; Clarke et al., 2016; Nolan et al., 2016; O'Donnell et al., 2011; Y. Zhang et al., 2017), fire management and mitigation strategies (Bearman et al., 2015;

Bradshaw et al., 2018; Enright and Fontaine, 2014; Kanowski et al., 2005; Volkova and Weston, 2019), terrestrial flora and fauna (Banks et al., 2011; Bowd et al., 2019; Keith et al., 2014; Lunn et al., 2018; Muñoz-Rojas et al., 2016), post-fire run-off, erosion and hydrology (Feikema et al., 2011; Heath et al., 2014; Lane et al., 2008; Nyman et al., 2011; Sheridan et al., 2007; Townsend and Douglas, 2000), physical water quality parameters (Chessman, 1986; Harrison et al., 2014; Smith et al., 2012), stream macroinvertebrates and fish (Robson et al., 2018; Schäfer et al., 2010; Stoessel et al., 2012), and the social, economic, and human health consequences of wildfire exposure (McFarlane and Van Hooff, 2009; Parslow et al., 2006; Price and Bradstock, 2013; Sherry et al., 2013; Stephenson et al., 2013). Only a small number of studies investigated impacts on aquatic microbes directly, including a 2003-2017 study along the Kimberley coast (Western Australian) which showed positive correlations between chlorophyll-a and black carbon – a marker for biomass burning (D. Liu et al., 2022), and a 2007 study in Gippsland Lakes (Victoria) which documented an unprecedented cyanobacterial bloom following local wildfires (Cook and Holland, 2012).

1.7 The 2019-20 Black Summer wildfires

Ignited in September of 2019, the 2019–20 “Black Summer” wildfires in Australia represent one of the most severe and far-reaching fire seasons in recorded history, offering a unique opportunity to deepen our understanding of the broader impacts of large wildfire events. In the lead up to the fire season, 2019 was Australia’s warmest and driest year on record (Bureau of Meteorology, 2019). Over 95% of the continent had a Forest Fire Danger Index (FFDI) in the top 10% for Spring, and ~60% featured recording-breaking FFDI values (Filkov et al., 2020). Under these extreme conditions, lightning was a major ignition source, responsible for ~75% of significant fires in NSW (Owens and O’Kane, 2020) and a conservative ~23% of ignitions across south-eastern Australia (Levin et al., 2021). Spanning five consecutive months, the fires burned across multiple states before being extinguished by rainfall in February 2020 (Boer et al., 2020; Bowman et al., 2020). During this time, approximately 30 million hectares - or ~20% of Australian forest - was burned, setting a global record for the largest burn area of high fire severity (Collins et al., 2021). The event generated unprecedented emissions in both volume and altitude, driven by a super-outbreak of 38 pyroconvective events that injected smoke to heights comparable to moderate volcanic eruptions, allowing plumes to circulate around the Southern Hemisphere for over a year (Hirsch and Koren, 2021; Peterson et al., 2021, 2018).

Current estimates indicate that up to 3 billion mammals, reptiles, birds and amphibians perished in the fires (WWF Australia, 2020), along with the destruction of thousands of homes and the loss of 33 human lives (Filkov et al., 2020). Furthermore, smoke exposure led to 417 deaths in humans and 4456 hospitalisations due to cardiovascular, respiratory and asthma-related issues (Borchers Arriagada et al., 2020). While these impacts on terrestrial systems and human health are increasingly well documented, there is comparatively little known about impacts of aerosol composition on aquatic environments.

Marine observations during the 2019-20 Black Summer fires revealed anomalous, widespread phytoplankton blooms in oceanic regions south of Australia, which was attributed to dry deposition of Fe from overhead smoke plumes (Li et al., 2021; Tang et al., 2021; Wang et al., 2022; Weis et al., 2022). One study examining this bloom in greater detail reported enhanced chlorophyll pigmentation, increased fluorescence-based photosynthetic efficiency, and shifts in community structure inferred from changes in cell size and shape, compared to pre-bloom phytoplankton (Weis et al., 2022). In estuaries, observations in benthic sediments before and after the 2019-20 fires revealed increased abundances of green algae and bacteria associated with effluent pollution, iron and sulfate reduction, and organic matter degradation, alongside a decrease in dinoflagellates, nematodes, and nitrifying bacteria (Bracewell et al., 2023). These changes were more pronounced in estuaries with burnt riparian vegetation, compared to those with intact vegetation buffers or systems in unburnt catchments (Bracewell et al., 2023).

While these aquatic studies offer valuable insight into microbial responses to extreme wildfire events, documented impacts on estuarine systems remain scarce - despite 30% of catchments along the New South Wales (NSW) coastline burning during the 2019-20 Black Summer fires (Fryirs et al., 2022). The south coast was the most severely affected, with 52% of both catchment area and stream length burned, peaking at 74% stream length in the Clyde catchment (Fryirs et al., 2022). Although estuaries in this region are considered relatively pristine by national standards, the extent of burning and aerosol exposure in the Clyde catchment underscores its importance for assessing fire impacts. Notably, the responses of planktonic microbes inhabiting the water column of estuaries have yet to be examined. Given the proximity of these fires to the coast, understanding their effects on estuarine microbial communities is imperative for effective management and forecasting – particularly in fire-prone regions like Australia.

1.8 Research aims and objectives

The preceding sections highlight several key gaps in knowledge that motivate the research presented in this thesis. Despite Australia's status as one of the most fire-prone nations on Earth, the physical and chemical properties of aged plumes located downwind of the emission source remain poorly constrained beyond individual elements like Fe (Section 1.5). Furthermore, while wildfire aerosols have been shown to influence aquatic microbial communities in marine and freshwater systems, estuarine responses remain largely unexamined – particularly for planktonic communities inhabiting the water column (Section 1.6). This gap is especially significant given that 30% of NSW coastal catchments burned during the 2019-20 Black Summer fires, yet no studies had investigated the effects of these emissions on estuarine microbial dynamics at the time (Section 1.7). Together, these gaps underscore the need for an interdisciplinary study that integrates atmospheric and aquatic microbial approaches to characterise wildfire-enriched aerosols and assess their ecological consequences for estuarine systems.

In this thesis, I aimed to characterise the bioactive properties of aged wildfire PM and determine its impact on planktonic estuarine microbial dynamics following dry deposition. The research focused on aged wildfire plumes sampled in Sydney, Australia during the 2019–20 Black Summer fires and on estuarine systems along the south coast of NSW, primarily in and around the Clyde catchment (see Figure 1.6B for estuary locations). An interdisciplinary approach was employed, integrating techniques from atmospheric science (Chapters 2 and 3) and aquatic microbial ecology (Chapters 4 and 5) to address this aim. As PM was sampled using HVAC filters, the collected material represents mixed-source rather than exclusively wildfire-derived particles, a limitation common to in situ aerosol sampling approaches not deployed at the emission source. However, source apportionment indicates that the composition was strongly influenced by fire emissions and fire-mobilised material, with aged wildfire smoke and associated soil-derived components together accounting for the majority of analysed mass. Accordingly, the material is described throughout this thesis as "wildfire-enriched" PM, and findings are interpreted within this context. The specific aims and objectives of each data chapter are outlined below.

In Chapter 2 – *Fine particle pollution during megafires contains potentially toxic elements* – I aimed to determine the physical and chemical attributes of aged wildfire PM in relation to its

potential toxicity to the biosphere, including aquatic and terrestrial environments, as well as human health. Using the novel approach of "filter forensics" (Figure 1.5), this chapter captures and characterises PM enriched by Black Summer fire emissions, analysing the size distribution of particulate filter extracts and the concentration and solubility of potentially toxic trace elements and ions listed in Australia's National Pollutant Inventory (NSW Department of Climate Change, Energy, the Environment, 2025). These assessments are supported by atmospheric concentration analyses and meteorological source attribution to evaluate the extent and likely sources of high PM exposure. To contextualise results, ambient urban PM was also sampled and analysed in the same way to enable comparisons.

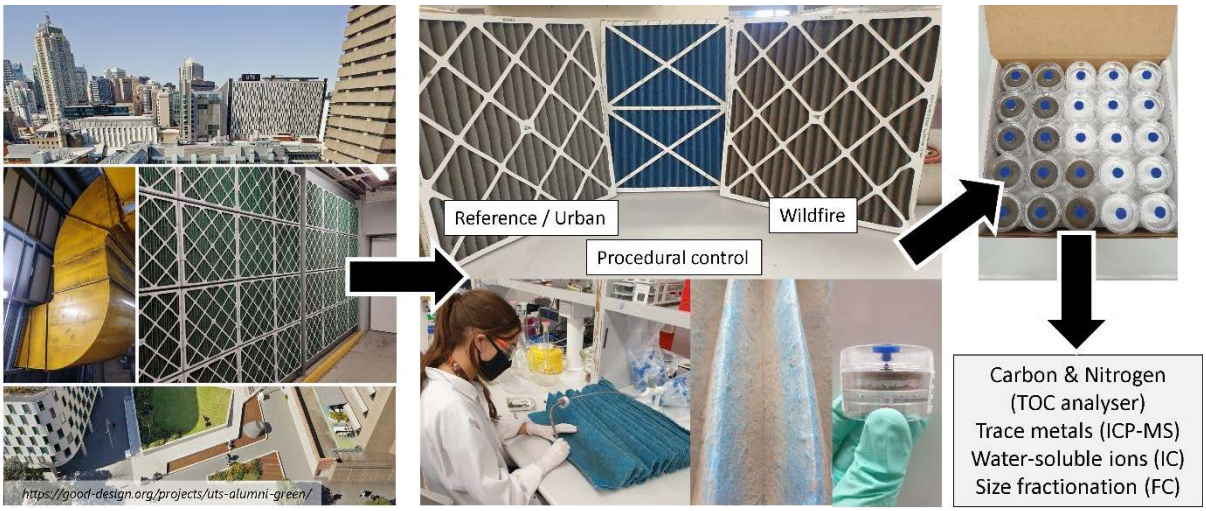


Figure 1.5 Schematic of the various stages of particle capture and extraction using the filter forensics approach. From left to right: HVAC filter room at particle capture site (University of Technology Sydney, Australia); unprocessed HVAC filters from different time points and the sample extraction process; subset of sample collected and major physical and chemical analyses for downstream processing to be conducted for Chapters 2 and 3.

In Chapter 3 – *Nutrient profile and sources of aerosols collected during intense wildfires in the Southern Hemisphere* – I aimed to determine the composition and sources of nutrients in aged wildfire PM relevant to aquatic and terrestrial ecosystems. Building on Chapter 2, this chapter examines the concentration and solubility of various macro- and micronutrients in PM enriched by Black Summer fire emissions and ambient urban PM. This analysis is supported by chemical source attribution to identify and partition the likely sources of aeolian nutrients.

16In Chapter 4 – *Acute exposure to wildfire-enriched aerosols elicits divergent microbial responses across multiple Australian estuaries* – I aimed to investigate the acute effects of aged wildfire PM on planktonic microbial populations across multiple estuary systems. In this chapter, natural microbial communities were collected from five south coast estuaries (Figure 1.6, coloured diamonds) and incubated for 24 hours with PM enriched by Black Summer fire emissions (from Chapters 2 and 3) under two deposition scenarios, examining changes in the abundance and/or physiology of viruses, bacteria and phytoplankton (Figure 1.7).



Figure 1.7 Series of images demonstrating the estuary sampling procedure employed for sample collection in Chapters 4 and 5 ("A") and map depicting locations of estuaries sampled in Chapter 4 (coloured diamonds) as well as location of PM sampling and air quality monitoring (black diamonds).

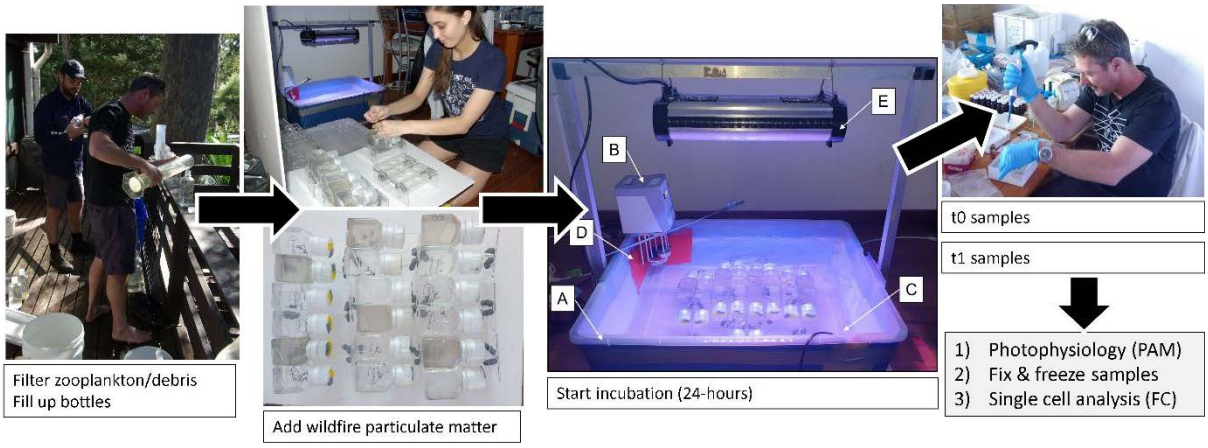


Figure 1.8 Schematic depicting an overview of the setup and procedure for incubation experiments in Chapter 4. From left to right: filtration of estuary water and filling of bottles; bottles dosed with PM enriched by Black Summer fire emissions in two deposition scenarios and secured; 24-hour incubation initiated in temperature- and light-controlled bath; initial samples taken and stored for measurement and downstream processing. This process was repeated for each estuary in Chapter 4.

In Chapter 5 – *Aerosols generated by extreme wildfires elicit dose- and time-dependent changes in estuarine microbial communities* – I aimed to examine longer-term responses of planktonic microbial communities to aged wildfire PM over varying doses in a single estuary. In this chapter, microbial communities were collected from the Clyde River (Figure 1.6, green diamond) and incubated for 5-10 days with PM enriched by Black Summer fire emissions under twelve continuous deposition scenarios, examining changes in cell abundance, physiology and community composition of viruses, bacteria and phytoplankton (Figure 1.8).

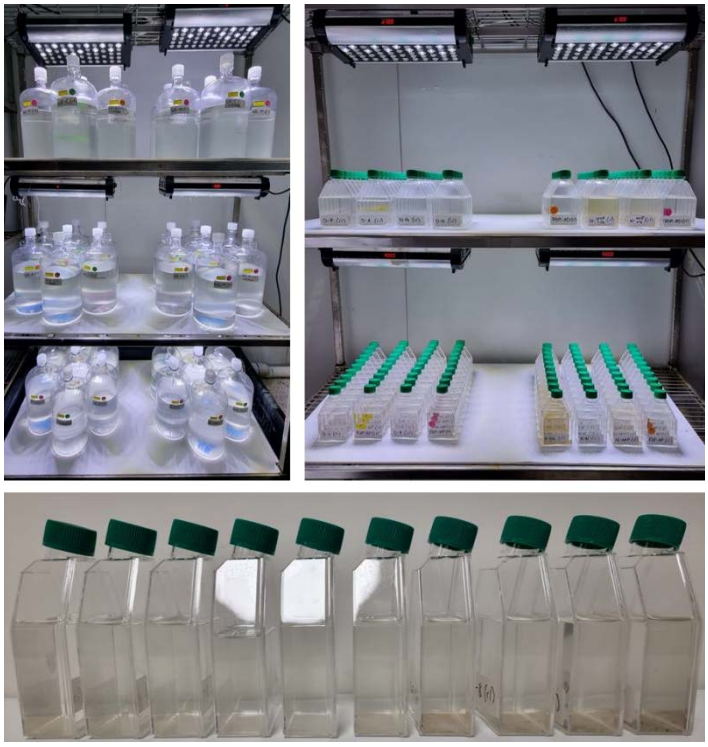


Figure 1.9 Series of images depicting the overall set up of incubation experiments in Chapter 5, including two continuous deposition scenarios running for 10-days in bottles (top-left image) and ten continuous scenarios running for 5-days in flasks (top-right image). Bottom image depicts the concentration gradient of PM enriched by Black Summer fire emissions added to vessels.

In my final chapter – *Summary and significance* – I briefly summarise the key findings and methodological considerations of this thesis before discussing its contributions to the field. I then explore its broader relevance by demonstrating how these insights on wildfire-enriched PM and estuarine microbes have been applied to historical datasets in collaboration with the NSW Government (Department of Climate Change, Energy, the Environment and Water). This collaboration aimed to better understand the effects of extreme wildfire events on estuarine water quality across NSW. The chapter concludes with a discussion of future research directions and final reflections.

2. Fine particle pollution during megafires contains potentially toxic elements

Raissa L Gill [a, b, #], Robert Fleck [b], Ky Chau [b], Mika T Westerhausen [c], Thomas Lockwood [c], Jake P Violi [d], Peter J Irga [e], Martina A Doblin [a, f], Fraser R Torpy [b]

[a] Productive Coasts, Climate Change Cluster, University of Technology Sydney, Ultimo, NSW, 2007, Australia

[b] Plants and Environmental Quality Research Group, School of Life Sciences, University of Technology Sydney, Ultimo, NSW, 2007, Australia

[c] School of Mathematical and Physical Sciences, University of Technology Sydney, Ultimo, NSW, 2007, Australia

[d] School of Chemistry, University of New South Wales, Kensington, NSW, 2033, Australia

[e] Plants and Environmental Quality Research Group, School of Civil and Environmental Engineering, University of Technology Sydney, Ultimo, NSW, 2007, Australia

[f] Sydney Institute of Marine Science, Mosman, NSW, 2088, Australia

[#] Corresponding Author: raissa.l.gill@student.uts.edu.au; PO Box 123 Ultimo, NSW, 2007, Australia

Chapter 2 is currently published in the *Journal of Environmental Pollution*, available at: https://doi.org/10.1016/j.envpol.2024.123306

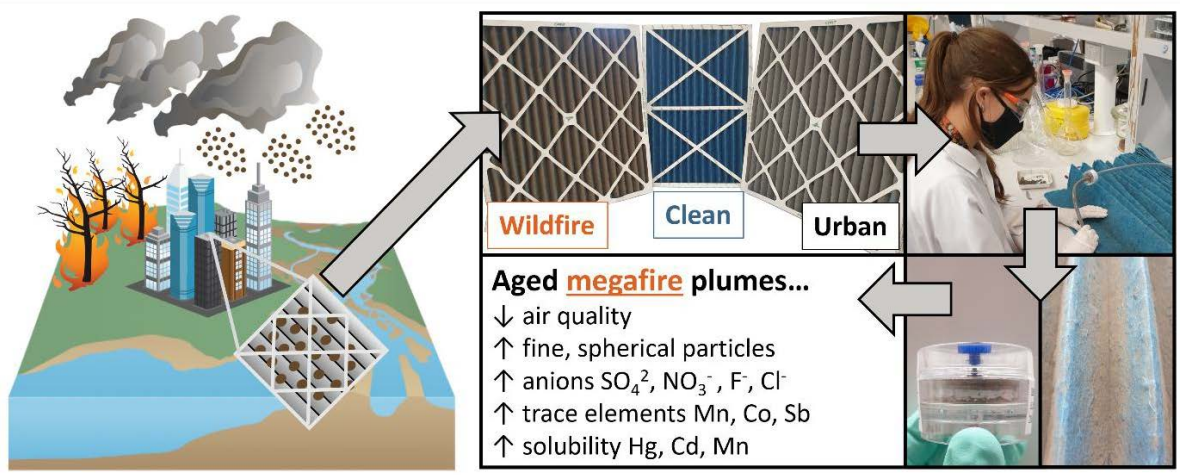
Highlights

- Black Summer wildfires increased particulate matter concentrations in Sydney.
- Aged wildfire particles were finer and more spherical than ambient urban particles.
- Wildfires were a major source of SO_4^{2-}, NO_3^- and F^- ions, and minor source of Cl^-.
- Smoke plumes were enriched with dissolved Mn and particulate forms of Mn, Co and Sb.
- Wildfires enhanced Hg solubility and extended the range for Hg, Cd and Mn solubility.

Abstract

Wildfires that raged across Australia during the 2019-2020 'Black Summer' produced an enormous quantity of particulate matter (PM) pollution, with plumes that cloaked many urban centres and ecosystems along the eastern Australian seaboard. This has motivated a need to understand the magnitude and nature of PM exposure, so that its impact on both built and natural environments can be more accurately assessed. Here we present the potentially toxic fingerprint of PM captured by building heating, ventilation, and air conditioning filters in Sydney, Australia during the peak of the Wildfires, and from ambient urban emissions one year later (Reference period). Atmospheric PM and meteorological monitoring data were also assessed to determine the magnitude and source of high PM exposure. The wildfires were a major source of PM pollution in Sydney, exceeding the national standards on 19 % of days between November-February. Wildfire particles were finer and more spherical compared to Reference PM, with count median diameters of 892.1 ± 23.1 versus 1484.8 ± 96.7 nm (mean ± standard error). On an equal-mass basis, differences in potentially toxic elements were predominantly due to higher SO_4^{2-}-S (median 20.4 vs 4.7 mg g^{-1}) and NO_3^--N (2.4 vs 1.2 mg g^{-1}) in Wildfire PM, and higher PO_4^{3-}-P (10.4 vs 1.4 mg/g) in Reference PM. Concentrations of remaining elements were similar or lower than Reference PM, except for enrichments to F^-, Cl^-, dissolved Mn, and particulate Mn, Co and Sb. Fractional solubilities of trace elements were similar or lower than Reference PM, except for enhanced Hg (12.1 vs 1.0 %) and greater variability in Cd, Hg and Mn solubility, which displayed upper quartiles exceeding that of Reference PM. These findings contribute to our understanding of human and ecosystem exposures to the toxic components of mixed smoke plumes, especially in regions downwind of the source.

Graphical abstract



Keywords

Aerosols; Air quality; Biomass burning; Filter forensics; Solubility; Source apportionment

Abbreviations

AHU = air handling unit
CMD = count median diameter
ESD = equivalent spherical diameter
FF = filter forensics
HVAC = heating, ventilation, and air conditioning
PM = particulate matter
$PM_{0.1}$ = ultra-fine particulate matter with aerodynamic diameter ≤0.1 μm
PM_1 = submicron particulate matter with aerodynamic diameter ≤1 μm, includes $PM_{0.1}$
$PM_{2.5}$ = fine particulate matter with aerodynamic diameter ≤2.5 μm, includes PM_1
PM_{10} = particulate matter with aerodynamic diameter ≤10 μm, includes $PM_{2.5}$
PM_{25} = particulate matter with aerodynamic diameter ≤25 μm, includes PM_{10}
PTE = potentially toxic element
TSP = total suspended particles

2.1 Introduction

Climate change is associated with conditions more favorable for wildfires in many locations by acting on drivers of heat and water availability in the atmosphere and terrestrial landscape (Aldersley et al., 2011; Pechony and Shindell, 2010). Increasing wildfire frequency and severity have already been observed in many regions, including the recent megafires in Australia, Brazil, California, and Russia (Bowman et al., 2020; Huang et al., 2015). Australia is acknowledged as the most fire-prone continent due to the high fuel load associated with its endemic eucalypt forests (Boer et al., 2020) and the propensity for fuel dryness, due to the continent's high solar radiation, low relative humidity, and prolonged drought periods (Nolan et al., 2016). During spells of hot, dry, and windy weather, these conditions enable wildfires (known locally as bushfires) to spread quickly across a highly flammable landscape. The 2019-2020 Black Summer Wildfires were an extreme instance, burning 30.4 Mha of land (Borchers Arriagada et al., 2020) with substantial impacts to both human (Borchers Arriagada et al., 2020; Johnston et al., 2021) and animal (Ward et al., 2020) morbidity and mortality. Furthermore, the vast quantity of particulate matter (PM) emitted into the atmosphere (Hirsch and Koren, 2021; van der Velde et al., 2021) can travel great distances downwind from active fire locations (Peterson et al., 2021), impacting humans and biota distant from the source.

During a wildfire, the primary route of PM exposure for humans is inhalation. Its toxicity in mammals is attributed to large quantities of deeply inhalable fine particulates ($PM_{2.5}$ - aerodynamic diameter ≤2.5 μm), the dominant size fraction of pyrogenic PM (Reid et al., 2005). This fraction not only penetrates the gas exchange region of the respiratory tract (Miller et al., 1979; Pinkerton et al., 2000), but the ultrafine portion ($PM_{0.1}$ - aerodynamic diameter ≤0.1 μm) can cross the alveolar-capillary membrane, where it circulates in the blood (Nemmar et al., 2002). Toxicity may act on cell viability, cell apoptosis, inflammation, oxidative stress, and genotoxicity (Dong et al., 2017), leading to adverse respiratory and cardiovascular health effects (Reid et al., 2016). Regional estimates during the 2019-2020 Black Summer attributed 417 mortalities and 4456 hospitalisations to wildfire PM exposure (Borchers Arriagada et al., 2020). While PM quantity and size are key causative factors for adverse health outcomes during wildfire, recent evidence suggests that wildfire $PM_{2.5}$ may be more toxic than equal doses of ambient $PM_{2.5}$ (Aguilera et al., 2021; Franzi et al., 2011; Wegesser et al., 2009). This is especially important for water-soluble

elements, as they possess higher bioavailability and may cause greater injury compared to their insoluble counterparts (Costa and Dreher, 1997).

Given the magnitude of PM pollution during the 2019-2020 Wildfires, there was also significant likelihood for ecotoxicological effects to occur upon the PM's deposition. Acidic compounds like sulfates and nitrates which are associated with secondary aerosol formation during transport (Akagi et al., 2011; Li et al., 2015) can reduce the calcium and dissolved organic carbon content of soils that lack sufficient buffering, leading to reduced plant growth and mortality (Battles et al., 2014; Monteith et al., 2007). In aquatic systems, the deposition of smoke-derived metals like copper (Sparks and Wagner, 2021) can have toxic effects on marine phytoplankton (Paytan et al., 2009), with implications for grazing and bioaccumulation in marine food webs. While nutrient enrichment has been observed in ocean waters surrounding Australia during wildfires (Li et al., 2021; Tang et al., 2021), deposition-induced ecotoxicity has been insufficiently studied, especially given that observations in both terrestrial and aquatic environments closer to the source of fires are very limited.

The highly unpredictable and dangerous nature of wildfires presents a unique set of challenges for collecting representative PM samples, so observations that capture the fingerprint of wildfire-influenced plumes are highly valuable for informing their potential impacts. Given the longevity and reach of megafire plumes like those observed during the 2019-2020 Black Summer (Peterson et al., 2021), examining aged PM that has undergone atmospheric processing and mixing is imperative due to its influence on particle size and composition (Kanakidou et al., 2005) as well as its relevance for human exposure in urban centres. Here we gathered a retrospective, four-month sample of PM in Sydney's Central Business District (CBD) immediately after the Black Summer Wildfires and from ambient urban emissions one year later for comparison. This study uniquely describes PM to which Australia's largest urban population was exposed during the 2019-2020 fires, as well as providing previously undocumented atmospheric concentration analyses, source apportionment, particle size distributions, and dissolved and particulate fractions of potentially toxic trace elements and ions (PTEs) listed in Australia's National Pollutant Inventory (NPI Australia, 2015). We anticipated that because of its mixed pyrogenic and urban origin, analysis of the PM fingerprint would reveal size distributions and elemental concentrations that deviated strongly from ambient urban emissions.

2.2 Material and methods

2.2.1 Study site

The study site (33.8832° S, 151.2005° E, University of Technology Sydney (UTS) Ultimo campus) is in Sydney's CBD, the most populated city in Australia (5.3 million in 2022) (Australian Bureau of Statistics, 2023). Sydney is situated in a low-lying basin between the eastern seaboard and large areas of sclerophyll forest, acting as a natural trap for fine PM pollution due to natural geographic and meteorological conditions that hold PM within the basin (Cohen et al., 2011). Sydney's climate is classified as temperate with no dry season and hot summers (Cfa Köppen-Geiger classification) (Beck et al., 2018). During the Summer months, local sources of fine particles are predominantly coal-burning power generation and diesel vehicles (50-70 %), as well as industrial sources (30-50 %) (Cohen et al., 2016a). Coarser particles include soil, sea-spray, and industrial activities (Cohen et al., 2016a).

2.2.2 Sample collection

Building heating, ventilation, and air conditioning (HVAC) filters were used to collect and extract PM arriving in Sydney's CBD during the peak of the Black Summer Wildfires (Mahdavi and Siegel, 2020). The strength of this approach is its ability to bulk-capture PM without a priori notice of catastrophic events such as wildfires and was used here to collect sufficient mass for both this study and ongoing experimentation. The analysis of HVAC-derived PM, known as filter forensics (FF), yields a spatially and temporally integrated sample that is indicative of exposure across a broader sampling region and period. This is advantageous when sampling densely concentrated plumes of variable source location or conditions, as these may provide a skewed snapshot of the aerosol(s) of interest. FF yields relatively similar trace element concentrations (Mahdavi et al., 2021) and size distributions for particles spanning 1-10 μm (Mahdavi et al., 2021; Mahdavi and Siegel, 2020), with limited evidence of ongoing chemical transformation on the filter surface after its deposition (Weschler and Nazaroff, 2010; Xu et al., 2015). For particles <1 μm, the limit of detection varies amongst studies, though sizes down to 0.45 μm have been achieved (Dev et al., 2022; Mahdavi et al., 2021; Mahdavi and Siegel, 2020; Stephens and Siegel, 2012). More information on the representativeness of FF sampling can be found in the Supplementary Material (Text 2.1).

Building HVAC filters were retrieved from two mechanically ventilated, adjoined buildings (Central Buildings 4 and 7), each featuring an independent centralised HVAC system with either south-west (CB4) or north-west (CB7) facing air intake ducts. Both buildings drew outdoor air into their respective air handling unit (AHU) through straight ducting, where it was filtered directly by one of several primary HVAC filters before being secondarily filtered for indoor circulation. Filters are replaced on a four-month rotation. HVAC filters from CB4 (n = 12) and CB7 (n = 9) AHUs were in service for 120 days during the peak of the Wildfires (1 November 2019 - 28 February 2020; Fig. S2.1A). Given that PM from the two buildings featured similar particle size distributions (two-sample z-test: p = 0.240) and chemical composition (PERMANOVA: p = 0.227; PERMDISP: p = 0.821), these samples were analysed collectively. HVAC filters were also retrieved one year later from Building 4 AHU (n = 12) as a Reference for ambient urban PM (2 November 2020 - 1 March 2021; Fig. S2.1B). Building HVAC operative settings were kept consistent between study periods and AHUs.

All filters were 594 × 594 mm Aeropleat III MERV 8 type (Camfil, Sweden) with a pleat depth of 44 mm (filter airflow rate: 3400 $m^3 h^{-1}$) and a clean-filter, minimum efficiency reporting value (MERV) of ≥70 % for $PM_{3\text{-}10}$ and ≥20 % for $PM_{1\text{-}3}$. In practice, runtime increases filtration efficiency whereby captured PM acts as a secondary layer for particle interception and impaction, increasing the effectiveness of $PM_{0.1\text{-}0.3}$ capture by up to 80 % (Alavy and Siegel, 2020; Hanley et al., 1994). To control for the extraction process, four unused filters of identical grade, material, and supplier were also sampled and analysed (Procedural control; Fig. S2.1C).

2.2.3 Sample extraction

PM was extracted from the filters using a similar methodology to Mahdavi and Siegel (2020). Briefly, a vacuum sampler was constructed by fitting polyvinyl tubing (8 mm) either side of a sealed cassette which housed a mixed cellulose ester filter (37 mm, pore size 0.8 µm) backed with a cellulose pad (ZEF728MCE; Zefon International, USA). One end of the sampler was encased with a 25 µm pre-screen (XTRECHT03; Allied Filter Fabrics, Australia) as an exclusionary mechanism for HVAC filter fibers and particles ≥25 µm. The other end was connected to a vacuum with an unobstructed inlet flow rate of 100 L min^{-1} (pressure -70 to -90 kPa). For each extraction, the HVAC filter mesh was removed from its frame with non-metal tools. Sealed cassettes were weighed prior to sampling using an analytical balance (A200S; Sartorius,

Germany) and fitted to the vacuum sampler. The head of the sampler was held flat against the filter mesh and vacuumed whilst moving horizontally across the filter pleats. This was repeated three times along each pleat to increase particle recovery. The sampler headpiece was periodically cleared of larger material to ensure unobstructed vacuum pressure, and the sealed cassette was changed when suction diminished. To avoid contamination between HVAC filters, the entire assembly (tubing, cassette, and pre-screen) was replaced between each filter. Extracted mass was calculated by subtracting the initial and post-collection weights of the sealed cassette under standardised conditions. PM analyses were conducted on a subset of extracted mass.

2.2.4 Sample processing

To prepare samples for analysis, loose PM within the cassettes was carefully transferred into sterile 50 mL centrifuge tubes (Falcon, USA) by rinsing three times with fresh Milli-Q water (18.2 Ω; Millipore, Germany). The filter paper containing embedded PM was placed in the tube using acid-washed plastic forceps. Tubes were then topped up to 50 mL with Milli-Q, sealed, shaken, and left for 20 min. To extract embedded PM from the cassette filters, the solutions were sonicated for 15 min. Pilots indicated that this was sufficient to remove the majority of mass without filter destruction, with only 4.2 ± 1.3 % mean ± standard deviation (sd) remaining in the filter (n = 9). Sonicated cassette filters were then transferred to a new centrifuge tube, and the remaining particulate material separated through centrifugation (23 °C for 15 min at 7.826 g) (Model 5404; Eppendorf AG, Germany). The liquid filtrate was carefully removed for dissolved analyses, leaving behind a firm pellet for the particulate fraction. The dissolved fraction was further filtered through a sterile, pre-flushed 0.22 µm pore size polyethersulfone membrane syringe filter (Millex-GP Filter; Millipore, Germany). Several aliquots of the dissolved and particulate fractions were set aside for downstream processing, with the cassette filter preserved for trace elements. Extracts were stored at -80 °C until analysis. Prior to analysing samples, particulate extracts were verified gravimetrically to account for potential particle losses during sample extraction, storage, and processing. Recoveries were 99.0 ± 4.6 % (mean ± sd) of initial post-extraction weights. Sample weights were adjusted accordingly prior to mass correction.

2.2.5 Airborne concentration and source analyses

Atmospheric PM and meteorological data recorded at the nearest air monitoring station (4 km away) in Rozelle (33.8658° S, 151.1625° E) were obtained from the NSW air quality monitoring network (Department of Planning and Environment, 2023; Riley et al., 2020). Hourly and daily-mean measurements spanning pre- to post-HVAC sampling (1 May 2019 - 1 May 2021) were retrieved for the following variables: $PM_{2.5}$, PM_{10}, wind direction, wind speed, temperature, relative humidity, rainfall, solar radiation. Rozelle and the HVAC sampling location are located 0.7-1 km away from high-density traffic at an elevation of 22 and 26.7 m respectively. Traffic count data recorded from the nearest sensor on Parramatta Road (#19065, 33.887417° S, 151.173325° E) were retrieved from the NSW Traffic Volume Viewer (Transport for NSW, 2023). Mean daily counts for each month during the Wildfire and Reference periods were obtained for both eastbound and westbound traffic. This station is located approximately 3 km away from both HVAC and Rozelle sites on the main arterial road that would influence traffic-related air pollution at these locations.

The importance of local versus remote sources of PM pollution were assessed using polar plots in the openair package (Carslaw and Ropkins, 2012) for R V4.2.1 (R Core Team, 2021). These were configured to a conditional probability function (CPF) set to national standards of 50 μg m^3 PM_{10} and 25 μg m^3 $PM_{2.5}$ (Department of the Environment and Heritage, 2005). This analysis partitions the probability of exceeding these concentrations by wind direction and speed and is indicative of the direction and proximity of source(s) contributing to local concentrations (Uria-Tellaetxe and Carslaw, 2014). This analysis was supplemented by Hybrid Single-Particle Lagrangian Integrated Trajectory (HYSPLIT) modelling using the NOAA Air Resources Laboratory web-based system (V5.2.0) (Rolph et al., 2017; Stein et al., 2015) to generate air mass back-trajectories and identify possible source regions. Initial air parcels were generated at 00:00 on the 1st of November 2019 (UTC). These were run backwards in time for 72 h each, with new trajectories released every 6 h across the 4-month wildfire sampling window. All air parcels arrived at the HVAC sampling location (33.8832° S, 151.2005° E) at an altitude 0.5 times the planetary boundary level (PBL) to ensure trajectories did not fall prematurely out of suspension. HYSPLIT was driven by 6-hourly meteorological data from NOAA's Global Forecast System (GFS) at a spatial resolution of 0.25° (approximately 25 km^2). Regions associated with national standard exceedances (>50 μg m^3 PM_{10} and >25 μg m^3 $PM_{2.5}$) were calculated using gridded percentile differences in the trajLevel function of the openair package (Carslaw and Ropkins, 2012) for R (R Core Team, 2021). To aid interpretations, confirmed fire locations recorded throughout the 2019-2020 Black Summer,

including single fires or the perimeters of burnt zones, were obtained from the National Indicative Aggregated Fire Extent Dataset (Department of Climate Change, Energy, 2020) and visualised in R (R Core Team, 2021) using the ggplot2 (Wickham, 2016), ggspatial (Dunnington, 2023), ozmaps (Sumner, 2021), sf (Pebesma, 2018), and shapefiles (Stabler, 2022) packages.

2.2.6 Particle size and morphology

Particle size analysis was conducted using a Cytoflex LX flow cytometer (C40321; Beckman Coulter, USA) operated using CytExpert software (V2.1; Beckman Coulter, USA). Samples were prepared by resuspending the particulate extracts in Milli-Q and combining with the dissolved fraction (1:1 ratio) following 10 min sonication. Samples were analysed after vortexing (30 s) to determine particle count and equivalent spherical diameters (ESD). Milli-Q blanks were run between each sample until events read <100 µL min^{-1}. Solutions were diluted 1:2 with Milli-Q and re-analysed if the abortion rate was ≥2.5 %. Particle aggregates were assessed by plotting FSC-H × FSC-A and checking for linear correspondence (deviation from linearity indicating aggregate presence; R^2 > 0.99). For calibration, six suspensions of non-fluorescent polystyrene microspheres (Flow Cytometry Size Calibration Kit; Thermofisher, USA) of known diameters (1-15 µm) were prepared as above in Milli-Q (linear calibration of FSC-A × SSC-A: R^2 > 0.99). All data were processed in FlowJo software (V10.8.1; BD, USA). Specific instrument parameters and settings can be found in the Supplementary Material (Table 2.1).

To examine particle morphology, composite samples from three individual cassettes (1:1:1 mass ratio) were imaged using a field emission scanning electron microscope (SEM) with the GEMINI column (Supra 55VP; Carl Zeiss, Germany). Images were taken at a 5 kV accelerating voltage to improve imaging of fine carbonaceous particles, at 100-500× magnification.

2.2.7 Potentially toxic elements

Major ion analyses were performed on a subset of the Wildfire and Reference sample extracts using high-pressure ion chromatography (Integrion HPIC; Thermofisher, Australia). Dissolved sample aliquots were diluted 1:10 to 1:50 with Milli-Q to avoid swamping the chromatograph. The mass concentrations of the following PTEs (and Na+) were determined: Cl^-, F^-, Na^+, NH_4^+-N, NO_2^-

-N, NO_3^--N, PO_4^{3-}-P, SO_4^{2-}-S. Six-point calibration curves (0.01-20 ppm) were prepared from mixed single element standards (TraceCERT; Sigma-Aldrich, Australia) in Milli-Q.

Trace element (TE) analysis was performed on dissolved, particulate and filter extracts using solution nebulization inductively coupled plasma mass spectrometry (SN ICP-MS; 7700x series; Agilent, Australia). Particulate and filter samples were vacuum dried overnight, then digested in 1:1 69 % HNO_3/34 % HCl and made to volume with Milli-Q. Dissolved samples were digested in 3 % HNO_3/1 % HCl. Samples were diluted 1:100 to 1:3000 with Milli-Q before running on SN-ICP-MS to ensure they fell within calibration. The mass concentrations of the following PTEs were determined: As, B, Be, Cd, Co, Cr, Cu, Hg, Mn, Ni, Pb, Sb, Se and Zn. Calibration points spanned twelve concentrations (0-5 ppm) and was prepared from a 68-elemental standard (ICP-MS68A-500; Choice Analytical, Australia) in a mixture of 2 % HNO_3/1 % HCl (Seastar Baseline®; Choice Analytical, Australia). An online internal standard of 100 ppb Rhodium solution in 2 % HNO_3/1 % HCl was used to normalise matrix effects.

Quality control involved running blanks, duplicate PM samples (n = 3), mixed calibration standards and/or Certified Reference Material (NCS DC 73016a and NCS ZC 71008; NCS Testing Technology Co, China) every 15-25 reads. Blanks read low and stable (ions <0.05 ppm and TEs <10 ppb), duplicate variance was within ±5 (ions) or ±10 (TEs) %, and recoveries were within 94-111 % of expected values for all PTEs listed, except B and Se (excluded from further analysis). Specific HPIC and SN ICP-MS parameters can be found in the Supplementary Material (Tables 2.2 and 2.3).

2.2.8 Data analysis

For airborne analyses, differences in PM concentration and meteorology between the two study periods were assessed separately by Permutational Analysis of Variance (PERMANOVA) on a Euclidean distance matrix with 999 permutations. Daily mean traffic counts across all months/directions spanning the two study periods were assessed by Analysis of Variance (ANOVA). The proportion of $PM_{2.5}$ mass within PM_{10} was calculated from daily mean mass

concentrations (μg m^3) for both study periods and expressed as a percentage. Comparisons were performed using PERMANOVA.

For size analyses, overall differences in the particle number distributions between the two periods were assessed by a two-sample z-test. Individual particles of varying ESDs were allocated to the appropriate size fraction (<PM_{10}, $PM_{2.5-10}$ <$PM_{2.5}$, <PM_1, $PM_{0.1-1}$, <$PM_{0.1}$), standardised to analysed sample mass, and used to calculate the proportion of particles falling within various size fractions. The latter was calculated from binned particle counts standardised to PM mass (number of particles per μg) and is expressed as a percentage for both study periods. Count median diameters (CMD) were calculated as the median ESD of particles within a given size fraction. Individual PERMANOVAs were used for size metric comparisons.

For chemical analyses, procedural control data were first subtracted from concentrations of both study periods to remove contributions from the extraction process. Given that PM extractions from the HVAC filter mesh were not 100 % efficient, and we did not have the means to quantify infiltration rate through the building envelope, PTE concentrations were standardised by analysed PM mass (μg g^{-1} PTE in PM) as opposed to air volume and pollutant loading (μg m^3 PTE in air). The fractional solubility of each trace element was expressed as a percentage of analysed sample mass. To assess differences in the overall chemical composition between the two study periods, the concentration matrix comprised of all PTEs were compared by PERMANOVA and Permutational Multivariate Analysis of Dispersion (PERMDISP - analogous to Levene's test for equality of variance). Elements that contributed the most to these differences were then identified by the magnitude of vectors in Principal Components Analysis (PCA), which was calculated based on Euclidean distance of the standardised concentration matrix (μg g^{-1} PTE in PM) and visualised on a -1 to 1 biplot. Compositional data were summarised by medians and lower/upper quartiles (q1-q3) as many elements had skewed distributions. Individual differences for each PTE were tested by PERMANOVA and PERMDISP as appropriate. Pearson correlations between Na^+ and Pb were used to assess potential associations with sea salt and anthropogenic sources, respectively.

All data analysis and visualization were performed in R (R Core Team, 2022) using the following packages: BDSA (Arnholt and Evans, 2021), dplyr (Wickham et al., 2021), ggplot2 (Wickham, 2016), ggpubr (Kassambara, 2020), and vegan (Oksanen et al., 2022).

2.3 Results and discussion

2.3.1 Particle pollution in Sydney's CBD during the Black Summer Wildfires

Throughout the 2019-2020 Black Summer, wildfires burned across the entire continent, including locations to the north, south and west of Sydney's CBD (Fig. 2.1A). The fires emitted burnt vegetation, smoke, and surface soil entrained during pyro-convection into the atmosphere (Gaudichet et al., 1995; Wagner et al., 2018); these PM-rich plumes were then carried by winds to Sydney, mixing with urban particles and impacting the air quality of Australia's largest human population.

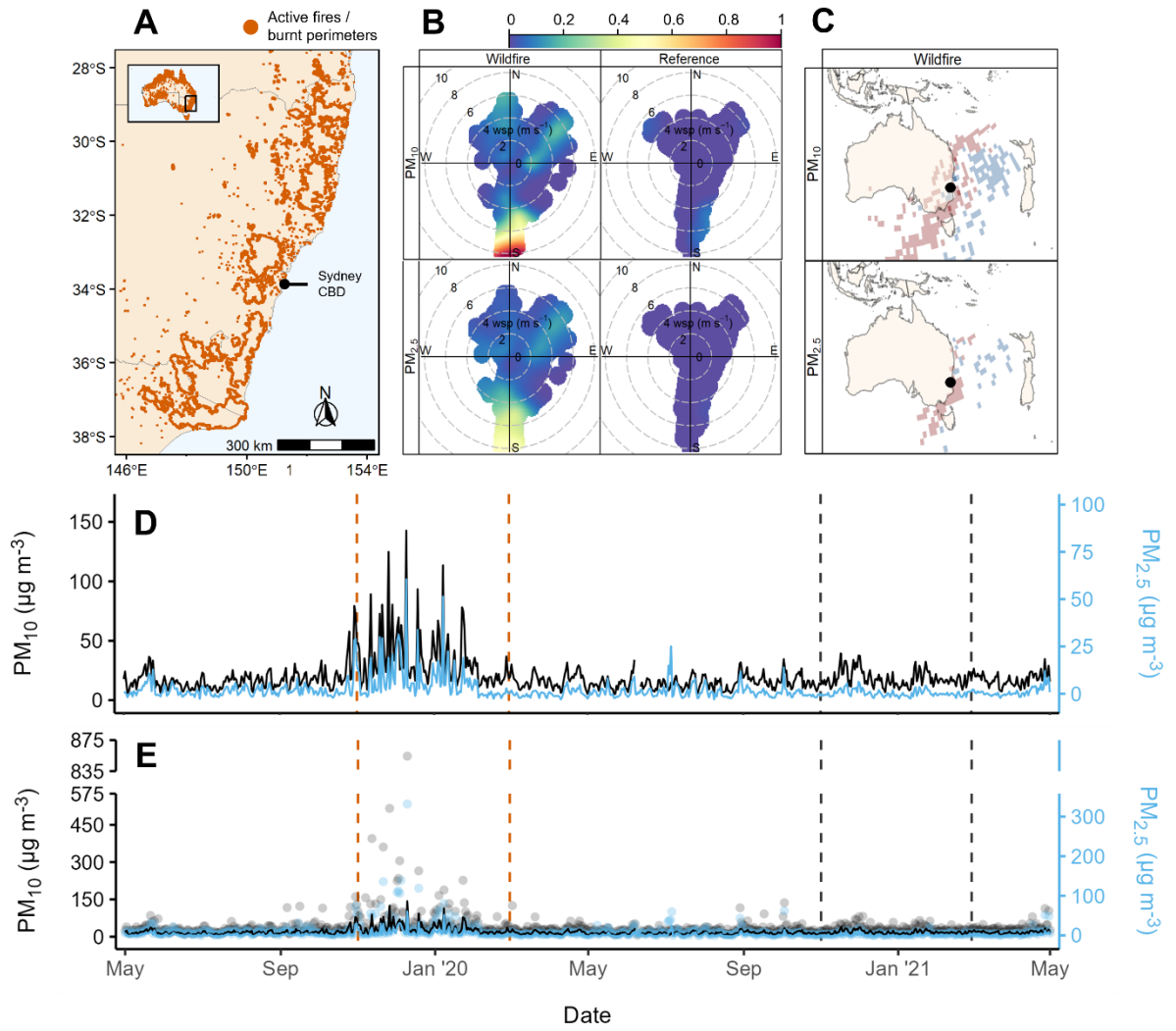


Figure 2.1 Airborne concentration and source analysis of PM pollution in Sydney's CBD during the 2019-2020 Black Summer Wildfires and 2020-2021 Reference period. A) depicts location of HVAC sampling relative to confirmed fire cases (orange points as single fires or perimeters of burnt zones); B) polar plots for the two study periods (Wildfire and Reference) by pollutant (PM_{10} and $PM_{2.5}$), where colour denotes the probability of exceeding hourly concentrations of 50 µg m^3 PM_{10} and 25 µg m^3 $PM_{2.5}$ by wind direction and wind speed; C) regional back-trajectory analysis of Wildfire period depicting origin of air-masses associated with exceeding 50 µg m^3 PM_{10} and 25 µg m^3 $PM_{2.5}$ (red/blue regions indicate highest/lowest probabilities); D) daily mean concentration of PM_{10} (black) and $PM_{2.5}$ (blue); E) daily mean (solid line) and hourly maximum (point) concentrations. Dashed lines on D) and E) depict periods of Wildfire (orange) and Reference (black) HVAC sampling (n = 120 days).

Daily PM concentrations at the Rozelle monitoring station, located 4 km away from the HVAC units where PM was sampled, exceeded the national standards (50/25 µg m^3 PM_{10} $PM_{2.5}$) (Department of the Environment and Heritage, 2005) on 19 % of days over the four-month sampling period. Exceedances occurred most frequently during higher velocity (6-8 m s^{-1}) south-westerly winds (Fig. 2.1B), indicating that a substantial portion of particles in the Wildfire

samples were attributable to remote sources, rather than local anthropogenic sources. Regional air-mass trajectories suggest that these PM-rich plumes originated from fires south/south-west of Sydney along the eastern and south-eastern coastline, especially the $PM_{2.5}$ fraction (Fig. 2.1C). There was evidence for a secondary region located north/north-east of Sydney that contributed mostly to elevated concentrations of PM_{10} (Fig. 2.1C). However polar plot analyses indicate that this source was relatively minor (Fig. 2.1B). These results are consistent with documented fire cases presented here (Fig. 2.1A) and by Li et al. (2021), with smoke plumes cloaking the east and south-eastern coastline and extending across the Tasman Sea (Li et al., 2021).

Generally, over the four-month Wildfire period, daily concentrations of PM_{10} and $PM_{2.5}$ were 34.4 ± 2.2 and 16.6 ± 1.5 µg m^3 respectively (mean ± standard error (se); Fig. 2.1D), with maximum hourly concentrations of up to 854.3 (PM_{10}) and 533.5 ($PM_{2.5}$) µg m^3 (Fig. 2.1E). During non-wildfire Reference conditions, daily concentrations were 2-3 times lower ($p = 0.001$) at 18.3 ± 0.6 µg m^3 PM_{10} and 6.0 ± 0.3 µg m^3 $PM_{2.5}$ (Fig. 2.1D). While occasional spikes of up to 81.8 µg m^3 occurred (Fig. 2.1E), these concentrations were not sustained over any 24-h mean period. Fine particles during the Wildfire period comprised 38.1 % (median, q1-q3 31.9-50.0) of airborne PM_{10} mass. This was elevated compared to Reference conditions (32.1 %, 27.9-35.7; $p = 0.001$) and the equivalent months before (2018-2019: 33.8 %, 33.0-35.1; $p = 0.014$) and after (2021-2022: 31.0 %, 30.9-31.5; $p = 0.001$) this study, demonstrating that the 2019-2020 plumes were especially enriched with fine, hazardous particles.

Given the HVAC units collected distant and proximate sources of particulates, the Wildfire PM captured and analysed in this study is likely of mixed pyrogenic and urban origin. This is supported by an ensemble of meteorological variables ($p > 0.05$; Fig. S2.2) and traffic counts ($p = 0.342$; Table S2.4), which indicate that there was no significant change in local conditions between study periods (see Figure 2.2 and Table 2.4 in the Supplementary Material).

2.3.2 Impact of wildfires on particle size and morphology

While most particles recovered were within the PM_{10} size fraction for both study periods (>95 %; Table 2.1), the size distribution of Wildfire samples were significantly finer than the Reference

period (p = 0.001; Fig. 2.2), with lower CMDs and a higher proportion of $PM_{2.5}$ (p = 0.001; Table 2.1). Approximately 83 % of Wildfire particles were within the $PM_{2.5}$ fraction, compared to only 67 % in the Reference period. These samples featured CMDs of 892.1 ± 23.1 and 1484.8 ± 96.7 nm, respectively. Given that both biomass and fossil fuel combustion emit fine particles (Reid et al., 2005; Sparks and Wagner, 2021; Wu and Boor, 2021), this increase in $PM_{2.5}$ may be a result of Sydney's distance from the fires (Fig. 2.1A), with coarser particles settling out faster than fine PM along the smoke plumes' trajectory (Arimoto et al., 1997). Alternatively, prolonged exposure to heavily polluted air could have differentially enhanced the fine PM trapping efficiency of the Wildfire HVAC filters, generating a stronger clogging effect compared to the less polluted Reference filters. This potential effect was analysed independently and found to be negligible (Supplementary Material, Text 2.2), and thus the differences found here between the two study periods remain valid.

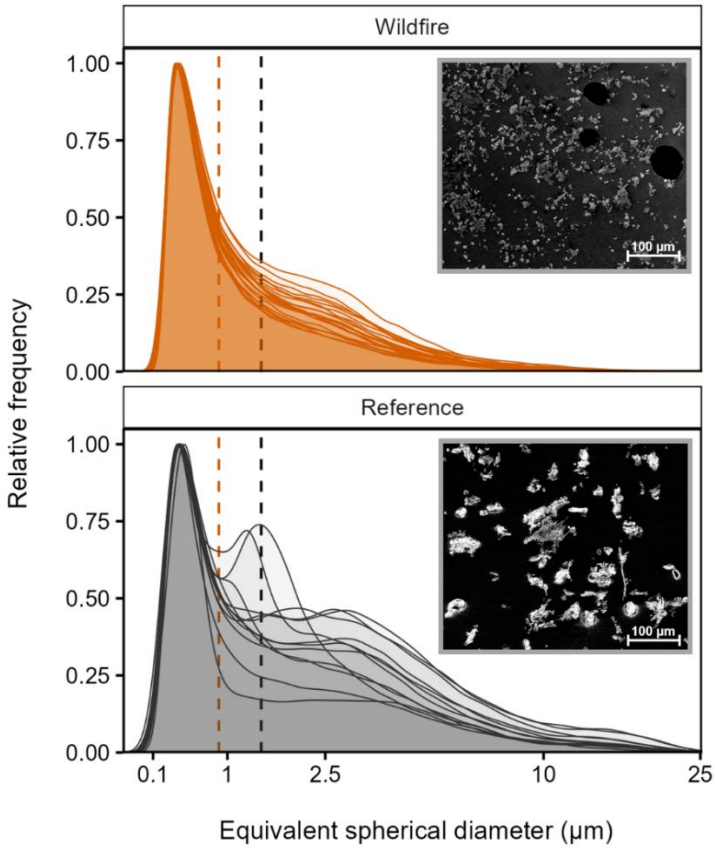


Figure 2.2 Particle number size distributions of Wildfire (n = 21) and Reference (n = 12) PM. Individual solid lines depict replicates, where dashed lines denote the mean count median diameters for the Wildfire (orange) and Reference (black) periods. SEM images show the size and morphology of PM sample composites. Overall size distributions differed significantly between study periods (two-sample z-test: p = 0.001). Wildfire filters collected from the two buildings did not differ (two-sample z-test: p = 0.240).

Table 2.1 Particle size metrics of Wildfire (n = 21) and Reference (n = 12) PM (mean ± se). Significant PERMANOVA ($P_{(p\text{-}aov)}$) comparisons are denoted by stars (***p ⩽ 0.001; **p ⩽ 0.01; *p < 0.05), where ns indicates non-significant (p > 0.05). Bold values denote finer particle metrics.

Metric	Wildfire	Reference	$P_{(p\text{-}aov)}$
Proportion of particle number by size fraction (%)			
$PM_{0.1}$	0.0 ± 0.0	0.0 ± 0.0	ns
$PM_{0.1\text{-}1}$	**54.6 ± 1.0**	39.1 ± 1.8	***
PM_1	**54.6 ± 1.0**	39.1 ± 1.8	***
$PM_{2.5}$	**83.0 ± 0.7**	66.9 ± 1.8	***
PM_{10}	**99.5 ± 0.1**	96.8 ± 0.4	***
Count median diameter by size fraction (nm)			
$CMD_{0.1}$	78.0 ± 7.4	58.2 ± 8.6	ns
$CMD_{0.1\text{-}1}$	511.2 ± 2.7	**494.9 ± 5.7**	**
CMD_1	511.2 ± 2.7	**494.9 ± 5.7**	**
$CMD_{2.5}$	**712.2 ± 10.6**	819.4 ± 39.9	**
CMD_{10}	**886.0 ± 22.9**	1403.4 ± 87.8	***
CMD	**892.1 ± 23.1**	1484.8 ± 96.7	***

Previous observations indicate that wildfire PM consists mainly of $PM_{0.1\text{-}1}$, with log-normal number size distributions and finer particles relative to ambient conditions (Alonso-Blanco et al., 2012; Okoshi et al., 2014; Reid et al., 2005; Sparks and Wagner, 2021). Wildfire PM in this study was also log-normally distributed (Fig. 2.2) and featured a higher proportion of $PM_{0.1\text{-}1}$ than the Reference samples (p = 0.001; Table 2.1). However, the CMDs observed for this fraction ($CMD_{0.1\text{-}1}$) were larger than previous aged wildfire smoke observations (511 vs 120-340 nm; Table 2.1) (Alonso-Blanco et al., 2012; Okoshi et al., 2014; Reid et al., 2005). Furthermore, while particles as small as 21.5 nm were detected by flow cytometry (confirmed by SEM), the abundance of ultrafine PM was extremely rare in both study periods (up to 0.002 %; Table 2.1). Electron microscopy detected finer and more spherical particles during the Wildfire period (Fig. 2.2). Observations of residential MERV11 filters during a smoke episode showed particle morphology and chemistry similar to wildfire-generated tar balls (Sparks and Wagner, 2021). Enhanced sphericity is consistent with the photochemical aging of smoke plumes, where processes such as coating by secondary aerosols and gas-to-particle conversion produce more physically rounded particles compared with fresh emissions (Giordano et al., 2015; Pósfai et al., 2003; Ruellan, 1999).

There are many possible reasons for the differences observed in particle sizes between wildfire studies, such as: concentration-enhanced coagulation of particles during atmospheric transport (especially given that emissions were record-breaking) (Hirsch and Koren, 2021); greater contributions from coarse mineral particles entrained during strong wildfire-driven winds and thunderstorms (Peterson et al., 2021, 2018); and <1 µm particle losses due to constraints of the FF approach. The latter may include: fine PM passing through the HVAC filter; agglomeration of fine PM to coarser particles during dust cake formation or within the 25 µm pre-screen; and strong particle-to-surface forces preventing retrieval of fine PM from the filter mesh (Mahdavi et al., 2021; Mahdavi and Siegel, 2020). Existing observations during the 2019-2020 Wildfires in Tumbarumba, Australia (464 km south-west of HVAC sampling site) found median particle diameters of 280-500 nm associated with PM_{10} in smoke (Li et al., 2021). Given the above, it is likely that constraints of the FF approach prevented the retrieval of a portion of particles in the PM_1 fraction, though to what extent is unknown. Nonetheless, the relative impact of the Wildfires on particle size relative to the Reference period remained evident.

2.3.3 Potentially toxic elements: chemical composition and solubility

The potentially toxic fingerprint of Wildfire PM was distinct compared to the Reference period, varying in both the centre ($p = 0.001$) and spread ($p = 0.026$) of clusters in the PCA (Fig. 2.3). Broadly, Wildfire PM was characterised by higher concentrations of acidic ions, including SO_4^{2-}-S and NO_3^--N ($p = 0.001$; Fig. 2.3 and Table 2.2). Both study periods displayed varying concentrations of Cl^- and Na^+ (Fig. 2.3), though concentrations were higher in Wildfire samples ($p = 0.001$; Table 2.2). During Reference conditions, Cl^- displayed strong associations with NO_3^--N ($r = 0.99$), Na^+ (0.98) and SO_4^{2-}-S (0.92), indicative of aged sea salt (Zhang and Chan, 2023) from adjacent waters (Fig. 2.1A). However, the disparity between vector positions in the PCA indicates that Na^+ did not solely explain the variation in Cl^- (Fig. 2.3), with weaker (but still strong) associations in Wildfire PM ($r = 0.92$ vs 0.98). Further, Cl^- displayed low-moderate correlations with SO_4^{2-}-S (0.41 vs 0.92) and NO_3^--N (0.13 vs 0.99), indicating little association with aged sea salt.

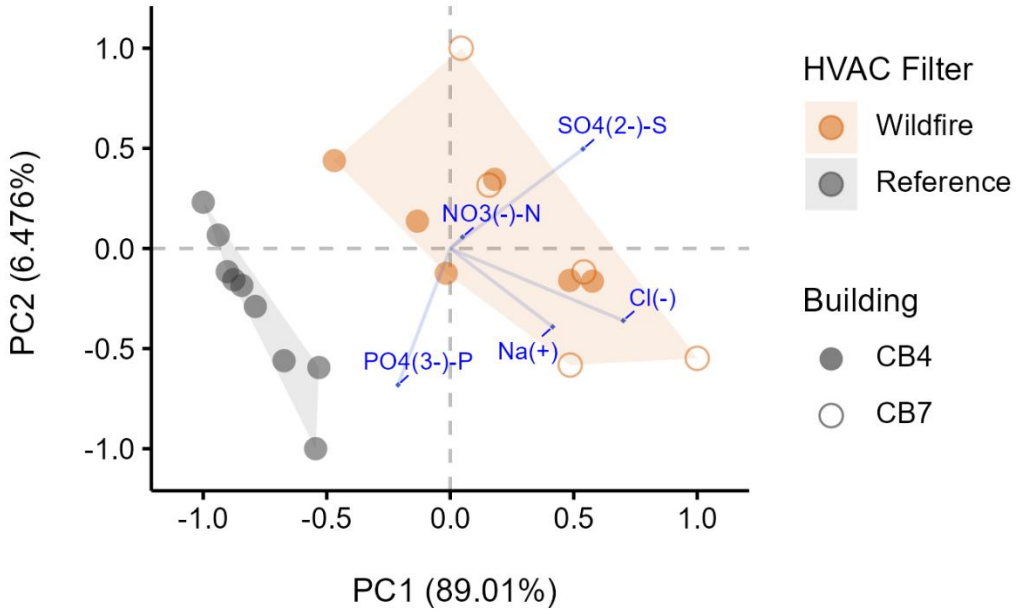


Figure 2.3 Principal Components Analysis (PCA) biplot depicting differences in the potentially toxic fingerprint of Wildfire (orange, n = 12) and Reference (black, n = 9) PM. Points closer together have more similar mass composition and vice versa. Blue vectors represent the direction and magnitude of elements driving the greatest differences amongst samples. Study periods differed significantly in both the centre (PERMANOVA: p = 0.001) and spread (PERMDISP: p = 0.026) of PCA clusters. Wildfire filters collected from the two buildings (closed/open circles) did not differ (PERMANOVA: p = 0.227; PERMDISP: p = 0.821).

Table 2.2 Potentially toxic ions (and Na^+) in Wildfire (n = 12) and Reference (n = 9) PM (median, q1-q3). Significant differences between periods (PERMANOVA ($P_{(p\text{-}aov)}$) are denoted by stars (***p ⩽ 0.001; **p ⩽ 0.01; *p < 0.05), where ns indicates non-significant (p > 0.05). Bold values denote higher median concentrations (mg/g or µg/g). LOD = limit of detection.

	Wildfire	**Reference**	**$P_{(p\text{-}aov)}$**
mg/g			
Cl^-	**34.7 (30.5-45.5)**	15.8 (15-3-21.1)	***
Na^+	**24.5 (21.9-31.9)**	11.5 (8.8-15.5)	***
NO_3^--N	**2.4 (2.3-4.1)**	1.2 (1.0-1.6)	***
PO_4^{3-}-P	1.4 (0.7-5.5)	**10.4 (9.9-12.4)**	***
SO_4^{2-}-S	**20.4 (15.6-28.5)**	4.7 (4.1-6.2)	***
µg/g			
F^-	**334.9 (230.3-384.8)**	<LOD	***
NH_4^+-N	0.0 (0.0-216.3)	**466.2 (0.0-478.5)**	*
NO_2^--N	0.0 (0.0-13.6)	**19.2 (16.1-21.7)**	*

Compared with ambient emissions, these results suggest an alternative source of SO_4^{2-}-S and NO_3^--N during the fires, and an additional, minor source of Cl^-. This is consistent with observations during the 2019-2020 Black Summer, which document chlorine perturbations due to oxidized organics and sulfates (Bernath et al., 2022; Solomon et al., 2023) and nitrate-enriched smoke (Perron et al., 2022; Simmons et al., 2022). Furthermore, it is well established that Cl, NO_x and SO_2 are gaseous species formed during combustion (Akagi et al., 2011; Benedict et al., 2017), and that the aging of particles during transport serves to increase inorganics through secondary aerosol production (Akagi et al., 2011; Li et al., 2015; Pósfai et al., 2003). These species tend to be ubiquitous wildfire by-products across the globe, including in Canada, south-east Asia, and the United States (Adam et al., 2021; Harper et al., 2019). In contrast, PM captured during the Reference period was enriched with PO4(3-)-P ($p = 0.001$; Fig. 2.3 and Table 2.2), likely due to greater contributions from fossil fuel combustion (Wang et al., 2015). By mass, these three PTEs (SO_4^{2-}-S, PO_4^{3-}-P, NO_3^--N) were the major drivers of variation between the two study periods given their orthogonal positioning relative to clusters in the PCA (Fig. 2.3). This is consistent with historical observations in Western Australia, where oxalate, nitrate and sulfate were the most reliable tracers for biomass burning in 2015-2018 (Strzelec et al., 2020a). The first two principal components explained 95.5 % of the variability amongst samples, indicating that these differences were well represented. The remaining PTEs were generally less abundant with lower mass contributions to the PCA (<5 %), however many exhibited significant shifts between the two study periods (Table 2.2, Table 2.3).

Table 2.3 Potentially toxic trace elements in Wildfire (n = 12) and Reference (n = 9) PM (median, q1-q3). Significant PERMANOVA ($P_{(p\text{-}aov)}$) and PERMDISP ($P_{(p\text{-}disp)}$) comparisons are denoted by stars (***p ⩽ 0.001; **p ⩽ 0.01; *p < 0.05), where ns indicates non-significant (p > 0.05). Bold values denote higher median concentrations (µg/g) / solubilities (%) and wider quartile ranges (solubility only). LOD = limit of detection.

	Dissolved			**Particulate**			**Solubility**			
	Wildfire	**Reference**	**$P_{(p\text{-}aov)}$**	**Wildfire**	**Reference**	**$P_{(p\text{-}aov)}$**	**Wildfire**	**Reference**	**$P_{(p\text{-}aov)}$**	**$P_{(p\text{-}disp)}$**
	µg/g						%			
As	<LOD	<LOD	ns	<LOD	<LOD	ns	<LOD	<LOD	ns	ns
Be	<LOD	<LOD	ns	<LOD	<LOD	ns	<LOD	<LOD	ns	ns
Cd	0.1 (0-0.1)	0.2 (0.1-0.2)	ns	0.3 (0.2-0.4)	**1.7** (1.5-2.2)	***	17.2 **(5.4-25.4)**	6.5 (4.3-8.0)	ns	**
Co	1.2 (0.9-1.6)	1.2 (1.1-1.5)	ns	**13.6** (13.0-16.4)	7.9 (7.0-8.8)	***	7.0 (5.3-10.3)	**13.3** (12.2-15.0)	**	ns
Cr	0 (0-0)	0 (0-0)	ns	119.6 (93.0-135.6)	147.6 (108.7-160.2)	ns	0 (0-0)	0 (0-0)	ns	ns
Cu	39.8 (27.5-47.9)	**83.7** (80-100.9)	***	775.7 (593.9-1011.3)	742.5 (653.9-772.8)	ns	5.2 (3.6-5.7)	**10.1** (9.4-12.0)	***	ns
Hg	7.2 (2.9-13.5)	13.2 (7.6-25.6)	ns	45.8 (33.3-75.7)	**848.6** (243.4-1132.1)	***	**12.2 (4.7-25.5)**	1.0 (0.8-10.1)	*	*
Mn	**108.0** (85.5-163.8)	28.6 (27.8-31.8)	***	**870.3** (719.7-986.5)	303.4 (290.1-349.3)	***	10.1 **(8.2-18.2)**	8.5 (7.7-9.0)	ns	*
Ni	3.4 (2.9-5.9)	**38.1** (33.9-42.2)	***	63.9 (52.1-70.8)	**222.9** (139.3-237.8)	***	5.8 (4.8-8.2)	**15.7** (12.8-19.6)	***	ns
Pb	0.1 (0.1-0.3)	**0.4** (0.4-0.5)	**	68.2 (59.0-80.5)	**129.6** (120.8-143.2)	**	0.2 (0.1-0.4)	0.3 (0.3-0.4)	ns	ns
Sb	1.7 (1.2-3.2)	2.7 (2.5-2.9)	ns	**64.1** (50.0-90.1)	17.4 (15.7-29.5)	***	2.7 (2.0-4.4)	**12.7 (9.3-15.6)**	***	***
Zn	199.8 (123.8-479.2)	283.8 (163.8-293.9)	ns	3699.4 (2618.6-3944.6)	3734.7 (3495.0-3795.2)	ns	4.2 (3.2-13.3)	7.1 (4.2-8.7)	ns	ns

Interestingly, Wildfire PM contained substantially more F^- than Reference samples ($p = 0.001$; Table 2.2). The primary source of F^- emissions in Australia tend to be industrial (NPI Australia, 2015), however recent evaluations have shown global biomass burning to be a major source of F-containing particles, comparable to and often exceeding that of coal combustion and other anthropogenic sources (Jayarathne et al., 2014). While F^- was not targeted in other Black Summer monitoring, increases in F^- concentration have been related to distal fires east and north-west of Poland (Lewandowska et al., 2013). Reports of NH_4^+ demonstrated 1.7-fold enrichment (Perron et al., 2022) and significant correlations ($R^2 = 0.87$) with Carbon Monoxide (biomass burning tracer) (Simmons et al., 2022). Comparatively, we detected almost no NH_4^+-N and little NO_2^--N (Table 2.2). Further, these elements were both higher during Reference conditions (though effects were marginal; $p = 0.029$ and 0.045 respectively; Table 2.2). Given that wildfires emit significant quantities of NH_3 (Campbell et al., 2022) and the degree of NO_3^--N enrichment observed in this study (2-fold vs 1.5-fold in (Perron et al., 2022)), this discrepancy is likely due to differences in oxidative particle formation during atmospheric transport, where NH_3 and NO_2 were converted more efficiently to NO_3 compounds (Lindaas et al., 2021a, 2021b).

Particulate matter arriving in Sydney during the Wildfires displayed comparatively low concentrations of most trace elements relative to the Reference period, including fraction(s) of Cu, Cd, Hg, Ni and Pb (Table 2.3). This could be expected given these elements are major atmospheric by-products of non-ferrous metal production, coal and oil combustion, and vehicular traffic worldwide (Grigoratos and Martini, 2015; Pacyna and Pacyna, 2001). Meanwhile, Wildfire PM contained higher concentrations of particulate Co and Sb, and both fractions of Mn (Table 2.3). Correlation analyses with Pb (a common marker for anthropogenic activity) suggest a predominantly urban source of Co and Mn in the Reference samples ($r = 0.91$ and 0.97) and an alternative source during the Wildfires (0.21 and 0.10). Co and Mn in Australian aerosols are often associated with mineral dust when found offshore (Strzelec et al., 2020b, 2020a), indicating that these PTEs probably originated from soil that was entrained during strong pyrogenic winds (Wagner et al., 2018). This is consistent with previous wildfire smoke observations in Sydney (Isley and Taylor, 2020). Interestingly, Sb exhibited moderate associations with Pb in both study periods, indicative of a mixed-urban source, but had distinct associations with the other PTEs: in Reference PM, Sb was associated with Co ($r = 0.79$ vs -0.07), Mn (0.70 vs -0.40) and Pb (0.66 vs 0.55), whereas Wildfire samples were associated with Cu (0.95 vs 0.13), Cr (0.79 vs -0.31) and Pb (0.55 vs 0.66). Despite ranking seventh for global production (Britt and Senior, 2021), Sb remains unreported in Australian wildfire monitoring, yet has significant potential for remobilisation from

current and historical mining sites (Telford et al., 2009), waste-disposal sites (Wilson et al., 2014) and shooting ranges (Sanderson et al., 2014).

While prior observations during the Black Summer Wildfires also detected Mn enrichment in aerosols and sediment deposits (Barros et al., 2022; Perron et al., 2022), Co and Sb were not targeted by these studies, nor did we detect enrichment of other PTEs like As, Cu, Cr, Ni, Pb and Zn (Barros et al., 2022; Biswas et al., 2021; Perron et al., 2022). This is likely due to differences in sampling technique, where airborne samples are influenced by pollutant loading (which was exceptionally high during the Wildfires) and the current study assessed differences on an equal-mass basis. Therefore, we emphasise that our results are likely to be conservative when assessing the impact of wildfires on PTE exposure. Future studies should aim to pair FF with HVAC systems information to estimate atmospheric PTE exposures (Mahdavi et al., 2021) and include airborne sampling techniques where possible for methodological comparisons.

The solubility of Wildfire PTEs were either equal to (Cd, Cr, Mn, Pb, Zn; $p \geq 0.076$) or lower than (Co, Cu, Ni, Sb; $p \leq 0.01$) the Reference period, except for Hg ($p = 0.025$) (Table 2.3). Given that both anthropogenic and biomass combustion sources are associated with high trace element solubilities (Baker et al., 2006b; Mahowald et al., 2018), a differential enhancement of Hg is likely due to high-temperature induced volatilisation and emission of anthropogenic deposits on vegetation, litter, and soil (Howard et al., 2019). This is consistent with observations of wildfire ash, where Hg had the highest solubility of all elements analysed (Harper et al., 2019). While the central tendency of PTE solubilities were generally higher in Reference PM, the upper range and level of dispersion was either similar (Co, Cr, Cu, Ni, Pb, Zn; $p \geq 0.196$) or greater (Cd, Hg, Mn) than Reference PM for all trace elements except Sb (Table 2.3). This was expected given that HVAC filters received substantial contributions from a variety of smoke plume populations, sampling emissions of different source locations and characteristics (e.g., organic/inorganic particle matrix; moisture content; reactions with co-emitted organics, oxidisers, acidic species; photochemical processing and mixing; plume age, etc.) (Andreae, 2019; Baker et al., 2006b; Desboeufs et al., 2005; Hsu et al., 2010; Longo et al., 2016; Yang et al., 2023).

The PTEs detected in this study have a wide range of toxic effects at relatively low concentrations on diverse biota. In humans, ions like F^- are extremely permeable across biological membranes,

where their inhalation even in low concentrations elicits acute airway inflammation (Lund et al., 1999), and epithelial lung cell apoptosis at high concentrations (Refsnes et al., 2003). Similarly, trace elements such as Mn and Cu are major contributors to oxidative stress (Fujitani et al., 2017), while soluble forms of Hg can rapidly absorb and spread to all major organs in the human body (Park and Zheng, 2012). Upon their deposition, anions (mainly SO_4^{2-} and NO_3^-) may acidify surface waters and forest-floor soils (Battles et al., 2014; Lawrence et al., 1995; Lydersen et al., 2014) impacting acid-sensitive organisms, whilst PTEs like F^- and Mn may elicit direct toxicity in receiving environments (Alexakis, 2020; Golding et al., 2023; Wang et al., 2022). These impacts vary in their scale, from cellular (e.g., oxidative stress; DNA degradation, etc.) to organism level (impaired development, behaviours, and function), to populations (prolific growth of algae; mass fish kills) up to widescale ecosystem disturbances (trace element mobilisation; reduced nutrient storage; altered trophic flows and food availability) (Ding et al., 2022; Fornasiero, 2001; Leduc et al., 2013; McNulty and Newman, 1961; Monteith et al., 2007; Muniz, 1990; Wang et al., 2022). These impacts tend to be long-lived given that many trace elements are not readily biodegradable, persisting in the organism and environment for decades, even after removing the source (Gall et al., 2015).

2.4 Conclusions

The 2019-2020 Black Summer Wildfires were a major remote source of particle pollution in Sydney, especially fires originating on the south and south-east coast of Australia. Throughout HVAC sampling, daily mean PM concentrations were 2-3 times higher than the Reference period and exceeded the national standards on 19 % of days across the four-month sampling window. The wildfires were a significant source of $PM_{2.5}$ mass, comprising 31.9-50.0 % (q1-q3) of PM_{10} compared to only 27.9-35.7 % during Reference conditions. In this study, we show that particles collected during the Wildfires were significantly finer and more spherical than ambient urban PM. Particle number size distributions were finer, with 83.0 ± 0.7 versus 66.9 ± 1.8 % of particles <2.5 µm, and CMDs of 892.1 ± 23.1 and 1484.8 ± 96.7 nm, respectively. On an equal-mass basis, aged mixed wildfire-urban particles were a major source of acidic ions, including SO_4^{2-}-S (20.4 vs 4.7 mg g^{-1}) and NO_3^--N (2.4 vs 1.2 mg g^{-1}). Wildfire samples were also enriched with other PTEs, including Cl^- (34.7 vs 15.8 mg g^{-1}), F^- (334.9 µg g^{-1} vs < LOD), dissolved Mn (108.0 vs 28.6 µg g^{-1}), and particulate forms of Mn (870.3 vs 303.4 µg g^{-1}), Co (13.6 vs 7.9 µg g^{-1}), and Sb (64.1 vs 17.4 µg g^{-1}). Wildfire PM featured higher Hg solubility (12.1 vs 1.0 %) and displayed a greater range of Hg (q1-q3 4.7-25.5 vs 0.8-10.1 %), Cd (5.4-25.4 vs 4.3-8.0 %), and Mn (8.2-18.2 vs 7.7-9.0 %)

solubilities. Together, Wildfire PM displayed significant potential for toxicity given these elements are highly mobile, bioavailable, and persistent in the environment. Therefore, inhalation and deposition of this material had a high probability of negative impacts in the Sydney human population and on surrounding ecosystems.

Funding

This work was supported by the Faculty of Science and Climate Change Cluster at the University of Technology Sydney (UTS) through provision of operation funds and equipment, as well as the NSW Department of Planning and Environment (DPE) through in-kind contributions of expertise and the provision of consumables. RLG was supported by an Australian Government Research Training Program Scholarship at UTS.

CRediT authorship contribution statement

Raissa L. Gill: Writing - review & editing, Writing - original draft, Visualization, Methodology, Investigation, Formal analysis, Data curation, Conceptualization. **Robert Fleck:** Writing - review & editing, Methodology, Investigation, Conceptualization. **Ky Chau:** Writing - review & editing, Investigation. **Mika T. Westerhausen:** Writing - review & editing, Methodology, Investigation. **Thomas E. Lockwood:** Writing - review & editing, Methodology, Investigation. **Jake P. Violi:** Writing - review & editing, Investigation. **Peter J. Irga:** Writing - review & editing, Conceptualization. **Martina A. Doblin:** Writing - review & editing, Supervision, Conceptualization. **Fraser R. Torpy:** Writing - review & editing, Supervision, Methodology, Conceptualization.

Declaration of competing interest

The authors declare that they have no known competing financial interests or personal relationships that could have appeared to influence the work reported in this paper.

Acknowledgements

The authors acknowledge the Climate and Atmospheric Science Branch from the NSW Department of Planning and Environment (DPE) for provision of atmospheric PM and meteorological data, and Transport for NSW for the provision of traffic count data. The authors gratefully acknowledge the NOAA Air Resources Laboratory (ARL) for the provision of the HYSPLIT transport and dispersion model and READY website (ready.noaa.gov) used in this publication. We acknowledge the Department of Climate Change, Energy, the Environment and Water as well as the following providers for their contributions to the National Indicative Aggregated Fire Extent Datasets: NSW Rural Fire Service, Northern Australian Fire Information (NAFI), QLD Fire and Emergency Service, QLD Department of Environment and Science, SA Country Fire Service, SA Department for Environment and Water, Tasmanian Fire Service, TAS Department of Primary Industry, Parks, Water and Environment, VIC Department of Environment, Land, Water and Planning, WA Department of Biodiversity, Conservation and Attractions. For the symbols used to assemble the graphical abstract, we acknowledge Tracey Saxby and Jane Hawkey from the Integration and Application Network (ian.umces.edu/media-library) for the following artworks: Estuary 3D: braided river mouth; Climate change: wildfire; Urban: city 1; Industry 2; Sediment. The Sediment symbol was modified by cropping it from the original. All symbols are licensed under a Creative Commons Attribution-ShareAlike 4.0 International (CC BY-SA 4.0) license (creativecommons.org/licenses/by-sa/4.0). Finally, the authors would like to acknowledge the three anonymous reviewers for their insightful feedback which improved the manuscript.

3. Nutrient profile and sources of aerosols collected during intense wildfires in the Southern Hemisphere

Raissa L Gill [a b #], Robert Fleck [b], Ky Chau [b], Mika T Westerhausen [c], Thomas Lockwood [c], Jake P Violi [d], Peter J Irga [e b], Fraser R Torpy [b], Martina A Doblin [a f]

[a] Productive Coasts, Climate Change Cluster, University of Technology Sydney, Ultimo, NSW, 2007, Australia

[b] Plants and Environmental Quality Research Group, School of Life Sciences, University of Technology Sydney, Ultimo, NSW, 2007, Australia

[c] School of Mathematical and Physical Sciences, University of Technology Sydney, Ultimo, NSW, 2007, Australia

[d] School of Chemistry, University of New South Wales, Kensington, NSW, 2033, Australia

[e] Plants and Environmental Quality Research Group, School of Civil and Environmental Engineering, University of Technology Sydney, Ultimo, NSW, 2007, Australia

[f] Sydney Institute of Marine Science, Mosman, NSW, 2088, Australia

[#] Corresponding Author: raissa.l.gill@student.uts.edu.au; PO Box 123 Ultimo, NSW, 2007, Australia

Chapter 3 is currently under review in the *Journal of Environmental Pollution*.

Highlights

- Macronutrients in mixed smoke plumes were mostly OC, then SO_4^{2-} (as S) > N ≈ P ≈ K.
- Aged smoke was rich in combustive/secondary ions like SO_4^{2-}, NO_3^-, $C_2O_4^{2-}$ and K^+.
- Smoke plumes were enriched with mineral dust elements, including total Fe and Mn.
- Pb-contaminated soil was a major source of aerosols during the wildfires.
- Dust elements like Ca, Mg, and Cd were rapidly dissolved in wildfire-enriched samples.

Abstract

Australia is a major source of aerosols in the Southern Hemisphere, including mineral dust and wildfire smoke. Bioactive nutrients and toxicants in these emissions vary widely in composition, especially for wildfires, making it difficult to predict their ecological impact. The 2019-20 Black Summer wildfires provided a unique opportunity to examine how extreme fires influence bioactive aerosols. To quantify the composition and sources of wildfire-enriched nutrients, we analysed particulate matter in Sydney during the Black Summer (2019-20) and in ambient urban emissions one year later (2020-21). Macronutrients in wildfire-enriched samples were dominated by organic carbon (OC ~107 mg g^{-1}), sulphate (~28 mg g^{-1}) and similar amounts of nitrogen (N), phosphorus (P) and potassium (K) (~7 mg g^{-1} each). Approximately half of the N and K were water-soluble (~45-50%), whereas the majority of OC (~90%) and P (~99%) remained in the particulate phase. Micronutrients followed the order of iron > calcium (Ca) > magnesium (Mg) > manganese > silica > molybdenum > cobalt > cadmium (Cd), with Ca (~46%), Mg (~48%) and Cd (~17%) displaying high solubility. Per-mass, urban aerosols contained more OC, N, P and Cd and featured higher fractional solubilities. Wildfire-enriched samples likely originated from aged wildfire smoke (~33%), lead-contaminated soil (~32%), soil and sea-spray (~13%), and sea-spray (20%). In contrast, urban samples were predominately linked to vehicular exhaust (47%) and household liquid fuels and vehicular traffic (~32%). Given projections of more extreme fire weather, our results highlight Australia's role as a complex source of both nutrients and contaminants in the Southern Hemisphere.

Keywords

Aerosols; Biomass burning; Organic compounds; Source apportionment; Trace metals; Water-soluble ions.

Abbreviations

HVAC = heating, ventilation, and air conditioning
MDL = method detection limit
NPI = National Pollutant Inventory
PMF = positive matrix factorisation

3.1 Introduction

Aerosols are suspensions of small solid or liquid particles in the atmosphere, with diameters ranging between 1 nm and 100 µm (Mahowald et al., 2011). They can be classified as natural or anthropogenic in origin and have diverse chemical composition, including liquid and solid phases, nutritional and toxic elements, and a wide range of fractional solubilities (Mahowald et al., 2011, 2017). Aerosols can remain suspended anywhere from <1 day to >3 months depending on particle properties, meteorological conditions, emission characteristics and surface properties (Khaykin et al., 2020; Textor et al., 2006). During suspension, aerosols are subject to atmospheric transport and processing via wind currents (Longo et al., 2016) and can be dispersed great distances over large areas of land and ocean (e.g. (Wang et al., 2022)). The removal of aerosols from the atmosphere occurs through gravitational settling, turbulent collision, or via precipitation, and is a significant pathway for delivering bioactive material to downwind ecosystems, where it can impact biological processes (Mahowald, 2011).

The Australian continent has been long recognised as a region of global significance for naturally sourced aerosols, contributing 6 % to global mineral dust (Tanaka and Chiba, 2006) and 6-8 % of biomass burning emissions (Ito and Penner, 2004; Van Der Werf et al., 2006). Large dust storms regularly uplift surface particles from Australian landscapes and transport them (Gabric et al., 2016, 2010; Mackie et al., 2008; McTainsh and Pitblado, 1987), and plumes from frequent wildfires (known as “bushfires” in Australia) (Williams et al., 2012) disperse burnt vegetation, smoke, and entrained mineral dust (Paris et al., 2010; Wagner et al., 2018). While aerosols from both dust storms and wildfires can have bioactive effects upon their deposition, mineral dust alone tends to be relatively insoluble - especially in phosphorus and iron - possibly due to its coarser particle size and lower surface area-to-volume ratio, degree of atmospheric processing, and/or chemical composition (Baker and Jickells, 2006; Liu et al., 2022). Subsequently, the bioavailability and impact of dust on receiving environments is highly dependent on atmospheric transport, where physical and chemical processes can increase its solubility as the plume ages (Mahowald et al., 2005; Perron et al., 2020b; Winton et al., 2016). In contrast, particles that comprise wildfire emissions (including entrained mineral dust) tend to be fine and highly soluble due to oxidation during combustion, the presence of organic acids and inorganic ions, and atmospheric oxidation and gas-to-particle conversion of co-emitted gases like SO_2 and VOCs (Mahowald et al., 2018; Reid et al., 2005; Winton et al., 2016).

While it is well understood that mineral dust is the dominant source of aerosol iron in the northern hemisphere (Fung et al., 2000; Mahowald et al., 2009), the aeolian supply of soluble iron in the southern hemisphere is predominately driven by wildfires (Hamilton et al., 2020). Its deposition in the ocean can stimulate phytoplankton growth when carbon and nitrogen fixation are limited by iron availability (Hamilton et al., 2020; Tang et al., 2021; Wang et al., 2022). Besides iron, wildfires may provide a source of other aeolian nutrients, including organic carbon (Jurado et al., 2008), nitrogen (Campbell et al., 2022; Chen et al., 2010), phosphorus (Barkley et al., 2019; Mahowald et al., 2005), potassium (Sparks and Wagner, 2021) and sulfur (Koplitz et al., 2021). Depending on the quantity and nature of aeolian supply, aerosols have diverse impacts on terrestrial, aquatic and marine habitats, altering local biogeochemistry, ecosystem processes and biota (Gomez Isaza et al., 2022; Hamilton et al., 2022; Ito et al., 2020). Predicting the aeolian supply of wildfire-derived nutrients is inherently complex, largely due to variations in emission source, meteorological conditions, atmospheric processing, and deposition modes (Hamilton et al., 2020; Reid et al., 2005). This is further complicated by the paucity of information on wildfire aerosol composition, where researchers must overcome several challenges to obtain such datasets: e.g., fixed observation sites are not necessarily located within fire zones; working in proximity to smoke and flames presents logistical and safety risks; access to suitable aerosol samplers may be limited; it can be difficult to amass sufficient material for analysis whilst meeting analytical detection limits; variability in sampling equipment and locations between studies can hinder comparability, etc. Therefore, documenting the impact of extreme fire events on aeolian nutrition is highly valuable for informing the potential impacts of wildfires on receiving environments.

Global fire frequency and severity will continue to increase with climate change as temperature and precipitation patterns generate more fire-prone weather (Aldersley et al., 2011; Canadell et al., 2021; Pechony and Shindell, 2010). Accordingly, record-breaking high temperatures in Australia preceded by years of prolonged and severe drought (Bureau of Meteorology, 2019) fuelled the most extreme wildfire season on record, known colloquially as the Australian 2019-20 Black Summer (Boer et al., 2020). The wildfires were ignited in September 2019 and developed across several states, burning ~20% of Australia's eucalypt forest (~30.38 Mha) until rain extinguished or eased conditions in February 2020 (Boer et al., 2020; Bowman et al., 2020). During this time, the fires emitted record-breaking quantities of pyrogenic aerosols at unprecedented altitudes; these were comparable to the plume injections of moderate volcanic eruptions (Hirsch and Koren, 2021; Peterson et al., 2021, 2018) and encircled a portion of the

southern hemisphere for over a year (Peterson et al., 2021). Here we describe the concentration and sources of aeolian nutrients captured in Sydney, Australia during the peak of the 2019-20 Black Summer wildfires, and how it compared to ambient urban aerosols sampled one year later. Given the magnitude and extent of bushland burnt throughout the fires, we anticipated that these samples would contain mainly natural aerosols from far-reaching, vegetative locations, with substantial enrichments to organic carbon and soluble forms of nutrients.

3.2 Material and methods

3.2.1 Aerosol capture and extraction

Aerosols were captured at the University of Technology Sydney (Ultimo campus, Sydney, Australia) by building HVAC filters. These air intakes drew a mix of Black Summer emissions and ambient urban aerosols ("Wildfire-enriched" henceforth) through seventeen primary HVAC filters (594 x 594 x 44 mm, Aeropleat III MERV 8 filters; Camfil, Sweden) from November 2019 to February 2020 (inclusive). As a point of reference, twelve primary filters were also retrieved one year later (aerosols captured from November 2020 – February 2021) to analyse the nutrient profile of urban-derived particles only ("Urban"). Four unused filters were also sampled and analysed as a control for the extraction procedure ("Procedural Control"). HVAC filters are not typically used for aerosol sampling but were used in this study to evaluate the nature of material being trapped in typical building air intake systems and as a source of bulk particulate matter for use in further experiments. Embedded particles were extracted from the primary filters using a similar technique to Mahdavi and Siegel (2020), which employed vacuum sampling to extract particles embedded in the filter mesh into enclosed cassettes. Extracted mass was determined gravimetrically and used to standardise chemical concentrations (mg analyte per g^{-1} aerosol mass). Each replicate primary filter yielded between 3-5 cassettes of particulate material; we analysed a subset of 12 wildfire-enriched and 9 urban replicates for this study. More details on the sample collection and extraction method are described elsewhere (Gill et al., 2024).

3.2.2 Chemical analyses

In preparation for analysis, loose particles in each cassette were transferred into sterile plastic tubes (Falcon, USA) by rinsing with Milli-Q water (MQ) (18.2 Ω; Millipore, Germany). The filter

paper was transferred using acid-washed forceps. Tubes were then filled to 50mL with MQ, shaken, and sonicated for 15 min. Filter paper was removed and set aside for trace element analysis, while the remaining extract was centrifuged (7.826 xg, 15 min) to separate the dissolved and particulate nutrient fractions. The liquid filtrate was filtered through 0.22 µm (Millex-GP Filter, Millipore, Germany) into another tube to remove any remaining particles, leaving behind a solid pellet of particle mass. All samples were stored at -80 °C until analysis.

3.2.2.1 Carbon and nitrogen

All carbon and nitrogen analyses were conducted on a TOC-L Total Organic Carbon Analyser (Shimadzu, Japan) with a TNM-L Total Nitrogen unit (Shimadzu, Japan), and operated using TOC-Control L software (V.1.06, Shimadzu, Japan). Prior to each run, the flow line contents were replaced and washed twice, and the catalyst was conditioned by triplicate MQ injections until blanks read low and stable (<1 mg L^{-1} for carbon and <0.05 mg L^{-1} for nitrogen, respectively). Injection volume was set to 40 µL with 3-5 technical replicates per sample. For calibration, triplicate five-point calibration curves (0-10, 0-20, 0-100 mg L^{-1}) were prepared from Potassium Hydrogen Phthalate in MQ or 0.22M Hydrochloric acid (HCl) (R^2 >0.99 in all cases).

For analysis, dissolved sample aliquots were diluted between 1:2-1:5 with MQ and decanted into acid-washed 40 mL autosampler vials with no headspace. Samples were analysed in TC/TN mode first to quantify total dissolved carbon (DC) and nitrogen (DN), followed by NPOC mode for dissolved organic carbon (DOC) after acidification with 1M HCl (pH 2-3) and sparging for 10 min with CO_2-free gas. Particulate samples were freeze dried for three days to remove any remaining liquid (freeze-dried mass within ±5% of initial extracted mass). Upon return to room temperature, dried mass was weighed into vials and diluted with ~37 mL 0.22M HCl to a final concentration of 149.83 ± 32.29 mg L^{-1}. Samples were sonicated for 10 min to disrupt any clumps and magnetic stirrer bars were added to maintain particles in suspension during analysis. Samples were sparged for 10 min and then analysed in NPOC/TN mode to quantify particulate organic carbon (POC) and particulate nitrogen (PN), with a single read per injection to minimise particle settling time (n = 3-4 reads per vial). The median of technical replicates was taken as the final concentration of each sample.

For quality control, MQ blanks, duplicate samples, matrix spikes (spiked with $C_8H_5KO_4$ and KNO_3), calibration standards ($C_8H_5KO_4$ and KNO_3), independent standards (99% Glycine in MQ/HCl - 502-211; LECO, USA), and Certified Reference Materials (CRM) were run every ~20 samples. CRMs included Stream Sediment (NCS DC 73016a) and Agricultural Soil (NCS ZC 71008) (NCS Testing Technology Co, China). Blanks read low and stable (<0.6 mg L^{-1} carbon and <0.03 µg L^{-1} nitrogen) and recoveries were within ±5 % of expected values in all cases.

3.2.2.2 Trace elements

A solution nebulization inductively coupled plasma mass spectrometer (SN ICP-MS; 7700x, Agilent, Australia) was employed to determine the trace element content of the dissolved, particulate, and filter paper sample fractions. For calibration, a 12-point calibration curve (0-5 mg L^{-1}) was made from a 68-elemental standard (ICP-MS68A-500; Choice Analytical, Australia) in 2 % HNO_3/1 % HCl (Seastar Baseline®; Choice Analytical, Australia). An online internal standard was used to normalise any matrix effects (100 µg L^{-1} Rhodium in 2 % HNO_3/1 % HCl). For analysis, particulate/filter samples were vacuum dried overnight at room temperature, then digested in 5 mL of 69 % HNO_3 and 5 mL of 34 % HCl made to a volume of 50 mL with MQ. Dissolved samples were diluted in 2 % HNO_3/1 % HCl. Samples were diluted between 1:100-1:3000 with 2 % HNO_3/1 % HCl diluent to ensure they fell within instrument calibration range. Several nutritional trace elements were quantified for this study, including Ca, Cd, Co, Cu, Fe, K, Mg, Mn, Mo, P, Se, Si and Zn. Additional elements were also analysed (Al, Na, Sn, Sr, Ti, V) or compiled from previous work (As, Be, Cd, Cr, Hg, Ni, Pb, Sb) to aid with source appointment (section 3.2.3). Quality control involved running MQ blanks, duplicate samples, and CRMs (same as above) every ~20 reads. Blanks read low and stable (<10 µg L^{-1} if detected), and recoveries were within ±10 % for all elements studied except Se (excluded from further analysis).

3.2.2.3 Major ions

Major cation and anion analyses were conducted on the soluble sample aliquots using a high-pressure ion chromatograph (HPIC, Thermofisher, USA) configured with a Dionex auto-sampler and conductivity detector (AS-AP). The HPIC was calibrated using a 6-point (0-20 mg L^{-1}) calibration curve made from mixed single ion (1000 mg L^{-1}) standards (TraceCERT, Sigma-Aldrich, Australia). Specific parameters are the same as in Gill et al., (2024). For analysis, dissolved sample aliquots were diluted between 1:10 and 1:50 with MQ to avoid overloading the column. The nutritional ions targeted for this study are provided below, reported on an elemental-

equivalent basis where applicable: Ca^{2+}, K^{+}, Mg^{2+}, NH_4^{+}-N, NO_2^{-}-N, NO_3^{-}-N, PO_4^{3-}-P, SO_4^{2-}-S. Three additional ions were also analysed as above ($C_2O_4^{2-}$-C) or compiled from previous work (Cl^{-}, Na^{+}) for source apportionment purposes (section 3.2.3). Quality control checks included blanks, duplicates, and calibration standards every ~20 reads. Blanks read low and stable (<0.05 mg L^{-1} for all ions) and recoveries fell within ±8 % of expected values for all ions studied. Final ionic concentrations are expressed in their elemental form.

3.2.3 Source apportionment

Positive Matrix Factorisation (PMF) was performed to elucidate the sources of aeolian nutrients in this study. This factor-based receptor model decomposes chemical composition data to identify and profile 'factors', i.e., combinations of chemical analytes from which a common source is inferred. Sources are then assigned based on the partitioning of chemical tracers and knowledge of local source profiles. PMF has been successfully implemented for a variety of scenarios (e.g., contaminated soil, dust storms, stormwater runoff), where its key advantage over other geostatistical approaches (e.g., correlation, principal components analysis) is the ability to distinguish between factors that share common chemical analytes. This is essential when sampling aerosols from two major combustion sources (fossil fuels and biomass). PMF also incorporates method detection limits and analytical uncertainties, increasing the robustness and accuracy of the model.

Receptor modelling was performed using the US Environmental Protection Authority's PMF software and guidelines (v5.0.14; Norris et al., 2014). The input data matrix was comprised of the nutrients targeted in this study, along with several chemical tracers and potentially toxic elements compiled previously (Gill et al., 2024). A full list of analytes is provided below, which includes the mass concentrations (mg g^{-1}) of both wildfire-enriched and urban samples: total fractions of OC, N, and trace elements (Al, As, Be, Ca, Cd, Co, Cr, Cu, Fe, Hg, K, Mg, Mn, Mo, Na, Ni, P, Pb, Sb, Si, Sn, Sr, Ti, V, Zn), as well as dissolved ions ($C_2O_4^{2-}$-C, Ca^{2+}, Cl^{-}, F^{-}, K^{+}, Mg^{2+}, Na^{+}, NH_4^{+}-N, NO_2^{-}-N, NO_3^{-}-N, PO_4^{3-}-P, SO_4^{2-}-S). Non-sea-salt concentrations were determined for K^{+} (nss-K^{+}) and SO_4^{2-} (nss-SO_4^{2-}) using Equations (1) and (2) below. Total fractions were derived by summing the dissolved and particulate concentrations where applicable. Several combinations of chemical species were used to guide the interpretation of PMF factors, including analytes indicative of oceanic (Cl^{-}, Na^{+}), crustal (Al, Si, Ti), anthropogenic (Hg, Ni, Pb), combustion (nss-

K^+) and combustion/secondary aerosols ($C_2O_4^{2-}$-C, NO_3^--N, nss-SO_4^{2-}) (Strzelec et al., 2020b and references therein). While these latter species may be directly emitted during combustion or derived from sources like marine dimethyl sulfide (in the case of SO_2), they primarily form through atmospheric oxidation of precursor gases emitted during combustion of biomass or fossil fuels (Zhang et al., 2017). In this instance, VOCs are oxidised to $C_2O_4^{2-}$ (and other secondary organic aerosols), NO_x to NO_3^-, and SO_2 to SO_4^{2-} (Hallquist et al., 2009; Riemer et al., 2019). All chemical analytes were input to PMF software prior to blank correction.

$$[\text{nss-}SO_4^{2-}] = [SO_4^{2-}] - [Na^+] \times 0.253 \quad (1)$$

...where 0.253 is the mass ratio between Na^+ and SO_4^{2-} in sea-spray (Keene et al., 1986).

$$[\text{nss-}K^+] = [K^+] - [Na^+] \times 0.037 \quad (2)$$

...where 0.037 is the mass ratio between K^+ and Na^+ in sea-spray (Keene et al., 1986).

As per EPA guidelines (Norris et al., 2014), the method detection limit (MDL) of each analyte was defined as three times the standard deviation of the Procedural Control filter, while uncertainty was calculated as the median variance between split PM samples that were analysed separately (n = 3). The data quality of each analyte was classified using the signal to noise ratio (S/N), where “bad” analytes were defined as those with ratios <0.2, “weak” analytes between 0.2-2, and “strong” analytes >2. “Bad” analytes were excluded from further analysis, and the uncertainty of “weak” analytes was increased by a factor of three to reduce the impact of barely detectable analytes on the overall model fit. Mass Balance (MB), calculated as the sum of chemical analytes for each sample, was classified as "weak" given its inclusion was for factor resolution/model diagnostic purposes only. In initial model runs, the scaled residuals of NH_4^+-N, NO_2^--N and V were consistently unstable and contributed poorly to model fit, even when reclassified as "weak". These analytes were subsequently reclassified as "bad" to exclude them from the model. The final input data matrix was comprised of 3 "bad", 1 "weak" and 33 "strong" analytes. Extra modelling uncertainty was set to 5% to improve goodness of fit (“Q”) parameters, which reflect how well the PMF solution fits the input data.

Three- to eight-factor solutions were explored on the combined dataset of both wildfire-enriched (n = 12) and urban (n = 9) samples (total n = 21). For each solution, 100 individual model runs

were initiated at a random starting point or "seed". Initial screening of possible solutions were based on the following four criteria (Cohen et al., 2016b): 1) all factors were driven by >1 analyte; 2) all factors contributed positively to reconstructed mass balance, with mean contributions >1 %; 3) linear regressions between observed and predicted analytes were significant ($p < 0.05$) with positive coefficients; 4) the solution had a Q_{true}/Q_{robust} (goodness-of-fit) ratio between 0.7-1.1, where <0.7 indicates too many factors being fit or the uncertainty estimate of an analyte(s) is too large (for >1.1 the reverse applies). Based on these criteria, we identified three possible solutions: 3-, 4- and 6-factors. The optimal solution was then selected based on three additional indicators: 1) a Q_{true}/Q_{robust} ratio close to 1, which indicates negligible impact of high, uncertainty-scaled residuals; 2) satisfactory (>0.7) R^2 values for linear regressions between observed and predicted analytes; 3) the interpretability of factors as relevant source fingerprints. The 3- and 4-factor solutions yielded Q_{true}/Q_{robust} ratios of between 0.83 and 0.85. However, 14 analytes in the 3-factor solution and 8 in the 4-factor solution showed substantial deviation from observed values ($R^2 < 0.7$), and the factors were difficult to interpret due to limited differentiation between sources. The 6-factor solution had a Q_{true}/Q_{robust} ratio of 0.99, only 1 analyte with R^2 <0.7 (copper: R^2 0.57), and clearly differentiated, interpretable factors. Inspection of observed versus predicted values for copper revealed two anomalous samples from the urban study period (24 and 50 % discrepancy), however its impact on model fit was negligible with remaining sample errors for copper all <1 %. Therefore, this solution was considered suitable to examine the sources of aerosols in this study.

3.2.4 Data analysis

Given that many nutrients displayed skewed distributions for concentration and/or solubility data, PERMANOVAs were used to identify differences between the wildfire-enriched and urban sample types. This was performed individually for each nutrient using Euclidean distance and 999 permutations. Data was then summarised as medians and lower/upper quartiles (Q1/Q3) for subsequent plotting and reporting. For source apportionment, mean factor profiles and contributions of the final 6-factor model were exported from EPA PMF software (Norris et al., 2014). This data was plotted and interpreted using selected chemical tracers and knowledge of source profiles from the literature (see section 3.2.3). All data analysis and plotting were performed in R software (v4.4.2, R Core Team, 2021) using the following packages: dplyr (Wickham et al., 2021); ggplot2 (Wickham, 2016); vegan (Oksanen et al., 2022).

3.3 Results

3.3.1 Macronutrients

The macronutrient profile of aerosols captured during both austral Summers is presented below (Figure 3.1). On a per mass basis, wildfire-enriched macronutrients were comprised mostly of OC, with a median concentration of ~107 mg g^{-1} (Q1-Q3; 77-119 mg g^{-1}) and ~10% (8-12 %) fractional solubility in water. Sulphur (as indicated by SO_4^{2-}-S) followed as the next most abundant macronutrient, contributing ~28 mg g^{-1} (20-30 mg g^{-1}) to sample mass in the dissolved phase. Remaining elements contributed ~7 mg g^{-1} each to sample mass, including N (7-10 mg g^{-1}), K (6-7 mg g^{-1}) and P (4-10 mg g^{-1}). Around half of the N and K was readily dissolved in water, with fractional solubilities of ~45 % (37-47 %) and ~50 % (45-54 %), respectively. This includes ~4 mg g^{-1} of K^+ (3-4 mg g^{-1}), ~2 mg g^{-1} of NO_3^--N (2-4 mg g^{-1}), and near-detection levels of NH_4^+-N (LOD-216 µg g^{-1}) and NO_2-N (LOD-14 µg g^{-1}). P was detected mostly in the particulate phase with ~0.9 % (0-5 %) solubility and ~680 µg g^{-1} of PO_4^{3-}-P (420-1149 mg g^{-1}; Figure 3.1).

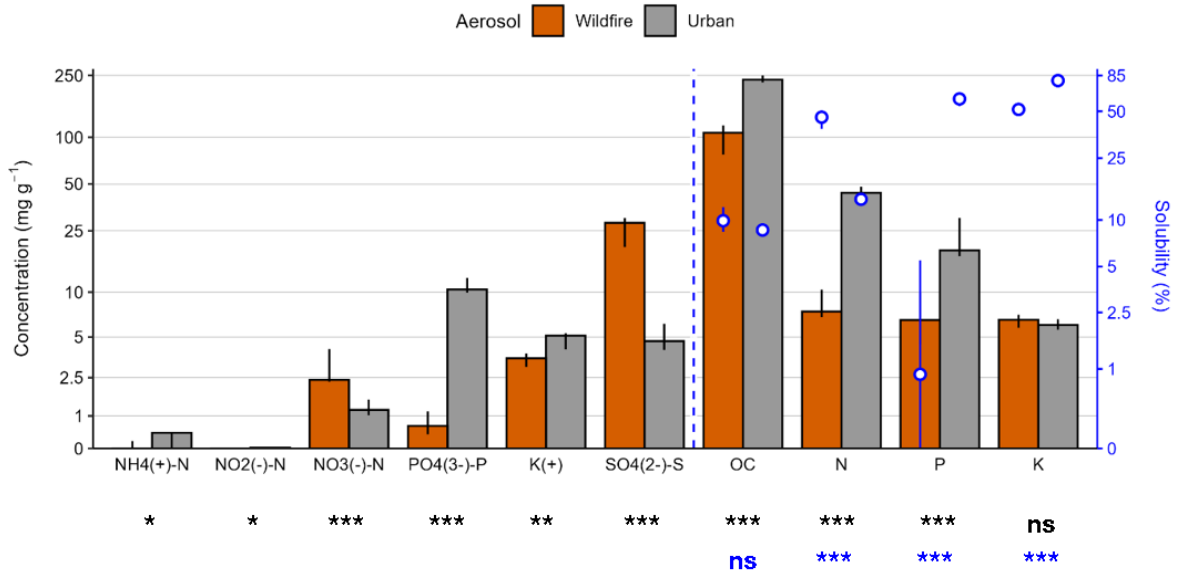


Figure 3.1 Macronutrient content of aerosols sampled in Sydney, Australia during the 2019-20 Black Summer wildfires (n = 12) and ambient urban conditions (2020-21, n = 9). Solubilities for non-ionic analytes (right-side of vertical dashed line) are denoted by blue points and the second y-axis, where values closer to 100% indicate that the element is primarily in the dissolved fraction. All data are shown as medians and upper/lower quartiles on a natural log scale, and statistical significance of wildfire-enriched versus urban comparisons are shown below the x-axis.

In ambient urban samples, OC remained the most abundant macronutrient and was detected at a similar level of solubility (~8 %, p = 0.118) but at twice the mass concentration (~235 mg g^{-1}, p = 0.001; Figure 3.1). N followed in second place, with concentrations ~6 times higher than fire-affected samples (~44 mg g^{-1}, p = 0.001). However, N was detected mainly in the particulate phase, with lower solubility (~13 %, p = 0.001), less NO_3^--N (~1 mg g^{-1}, p = 0.001), and marginally higher (p < 0.05) but negligible levels of NH_4^+-N (~466 µg g^{-1}) and NO_2^--N (~19 µg g^{-1}). P and PO_4^{3-}-P were the next highest in concentration (~19 and ~10 mg g^{-1}, respectively), with the former being detected mostly in the dissolved phase (~58 %). This far exceeded fire-affected samples in concentration and solubility (p = 0.001). K was ranked next highest with similar concentrations to wildfire-enriched samples (~6 mg g^{-1}, p = 0.267). However urban samples contained highly dissolved forms of K (~77 %) that exceeded wildfire-enriched solubilities (p = 0.001), including ~5 mg g^{-1} of K^+ ($p \leq 0.01$). The final macronutrient SO_4^{2-}-S was detected in similar levels to K^+ (~5 mg g^{-1}), which was significantly lower than that of samples (p = 0.001; Figure 3.1).

3.3.2 Micronutrients

For micronutrients (Figure 3.2), wildfire-enriched aerosols were mostly comprised of particulate Fe, with a mass concentration of ~50 mg g^{-1} (46-54 mg g^{-1}) and ~0 % (0-0.04 %) fractional solubility. Ca and Mg followed as the next most abundant micronutrients, with concentrations of ~33 mg g^{-1} (21-35 mg g^{-1}) and ~12 mg g^{-1} (12-14 mg g^{-1}), respectively. About half the Ca and Mg were readily dissolved in water, with solubilities of ~46 % (42-56 %) and ~48 % (42-54 %), respectively. This is consistent with measurements of water soluble Ca^{2+} and Mg^{2+} ions, which yielded mass concentrations of ~16 mg g^{-1} (15-19 mg g^{-1}) and ~7 mg g^{-1} (6-8 mg g^{-1}), respectively. Remaining micronutrients were present at lower concentrations and include the following: Zn ~4 mg g^{-1} (3-4 mg g^{-1}); Mn ~1 mg g^{-1} (0.9-1.1 mg g^{-1}); Cu ~816 µg g^{-1} (628-1054 µg g^{-1}); Si ~342 µg g^{-1} (243-762 µg g^{-1}); Mo ~28 µg g^{-1} (20-32 µg g^{-1}); Co ~15 µg g^{-1} (14-18 µg g^{-1}); Cd ~0.4 µg g^{-1} (0.3-0.5 µg g^{-1}). These analytes were mostly in the particulate phase, with upper quartiles for solubility all <25 %. Specific fractions are as follows: Zn ~4 % (3-13 %); Mn ~10 % (8-18 %); Cu ~5 % (4-6 %); Si ~0 % (0-0 %); Mo ~4 % (3-6 %); Co ~7 % (5-10 %); Cd ~17 % (5-23 %) (Figure 3.2).

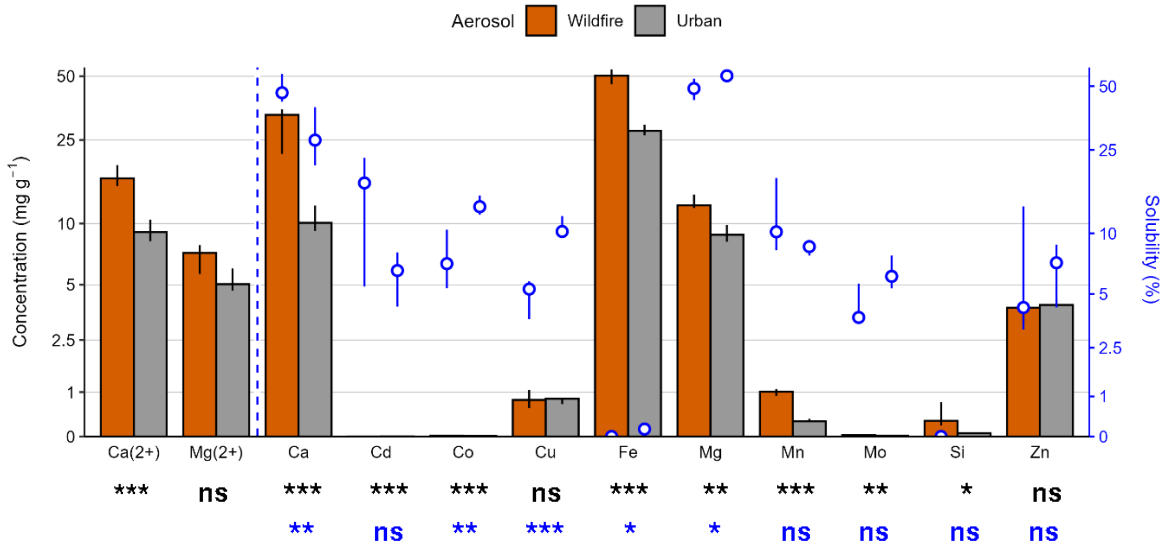


Figure 3.2 Micronutrient content of Black Summer wildfire (2019-20, n = 12) and ambient urban aerosols (2020-21, n = 9). Solubilities of trace elements (right of dashed line) are indicated by blue points and the second axis. All values are displayed as medians and upper/lower quartiles on a natural log scale, and statistical significance of wildfire-enriched versus urban comparisons are shown below the x-axis.

In ambient urban conditions (2020-21), Fe remained the most abundant micronutrient detected however at half the mass concentration (~28 mg g^{-1}, p = 0.001) and with marginally higher solubility (~0.2 %, $p \leq 0.05$) compared to wildfire-enriched aerosols (Figure 3.2). As above, Ca (~10 mg g^{-1}) and Mg (~9 mg g^{-1}) were ranked next but at concentrations ~1.3 to 3.3 times lower than wildfire-enriched samples ($p \leq 0.01$). These displayed less dissolved Ca (~27 %, $p \leq 0.01$) and marginally higher dissolved Mg (~55 %, $p < 0.05$) relative to wildfire-enriched fractions. Accordingly, Ca^{2+} ions were almost 50 % lower than in wildfire-enriched samples (~9 mg g^{-1}, p = 0.001), while Mg^{2+} ions did not differ (~5 mg g^{-1}, p = 0.097). Zn (4 mg g^{-1}) then Cu (~842 µg g^{-1}) were the next most abundant micronutrients, with solubilities of ~7 % and ~10 %, respectively. These were similar to measurements of wildfire-enriched aerosol ($p \geq 0.476$), except for Cu solubility which was higher in urban samples (p = 0.001). Mn (~332 µg g^{-1}), Si (~71 µg g^{-1}), Mo (~15 µg g^{-1}) and Co (~9 µg g^{-1}) followed in concentration, and were all lower than in wildfire-enriched samples ($p \leq 0.05$). These analytes were mostly in the particulate phase, with solubilities of ~9 % (Mn), ~0 % (Si), ~6 % (Mo) and ~13 % (Co), respectively. This is similar to wildfire-enriched fractions ($p \geq 0.091$), except for Co which was more soluble in urban samples (p = 0.003). Cd comprised the smallest portion of urban micronutrients (~2 µg g^{-1}), however was significantly more abundant than in wildfire-enriched aerosols (p = 0.001) with a similar level of solubility (~6 %, p = 0.997; Figure 3.2).

3.3.3 Aerosol sources

This study identified several potential sources of aerosols influencing the Sydney region across both austral Summers, including aged wildfire smoke (F1), Pb-contaminated soil (F2), soil and sea-spray (F3), sea-spray (F4), household liquid fuels and vehicular traffic (F5), and vehicular exhaust (F6). These PMF-resolved chemical signatures are shown in Figure 3.3A below, with contributions to wildfire-enriched and urban samples in Figure 3.3B.

Factor 1 (F1) was characterised predominately by combustion/secondary aerosol tracers (red points, Figure 3.3A), displaying the highest (62% nss-SO_4^{2-}-S > 58 % NO_3^--N > 42 % $C_2O_4^{2-}$-C) and second highest (30 % nss-K^+) contributions amongst all source factors identified. Oceanic and crustal tracers also contributed moderately to F1 (33 % Cl^- > 24 % Na^+ and 23 % Al > 22 % Ti > 21 % Si, respectively; blue/brown points), while anthropogenic tracers displayed little association (<16 %; grey points). This suggests that this source likely originated from outside Sydney's harbour and highly urbanised CBD. Among the non-tracer analytes (white points), F1 was the only source of F^- (100 %) and contained substantial contributions from many analytes of known crustal origins (52 % Ca^{2+} > 48 % Sb > 47 % Mg^{2+} > 39 % Mo > 36 % Mg > 26 % Ca > 25 % Fe ≈ 25 % Cu > 23 % Co > 19 % Mn > 18 % Cr). In the wildfire-enriched samples, F1 accounted for 44 % (35-53 %) of total analysed mass (Figure 3.3B). Comparatively, urban samples were ~4 %. Given the above findings, the bulk of this fraction was likely derived from aged wildfire smoke, with secondary contributions from sea-salt and mineral dust that became entrained on emission or during aeolian transport.

Factor 2 (F2) was dominated by crustal tracers (41 % Si > 33 % Ti > 19 % Al) and the anthropogenic tracer Pb (31 %), with first-ranked contributions for all these analytes except Al (Figure 3.3A). The combustion/secondary tracer NO_3^--N also contributed moderately to F2 (14 %), while remaining tracer contributions were <10 %. Accordingly, F2 had substantial contributions from many analytes of known soil and/or urban origins (31 % Cu ≈ 31 % Cr > 29 % Mo > 28 % Fe > 27 % Sb > 22 % Zn > 20 % Mn > 20 % Co). Despite the prevalence of Pb, F2 was ~3 times more prominent in the wildfire-enriched samples compared with urban emissions, accounting for 22 % (1-25 %) versus 7 % (6-10 %) of analysed sample mass (Figure 3.3B). Wildfire-enriched sample contributions were also more variable with a considerable left skew, which indicates that this source was not consistently emitted or aerosolised. Together, these results suggest that these

aerosols were derived from Pb-contaminated soil that became entrained during strong, fire-driven winds, and were then transported by air to Sydney.

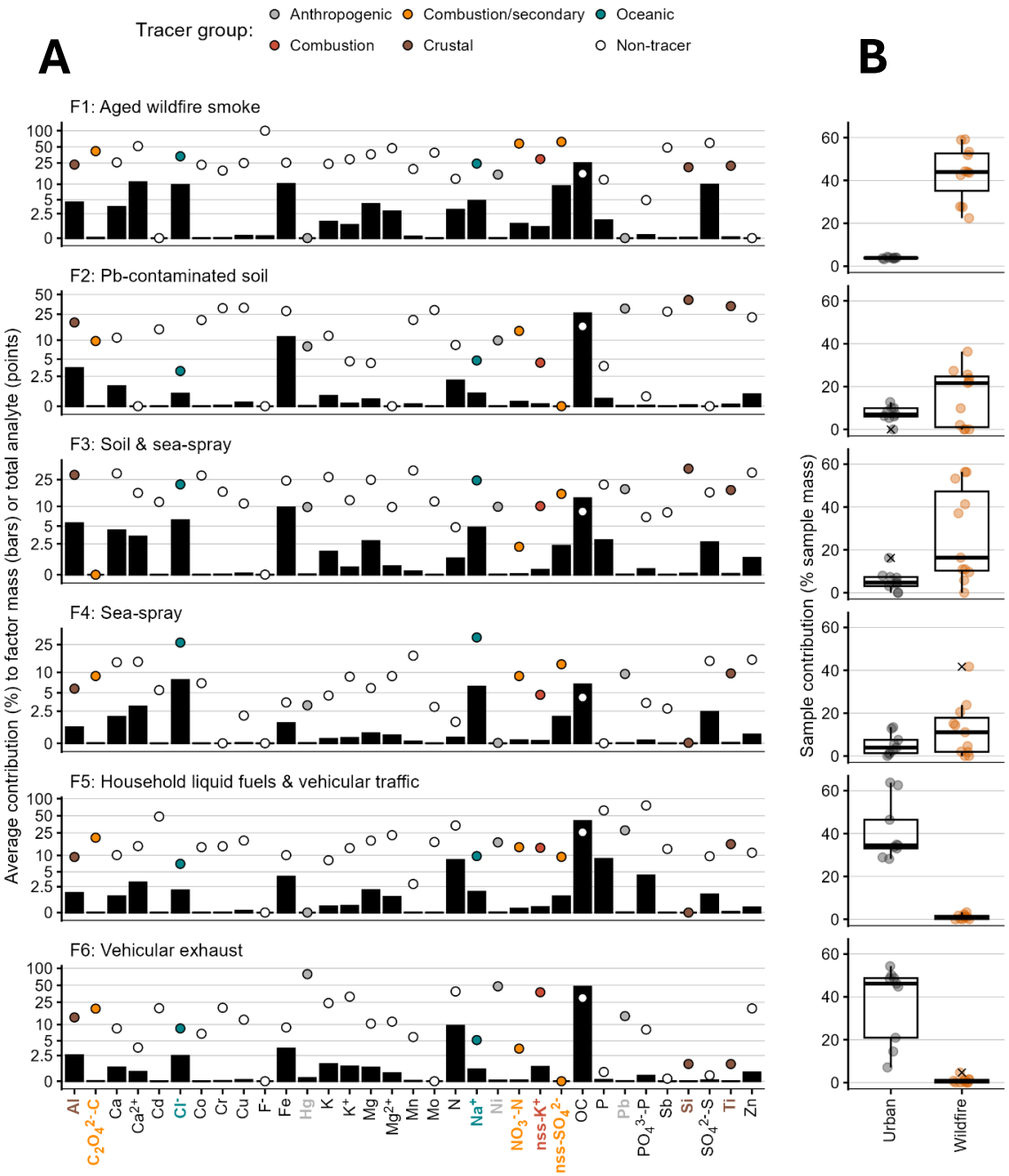


Figure 3.3 PMF-resolved source profiles (A: left subplots) and sample contributions (B: right subplots) for aerosols captured in Sydney, Australia during Black Summer wildfire (2019-20, n = 11) and ambient urban conditions (2020-21, n = 9). Factors 1-6 (F1-F6) are displayed by row and labelled according to its deduced source (see Results). For left subplots (A), analytes are shown along the x-axis, with the y-axis indicating average contributions (%) to each factor's mass (bars) or to total analyte mass as measured across all factors (points). Analytes used as chemical tracers in this study are coloured according to its source classification. Right subplots (B) show each factor's contribution (%) to wildfire-enriched (orange) and urban (grey) sample mass (%). All values are displayed on a natural log scale.

Similar to F2, Factor 3 (F3) was primarily influenced by crustal tracers (36 % Si > 29 % Al > 18 % Ti) and non-tracer soil analytes (34 % Mn > 32 % Zn > 31 % Ca > 29 % Co > 27 % K > 25 % Mg > 24 % Fe > 21 % P). Among the six factors, F3 was the largest source of Al and second-largest for Si (Figure 3.3A). However, F3 also displayed moderate contributions from oceanic tracers (24 % Na^+ > 21 % Cl^-), with Na^+ tied at second amongst the six-factor rankings, and remaining tracer contributions were < 20 %. Like F2, F3 contributions to wildfire-enriched samples were ~3 times higher than urban emissions at 16 % (10-47 %) versus 5 % (3-7 %), respectively (Figure 3.3B). F3 was also heavily skewed but in the opposite direction to F2, suggesting that this source was also emitted or aerosolised inconsistently. These results suggest that wind-swept soil is the primary source contributing to this factor, with secondary contributions from sea-salt particles that were either entrained on emission or mixed during aeolian transport. Therefore, F3 was denoted as soil and sea-spray.

Factor 4 (F4) was solely influenced by tracers of sea-spray (32 % Na^+ > 27% Cl^-), which ranked first (Na^+) and second (Cl^-) amongst the factors (Figure 3.3A). Remaining contributions of all analytes were < 20 %. While median F4 contributions to wildfire-enriched samples were ~3 times higher than urban emissions (11 % versus 4 %), there was substantial overlap between sample types with quartile ranges of 2-18 % versus 1-8 %, respectively (Figure 3.3B). Both sample types were considerably skewed, indicating that F4 was not consistently aerosolised. Given the above, F4 is likely derived from sea-spray particles that were either entrained from coastal water and estuaries along the sampled plume's trajectory and/or emitted locally from Sydney Harbour.

Factors 5 (F5) and 6 (F6) had negligible impact on wildfire-enriched sample mass (~1 %), but together they comprised ~81 % of the urban samples with median contributions of 34 % (33-46 %) and 46 % (21-49 %), respectively (Figure 3.3B). Accordingly, these factors were predominately influenced by tracers of urban activity, with secondary contributions from combustion/secondary sources (Figure 3.3A). Specifically, F5 displayed the second-highest Pb (28 %), $C_2O_4^{2-}$-C (21 %), Ni (17 %), and NO_3^--N (14 %) of all factors, while F6 had the highest levels of Hg (79 %), Ni (48 %) and nss-K^+ (38 %). Remaining tracer contributions were < 20 % for both factors. Amongst the non-tracer analytes, F5 and F6 were the greatest source of macronutrients on an equal-mass basis, where they each contributed 26-30 % to OC and 34-39 % to TN, respectively. F5 also displayed the highest P (62 %) and PO_4^{3-}-P (76 %) contributions. Besides nutrients, F5 was the primary source of Cd (49 %) and second-highest contributor to Mg^{2+} (23 %),

and F6 was the second-highest contributor to Cd (20 %) and Cr (20 %). While both F5 and F6 share urban origins, their distinct chemical signatures suggest that these aerosols were emitted from different sources.

The Australian National Pollutant Inventory (NPI), which publishes source emission estimates for 93 potentially toxic substances each year, indicates that motor vehicles dominated diffuse emissions of NO_x (69,000 kg) > Pb (16 kg) > Cd (5.9 kg) > Cr(III) (0.15 kg) > Hg (0.052 kg) in the Ultimo suburb for the urban sampling period (2020-21), whilst liquid fuel burning (domestic) was the sole emitter of TP (0.015 kg). Ni was emitted in similar quantities by both sources (0.11 and 0.13 kg, respectively), while Cr(VI) was primarily emitted by barbeques (0.021 kg). Similar trends were observed at the broader level of Sydney's Local Government Area (LGA) for all analytes. Based on the NPI emission profile and PMF analysis, F5 likely originated primarily from household liquid fuels used for room/water heating and cooking, as evidenced by high contributions to P and PO_4^{3-}-P. Secondary contributions to Pb, Ni, Cd and Mg^{2+} are often associated with non-exhaust traffic emissions (non-combustion related), including brake abrasion products and resuspended road dust (McKenzie et al., 2009), while elevated $C_2O_4^{2-}$-C and NO_3^--N are likely indicative of combustion emissions from tailpipe exhaust (Qin et al., 2017; Wang et al., 2007). Therefore, F5 was denoted as household liquid fuels and vehicular traffic (including both exhaust and non-exhaust sources). In contrast, F6 displayed substantially lower contributions from liquid fuel burning and non-exhaust markers but was characterised by elevated Hg and nss-K^+. Considering that the NPI identifies motor vehicles as the primary source of Hg, this signature is consistent with emissions from unleaded, petroleum-based fuel combustion, in which Hg and nss-K^+ are significant trace constituents (Spencer et al., 2006; Wilhelm et al., 2006). These observations suggest that F6 was derived predominately from vehicular exhaust emissions.

3.4 Discussion

To gain insight into how these high-intensity fires impacted biogeochemistry, we sampled aerosols arriving in Sydney, Australia during the 2019-20 Black Summer fires, and analysed the composition and source(s) of nutrients that comprised its plumes. Urban aerosols were also sampled one year later as a reference for ambient emissions. Given the longevity and reach of

wildfire emissions, our results are likely relevant across a wide geographic area and for multiple compartments (e.g. air, water, soil) of the Earth system.

Typically, fresh nutrient-bearing particles emitted from biomass burning are comprised of OC, followed by N and inorganic ions (K^+, NO_3^-, SO_4^{2-}, and/or Ca^{2+}) (Reid et al., 2005). These are released both as primary aerosols – derived directly from the combustion of biomass during fire propagation – and as secondary aerosols formed through the atmospheric transformation of primary gas emissions like CO_2, NO_x and SO_2 (Akagi et al., 2011; Fiedler et al., 2011; Huang et al., 2024; Li et al., 2003; Pósfai et al., 2003; Reid et al., 2005). In this study, the nutrient profile of Black Summer particles was comprised mostly of OC (Figure 3.1), with significant enrichment of NO_3^-, SO_4^{2-} and Ca^{2+} relative to ambient conditions (Figures 3.1 and 3.2). Primary tracers of combustion (K^+) were also highly prevalent across wildfire-enriched samples, as well as tracers of combustive and/or secondary processes ($C_2O_4^{2-}$, NO_3^-, SO_4^{2-}) (Figure 3.3). While these findings are broadly consistent with known emissions from fresh smoke plumes, wildfire-enriched samples in this study had lower mass-per-mass fractions of OC (107 mg g^{-1}), N (7 mg g^{-1}) and K^+ (4 mg g^{-1}) compared with urban samples (235 mg g^{-1} OC, 44 mg g^{-1} N, 5 mg g^{-1} K^+). This likely reflects a combination of factors. First, most plumes reaching our Sydney-based sampling location had undergone atmospheric processing and mixing during transport (Hirsch and Koren, 2021; Peterson et al., 2021). This is supported by our PMF analysis, which identified aged wildfire smoke as the largest component of wildfire-enriched samples in this study (~44 %, Figure 3.3). Aged smoke tends to be enriched with inorganic ions associated with secondary aerosol formation ($C_2O_4^{2-}$, NO_3^-, SO_4^{2-}) and contains less OC and K^+ from primary emissions (Reid et al., 2005). Second, the high severity of the Black Summer fires likely promoted more complete fuel combustion due to elevated temperatures, resulting in lower particulate OC and K^+, and enhanced elemental carbon (Rau, 1989). Third, many anthropogenic sources including motor vehicles emit significant quantities of OC, N and K (Song et al., 2006), so while mass-per-mass concentrations of these species appear lower in the wildfire samples, they were likely elevated in atmospheric concentration due to the exceptionally large PM load during the fires.

Wildfire-enriched samples were also enriched with mineral dust elements, including Fe, Ca, Mg, Mn, Si, Mo and Co (Figure 3.2) (Radhi et al., 2011; Strzelec et al., 2020a). These micronutrients were likely uplifted from surface soils by strong, fire-driven winds and subsequently incorporated into smoke plumes (Wagner et al., 2018). As expected, they were mainly associated with the two

mixed-soil factors identified in this study - Pb-contaminated soil and a combined soil and sea-spray source (Figure 3.3). Together, these constituted more than one third of analysed particle mass of wildfire-enriched samples, with contributions of ~22 % and ~16 %, respectively (Figure 3.3). Aged wildfire smoke was identified as an additional source of these elements (after burnt biomass and secondary aerosols), where further differentiation between sources was not possible (Figure 3.3). This may relate to our sampling approach, which employed composites that were integrated over the entire four-month period. Interestingly, despite P (phosphorus) often being considered a key constituent of mineral dust (Myriokefalitakis et al., 2016), this macronutrient was more abundant in the urban samples (Figure 3.1), where it was associated with household liquid fuels (Figure 3.3). This could be expected given that P was mostly detected as PO_4^{3-}, which tends to be associated with anthropogenic rather than mineral sources (Mahowald et al., 2008). Nonetheless, P was still present in the wildfire-enriched samples (Figure 3.1), where it was associated with the soil and sea-spray factor (Figure 3.3). Similar results were found for mixed-source micronutrients including Cd, Cu and Zn (Figures 3.2 and 3.3), with possible origins in crustal material and/or legacy anthropogenic deposits. As with other analytes, differences in aerosol loadings between the 2019-20 and 2020-21 sampling periods (see time series in (Gill et al., 2024)) likely resulted in elevated atmospheric concentrations during the fires, despite their lower mass contributions. Our results align with previous observations during the 2019-20 Black Summer wildfires, which report high loadings of mineral dust aerosols (Li et al., 2021), including Fe (Perron et al., 2022; Tang et al., 2021) and Mn (Perron et al., 2022), as well as anthropogenic contaminants like Pb (Perron et al., 2022). Despite the elimination of leaded petrol in Australia in 2002, legacy Pb deposits may be volatilised or remobilised from burnt vegetation and surrounding soil, as seen in several wildfires near Sydney between 1994 and 2013 (Isley and Taylor, 2020; Wu et al., 2017). The role of the 2019-20 Black Summer wildfires as a vector for harmful contaminants was examined previously (Gill et al., 2024) and is of significant concern for areas surrounding past and present human activity.

While the 2019-20 Black Summer wildfires were a significant source of atmospheric nutrients, only a fraction of the aeolian supply was readily soluble, and thus bioavailable to ecosystems in the receiving depositional environment. Mineral dust elements are typically characterised by low solubility, with dissolved fractions reported as <1 % for Cd and Si, <2.7 % for Fe, ~1-7 % for Cu, ~5-18.6 % for Ca, Mg, P and Zn, and ~12-57 % for Mn (Baker et al., 2006b; Journet et al., 2008; Li et al., 2022; Mendez et al., 2010; Schroth et al., 2009; Sholkovitz et al., 2010; Zhang et al., 2015). However, when mineral dust becomes entrained within wildfire smoke plumes, interactions with

pyrogenic aerosols and atmospheric aging processes can substantially increase the solubility of associated elements (Jickells et al., 2005; Mahowald et al., 2018; Winton et al., 2016). Despite the prevalence of aged smoke during the Black Summer event (Figure 3.3), the solubility of most soil-derived elements remained within the ranges reported for mineral dust, except for Ca (~46 %), Mg (~48 %), and Cd (~17 %) which showed greater solubility (Figure 3.1). Given the paucity of data on the fractional solubility of Ca, Mg and Cd in wildfire-enriched aerosols, we propose - based on prior studies of ash and soil - that this enhancement reflects their association with labile carbonate and oxide phases that dissolve readily, unlike less soluble metals such as Cu, Fe, Ni and Pb which are typically bound to more refractory mineral or organic fractions (Caetano et al., 2003; Kubier et al., 2019; Sánchez-García et al., 2023). In context of the 2019-20 fire season, nutrients associated with soil likely underwent early stages of atmospheric processing enroute to Sydney, leading to the rapid dissolution of alkali earth elements (Ca, Mg) and Cd and suggests that deposition of wildfire-enriched aerosols may increase the alkalinity of receiving waters. However, given the longevity and reach of Black Summer's plumes, aeolian nutrients such as Fe are likely to be more soluble in regions downwind of Australia's mainland, especially in remote oceanic locations over the southern hemisphere. This is supported by measurements of aerosols in Tasmania during the 2018-19 and 2019-20 fire seasons, which show nearly double the Fe solubility in distal (>600 km) versus proximal (<200 km) emissions (Perron et al., 2022).

Climate change is projected to increase the frequency and severity of wildfire events in Australia (Di Virgilio et al., 2019). As such, an improved understanding of how these atmospheric perturbations influence biogeochemistry is warranted, especially in extreme instances like the recent 2019-20 Black Summer wildfires. Our results indicate that PM captured in Sydney during this period was predominantly shaped by wildfire emissions and fire-mobilised dust, with PMF analysis estimating that aged wildfire smoke (Factor 1) accounted for ~44% of analysed mass, and soil-related factors (Factors 2 and 3) a further ~38%, together representing ~82% of analysed sample mass. This material originated from a diversity of sources, including biomass smoke, secondary aerosols, mineral dust, legacy contaminants and sea-spray. Within these mixed plumes, we detected an array of bioactive nutrients, with substantial enrichment of water-soluble ions and trace elements. Ocean observations have demonstrated the importance of nutrient sources for biological responses, where the highest increase in oceanic primary producers (phytoplankton) during the 2019-20 Black Summer was associated with entrained mineral dust that was deposited close to Australia, compared with widespread biomass smoke

particles which elicited relatively weak phytoplankton responses (Li et al., 2021). This has been attributed to the provision of Fe which limits phytoplankton growth in these ocean regions (Doblin et al., 2016; Tang et al., 2021). Wildfire-enriched macronutrients displayed a median molar ratio of 39 : 2 : 1 : 1 : 4 for OC : N : P : K : SO_4^{2-}-S, highlighting the disproportionate supply of OC relative to major growth-limiting nutrients in aquatic and terrestrial ecosystems. Deposition of OC is likely to fuel bacterial activity in both systems, though its bioavailability depends on solubility and degradation pathways (Azam et al., 1983; Bodí et al., 2014; Nagata, 2000). N and P remain the dominant limiting nutrients globally, where they support growth, metabolism, protein synthesis and/or photosynthetic processes in a range of organisms (Chapin et al., 2011). The higher ratio of N : P in wildfire-enriched compared to urban aerosols implies a greater stimulatory effect in N-limited rather than P-limited systems, especially given the differences in solubility (Figure 3.1). Under changing environmental conditions, particulate P can be remineralised, potentially enhancing its availability post-deposition (Chambers et al., 1995; Li et al., 2017). S and K are key nutrients for plant growth (Kopriva et al., 2019; Leigh and Wyn Jones, 1984), where the former may also influence the acidification and acid-neutralising capacity of soils (Brahney et al., 2013). While the deposition of bioactive aerosols may alleviate nutrient limitation and increase productivity of receiving environments, excess input from severe wildfires like the 2019-20 Black Summer may also cause eutrophication and have adverse effects, such as proliferation of cyanobacteria and hypoxia (Smith and Schindler, 2009). Evidence of macronutrient delivery following the 2019-20 Black Summer fires have been documented in estuarine sediments (OC, N and P) (Barros et al., 2022) and freshwater catchments (DOC pulses) (Biswas et al., 2021), highlighting the importance of understanding ecosystem responses to wildfire-enriched inputs. This remains a priority area of research.

Funding

This work was supported by the Climate Change Cluster and the Faculty of Science at the University of Technology Sydney (UTS) through the provision of operational funding and equipment. Additional support was provided the NSW Department of Planning and Environment (DPE) through in-kind contributions of expertise and consumables. RLG was supported by an Australian Government Research Training Program Scholarship at UTS.

CRediT authorship contribution statement

Raissa L. Gill: Writing - review & editing, Writing - original draft, Visualization, Methodology, Investigation, Formal analysis, Data curation, Conceptualization. **Robert Fleck:** Writing - review & editing, Methodology, Investigation, Conceptualization. **Ky Chau:** Writing - review & editing, Investigation. **Mika T. Westerhausen:** Writing - review & editing, Methodology, Investigation. **Thomas E. Lockwood:** Writing - review & editing, Methodology, Investigation. **Jake P. Violi:** Writing - review & editing, Investigation. **Peter J. Irga:** Writing - review & editing, Conceptualization. **Fraser R. Torpy:** Writing - review & editing, Supervision, Methodology, Conceptualization. **Martina A. Doblin:** Writing - review & editing, Supervision, Conceptualization.

Declaration of competing interest

The authors declare that they have no known competing financial interests or personal relationships that could have appeared to influence the work reported in this paper.

Acknowledgements

The authors would like to acknowledge Dr Helen Price for her assistance with carbon and nitrogen analysis, including instrument calibration, training, and troubleshooting.

4. Acute exposure to wildfire-enriched aerosols elicits divergent microbial responses across multiple Australian estuaries

Raissa L. Gill [1, 2, #], Callum Muir [1], Aaron Wright [3], Colin Johnson [3], Robert Fleck [2], Peter Scanes [3], Fraser R. Torpy [2], Martina A. Doblin [1, 4]

[1] Productive Coasts, Climate Change Cluster, University of Technology Sydney, Ultimo, NSW, 2007, Australia

[2] Plants and Environmental Quality Research Group, School of Life Sciences, Faculty of Science, University of Technology Sydney, Sydney, NSW, Australia

[3] Estuary and Catchments Science, New South Wales Department of Planning, Industry and Environment, Sydney, NSW, Australia.

[4] Sydney Institute of Marine Science, Mosman, NSW, 2088, Australia

[#] Corresponding Author: raissa.l.gill@student.uts.edu.au; PO Box 123 Ultimo, NSW, 2007, Australia

Chapter 4 is currently presented as a draft manuscript in preparation for submission.

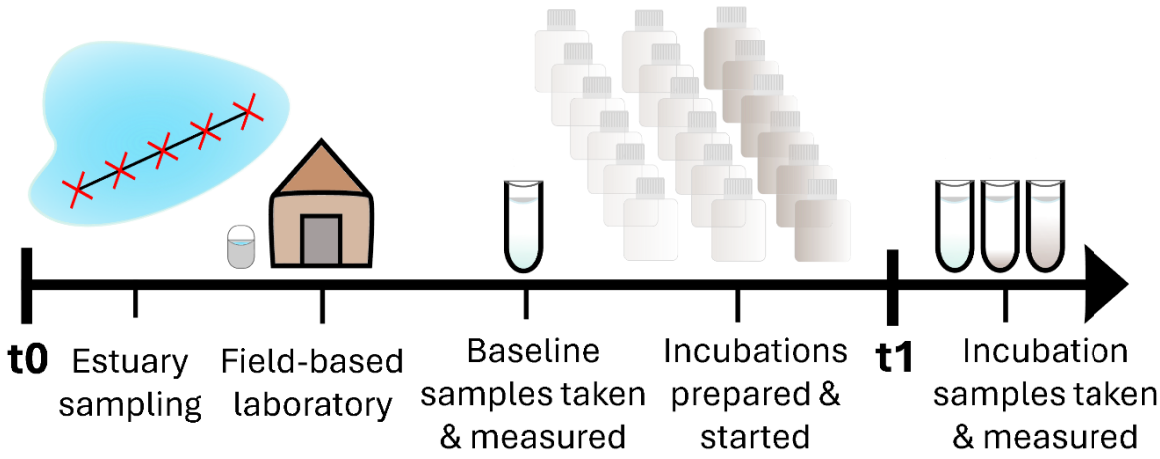
Highlights

- Under the average scenario for wildfire-enriched aerosol deposition, estuaries displayed divergent microbial responses, including heterotrophy, autotrophy, and no measurable response.
- Under the extreme deposition scenario, similar impacts were observed for all estuaries with a universal shift towards heterotrophy and high-DNA bacterial populations.
- Potential for inhibition of Photosystem II with exposure to toxic metals in wildfire-enriched particles, leading to a reduction in effective quantum yields of picophytoplankton.

Abstract

The Australian Black Summer 2019-20 wildfires were unprecedented in their magnitude and extent, however the impact to Australia's estuaries remain largely unexamined. Here we use atmospheric particulate matter (PM) captured during the fires to assess the acute response of aquatic microbial communities in five estuaries on the NSW South Coast of Australia. Natural communities were incubated with wildfire-enriched PM in concentrations indicative of average and extreme scenarios for dry deposition, modelled using empirical particulate data from the region. Changes to phytoplankton photophysiology and the abundances and traits of key microbial taxa (phytoplankton, bacteria, viruses) were quantified after ~24 hours of exposure. In the average scenario, the five estuaries exhibited divergent responses that fell broadly into three categories: 1) a heterotrophic response, 2) an autotrophic response, and 3) no detectable response. Heterotrophic responses were characterised by the following: an increase in the abundance of low-DNA bacteria and viruses; larger, more granular but less fluorescent *Synechococcus* cells; a decline in *Synechococcus* and eukaryote population; and a reduction in the effective quantum yield of phytoplankton communities. Shifts towards autotrophy were characterised by the opposite changes in microbial populations, and were moderately associated with larger, more acidic and less saline estuaries, with a history of nutrient limitation and more pigmented cyanobacterial populations, amongst other attributes. Under extreme wildfire conditions, however, responses converged across all estuaries, marked by the proliferation of more metabolically active bacteria (high-DNA containing), declines in the pigmentation of *Synechococcus*, and reduced effective quantum yields of phytoplankton populations, indicating the potential for metal-induced impairment of Photosystem II. These results highlight the acute response and relative flexibility of NSW estuaries to wildfire inputs; however, the mid-to-long-term effects of wildfire additions remains largely unknown. We recommend future studies perform longer-term incubations and monitoring programs, more detailed analyses such as changes in microbial community composition, and sample additional locations to improve our understanding of drivers of estuarine responses to wildfire.

Graphical abstract



Keywords

Wildfire aerosols; Atmospheric deposition; Aquatic microbes; Estuaries; Phytoplankton; Bacteria; Physiological traits; Flow cytometry

Abbreviations

Alpha (α)	relative rate of photosynthesis onset
AvDepth_m	average estuary depth (m)
BAC	heterotrophic bacteria
BRO	Lake Brou
C_µScm	conductivity (µS/cm)
CatSA_km2	catchment surface area (km^2)
CBD	central business district
CDOM_RFU	coloured DOM (RFU)
Cells/mL	cell abundance (cells/mL)
CHL	chlorophyll (green pigment)
CHL/µm	CHL autofluorescence per µm cell diameter
CHL_µgL	estuary CHL content (µg/L)
CLY	Clyde River
ColA_PtCo	apparent colour (Pt/Co)
ColT_PtCo	true colour (Pt/Co)
Depth_m	estuary depth (m)
DOM	dissolved organic matter
DO_mgL	dissolved oxygen (mg/L)
DO_perc	dissolved oxygen (%)
DN_µgL	dissolved N (µg/L)
DP_ugL	dissolved P (µg/L)
ESD(µm)	equivalent spherical diameter (µm)
EstSA_km2	estuary surface area (km^2)
EstVol_ML	estuary volume (ML)
EUK	eukaryotes
fDOM_QSU	fluorescent DOM (QSU)
fDOM_RFU	fluorescent DOM (RFU)
Fq'/Fm'	effective quantum yield
FSC	forward scatter (cell size proxy)
Fv/Fm	maximum quantum yield
HDNA	high-DNA containing bacteria
HVAC	heating, ventilation and air conditioning
LDNA	low-DNA containing bacteria
MOR	Moruya River
N	nitrogen
NH3N_ugL	ammonia as N (µg/L)
NOxN_ugL	nitrogen oxides as N (µg/L)
P	phosphorus
PE	phycoerytherin (orange pigment)
PE/µm	PE autofluorescence per µm cell diameter
PE_µg/L	estuary PE content (µg/L)
PE_RFU	estuary PE signal (RFU)
pH	pH
PHY	phytoplankton
PM	particulate patter
$PM_{2.5}$	PM with diameter <2.5 µm
PM_{10}	PM with diameter <10 µm, includes $PM_{2.5}$
PN_ugL	particulate N (µg/L)
PP_ugL	particulate P (µg/L)
PSII	photosystem II
(ratio)	abundance ratio
Sal_ppt	salinity (ppt)
Secchi_m	secchi depth (m)
Si	silicon
SiO2Si_ugL	silicon dioxide as Si (µg/L)
SPC_µScm	specific conductivity (µS/cm)
SRP_ugL	soluble reactive P (µg/L)
SSC	side scatter (related to cellular complexity)
SSC/µm	SSC per µm cell diameter
SYBR	nucleic acid stain
SYN	synechococcus
TAB	Lake Tabourie
Temp_C	temperature (°C)
TN_ugL	total N (µg/L)
TP_ugL	total P (µg/L)
TSP	total suspended particles (<100 µm)
Turb_NTU	turbidity (NTU)
TUR	Tuross River
VLP	virus-like particles
VSSC	violet side scatter (related to cellular complexity)

4.1 Introduction

During a wildfire, vast quantities of burnt vegetation and smoke are emitted into the atmosphere, including dust particles from surface soil which are entrained by fire-driven wind and pyro-convection (Gaudichet et al., 1995; Wagner et al., 2018). Wildfire aerosol and dust material can remain on the soil or in the air for prolonged periods and can be transported great distances before being deposited in aquatic environments by dry (gravitational settling) or wet (collision during rainfall and subsequent run off) depositional processes (Mahowald et al., 2011). On entry to the water column, this material begins to impact water quality and becomes available to a host of aquatic organisms (Bixby et al., 2015). Of particular interest are the aquatic microbes, which form the base of the aquatic food web via phytoplankton photosynthesis (Araujo-Lima et al., 1986), carbon cycling by bacteria (Azam et al., 1983), aided by viral lysis (Bratbak et al., 1994).

Aeolian wildfire inputs can vary greatly in their composition but are comprised predominately of organic matter and include bioactive material such as trace metals and water-soluble ions (Alves et al., 2010; Samsonov et al., 2012; Strzelec et al., 2020a; Yamasoe et al., 2000). Upon deposition to aquatic environments, these analytes can have significant impacts on estuarine and marine microbes (see summaries by Arrigo, 2005; Kolarova and Napiórkowski, 2021; & Merchant and Helmann, 2012). However, predicting responses remains complex as only a fraction of this material is soluble (and bioavailable) in aquatic environments (Perron et al., 2020b). The size of this soluble fraction varies greatly depending on factors such as particle mineralogy, pH, size, degree of atmospheric processing etc. (Marcotte et al., 2020; Park et al., 2013), with observations of between 0.1 and 98 % trace metal solubility over the Atlantic Ocean (Baker et al., 2013). This is further complicated by the presence of potentially toxic analytes in wildfire smoke like copper (Kelly et al., 2021; Sparks and Wagner, 2021), which can exert harmful effects on phytoplankton (Jordi et al., 2012; Paytan et al., 2009).

Many studies have recognised the fertilising role of aerosolised dust deposition to the ocean (Mahowald et al., 2018 and references therein), which provides iron and other nutrients sufficient to alter production at all levels of the microbial food web (Ardyna et al., 2022; Tsagaraki et al., 2017; Tsiola et al., 2017). Similar observations during wildfires remain considerably fewer, with most research to date focused on impacts to air quality, human health, the economy, and

terrestrial ecosystems. However growing recognition of wildfire impacts beyond land has spurred recent interest in the responses of aquatic ecosystems.

Estuaries are vital hubs of biological and human activity, serving as critical interfaces between land and sea. These transitional zones are among the most productive ecosystems on Earth (Douglas et al., 2022), providing essential services including carbon sequestration, nutrient cycling, water filtration, and nursery habitats for numerous fish and invertebrates (Douglas et al., 2022). Unlike the open ocean, estuaries are shallow, semi-enclosed, and located much closer to vegetation fuels, making them susceptible to high exposures from wildfire emissions.

Due to the inherent variability in estuary characteristics (e.g. physicochemistry, nutrient status, resident biota etc.), the impact of wildfire inputs has the potential to vary greatly (Smits et al., 2024). Given that many freshwater systems are phosphorus and nitrogen limited, it is likely that wildfire smoke plumes would enrich these ecosystems (Elser et al., 2007). Given the quantity of particulate matter (PM) emitted from wildfires, runoff from surrounding catchments that would also contribute ash and other wildfire debris, and time required to remineralise particulate forms of limiting nutrients the impacts could be long-lived (Chambers et al., 1995; Li et al., 2017). Conversely, the alleviation of nutrient limitation and increase in productivity of receiving environments may be constrained by the presence of toxic elements in wildfire aerosols (Harper et al., 2019; Paytan et al., 2009), the proliferation of harmful microbial taxa (Smith and Schindler, 2009), and water quality issues such as hypoxia (Smith and Schindler, 2009). Given that wildfire aerosol inputs to estuaries vary widely in quantity and composition – even from the same fire – controlled experimental approaches are necessary to identify key factors influencing estuary responses.

Devastating fire seasons are on the rise, with wildfires projected to increase in their frequency, severity and duration due to anthropogenically-driven climate change (IPCC, 2021). Certainly, increases in both wildfire frequency and spatial extent have been well documented in regions such as Canada (Kasischke and Turetsky, 2006) and the United States (Westerling, 2016), and is evidenced by several recent wildfires around the globe, including the 2017 Chilean fires (>500,000 ha burnt; (Bowman et al., 2019)) and 2019-20 Australian Black Summer fires (30.4 million ha burnt; (Bowman et al., 2020)). The latter was one of the worst fire seasons in recorded

Australian history, with significant consequences for human (Borchers Arriagada et al., 2020; Johnston et al., 2021) and animal (Ward et al., 2020) wellbeing, notwithstanding the vast quantity of pyrogenic aerosols emitted into the atmosphere (Hirsch and Koren, 2021). Given the proximity of the 2019-20 Black Summer wildfires to Australia's coastline, understanding their potential impacts on aquatic and marine ecosystems is vital for management, especially in fire-prone nations like Australia.

During severe wildfires, assessing the impact of atmospheric aerosol deposition on nearby estuaries is challenging - particularly within the water column, where pyrogenic inputs and exposed microbial communities are potentially rapidly diluted and dispersed through tidal and oceanic exchange (Roper et al., 2011). In contrast, surface runoff from burnt catchments can elevate estuarine nutrient concentrations for several months post-fire (Lane et al., 2008), enabling safer and more straightforward monitoring. However, these inputs depend on post-fire precipitation to mobilise deposited material through soil and vegetation, making them temporally and chemically distinct from dry deposition originating directly from overhead plumes (Adachi et al., 2022). In this study, we addressed this gap in knowledge by simulating the acute effects of wildfire smoke deposition across multiple estuaries on the NSW South Coast of Australia. Our aim was to characterise short-term microbial responses during active burning phases, which has significant implications for understanding risks to industries that rely on good water quality such as aquaculture.

4.2 Material and methods

4.2.1 Study region

Estuaries in the Southern Rivers region (NSW, Australia) were selected based on their proximity to Batemans Bay (35.7162° S, 150.1795° E), a town located ~280km from Sydney's Central Business District (CBD) on the South Coast of NSW, Australia. Estuaries in this region tend to be relatively pristine, with a population of ~11,300 people (as of 2016; Australian Bureau of Statistics 2016) and is a significant recreational and commercial hub for boating, fishing, and oyster farming. Batemans Bay and the majority of the South Coast were heavily impacted by the Australian Black Summer 2019-20 wildfires (Department of Climate Change, Energy, 2020), where estuaries suffered stream length burns of between 52 and 74 % (Fryirs et al., 2022). The

Currowan fire was the first to start in the South Coast region, and burned for 74 days from the 26th of November 2019 until the 9th of February 2020, at which point 80 % of land was impacted or burned, including mangroves all the way down to the waterline (Shoalhaven City Council, 2020).

Initially, six estuaries were selected for inclusion in this study, including three lagoons and three rivers: Clyde River (CLY), Moruya River (MOR), Tuross River (TUR), Lake Brou (BRO), Lake Tabourie (TAB), Lake Wollumboola (WOL). However, due to the highly unusual traits of one estuarine community during sampling (Lake Wollumboola), this site was removed from the study as it was incomparable to the other five sites and unrepresentative of NSW estuaries generally (Supplementary Figure 4.1). The location and physical characteristics of each of the estuaries included in this study are summarised below (Figure 4.1 and Supplementary Table 4.1).

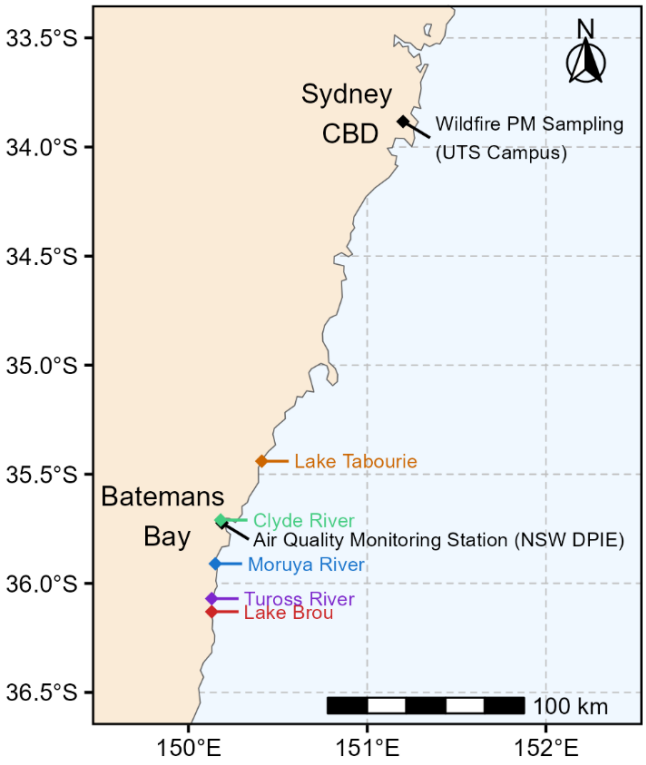


Figure 4.1 Site map of the five estuaries sampled near Batemans Bay on the South Coast of NSW, Australia (coloured diamonds). Also shown are the locations of particulate matter (PM) sampling in Sydney's CBD and air quality monitoring in Batemans Bay during the 2019-20 Black Summer wildfires (black diamonds). PM samples were collected at the University of Technology Sydney (UTS) Ultimo campus, and air quality data was obtained from the NSW Department of Climate Change, Energy, the Environment and Water (DCEEW).

4.2.2 Wildfire-enriched PM sampling

Experiments utilised PM captured in Sydney, Australia during the 2019-20 Black Summer wildfires, as described in Chapters 2 and 3 of this thesis. Briefly, suspended PM from ambient wildfire smoke was captured in Heating, Ventilation and Air Conditioning (HVAC) building filters in the Sydney CBD at the University of Technology Sydney (UTS) Ultimo campus (33.8832° S, 151.2005° E) between November of 2019 and February of 2020 (inclusive). A filter forensics approach was used to extract this material by vacuum through a 25 µm pre-screen into pre-weighed sealed cassettes. Three individual wildfire cassettes were combined to create a composite for use in bottle incubations, which was stored in dry dark conditions until required.

4.2.3 Estimating dry deposition flux of PM_{10}

The quantity of PM used in experimental incubations was determined by calculating two dry deposition flux scenarios using PM_{10} concentrations recorded by NSW DCCEEWs bushfire emergency monitoring station (Multi-channel EDT DustTrak – TSI 8543/8533, TSI, USA) deployed in Batemans Bay (35.7234° S, 150.1872° E) (Figure 4.1). This monitoring station comprises a light scattering laser photometer that provides concentrations of total suspended particulate (TSP – PM <100 µm diameter), PM_{10} and $PM_{2.5}$ (PM <10 and <2.5 µm diameter, respectively), and is recorded as hourly averaged concentrations in µg m^{-3} on NSW DCCEEW's rural air quality network (NSW Department of Climate Change, Energy, the Environment, 2021a). Given that 99.5 ± 0.1 % of PM captured during the Black Summer fires were <10 µm in diameter (based on filter-extracted material in our previous study: Gill et al., 2024), PM_{10} concentrations were considered representative for estimating deposition fluxes. Hourly averaged PM_{10} concentrations from the 10th of December 2019 (monitor deployment) to the 17th of April 2020 (decommissioned) were downloaded from the NSW Government's Air Quality API (NSW Department of Climate Change, Energy, the Environment, 2021b) using R software (R Core Team, 2021) and associated packages ('dplyr'; (Wickham et al., 2021), 'httr'; (Wickham, 2020), 'jsonlite'; (Ooms, 2014)). Daily concentrations were also calculated by averaging over the 24-hour period.

To quantify the mass of PM_{10} deposited on an estuary surface per unit area/time, the daily dry deposition flux (F) associated with each of these concentrations (C) was calculated as a function of dry deposition velocity (V) (Duce et al., 1991) (Equation 1). V is a function of various attributes influencing dry deposition, including particle size and meteorological conditions (i.e., wind

speed, humidity, air viscosity etc.). As such, this parameter was estimated to be 2 cm^{-1} s^{-1} based on estimates of dry deposition velocities for coarse particles in coastal and nearshore ocean regions (Duce et al., 1991). This is consistent with estimates used in other Australian-based studies (Perron et al., 2020b; Strzelec et al., 2020b; Winton et al., 2016).

$$F\ (g\ m^2\ d^{-1}) = (C\ \mu g\ m^3 \times 10^{-6}\ g\ \mu g^{-1}) \times (V\ cm^{-1}\ s^{-1} \times 10^{-2}\ m\ cm^{-1} \times 8.64{\times}10^4\ s^{-1}\ d^{-1}) \quad (1)$$

where F is the dry deposition flux ($g/m^2/d$), V is the dry deposition rate (cm/s), and C is the daily averaged concentration of PM_{10} in the atmosphere ($\mu g/m^3$).

4.2.4 Wildfire deposition scenarios

Two wildfire scenarios were selected based on estimates of dry deposition flux: 1) an "Average Scenario" of 0.17 g m^{-2} d^{-1}, reflecting the mean flux of PM_{10} in Batemans Bay during local wildfires (from 10th of December 2019 until 9th of February 2020 inclusive); 2) an "Extreme Scenario" of 4.95 g m^{-2} d^{-1}, reflecting the maximum hourly flux of PM_{10} in the same time frame. We assumed a consistent depth of 1m when converting surface area deposition fluxes (0.17 and 4.95 g m^{-2} d^{-1}) to water concentrations (0.17 and 4.95 mg L^{-1}), given that estuaries were generally shallow (Supplementary Table 4.1). Further, our focus here was to examine how resident microbes from different estuaries respond to the same quantity of PM, rather than attempting to recreate the exact concentration as a function of varying estuary depth.

4.2.5 Estuary field sampling

Estuary sampling was undertaken during the austral Autumn period (between the 18th of April and 19th of May 2021 inclusive) in collaboration with NSW DCCEEW, using field procedures consistent with the NSW Government's state-wide estuary monitoring program (Hallett et al., 2016; Office of Environment and Heritage (OEH), 2016). A powered vessel or manned canoe equipped with a calibrated water quality sonde (YSI EXO 2, Yellow Springs Instruments; OH, USA) at a depth of ~0.5 m was deployed, and a 1 L vertical pole sampler was used for water collection. All equipment was rinsed twice with local estuary water. The probe recorded date, time, GPS location, depth, and various water quality variables (temperature, dissolved oxygen, conductivity, specific conductivity, salinity, pH, turbidity, phycoerythrin fluorescence, chlorophyll fluorescence, fluorescent dissolved organic matter). These variables are

summarised in the supplementary material, including abbreviations used in subsequent figures (Supplementary Table 4.2). Sampling was performed at five points along a transect spanning ~200 m (~40 m apart), where 1 m integrated water samples were collected and combined for a single composite sample. Several aliquots of estuary water were also taken for nutrient analyses, including total, filtered and unfiltered fractions of nitrogen, phosphorus and silica. Dissolved samples were collected by a pre-flushed 0.22 µm syringe filter into sterile tubes, which were frozen until analysis. All samples were transported to a field-based laboratory within ~2 h of collection. All samples were taken in the morning during the falling of the tide. The date/time of sampling and prevailing conditions are summarised in the supplementary material (Supplementary Table 4.3).

4.2.6 Experimental bottle incubations

A field-based laboratory was set up in the Batemans Bay area to ensure experiments with living microbial communities could be conducted within 3 h of collection. An incubation bath was constructed (Figure 4.2) using a large, clear plastic container (90 L capacity) insulated with rubber matting on the exterior to reduce heat loss (Figure 4.2A). The bath was filled with tap water and a constant temperature of 19.5 ± 1.5 °C (min/max) was achieved using a heating immersion circulator (EH (v.2), Julabo GmbH, Germany) fixed to the interior corner of the bath (Figure 4.2B), supplemented with an additional pump (Maxi 102 Power Head, Aqua One, Australia) for mixing (Figure 4.2C). A custom-made LED light source with a cool white spectral output was suspended on a mounting frame to illuminate the bath at a surface irradiance of 195 ± 15 µmol photons m^{-2} s^{-1} (min/max) (Figure 4.2E). This was set to a 12:12 light:dark cycle, consistent with the timing of sunrise/sunset in Batemans Bay (sunrise at ~7:00, sunset at ~19:00 AEDT).

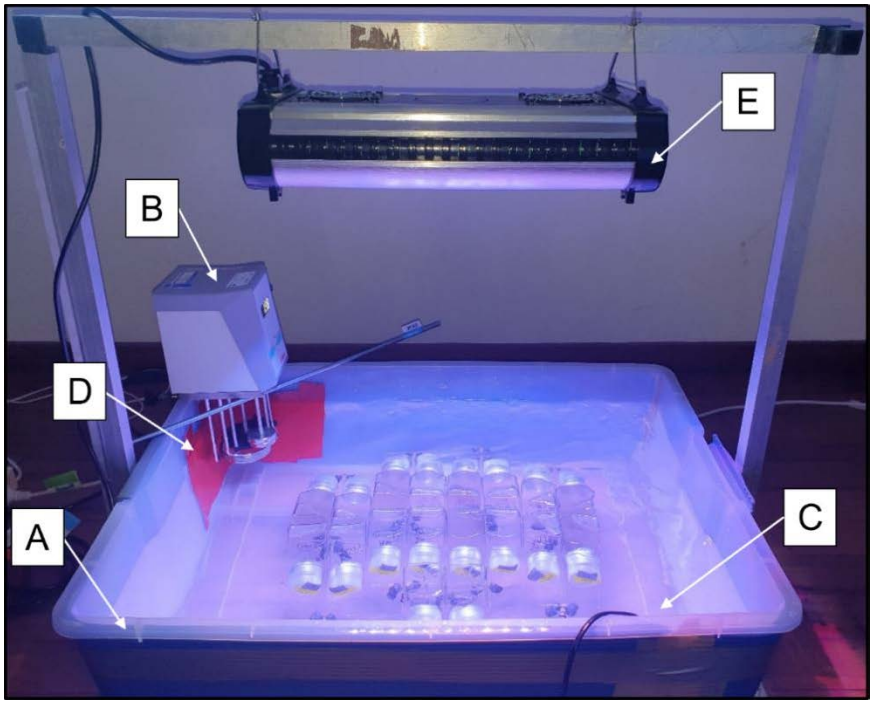


Figure 4.2 Photograph of the incubation bath used to conduct 24-hour bottle incubation experiments. The bath was constructed using a 90 L plastic container insulated with rubber matting (A) and was heated with a heating immersion circulator (B) supplemented with an additional pump (C) for mixing. The interior corner was protected against the heating element using thermally resistant mounting tape (D). An LED light with a cool white spectral output was used to illuminate the bath (E).

Upon immediate return from field sampling, estuary water was filtered through a clean 200 µm nylon mesh to remove mesozooplankton and debris, and samples (n=3) were taken to enumerate the baseline microbial community ("Estuary Baseline"). Incubation vessels were then filled with <200 µm estuary water, including eighteen 170 mL clear narrow-mouth polycarbonate bottles (Nalgene 2015 series, ThermoFisher Scientific, USA). Wildfire-enriched PM described above (section 4.2.2) was added as a single dose in concentrations corresponding to the Average Scenario (n=6) and Extreme Scenario (n=6) for dry deposition (section 4.2.4). This was achieved by adding pre-weighed portions to filtered estuary water to create stock solutions, which was subsequently dispensed into incubation bottles following homogenisation by vigorous mixing for 1 minute. Remaining incubation bottles (n=6) were dispensed with filtered estuary water that was PM-free and run simultaneously as a control ("Control Incubation"). Incubation bottles were sealed and parafilm was applied around the neck and lid for additional leak protection. Incubation bottles were then submerged (~15 cm below surface) and randomly distributed across the bottom of the bath, centred under the overhead light (Figure 4.2). The time of

incubation onset was noted, and bottles were removed ~24 hours later the next day for sample measurement and preservation.

4.2.7 Photophysiological traits

4.2.7.1 Analysis preparation

Photophysiology was assessed using a pulse amplitude modulated fluorometer (Water-PAM) and WinControl software (Heinz Walz GmbH, Germany). In preparation, samples were first gently inverted several times to homogenise microbes and 3 mL aliquots were transferred to glass tubes and dark adapted for 30 minutes. Meanwhile, an additional aliquot was taken to blank the Water-PAM against local background fluorescence and to adjust gain settings. This was achieved by syringe-filtering the aliquot through a 0.22 µm Sterivex filter into a clean cylindrical quartz cuvette (to remove picophytoplankton) and checking chlorophyll-a fluorescence for negligible emission using a single saturating pulse of blue light (460 nm; pulse duration = 0.6 s; pulse intensity = 893.9 ± 19.3 µmol photons m^{-2} s^{-1}). If fluorescence was detected, the aliquot was filtered again and re-checked. After the Water-PAM was blanked, gain settings were adjusted to a base fluorescence of ~150 (gains varied between 22 and 26 across estuaries).

4.2.7.2 Sample measurement

Following 30 minutes of dark adaptation, samples were carefully transferred in the dark into a clean cuvette and placed in the emitter-detector unit of the Water-PAM. Once fluorescence stabilised (~60 s), a single saturating pulse was emitted (as above) to measure dark-adapted minimum (F0) and maximum (Fm) fluorescence yields. When fluorescence re-stabilised (~60 s), a rapid light curve (RLC) was initiated whereby phytoplankton were exposed to 10 seconds of irradiance at nine incremental steps over 90 seconds, with pulses ranging from 0 to 893.9 ± 19.3 µmol photons m^{-2} s^{-1}. Fluorescence yields were taken before and after each light step under actinic light, giving F' and Fm' respectively. After photophysiological measurement, samples were transferred to 2 mL cryogenic vials (Corning, USA) containing a fixative (paraformaldehyde, 1 % v/v final concentration) (Emgrid Australia, Australia). Vials were gently mixed and after 15 minutes snap frozen in liquid nitrogen. These were then stored at –80 °C until flow cytometric analysis back at the university laboratory.

4.2.7.3 Verification

Actinic light levels were checked upon return to the university with a 4-pi light sensor fitted to an emitter-detector unit (Universal Light Meter & Data Logger (ULM-500), Heinz Walz GmbH, Germany), which detected light received in the centre of the same cuvette filled with Milli-Q water (Ω 18.2; Millipore, Germany). Light levels have been adjusted throughout and in subsequent calculations. Actinic light was also examined for each treatment by preparing PM in Milli-Q water and measuring as above. In this case, two independent measurements were made to minimise potentially skewed distributions due to particle settling effects, including: 1) starting at light level 1 through to 12, and 2) starting at light level 12 through to 1. There was no significant difference in light received by the emitter-detector unit ($p < 0.05$, Supplementary Figure 4.2). As such, light levels have not been treatment adjusted in subsequent calculations.

4.2.7.4 Data processing

Several photophysiological traits were derived from fluorescence yield measurements to assess the photosynthetic health of phytoplankton. Firstly, the maximum quantum yield of PSII (Fv/Fm) was derived from dark-adapted F0/Fm emitted before/after a single saturating pulse of light (Equation 2). This reflects the dark-adapted photosynthetic efficiency of open reaction centres in PSII, with higher values indicating that cells have the potential to generate greater rates of electron transport through their PSII centres (Genty et al., 1989). To understand photosynthetic efficiency under irradiated conditions, the effective quantum yield of PSII (Fq'/Fm') was derived from F'/Fm' emitted before/after each step of the RLC (Equation 3). This depicts the effective rate of electron transport through PSII under increasing light levels of the RLC. Both maximum and effective quantum yields were used to derive relative electron transport rates (rETR) (Equation 4).

$$F_v/F_m = \frac{(F_m - F_0)}{F_m} \quad (2)$$

where F_0 and F_m are the dark-adapted minimum and maximum fluorescence yields.

$$F_q'/F_m' = \frac{(F_m' - F')}{F_m'} \quad (3)$$

where F' and F_m' are the irradiated minimum and maximum fluorescence yields.

$$rETR = F_q'/F_m' \times E \quad (4)$$

where F_q'/F_m' is the effective quantum yield of PSII, and E is irradiance in µmol photons m^{-2} s^{-1}.

To compare RLCs, each was fitted to the equation of Platt et al. (1980) as has been done in previous studies (Ralph et al., 2002; Ralph and Gademann, 2005). Specifically, the rETRs for each individual RLC were fitted to a double exponential decay function using a non-linear Maquardt-Levenberg regression algorithm, which describes an initial linear photosynthetic response to increasing light followed by a plateau where the cells may become photoinhibited (Platt et al., 1980). Due to substantial variability in rETRs at the higher actinic light levels, curves were fitted up to actinic light level 9 (361.1 µmol photons m^{-2} s^{-1}) only. Curve fits were generally very good (R^2 ≥ 0.90), however those with poorer fit were inspected visually to determine if they had a substantial impact on the trajectory of the curve (they did not). Alpha ("α") which describes the relative rate of photosynthesis onset was derived from these curves as the initial slope. Other photophysiological traits (e.g. photosynthetic capacity, minimum saturating irradiance) were not examined further due to the low actinic light levels used. Curve fitting and alpha calculations were performed in R software (R Core Team, 2021) using the 'phytotools' package (Silsbe and Malkin, 2015).

4.2.8 Cellular abundance and functional traits

4.2.8.1 Analysis preparation

Abundances and traits of phytoplankton (PHY), bacteria (BAC), and virus-like particles (VLP) were quantified on a flow cytometer (Cytoflex LX, Beckman Coulter, USA) which was operated using CytExpert proprietary software. The flow cytometer was operated in plate mode with fresh Milli-Q water as sheath fluid and was deep cleaned prior to analysis with detergent (FlowClean Cleaning Agent, Beckman Coulter, USA). Calibration was performed using a suspension of fluorescent microspheres with known optical properties (CytoFLEX Daily QC Fluorospheres, Beckman Coulter, USA; 3 drops per 1 mL). The flow cytometer was then backflushed several times to flush out microspheres, and Milli-Q water was analysed to check background counts (≤10 events s^{-1}). Sample acquisition employed blue excitation (488 nm) and a variety of detectors, including red (690/50 nm), orange (585/40 nm), and green (525/40 nm) fluorescence, side scatter (SSC) (488 nm), Violet SSC (VSSC – greater resolution) (405 nm), and forward scatter (FSC) (488 nm). The fluorescent detectors allowed discrimination between populations based on their

natural chlorophyll (red; CHL) and phycoerytherin (orange; PE) pigment content, and the artificially stained nucleic acid content of cells (green; SYBR). SSC/VSSC signals reflect their level of complexity or granularity, whereas FSC signals are highly correlated with cell size. Once the flow cytometer was ready, frozen samples were thawed at room temperature for analysis.

4.2.8.2 Sample measurement

Bacteria and VLP were quantified first using methods described Marie, et al. (1999a, 1999b). Sub-samples (40 µL) were plated into 96-well flat-bottom cell culture microplates (200 µL working volume, Corning Costar, USA) and diluted in 0.22 µm filtered TE buffer (10 mM Tris-HCl, 1 mM disodium EDTA, pH = 8.0, Sigma-Aldrich, USA) stained with SYBR Green I (1:20,000 dilution, SYBR Green I Nucleic Acid Gel Stain – 10,000X concentrate in DMSO, Invitrogen, USA). Two controls were also prepared to set the gating threshold for background green fluorescence, including: 1) "Unstained sample" containing sample water diluted in unstained, 0.22 µm filtered TE buffer for each estuary, prepared by pooling replicates within each estuary; 2) "Stained buffer" containing stained, 0.22 µm filtered TE buffer. Plates were then incubated in the dark for 15 min until analysis. Acquisition was triggered by the green fluorescence signal (>1200 threshold to minimise contributions from unstained particles) and enumerated at a low flow rate for one minute (10 µL min^{-1}). These plates were prepared in batches of twelve samples at a time to ensure the stain remained active during data acquisition. Populations were gated in cytograms of VSSC versus green fluorescence signals, where VLP were defined as populations with green fluorescence above background levels (set by controls described above), but with lower fluorescence than the bacterial population (Marie et al., 1999a). The bacterial population was gated into high DNA (HDNA) and low DNA (LDNA) containing bacteria according to their green fluorescence, which generally indicates a two-fold difference in DNA content (Li et al., 1995) with HDNA bacteria being the active proportion of the bacterial community (dividing and/or actively metabolizing) (Jellett et al., 1996). VLP were enumerated as a single population as sub-populations were not observed. Additional cytograms of green versus red fluorescence signals were used to distinguish autotrophic (naturally fluorescent in red) from heterotrophic bacteria (Campbell et al., 1994; Monger and Landry, 1993).

After bacteria and VLP acquisition, phytoplankton plates were prepared by plating sub-samples (200 µL) into microplates and analysing them immediately. Acquisition was triggered on the forward scatter (FSC) signal (>8000 threshold to minimise contributions from detritus and VLP)

and enumerated at a high flow rate for two minutes (60 µL min^{-1} given abortion rates remained < 0.5 %). The following control was also analysed to set the gating threshold for background red fluorescence: "Filtered sample" containing 0.22 µm filtered sample water for each unique estuary, prepared by pooling replicates within each estuary. Populations were gated in cytograms of SSC versus red fluorescence signals to identify chlorophyll positive cells, which were gated as those with red fluorescence above background levels (set "Filtered sample" above). Cytograms of orange versus red fluorescence signals were then used to distinguish two sub-populations from chlorophyll positive cells; *Synechococcus* (low red and high orange fluorescence) and Eukaryotes (low orange and high red fluorescence) (Marie et al., 1999b). Given that *Prochlorococcus* populations (low orange and red fluorescence) can overlap substantially with detritus, the presence of this group was examined using nucleic acid staining (described above), but it was absent in all samples.

4.2.8.3 Cell size verification

After sample analysis, six suspensions of non-fluorescent spherical polystyrene microspheres with known particle diameters (1.1 - 14.9 µm, Flow Cytometry Calibration Kit, Thermofisher Scientific, United States) were added to Milli-Q water (1 drop per 2 mL) and analysed to estimate the size of phytoplankton cells. Beads were gated in cytograms of SSC versus FSC signals. Typical cytograms generated during flow cytometry acquisition are depicted in the supplementary (Supplementary Figure 4.3). All sample processing was completed in two, back-to-back sessions within 48 hours to minimise temporal and instrument-related variability.

4.2.8.4 Data processing

The abundance of several microbial populations, including VLP, heterotrophic bacteria (LDNA/HDNA) and phytoplankton (Eukaryotes/*Synechococcus*), were determined by the number of events per unit volume (cells mL^{-1}) falling within the gating parameters described above. Phenotypic traits of phytoplankton populations including cell size (FSC), granularity (SSC), chlorophyll (red autofluorescence) and phycoerytherin (orange autofluorescence) fluorescence, were quantified here as the median single-cell measurement for each population. Median FSC values were used to estimate cell size in µm by a simple linear regression between known particle diameters of calibration microspheres and their median FSC value (R^2 = 0.96). While many phytoplankton cells are not truly spherical in shape, we used these approximations as a general indication and to assess relative differences in size. To ensure granularity and pigment estimates

were not biased by cell size, they were normalised by dividing median trait values by the median cell size estimate in µm. The ratios of bacteria to phytoplankton, HDNA bacteria to total bacteria, and VLP to bacteria, were calculated by dividing the abundances of these populations against one another.

4.2.9 Statistical analysis

To examine how estuarine microbes responded to PM incubations, their abundances and traits were analysed collectively using the multivariate technique Principal Components Analysis (PCA). This analysis was performed only on samples that underwent incubation (i.e., excluding the Estuary Baseline). Each deposition scenario was normalised to the mean trait value of the Control Incubation to incorporate standing variation among the five estuaries. This was achieved by subtracting the mean of Control Incubations from each estuary, such that positive/negative values indicate the trait is of that magnitude higher/lower than the average Control incubation. The PCA was calculated by Euclidean distance on a correlation matrix, thus standardising each trait (0 mean ± 1 s.d.) to incorporate differences in the scale of measurement, whilst preserving the relative magnitude of differences among observations. PCA coordinates were rescaled to the interval [-1, 1] to allow equivalence with trait loadings.

Differences in trait clusters within the PCA were assessed by permutational analysis of variance (PERMANOVA) and pairwise PERMANOVA comparisons with a Bonferroni adjustment. This was performed on a standardised (0 mean ± 1 s.d.) dissimilarity matrix of traits using Euclidean distance and 999 permutations. A test of homogeneity of dispersions (PERMDISP) with pairwise PERMDISP comparisons (also with a Bonferroni adjustment) were also computed to aid with PERMANOVA interpretations and intra-estuary variation within treatments.

To examine whether variation in microbial responses between estuaries was associated with geomorphology, physicochemistry, or microbial traits at the time of sampling, we ran a series of Pearson correlation analyses with historical (DCCEEW) and/or t0 estuary data to determine their associations with the first principal component from the PCA (PC1). Estuary geomorphology was compiled from t0 measurements in this study as well as from DCCEEW's online estuary database (https://www.environment.nsw.gov.au/). These variables included average depth

along our sampling transect (m), catchment area (km^2), estuary surface area (km^2), estuary volume (ML), and mean depth of the entire water body (m). Physicochemistry was assessed using t0 water quality and nutrient parameters measured in this study or in previous field observations by DCCEEW. The latter used data compiled from previous field measurements by DPE between 2007-2020 (available online: https://data.nsw.gov.au/data/). Microbial traits were assessed using t0 measurements collected during estuary sampling in this study.

All analyses and graphics were generated using R (R Core Team, 2021) and the following packages: ggpubr, vegan, ggplot, dplyr (Dragulescu and Arendt, 2020; Kassambara, 2020; Oksanen et al., 2022; Silsbe and Malkin, 2015; Wickham, 2016; Wickham et al., 2019; Wilke, 2020).

4.3 Results and discussion

4.3.1 Estuary characteristics during sampling

In April 2021, natural microbial communities varied between five distinct estuaries surrounding Batemans Bay, including two lagoons (BRO, TAB) and three river systems (CLY, MOR, TUR) (Figure 4.1). At the time of sampling, phytoplankton abundances were on the order of 10^3 to 10^5 cells mL^{-1}, with bacteria and viruses an order of magnitude higher (between 10^5 and 10^6 cells mL^{-1}) (Figure 4.3A). Lagoons contained fewer phytoplankton, but more bacteria and viruses compared to rivers (Figure 4.3A; $p < 0.05$), with the largest difference observed for *Synechococcus* (Figure 4.3A, "Phytoplankton" facet). Across all five estuaries, phytoplankton cells were typically small and uniform in size, with median diameters ranging between 2.01 and 2.12 µm (estuary means) for eukaryotes, and between 1.96 and 1.98 µm for *Synechococcus* (Figure 4.3B, "ESD(µm)"). As expected, eukaryotes displayed higher granularity and chlorophyll fluorescence than *Synechococcus* cells - even after normalising to cell size (Figure 4.3B, "SSC/µm" and "CHL/µm"), and showed negligible phycoerytherin content (Figure 4.3B, "PE/µm"). On average, high-DNA bacteria (i.e. actively growing) accounted for 46–61 % of the total bacterial population in rivers, with more variable contributions for the two lagoons (27-70 %).

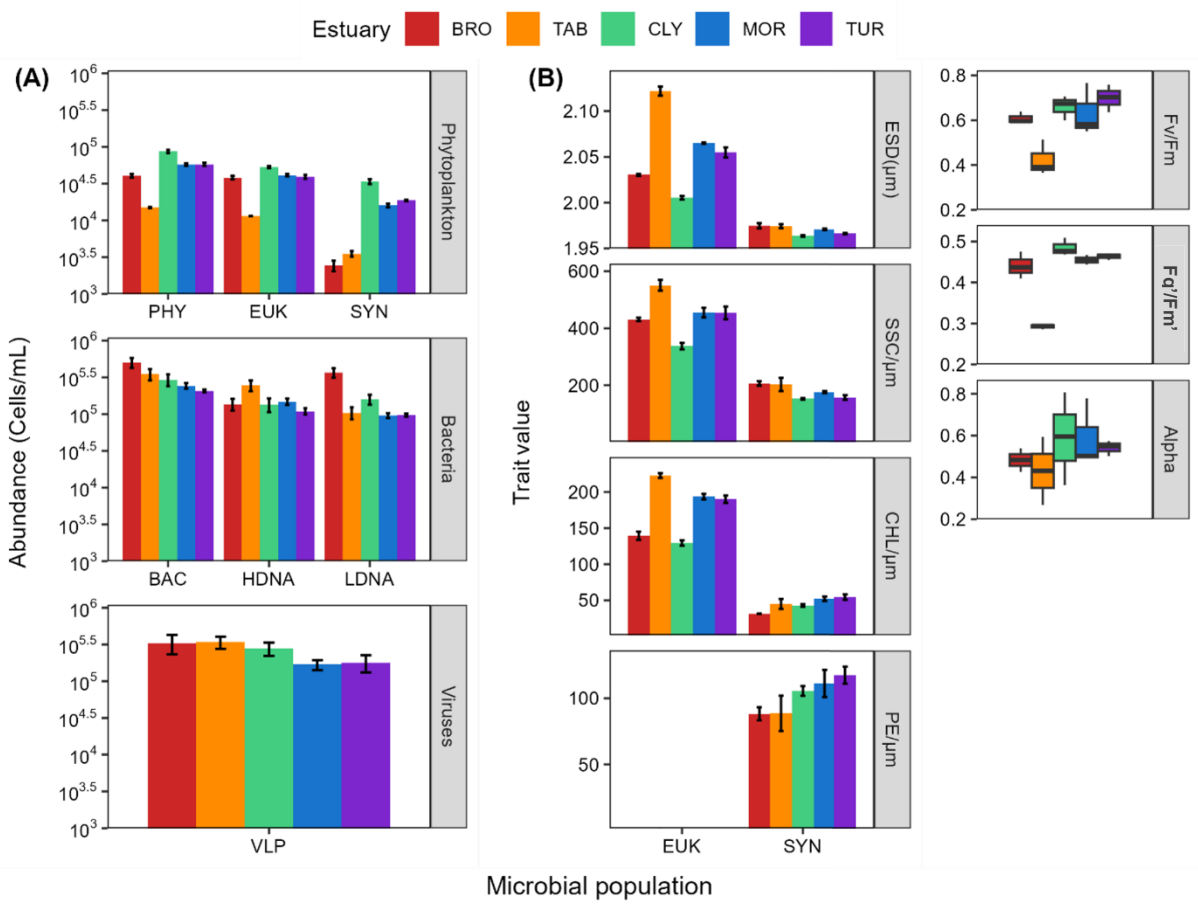


Figure 4.3 Abundances (A) and functional traits (B) of microbial populations (x-axis) in five estuaries (colour) surrounding Batemans Bay at the time of sampling (n = 3 per estuary). Flow cytometry measurements are depicted as means ± standard deviations (bars), whereas boxplots display the more variable PAM fluorometry results. Estuaries include Lake Brou (BRO), Lake Tabourie (TAB), Clyde River (CLY), Moruya River (MOR) and Tuross River (TUR). Microbial subpopulations include phytoplankton (PHY), eukaryotes (EUK), synechococcus (SYN), bacteria (BAC), high-DNA bacteria (HDNA), low-DNA bacteria (LDNA), virus-like particles (VLP). Functional traits include equivalent spherical diameter (ESD), side scatter (SSC), chlorophyll (CHL) and phycoerytherin (PE) autofluorescence, maximum (Fv/Fm) and effective (Fq'/Fm') quantum yields, and relative rate of photosynthesis onset (Alpha). All abbreviations are defined in the Abbreviations section at the start of this chapter.

The maximum quantum yield ranged from 0.55 to 0.77 in river systems (min/max) and 0.37 to 0.64 in lagoons (Figure 4.3B, "Fv/Fm"). Median values across estuary types ranged between 0.58-0.70 and 0.39-0.60, respectively. Under irradiated conditions, effective quantum yields were between 0.44-0.51 in rivers and 0.29-0.48 in lagoons, with medians of 0.45-0.48 and 0.29-0.44, respectively (Figure 4.3B, "Fq/Fm"). These results indicate that under saturating light levels, phytoplankton in rivers performed better than lagoons in terms of their photosynthetic efficiency. At non-saturating irradiance, rivers displayed higher rates of photosynthesis onset, ranging between 0.36-0.81 (0.50-0.60 median) versus 0.27-0.59 (0.43-0.48 median) in lagoons (Figure

4.3B, “Alpha”). This suggests that lagoons responded less readily to the onset of light exposure than rivers. This may be due to differences in estuarine hydrology, where river microbes must adapt to dynamic, fluctuating environments of varying light intensities, while lagoons are relatively stable and favour adaptations to low-lit or turbid conditions.

4.3.2 Assessment of wildfire aerosol inputs

From the 10th of December 2019 (monitor deployed) until local wildfires were extinguished (9th of February 2020), daily averaged PM_{10} concentrations in Batemans Bay ranged between 8.43 and 738.08 µg m^{-3} (min/max), with a mean of 96.63 µg m^{-3} (Figure 4.4). This is equivalent to a dry deposition flux of between 0.02 and 1.28 g m^{-2} d^{-1}, averaging at ~0.17 g m^{-2} d^{-1} (Figure 4.4). Daily concentrations peaked on the 1st of January 2020, with hourly observations reaching a maximum of 2863 µg m^{-3} on the day prior (12:00 on 31st December 2019) (Figure 4.4). In a scenario where this concentration is sustained over a 24-hour averaging period, the associated flux would be as high as 4.95 g m^{-2} d^{-1} (Figure 4.4). After local fires were extinguished (10th of February 2020 onwards), daily PM_{10} averaged at 12.02 µg m^{-3} with an hourly maximum of 48 µg m^{-3} (Figure 4.4B) falling back to within Australia’s guidelines for good air quality (< 50 µg m^{-3} PM_{10}) (Department of the Environment and Heritage, 2005).

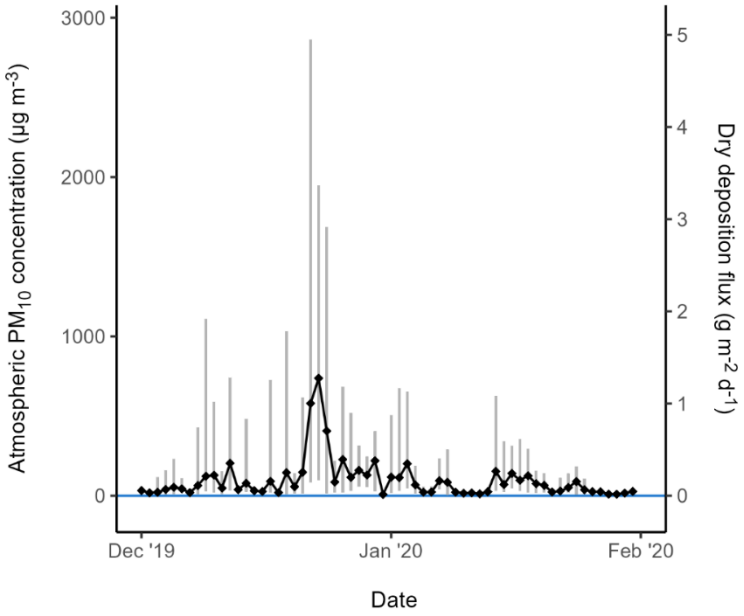


Figure 4.4 Atmospheric PM_{10} concentrations (µg m^{-3}) in Batemans Bay during the 2019-20 Australian Black Summer wildfires. The black line and diamonds represent the average daily PM_{10} concentration, with grey bars indicating the range (minimum to maximum) of hourly concentrations observed each day. The corresponding dry deposition flux of PM_{10} (g m^{-2} d^{-1}) is shown on the secondary y-axis (scaled equivalently), where black lines and diamonds denote the daily mean flux and grey bars represent the range. The blue line indicates the mean daily PM_{10} concentration (~12 µg m^{-3}) after local fires were extinguished on 9 February 2020, with an estimated flux of ~0.021 g m^{-2} d^{-1} (or ~21 mg).

Bottle incubations simulated two scenarios of dry deposition: 1) an "Average Scenario" representative of typical fluxes of wildfire PM_{10} into estuaries near Batemans Bay (0.17 g m^{-2} d^{-1}), and 2) an "Extreme Scenario" reflective of more intense wildfires in the future or locations with higher vegetation densities and emissions (4.95 g m^{-2} d^{-1}). These experiments utilised PM_{10} captured during the 2019-20 Black Summer wildfires in Sydney, Australia. While Sydney is a heavily urbanised location, the sheer magnitude of emissions was such that the bulk of PM mass had originated from remote sources (Gill et al., 2024), including aged wildfire smoke (~33 %), entrained Pb-contaminated soil (~32 %), soil and sea-spray (~26 %) (Gill et al., n.d). This material contained a complex mixture of potentially toxic and nutritional elements (Gill et al., 2024; Gill et al., n.d.), representing a poorly understood source of bioactive inputs to estuarine environments.

4.3.3 Overview of multivariate impacts of wildfire-enriched aerosols

The “trait scape” generated by principal component analysis (PCA) revealed complex shifts in the abundance and functional traits of estuarine microbes following exposure to wildfire-enriched aerosols. Linear combinations of normalised microbial traits explained ~62 % of the variability among estuary observations (Figure 4.5, PC1 and PC2), which is relatively high for ecological datasets. The nature of these differences is illustrated through PCA loadings (Figure 4.5D-E and Table 4.1), where individual trait contributions are indicated by their distance from the origin (0, 0) and alignment with principal axes. The positioning of samples in relation to these loadings indicates the relative magnitude and direction of the trait value, where loadings located in the same vicinity indicate a concurrent increase in trait values, and those on opposing sides of the axis indicate divergent responses.

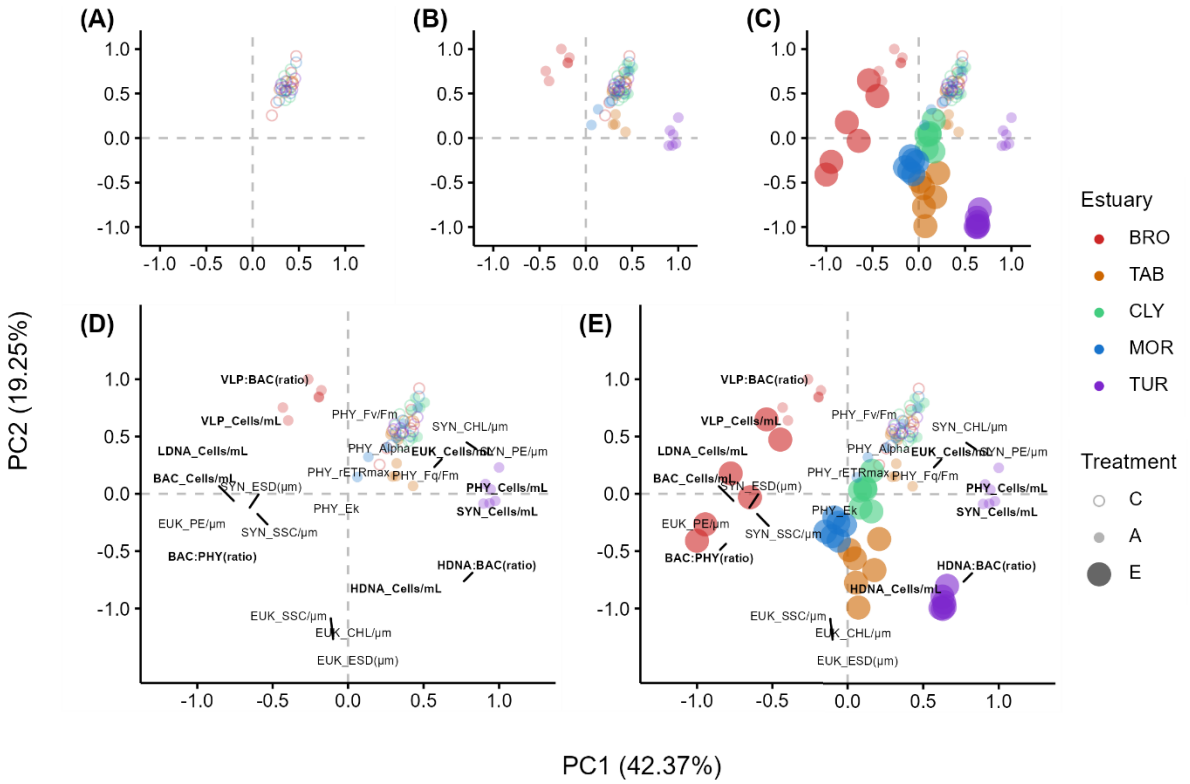


Figure 4.5 Principal components analysis (PCA) biplots depicting microbial traits in estuaries (colour) after 24-hour incubations with wildfire-enriched particles (n = 6 per estuary). Data was normalised to the mean of the Control Incubation for each estuary. Points indicate treatments: empty circles = Control Incubations (“C”); small filled circles = Average Scenario (“A”); large filled circles = Extreme Scenario (“E”). All panels display the same PCA biplot with treatments and loadings added sequentially: (A) Control Incubations; (B) + Average Scenario; (C) + Extreme Scenario; (D) A + B + loadings; (E) A + B + C + loadings. Loadings are labelled with population and trait abbreviations, as defined in the Abbreviations section at the start of this chapter. Bold loadings indicate cell abundance or population ratios. Axis percentages show the variance explained by PC1 and PC2.

Table 4.1 PCA loadings for microbial traits of estuaries following 24-hour incubations with wildfire-enriched particles (n = 6 per estuary). Columns under the "Average Scenario" (left-hand side) indicate divergent responses of estuaries observed along PC1, while the "Extreme Scenario" (right-hand side) depicts uniform responses of estuaries along PC2. Loadings are labelled with population and trait abbreviations, as defined in the Abbreviations section at the start of this chapter.

Average Scenario		**Extreme Scenario**	
Population / Trait	**PC1 Loading**	**Population / Trait**	**PC2 Loading**
EUK_PE/µm	-0.29	EUK_ESD(µm)	-0.44
LDNA_Cells/mL	-0.29	EUK_SSC/µm	-0.43
VLP_Cells/mL	-0.27	EUK_CHL/µm	-0.37
BAC:PHY(ratio)	-0.27	HDNA_Cells/mL	-0.32
BAC_Cells/mL	-0.25	HDNA:BAC(ratio)	-0.26
SYN_ESD(µm)	-0.22	BAC:PHY(ratio)	-0.14
SYN_SSC/µm	-0.20	SYN_Cells/mL	-0.09
VLP:BAC(ratio)	-0.15	SYN_SSC/µm	-0.05
EUK_SSC/µm	-0.03	SYN_ESD(µm)	-0.05
EUK_ESD(µm)	-0.01	EUK_PE/µm	-0.05
EUK_CHL/µm	0.04	BAC_Cells/mL	-0.03
HDNA_Cells/mL	0.07	PHY_Cells/mL	0.05
PHY_Fv/Fm	0.07	EUK_Cells/mL	0.08
PHY_Alpha	0.10	PHY_Fq/Fm	0.11
PHY_Fq/Fm	0.21	SYN_PE/µm	0.15
HDNA:BAC(ratio)	0.25	SYN_CHL/µm	0.15
SYN_CHL/µm	0.26	LDNA_Cells/mL	0.17
SYN_PE/µm	0.26	VLP_Cells/mL	0.17
EUK_Cells/mL	0.28	PHY_Alpha	0.18
PHY_Cells/mL	0.29	PHY_Fv/Fm	0.19
SYN_Cells/mL	0.30	VLP:BAC(ratio)	0.29

In control bottles without wildfire-enriched particles, microbial traits normalised to each estuary were relatively stable over the 24-hour period, forming a single tight cluster in the PCA (Figure 4.5A, empty circles). Under the Average Scenario of dry deposition, the geometric centre of this trait cluster did not shift relative to Control Incubations (PERMANOVA: $p = 0.147$), however trait variability increased markedly (PERMDISP: $p = 0.007$) (Figure 4.5B, filled circles). This was driven by divergent responses in Lake Brou and Tuross River (Figure 4.5B, lateral red and purple clusters), with the remaining three estuaries remaining virtually unimpacted (Figure 4.5B, middle cluster). Under the Extreme Scenario, the addition of higher concentrations of wildfire-enriched PM caused significant shifts in both the central position and dispersion of trait clusters in the

PCA, which differed from both controls and average treatments (PERMANOVA and PERMDISP: p = 0.001 in all cases) (Figure 4.5C, larger filled circles). In this instance, all five estuarine microbial communities shifted towards the lower quadrants of the PCA, indicating more convergent and pronounced functional changes.

4.3.4 Divergent heterotrophic response to average wildfire conditions

Trait loadings along PC1 indicate that Lake Brou exhibited a strong heterotrophic response to wildfire-enriched particle deposition under the Average Scenario (Figure 4.5D). Specifically, the abundances of low-DNA bacteria, viruses and total bacteria increased, with loadings of -0.29, -0.27 and -0.25, respectively (Table 4.1 and Figure 4.5D, left of axis), while *Synechococcus* (0.30), total phytoplankton (0.29) and eukaryotes (0.28) all declined (Table 4.1 and Figure 4.5D, right of axis). These loadings are consistent with observed changes in cell abundance shown below (Figure 4.6), where Lake Brou responded as above ("BRO" facet) and Lake Tabourie, Clyde River and Moruya River remained relatively stable ("TAB", "CLY" and "MOR" facets). Specifically, abundances in Lake Brou bottles increased by 175 ± 17 % for low-DNA bacteria, 120 ± 35 % for viruses, and 42 ± 8 % for total bacteria (mean ± sd), with mean counts rising from 1.3 to 3.5, 1.7 to 3.8, and 3.7 to 5.2 × 10^5 cells mL^{-1}, respectively (Figure 4.6, panels F, G and D). In contrast, *Synechococcus*, total phytoplankton, and eukaryotic picoplankton declined by 91 ± 4 %, 70 ± 6 %, and 64 ± 7 %, with mean abundances dropping from 1.5 to 0.1, 7.9 to 2.4, and 6.4 to 2.3 × 10^4 cells mL^{-1}, respectively (Figure 4.6, panels C, A and B).

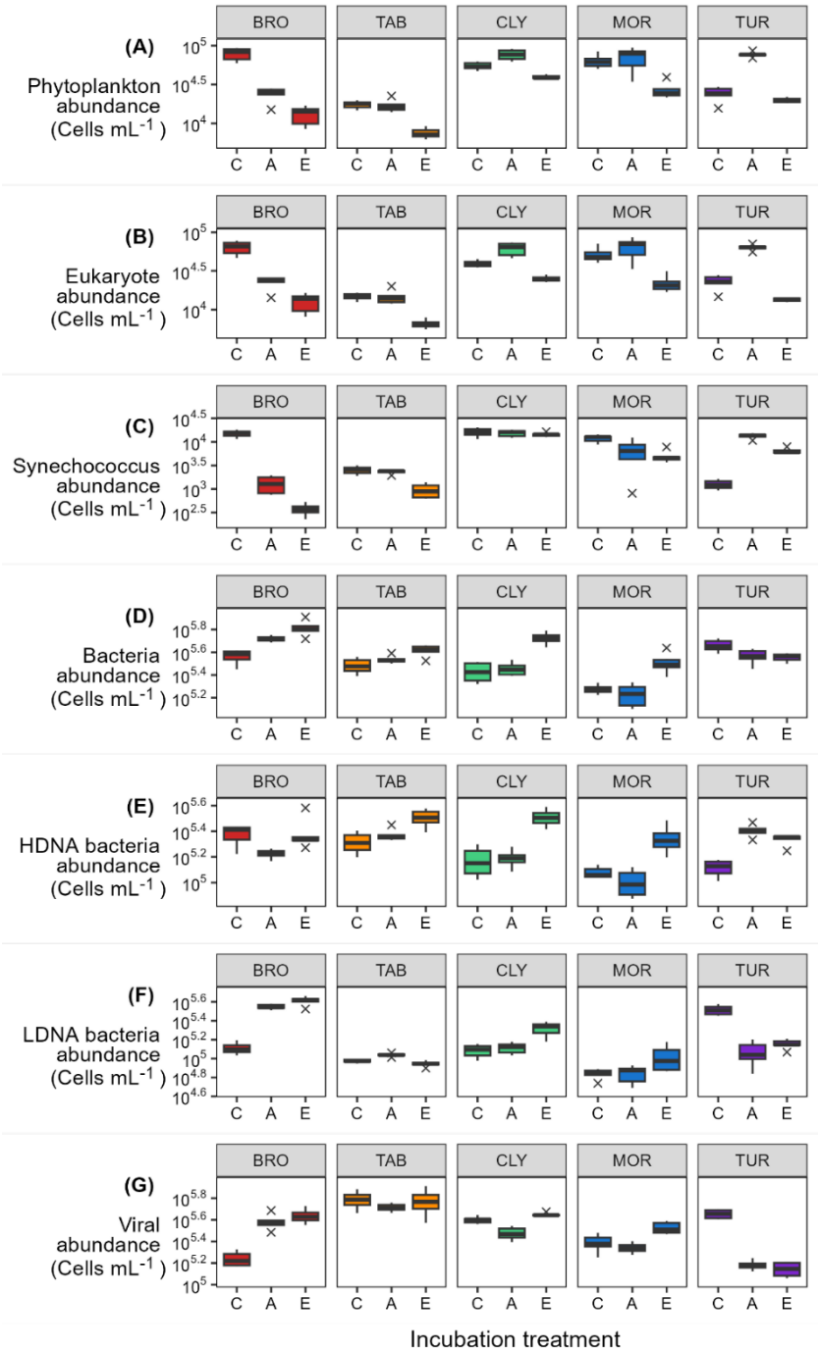


Figure 4.6 Abundance of microbial populations in five estuaries following 24-hour incubations with wildfire-enriched particles (n = 6 per estuary). Populations are depicted across rows (A) to (G) with estuaries separated by facet and incubation treatment along the x-axis. Cell abundances are shown on a natural log scale. All abbreviations are defined in the Abbreviations section at the start of this chapter.

These shifts were accompanied by increased ratios of bacteria-to-phytoplankton and viruses-to-bacteria (Table 4.1 and Figure 4.5D, left of axis), as well as a reduction in the ratio of high-DNA to total bacteria (Table 4.1 Figure 4.5D, right of axis). While observations of planktonic bacteria

during wildfires are limited, our findings align with studies of dust aerosols in marine populations, which typically lead to increased bacterial abundance, enhanced respiration, and shifts in microbial community composition (Guieu et al., 2014; Hou et al., 2019; Tsagaraki et al., 2017; Tsiola et al., 2017). Wildfire-enriched PM has also been demonstrated to reduce autotrophy and promote heterotrophy in coral symbionts (Qin et al., 2024). These responses are likely driven by the supply of soluble forms of organic carbon (Chapter 3), which fuels bacterial growth and may influence nutrient cycling and trophic flows (Azam et al., 1983). This is further supported by measurements of estuarine sediment before and after the 2019-20 wildfires, where fire-impacted estuaries showed increased abundance of bacteria involved in organic matter degradation, sulfate and iron reduction, and effluent pollution, alongside a decrease in nitrifying bacteria (Bracewell et al., 2023). Notably, these shifts were more pronounced in estuaries where wildfires had reached riparian zones, compared to those with intact vegetation buffers or unburnt catchments.

Interestingly, we also observed elevated phycoerythrin fluorescence in eukaryotic cells associated with this heterotrophic response, alongside declines in the chlorophyll and phycoerytherin fluorescence of *Synechococcus* populations, despite them becoming larger and more granular (Table 4.1 and Figure 4.5D, left of axis). We also observed a reduction in the effective quantum yield of phytoplankton populations (Table 4.1 and Figure 4.5D, right of axis). Since wildfire-enriched PM addition had no significant impact on light availability under the Average Scenario ($p > 0.05$; Supplementary Figure 4.4), these changes in phytoplankton cells are likely due to the direct or indirect effects of the particles themselves. One possible explanation for these changes is a shift in nutrient availability and stoichiometry that favours a transition toward cryptophytes (Li and Dickie, 2001). This interpretation is supported by observations from NSW estuarine sediments following the 2019–20 wildfires, which showed an increase in the relative abundance of the *Cryptomycotina* bacterial family—from ~0.02% to between ~0.05% and 0.15%—depending on the extent of vegetation buffer loss (Bracewell et al., 2023). Fire-induced changes in nutrient dynamics could also alter grazing pressure and restructure microbial communities or affect the metabolism of existing taxa in ways that influence their photosynthetic activity (Guo et al., 2022).

Alternatively, the presence of soluble metals in wildfire-enriched PM may have contributed to the decline in phytoplankton growth and photosynthetic efficiency. This interpretation aligns with

previous studies that demonstrate heightened sensitivity of *Synechococcus* to heavy metals relative to other phytoplankton groups (especially copper), even when nutrient conditions are favourable (de la Broise and Palenik, 2007; Debelius et al., 2011; Paytan et al., 2009). Concurrent increases in cell size and/or granularity with toxic metal exposure have also been reported in various aquatic microorganisms (Debelius et al., 2011; Franklin et al., 2001; Shoman et al., 2025). These effects may result from several processes, including: 1) damage to cell walls and membranes leading to structural deformation and increased permeability to sodium ions; 2) inhibited cell division causing the accumulation of photosynthetic products; 3) development or enlargement of intracellular structures such as membranous organelles and vacuoles that bind toxic metals; and 4) adsorption of toxic nanoparticle aggregates onto the cell surface (Franklin et al., 2001; Shoman et al., 2025; Visviki and Rachlin, 1994).

Collectively, these findings suggest that the deposition of wildfire-enriched particles during major wildfire events has the potential to rapidly shift the metabolism of estuary ecosystems, driving shifts in some estuaries towards heterotrophy and disrupting autotrophy. This may have significant implications not only for local trophic flows and aquaculture yields, but for surrounding estuaries that may depend on the organic matter produced by autotrophic systems to support their own metabolism (Cloern, 2007). Additional experiments are required to determine the extent to which these changes are sustained over longer time scales and its broader implications for aquatic microbes and ecosystem functioning.

4.3.5 Divergent autotrophic response to average wildfire conditions

On the opposing side of the PCA, this heterotrophic response observed in Lake Brou was mirrored by Tuross River, which displayed a strong autotrophic response under the Average Scenario for dry deposition (Table 4.1 and Figure 4.5D, right of axis). As above, these effects were evident in plots of microbial abundances (Figure 4.6) and relevant traits (Figure 4.7). Specifically, the abundances of heterotrophic microbes declined, including low-DNA bacteria (-65 ± 10 %; 3.3 to 1.2 × 10^5 cells mL^{-1}), viruses (-66 ± 3 %; 4.5 to 1.5 × 10^5 cells mL^{-1}) and total bacteria (-19 ± 12 %; 4.6 to 3.7 × 10^5 cells mL^{-1}) (Figure 4.5, panels F, G and D), while autotrophic populations like *Synechococcus* (964 ± 123 %; 0.1 to 1.3 × 10^4 cells mL^{-1}), total phytoplankton (218 ± 22 %; 2.4 to 7.7 × 10^4 cells mL^{-1}) and eukaryotes (177 ± 22 %; 2.3 to 6.4 × 10^4 cells mL^{-1}) grew significantly (Figure 4.5, panels C, A and B). Additionally, we also observed a 93 ± 20 % increase in high-DNA

bacteria, with counts rising from 1.3 to 2.5 $\times 10^5$ cells mL^{-1} (Figure 4.5, panel E). For traits, we observed no significant shift in effective quantum yields, indicating that photosynthetic efficiency was not impaired as it was in Lake Brou (Figure 4.7, panel "PHY Fq/Fm"). We also observed a decrease in the phycoerytherin fluorescence of eukaryotic cells and increases in both chlorophyll and phycoerytherin fluorescence of *Synechococcus* (Figure 4.7).

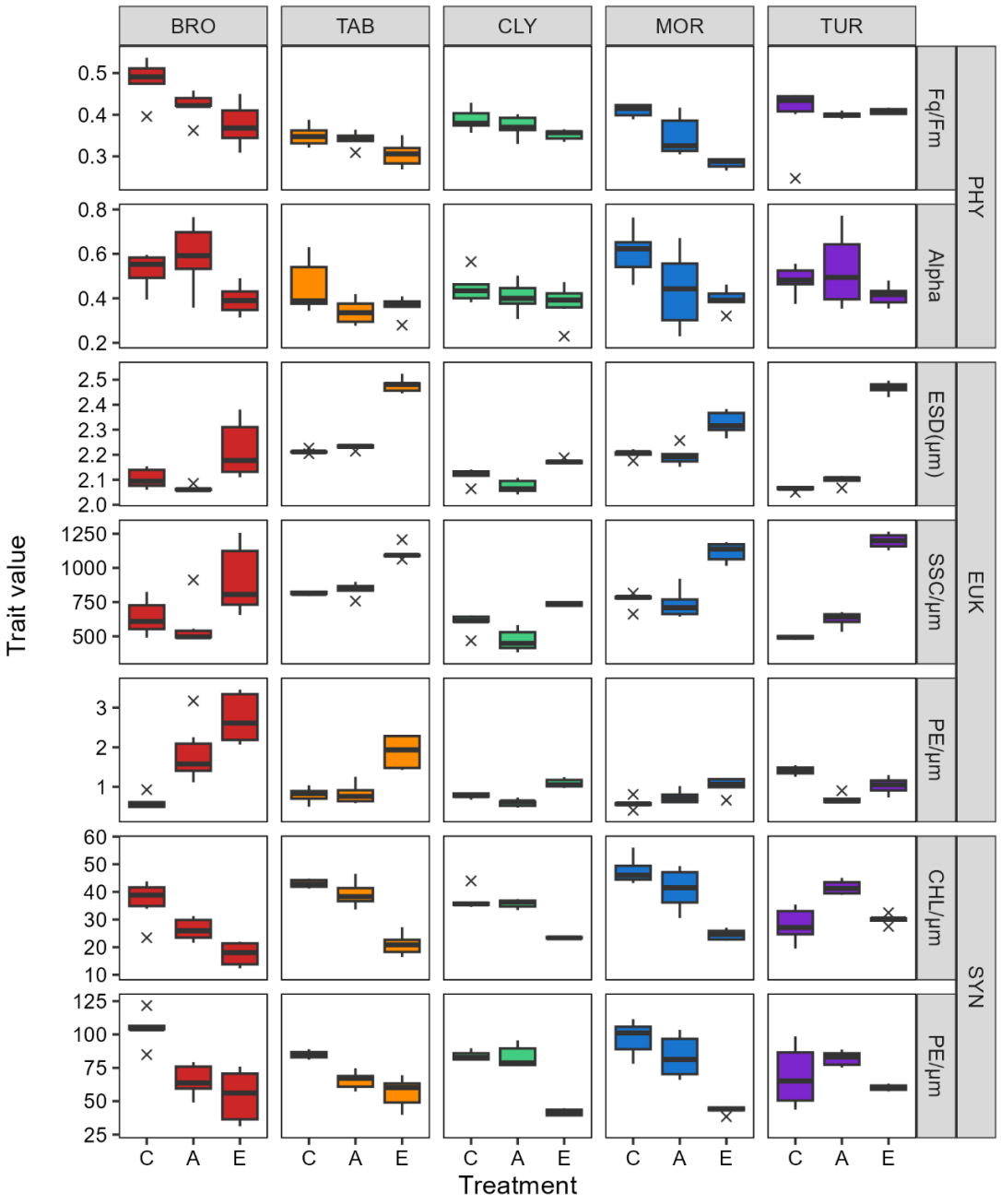


Figure 4.7 Functional traits associated with divergent microbial responses to the Average or Extreme Scenario of wildfire-enriched particle deposition in five estuaries (n = 6 per estuary). Populations and traits are denoted by right facets, while estuaries are denoted by top facets. All abbreviations are defined in the Abbreviations section at the start of this chapter.

Autotrophic responses like Tuross River are more commonly reported on in the literature compared with heterotrophic responses. Accordingly, several studies during the 2019-20 wildfires have identified prolonged and widespread phytoplankton blooms in marine areas south of Australia (Li et al., 2021; Tang et al., 2021; Wang et al., 2022; Weis et al., 2022). These communities exhibited distinct physiological changes to pre-bloom conditions, including increased chlorophyll pigmentation and fluorescence-based photosynthetic efficiency, along with shifts in community structure inferred from changes in particle shape/size (Weis et al., 2022). Our findings in Tuross River were broadly similar in that we observed a distinct stimulatory effect on phytoplankton populations, as well as increased photosynthetic fluorescence of *Synechococcus* cells. Beyond marine impacts, significant changes were also observed in benthic eukaryotes from five estuaries in NSW following the 2019-20 wildfire season that showed an increase in green algae and decrease in nematodes and dinoflagellates (Bracewell et al., 2023).

4.3.6 Convergent heterotrophic responses to extreme wildfire conditions

Trait loadings along PC2 indicate that higher concentrations of wildfire-enriched PM elicited a broadly consistent microbial response across the five estuaries (Figure 4.5E). Notably, we observed an increase in the abundance of high-DNA bacteria accompanied by elevated high-DNA to total bacterial ratios, with loadings of -0.32 and -0.26 respectively (Table 4.1 and Figure 4.5E, below axis). This growth occurred in all estuaries except Lake Brou, (Figure 4.5E), with cell abundances increasing by an average of 55 – 117 %. Interestingly, viral abundance did not scale with bacterial growth, suggesting a shift in community structure to one where bacteria are not controlled by viruses to the same degree as controls (Tsagaraki et al., 2017). The enrichment of high-DNA bacteria suggests a shift towards a more metabolically active or fast-growing bacterial community, likely reflecting increased resource availability from wildfire inputs. These microbial changes were accompanied by the following: (1) larger, more granular and pigmented eukaryotic cells in the absence of population growth (Figure 4.6, “EUK” facets), (2) reduced chlorophyll and phycoerytherin fluorescence of *Synechococcus* (Figure 4.6, “SYN” facets), (3) lower effective quantum yields of phytoplankton communities (Figure 4.7, “Fq/Fm” facets), and (4) slower rates of photosynthesis at the onset of irradiance (Figure 4.7, “Alpha” facets).

4.3.7 Potential drivers of wildfire responses

Correlation analyses revealed several potential drivers of estuarine microbial responses to wildfire incubations (Figure 4.8). Under the Average Scenario, we observed negative, moderate-to-strong correlations between PC1 - the primary axis along which estuary responses diverged - and water quality parameters at the time of sampling. These included conductivity, specific conductivity, and salinity (Pearson's r = -0.68 to -0.7; Figure 4.8, T0 column in "Water quality" facet). These parameters are indicators of brackishness, and followed a clear environmental gradient: Lake Brou, with a strong heterotrophic response, had the highest salinity (32.9 ppt), while Tuross River, which showed a strong autotrophic response, had the lowest (23.3 ppt). Estuaries with minimal responses had intermediate salinities (26.0 – 27.9 ppt), with similar trends for conductivity (Supplementary Table 4.2).

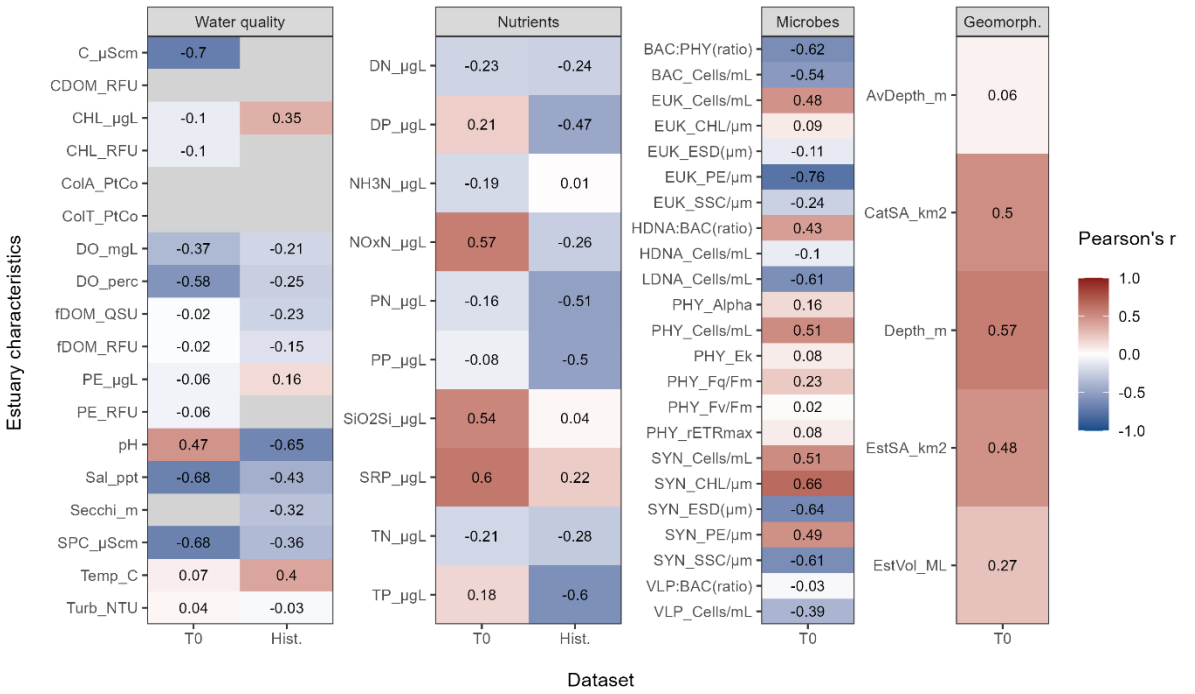


Figure 4.8 Heatmap depicting Pearson correlation coefficients (colour) between the horizontal trait axis (PC1) in Principal Components Analysis (PCA) (x-axis) and mean estuary characteristics at the time of sampling (t0) or in historical datasets (Hist.) (y-axis). Characteristics are grouped into four distinct facets, including (from left-right) water quality parameters, nutrients, microbial traits, and geomorphology. All abbreviations are defined in the Abbreviations section at the start of this chapter.

As the interface between land and sea, estuaries exhibit strong salinity gradients and tidal fluctuations that impose osmotic stress on microbes, driving shifts in the function and diversity of communities by selecting for osmoregulatory adaptations (Wu et al., 2024). As such, one possible explanation for our findings is that salinity structured communities in such a way that impacted their capacity to respond to wildfire inputs. Alternatively, higher salinity may have had indirect effects by enhancing the mobility of toxic metals (Jia et al., 2021; Zhao et al., 2013) in wildfire-enriched particles. High conductivity, associated with increased concentrations of major cations such as potassium, calcium, and magnesium, can further influence metal bioavailability by competing for sorption sites and prolonging their residence in the water column (Du Laing et al., 2009). Phytoplankton tend to display low tolerance for heavy metals, with previous studies documenting reduced cell counts, chlorophyll content, and primary production over short exposures (Nayar et al., 2004). On the other hand, heterotrophic bacteria may respond more favourably due to their broader range of metal resistance and detoxification strategies, potentially giving them a competitive advantage in more saline, metal-affected environments (Nayar et al., 2004). Future investigations should assess the potential for salinity and conductivity to modulate microbial responses to wildfire inputs, which may have significant implications for predicting estuarine resilience.

Heterotrophy was associated with a history of high pH in water quality records, while autotrophic responses were associated with more acidic historical conditions ($r = -0.65$; Figure 4.8, Hist. column in “Water quality” facet). In estuarine sediments, high pH is often associated with heavy metal adsorption and precipitation, while low pH may promote their release (Zhang et al., 2014). This shift may have influenced autotrophic responses either directly - by altering physiological tolerances - or indirectly, through changes in metal bioavailability or nutrient dynamics. Future research is needed to assess how extreme wildfire events disrupt or reshape long-term estuary dynamics, and the extent to which historical physicochemical properties influence responses to wildfire.

Correlations with estuary nutrients indicated that systems with higher levels of dissolved nutrients at the time of sampling – including oxidised forms of nitrogen, soluble reactive phosphorus, and silica ($r = 0.54$ to 0.6) – coupled with a history of low phosphorus and particulate nitrogen ($r = -0.47$ to -0.60), were more inclined to enrich phytoplankton in subsequent wildfire incubations (Figure 4.8, “Nutrients” facet). Labile nutrients tend to be immediately and easily

accessible to autotrophs, while particulate fractions tend to be less bioavailable and are associated with benthic sediments due to settling and extended leaching time (Sarkar et al., 2015). This suggests that the microbial communities from Tuross River may be primed to respond to nutrient enrichment favourably and quickly, given that historical nutrient inputs tend to be inaccessible.

This dynamic is supported by measurements of microbes during sampling, where autotrophic responses to wildfire-enriched particles were more prominent in systems with smaller (r = -0.64), less granular (r = -0.61), and more pigmented *Synechococcus* (r = 0.49 to 0.66) (Figure 4.8, "Microbes" facet). Compared with eukaryotes, cyanobacteria have highly effective strategies for nutrient uptake and storage, making them highly competitive in nutrient-limited environments (Reinl et al., 2021). These include the ability to: 1) fix their own source of nitrogen; 2) utilise both organic and inorganic forms of phosphorus; 3) release iron bound in sediment via siderophore production, scavenging and leaching; 4) more efficient uptake mechanisms for inorganic carbon and phosphate; and 5) greater storage capacity for excess nitrogen and phosphorus (Reinl et al., 2021 and references therein). Given that wildfire-enriched particles contained high levels of insoluble mineral dust elements like iron (Gill et al., n.d), incubations were likely to stimulate growth of cyanobacteria disproportionately to other phytoplankton due to differences in bioavailability. In contrast, heterotrophic responses were associated with higher abundances of bacteria (r = -0.54 to -0.61) as well as eukaryotes with higher phycoerytherin during sampling (r = -0.76) (possibly cryptophytes; Bracewell et al., 2023; Li and Dickie, 2001), indicating that these samples already had an abundance of microbes capable of efficiently exploiting organic carbon (Figure 4.8, "Microbes" facet). Overall, these results suggest that smaller, healthier phytoplankton populations with flexible nutrient strategies may buffer against heterotrophic responses to wildfire inputs.

Finally, we observed moderate associations between autotrophy and estuary geomorphology, including catchment area, estuary area, and transect depth (r = 0.48 to 0.57) (Figure 4.8, "Geomorph." facet). This suggests that larger estuaries may support stronger autotrophic responses. However, studies examining a larger number of estuaries (beyond n = 5) are needed to determine the significance of this potential driver. Lower saturated dissolved oxygen levels did display moderate correlations with autotrophic responses (r = -0.58), however absolute

concentrations were weakly associated (r = -0.37) (Figure 4.8, T0 column in “Water quality” facet).

4.3.8 Significance and conclusions

In this study, we demonstrate that wildfire-enriched aerosols can induce rapid and functionally significant shifts in estuarine microbes within just 24-hours. Despite all estuaries being exposed to the same wildfire-enriched aerosols, at the same concentration, and under the same controlled environmental conditions, acute microbial responses to the average wildfire scenario varied markedly across estuaries. We identified three distinct patterns: 1) no detectable response (Lake Tabourie, Clyde River, Moruya River), 2) a shift towards heterotrophy (Lake Brou), and 3) a shift towards autotrophy (Tuross River). Autotrophic responses were associated with larger, fresher, and more acidic estuaries, elevated levels of labile nutrients at the time of sampling, a history of nutrient limitation (particularly phosphorus), and smaller, more pigmented cyanobacterial populations. In contrast, heterotrophic responses were linked to smaller, more brackish, and alkaline estuaries with low labile nutrient availability, a history of nutrient enrichment, high abundances of non-photosynthetic bacteria, and the potential presence of cryptophytes. Further studies are needed to confirm the relative importance of these potential drivers.

Under the extreme wildfire PM scenario, however, responses converged across all estuaries, marked by the proliferation of high-DNA bacteria and impaired phytoplankton function. These findings highlight the vulnerability of coastal ecosystems to wildfire disturbance and emphasize the need to consider both toxic and nutritional components of wildfire-enriched aerosols as acute drivers of biogeochemical change in aquatic environments. They also leave open questions about the longer-term effects of wildfire-enriched aerosols and ash on estuarine ecosystems. As wildfires become more frequent and intense with climate change, understanding microbial responses will be essential for predicting both short- and long-term impacts on water quality, primary production, carbon cycling, and overall estuarine resilience.

Funding

This work was supported by the Climate Change Cluster and the Faculty of Science at the University of Technology Sydney (UTS) through the provision of operational funding and equipment. Additional support was provided the NSW Department of Planning and Environment (DPE) through in-kind contributions of expertise and consumables. RLG was supported by an Australian Government Research Training Program Scholarship at UTS.

CRediT authorship contribution statement

RLG, PS, FRT and MAD designed the study; PS facilitated and resourced field work; RLG, RF and FRT prepared wildfire-enriched particulate matter treatments; RLG performed air quality analysis; RLG, CM, AW, CJ and MAD collected estuary samples and contributed to experimental set up/pack up; RLG processed samples; RLG analysed & interpreted the data; RLG drafted the manuscript. All authors edited and reviewed the manuscript.

Declaration of competing interest

The authors declare that they have no known competing financial interests or personal relationships that could have appeared to influence the work reported in this paper.

Acknowledgements

We would like to acknowledge Dr. Michaela Larsson for her assistance with refining our protocols for gating of microbial populations in flow cytometry analysis.

5. Aerosols generated by extreme wildfires elicit dose- and time-dependent changes in estuarine microbial communities

Raissa L. Gill [1, 2, #], Alivia L. Price [1], Kittikun C. Songsomboon [1], Callum Muir [3], Aaron Wright [3], Robert Fleck [2], Colin Johnson [3], Peter Scanes [3], Fraser R. Torpy [2], Martina A. Doblin [1, 4]

[1] Productive Coasts, Climate Change Cluster, University of Technology Sydney, Ultimo, NSW, 2007, Australia

[2] Plants and Environmental Quality Research Group, School of Life Sciences, Faculty of Science, University of Technology Sydney, Sydney, NSW, Australia

[3] Estuary and Catchments Science, New South Wales Department of Planning, Industry and Environment, Sydney, NSW, Australia.

[4] Sydney Institute of Marine Science, Mosman, NSW, 2088, Australia

[#] Corresponding Author: raissa.l.gill@student.uts.edu.au; PO Box 123 Ultimo, NSW, 2007, Australia

Chapter 5 is currently presented as a draft manuscript in preparation for submission.

Highlights

- Microbial responses of viruses and bacteria were rapid but transient, with cell abundances returning to baseline levels within 1-2 days of wildfire exposure.
- Eukaryotes and chlorophyll-positive bacteria exhibited exponential increases in cell abundance with wildfire dose,
- Eukaryotic populations were not sustained over the full 10-days of the experiment, with a rapid collapse timed with a rise in viruses.
- Exposure to higher doses of wildfire-enriched particles significantly enhanced the diversity of bacterial assemblages, and reduced the diversity of eukaryotes

Abstract

Wildfires are increasing in frequency and severity worldwide, yet their impacts on aquatic ecosystems - particularly estuaries - remain poorly understood. Fire-derived nutrients and toxins have the potential to significantly alter estuarine microbial communities, which are central to ecosystem health and biogeochemical functioning. To address this gap, we incubated microbial communities from a pristine estuary in New South Wales, Australia with wildfire-enriched aerosols collected during the 2019-20 “Black Summer” wildfires, the most extreme fire season in Australia’s recorded history. Bottle incubations aimed to mimic dry deposition of aerosols from overhead smoke plumes using fluxes estimated from air monitoring data. This study features two distinct experiments: (1) a 5-day “Dose Response” experiment spanning twelve concentrations across the full range of estimated fluxes, and (2) a 10-day “Scenarios” experiment reflecting average and maximum local deposition conditions. Samples were collected and analysed for flow cytometry, photophysiology, eDNA and water quality. Results revealed concentration- and time-dependent effects that varied by microbial population. In the Dose Response experiment, viruses showed short-lived growth at low particle fluxes, while heterotrophic and phycoerythrin-containing bacteria required higher doses to elicit a stimulatory effect. Over five days, chlorophyll-containing bacteria and eukaryotes increased in abundance with particle dose, whereas *Synechococcus* declined. In the Scenarios experiment, a sharp decline in eukaryotes occurred on day 6 and persisted for the remaining four days, with cells exhibiting reduced size, complexity, and fluorescence. Despite this, cell abundances were similar across the two scenario treatments. Viruses and heterotrophic bacteria resurged approximately 24 hours later, with higher abundances observed in the Average compared to the Maximum Scenario. *Synechococcus* also rebounded from day 6, particularly under the Maximum Scenario, although it declined again toward the end of the experiment. By day 10, substantial shifts in microbial community composition were evident. Eukaryotic alpha diversity declined under the Maximum Scenario, with communities increasingly dominated by diatoms, particularly *Skeletonema* and *Chaetoceros*. In contrast, bacterial diversity increased under the same treatment, including higher relative abundance of Rhodobacterales, and reductions in PCC-6307 (Cyanobacteria) and Flavobacteriales, alongside changes in several rare taxa. These findings demonstrate that wildfire-enriched aerosols can alter the abundance and structure of estuarine microbial communities in a concentration- and time-dependent manner, with effects ranging from viral stimulation to acute toxicity to uninhibited growth. As wildfire activity intensifies globally, understanding the responses of aquatic microbes will be essential for predicting and managing the consequences of future fire seasons.

Keywords

Wildfire aerosols; Atmospheric deposition; Environmental DNA; Estuaries; Aquatic microbes; Community composition; Diversity; Dose response

Abbreviations

A = Average treatment
ANOVA = Analysis of variance
BAC = Bacteria
C = Control treatment
CBD = Central Business District
CHL+ = Chlorophyll-positive
DCCEEW = Department of Climate Change, Energy, the Environment and Water
DOM = Dissolved organic matter
eDNA = Environmental DNA
ESD = Equivalent spherical diameter
EUK = Eukaryotes
F0 = Dark-adapted minimum fluorescence
Fm = Dark-adapted maximum fluorescence
FSC = Forward scatter
Fv/Fm = Maximum quantum yield
HET = Heterotrophic bacteria
HVAC = Heating, ventilation and air conditioning
M = Maximum treatment
nMDS = Non-metric multidimensional scaling
PAM = Pulse amplitude modulated [fluorometry]
PCA = Principal component analysis
PE+ = Phycoerytherin-positive
PERMANOVA = Permutational analysis of variance
PHY = Phytoplankton
PM = Particulate matter
SIMPER = Similarity percentage [analysis]
SSC = Side scatter
SYN = Synechococcus
TSP = Total suspended particles
UTS = University of Technology Sydney
VLP = Virus-like particles

5.1 Introduction

Vegetation fires are an intrinsic component of Australia's natural landscape, playing a crucial role in maintaining biodiversity by creating habitats for wildlife and facilitating native plant reproduction (Kelly et al., 2020). Indigenous fire management practices have been integral to this process for thousands of years, with evidence suggesting that such practices began over 11,000 years ago (Fletcher et al., 2021). These traditional methods have fostered fire-tolerant ecosystems and have been associated with reduced bushfire risk and enhanced species richness (Fletcher et al., 2021). However, anthropogenic climate change is modifying natural fire regimes, with wildfires projected to increase in their frequency, severity and duration (IPCC, 2021). This trend is already evident in recent global disasters, including extreme fire events in Chile (>500,000 ha burnt; (Bowman et al., 2019), California (~1.9 Mha; (Ayars et al., 2023), Siberia (~4.7 Mha; (Descals et al., 2022), and Australia (~30.4 Mha; (Bowman et al., 2020). The 2019-2020 Black Summer wildfires exterminated nearly 3 billion mammals, reptiles, birds and amphibians (WWF Australia, 2020).

Beyond these immediate and localised impacts, the 2019-20 wildfires emitted far-reaching smoke plumes that travelled well beyond the burn zones, including downwind terrestrial areas, estuarine and coastal waters, and even remote ocean areas across the Southern Hemisphere (Peterson et al., 2021). While the consequences of these fires for air quality, human health, the economy, and terrestrial ecosystems are increasingly well understood, their impacts on aquatic biota remain relatively uncertain – particularly for estuaries. These coastal waterways are highly productive ecosystems that play critical roles in carbon sequestration, filtering contaminants, promoting biodiversity, and providing essential nursery habitats for commercially and ecologically important fish species (Gillanders et al., 2011; Hallett et al., 2016; Rönnbäck, 1999; Roy et al., 2001). They also support socio-economic systems and cultural values for indigenous Australians (National Oceans Office, 2002; Russell et al., 2015). Underpinning these ecosystem services are the microbial communities that fuel the base of estuarine food webs and drive key nutrient cycles that regulate water quality (Crump and Bowen, 2024). A recent review by Paul et al., (2022) highlights the varied impacts of wildfires for aquatic microbes, where across 25 studies, changes in algal diversity/richness/abundance pre- to post-fire remained unchanged in nearly half of studies (48%), with 28% seeing an increase, and 24% a decrease (Paul et al., 2022). Given the ecological and economic significance of Australia’s estuaries, improving our

understanding of how they are impacted by extreme wildfires is essential for managing the water quality impacts of future fire events.

A critical factor shaping how estuaries respond to wildfire events is the chemical composition of fire-derived inputs. Wildfires emit vast quantities of ash and smoke particles into the atmosphere, which are delivered to estuaries either directly from the atmosphere via gravity or via land runoff following precipitation. Ash refers to the coarse (2 – 2000 µm; (Balfour and Woods, 2013) partially burned residue that is typically found on the ground near its point of emission (Bodí et al., 2014), with particles larger than 10 µm usually settling within 24 hours (Textor et al., 2006). Ash consists primarily of charred organic matter (Bodí et al., 2014), along with trace elements and ions including calcium (Ca), aluminium (Al), iron (Fe), sulfate (SO_4^{2-}), chloride (Cl^-) and sodium ions (Na^+) (Harper et al., 2019). Upon entry to the water column, ash releases dissolved nutrients and trace metals that can stimulate microbial growth and alter community composition (Santín et al., 2015). For instance, during the 2017 Thomas Fires (USA), four-day bottle incubations with ash leachate supplied coastal microbes with an abundance of dissolved nutrients (organic carbon, nitrogen, silicic acid, iron, cobalt) and potentially toxic elements (copper, nickel), which ultimately provided "food for all" by supporting the growth of a diverse assemblage of eukaryotes (Ladd et al., 2023). Similarly, three-day incubations with ash from the 2017 Ria de Vigo wildfires (Spain) promoted growth of coastal phytoplankton and bacteria under nutrient-poor conditions – including potentially pathogenic taxa – yet had minimal effects when nutrients were high (Gutiérrez-Barral et al., 2024).

In contrast to ash, smoke is dominated by fine particles (<2.5 µm; (Reid et al., 2005)) that can remain airborne for up to one week in the planetary boundary layer to several months in the stratosphere (Peterson et al., 2021; Textor et al., 2006). Fresh smoke typically contains a mixture of organic and inorganic nutrients including organic carbon (OC), nitrogen (N) compounds, nitrate (NO_3^-), potassium ions (K^+), SO_4^{2-}, and Ca ions (Ca^+) (Reid et al., 2005). However, wildfire smoke is more than just burnt biomass: Fire-driven weather entrains mineral dust elements (e.g. Al, Fe, manganese, silica, titanium) and legacy contaminants (e.g., mercury, lead) from surrounding soil, with varying composition depending on local factors (e.g., soil type, vegetation, land use history) (Isley and Taylor, 2020; Wagner et al., 2018). As smoke plumes travel, atmospheric processing further alters their chemistry, oxidising OC, enriching them with acidic ions (e.g., NO_3^-, SO_4^{2-}) and increasing the solubility of crustal and anthropogenic metals (Akagi et

al., 2011; Baker and Jickells, 2006; Kanakidou et al., 2005). While estuaries within or near fire zones are vulnerable to immediate ash fallout during active burning, smoke with its longer atmospheric residence time poses a broader hazard by transporting highly soluble and potentially harmful constituents to both nearby and surrounding estuaries.

Studies of wildfire impacts on aquatic microbes are even scarcer for smoke than for ash, though available data indicate significant shifts in aquatic microbial dynamics. For example, three-day incubations in Lake Tahoe (USA) using smoke-derived total suspended particles (TSP) from the 2007 Angora Fire, favoured the growth of smaller picoplankton and filamentous cyanobacteria as opposed to larger nanophytoplankton by supplying nutrients with a high N:P ratio (as ammonium) (Mackey et al., 2013). Over longer time scales (2006 – 2020), wildfire-enriched $PM_{2.5}$ has been linked to an increase in lake cyanobacteria (USA) 2-7 days after exposure, which was likely due to phosphorus inputs (Olson et al., 2023). During the 2019-20 Black Summer wildfires (Australia), several studies have documented marine phytoplankton blooms due to smoke-derived nutrient deposition in downwind ocean regions using satellite imagery (Li et al., 2021; Tang et al., 2021; Wang et al., 2022; Weis et al., 2022). Weis et al. (2022) also demonstrated significant shifts in the composition and physiology of phytoplankton cells. However, despite 30 % of Australia's coastal catchments being burned during the 2019-20 Black Summer (Fryirs et al., 2022), little has been reported on the impacts of smoke deposition in estuaries.

To address this gap in knowledge, we used bottle incubation experiments to investigate how aquatic microbial communities collected from a pristine estuary on NSW's south-east of Australia respond to dry deposition of wildfire-enriched particulate matter (PM_{10}). Incubations were performed using particles captured during the 2019-20 Black Summer wildfires which were added over a range of concentrations reflecting estimated fluxes of dry deposition for 5-10 days. We aimed to mimic the dry gravitational settling of particles on the estuary surface from overhead smoke plumes, as would occur *during* active fire conditions, and to gain a mechanistic understanding of how aquatic microbes respond to these inputs. Our objectives were to identify potential thresholds for fertilisation and toxicity in different microbial populations, and to examine impacts on physiology and community composition.

5.2 Material and methods

5.2.1 Estuary field sampling

5.2.1.1 Study site

Sampling was conducted in Clyde River, Batemans Bay (35.7162° S, 150.1795° E), located ~280km from Sydney's Central Business District (CBD) on the South Coast of NSW, Australia. The Clyde River was examined previously in field experiments (Thesis Chapter 4) and was chosen for further testing after discussions with the NSW Department of Climate Change, Energy, the Environment and Water (DCCEEW) for several reasons; 1) the system was located in Batemans Bay which was heavily impacted by the 2019-2020 wildfires (74% stream length burned; (Fryirs et al., 2022), and 2) the system was relatively pristine, lacking significant runoff pollutants compared with the other estuaries routinely monitored by NSW DCCEEW. Clyde River is a tide dominated drowned valley with an open mouth to the sea, with significant recreational and economic significance to the population of Batemans Bay, hosting numerous oyster aquaculture leases. The river holds 50,737 ML of water with an estuary / catchment area of 17.5 and 1,723 km^2, respectively.

5.2.1.2 Sampling strategy

Estuary sampling was undertaken in collaboration with NSW DCCEEW, using field procedures consistent with the NSW Government's state-wide estuary monitoring program (Hallett et al., 2016; Office of Environment and Heritage (OEH), 2016), as previously described in Thesis Chapter 4. Briefly, on the 5th of May 2022, a powered vessel equipped with a calibrated water quality sonde (YSI EXO2, YSI Inc; OH, USA) and vertical pole sampler was used to sample at a depth of ~0.5 m along a three-point transect. The probe recorded date, time, GPS location, temperature, dissolved oxygen, conductivity, salinity, pH, turbidity, blue-green algae phycoerythrin (525 ± 15nm excitation), chlorophyll (470 ± 15 nm excitation), and fluorescent dissolved organic matter (365 ± 5 nm excitation). These are presented in Table 5.1 below. Water samples were filtered immediately through a 200 µm nylon mesh to remove mesozooplankton and debris. In total, ~400 L of water was collected and transported to the laboratory at University of Technology Sydney (UTS) for processing.

Table 5.1 Summary of water quality parameters across a three-point transect sampled in Clyde River in May 2022. Sites 1-3 reflect readings at each of the three points for water collection, while the Composite indicates the mean ± sd of values.

	Site 1		Site 2		Site 3		Composite	
	Mean	SD	Mean	SD	Mean	SD	Mean	SD
Temp. (°C)	18.8	0.1	19.2	0.0	19.2	0.0	19.1	0.2
DO (%)	81.2	0.3	82.6	0.2	85.4	0.2	83.1	2.1
DO (mg/L)	6.85	0.05	6.73	0.02	6.82	0.02	6.80	0.06
SPC (µS/cm)	26961	403	33902	708	38539	87	33134	5827
Sal. (ppt)	16.6	0.3	21.3	0.5	24.6	0.1	20.8	4.0
pH	7.71	0.01	7.91	0.02	8.01	0.00	7.88	0.15
Turb. (NTU)	0.96	0.04	3.11	1.20	0.93	0.07	1.67	1.25
BGA-PE (RFU)	1.9	0.1	2.5	0.1	2.5	0.1	2.3	0.4
BGA-PE (µg/L)	5.3	0.2	7.0	0.2	7.0	0.3	6.4	1.0
Chl (RFU)	0.29	0.04	0.54	0.03	0.44	0.02	0.42	0.12
Chl (µg/L)	3.8	0.1	4.7	0.1	4.3	0.1	4.3	0.5
fDOM (RFU)	8.14	0.05	6.50	0.21	5.03	0.03	6.56	1.56

5.2.2 Wildfire-enriched particulate matter

Wildfire-enriched particulate matter (PM) treatments utilised PM described in Gill et al. (2024). In brief, PM enriched by aged wildfire emissions in Sydney, Australia was captured in Heating, Ventilation and Air Conditioning (HVAC) building filters at the University of Technology Sydney (UTS) Ultimo campus (33.8832° S, 151.2005° E) between November 2019 and February 2020 (4 months). A filter forensics approach was used to extract this material by vacuum through a 25 µm pre-screen into pre-weighed sealed cassettes. Cassettes containing predominately PM_{10} (PM < 10 µm diameter) were stored in dry dark conditions until use in experimentation. A detailed description of the PM's composition, solubility, size and sources can be found in Gill et al., (2024) and Thesis Chapter 3. Wildfire-enriched PM treatments were prepared by transferring PM from three pre-weighed cassettes into a bottle containing 0.22 µm syringe-filtered water from the Clyde River. Each cassette was rinsed twice with filtered water to recover any remaining particles. Serial dilutions of this stock were then prepared using filtered estuary water to create solutions suitable for dosing each treatment with 1 mL d^{-1}.

5.2.3 Experimental design

In a previous investigation (Chapter 4), we examined the acute (24-hour) effects of wildfire-enriched PM on microbial communities across five estuaries. In this study, we focus on a single estuary to explore these impacts in greater detail over an extended period. To do this, we

conducted two experiments in which wildfire-enriched PM was added daily for 5–10 days at concentrations based on dry deposition fluxes measured in Batemans Bay during the 2019–20 Black Summer wildfires (see Chapter 3 for methods). The first experiment - *Dose response* - involved adding wildfire-enriched PM daily for five days at twelve concentrations ranging from of 0.01 to 5 g L^{-1} d^{-1}, covering the full range of hourly and daily deposition fluxes for the region. The second experiment – *Scenarios* - simulated two 10-day fluxes of dry deposition with PM added every day: an "Average" scenario calculated as the mean daily flux during the fire period, and a "Maximum" scenario reflecting the highest 10-day moving average. Both experiments included control incubations without wildfire-enriched PM addition (0 g L^{-1}) and were conducted with five replicates per treatment.

5.2.4 Experimental setup and sampling

Upon return from Clyde River, estuary water was gently swirled to homogenise microbes before being dispensed into several 250 mL flasks (Dose Response experiment) and 4 L bottles (Scenarios experiment) according to section 5.2.3 above. Baseline t0 samples (n = 3) were collected by carefully swirling estuary water to homogenise microbial communities, then preparing several aliquots for analysis by pulse amplitude modulated (PAM) fluorometry, flow cytometry, and environmental DNA (eDNA); sections 5.2.5 to 5.2.7). Additional estuary water was filtered twice through a 0.22 µm syringe filter and set aside for use in PAM analysis (section 5.2.4) and preparation of wildfire-enriched PM treatments (section 5.2.2). Vessels were then placed in a climate-controlled room (Figure 5.1) set to 20 °C and illuminated with ~200 µmol photons m^{-2} s^{-1} of light on a 12:12 cycle to simulate the diurnal light climate in surface waters of the Clyde River, NSW. Temperature logging iButtons (Thermochron; USA) deployed in the climate-controlled room confirmed water temperatures of ~20.6 ± 0.1 °C (mean ± sd), ranging from 19.5 to 22 °C (min/max) over the 10 days. The configuration of vessels during incubation was randomised daily to avoid systematic effects of light or shelf position. The next morning at sunrise, flasks and bottles were gently swirled three times before being sampled for flow cytometry analysis (section 5.2.6). Vessels were then dosed with 1 mL of wildfire-enriched PM solution (section 5.2.2) that had been shaken vigorously for 1 minute to resuspend settled particles. Vessels were resealed and gently swirled to homogenise the particles, before being randomly repositioned back on a shelf. Sampling and wildfire-enriched PM dosing was repeated daily for 5-10 days, depending on the treatment. At the end of the second experiment (Scenarios), additional samples were taken for PAM and eDNA analysis (as above), as well as measurement of physical water parameters (section 5.2.8).

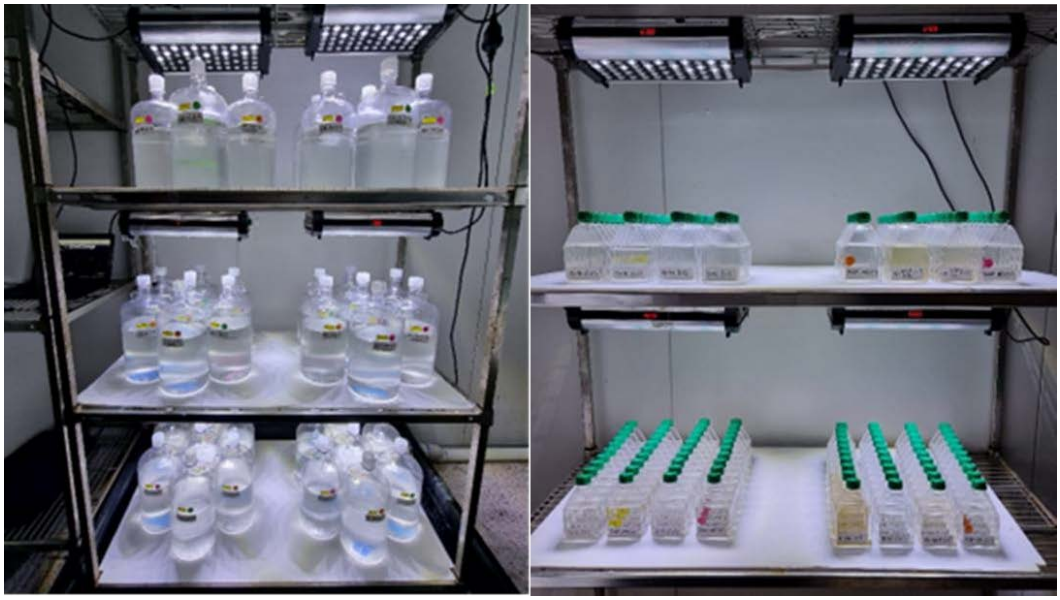


Figure 5.1 Photograph of the experimental set up for the “Scenario” experiment (left) and “Dose response” experiment (right).

5.2.5 PAM fluorometry

Photophysiology was assessed using a Water Pulse Amplitude Modulated fluorometer (Water-PAM) and WinControl software (Heinz Walz GmbH, Germany), as described previously (Thesis Chapter 4). Briefly, samples were syringe-filtered through a 0.22 µm filter into a clean quartz cuvette (to remove phytoplankton). Chlorophyll-a fluorescence was checked for negligible emission using a single saturating pulse of blue light (460 nm; pulse duration = 0.6 s; pulse intensity = 930 µmol photons m^{-2} s^{-1}). If fluorescence was detected, the sample was filtered again and re-checked. The Water-PAM was then blanked, and gain settings were adjusted to a base fluorescence ~49.90 (mean; gain = 20). For subsampling, incubation vessels were gently swirled to homogenise microbes, and 3 mL aliquots were dispensed into glass tubes and kept in the dark for at least 30 minutes. Dark adapted samples were then transferred into a clean cuvette and placed in the emitter-detector unit of the Water-PAM. After stabilisation (~1 minute), a single saturating pulse was emitted to measure dark-adapted minimum (F0) and maximum (Fm) fluorescence. These measurements were used to estimate the maximum quantum yield (Fv/Fm) of Photosystem II using Equation 1 below.

$$Fv/Fm = (Fm - F0) / Fm \quad (1)$$

where F0 and Fm are dark-adapted minimum and maximum fluorescence, respectively.

5.2.6 Flow cytometry

Vessels were gently swirled before subsampling 2 mL into cryotubes pre-loaded with Electron Microscope grade paraformaldehyde (1 % final v/v). Tubes were sealed, inverted, and snap-frozen in liquid nitrogen within 15 minutes, then stored at –80 °C until analysis. Samples were analysed by flow cytometry (Cytoflex LX, Beckman Coulter, USA) using CytExpert software, as described previously (Thesis Chapter 4). Briefly, the cytometer was operated in plate mode with blue excitation (488 nm) and fresh Milli-Q as diluent (18.2 Ω; Millipore, Germany). Daily calibration was performed using fluorescent quality control microspheres (CytoFLEX Daily QC Fluorospheres; Beckman Coulter, USA) and 1-15 µm non-fluorescent beads for size calibration (Flow Cytometry Size Calibration Kit; Thermofisher, USA). After calibration, the cytometer was flushed and cleaned to reduce background noise (≤10 events s^{-1}).

Sample analysis methods followed those outlines by Marie et al., (1999b, 1999a). Frozen samples were thawed at 35 °C for 15-20 minutes prior to analysis. For bacteria (BAC) and virus-like particles (VLP), vortexed samples were diluted 1:5 in 0.22 µm filtered TE buffer (10 mM Tris-HCl, 1 mM disodium EDTA, pH = 8.0, Sigma-Aldrich, USA) containing 1:20,000 SYBR Green I (SYBR Green I Nucleic Acid Gel Stain – 10,000X concentrate in DMSO; Invitrogen, USA). After 15 minutes of dark incubation, acquisition (10 µL min^{-1}) was triggered on green fluorescence (525/40 nm) using 0.22 µm filtered unstained samples and stained buffer to set fluorescence thresholds. Gating used violet side scatter (VSSC; 405 nm) and green fluorescence, where VLP were distinguished as SYBR-positive with lower fluorescence and VSSC than BAC. Bacterial autotrophs were further classified into chlorophyll-positive (CHL+ BAC) and phycoerytherin-positive (PE+ BAC) cells using red (690/50 nm) and orange (585/40 nm) autofluorescence. For phytoplankton (PHY), 200 µL of unstained, undiluted sample was analysed (60 µL min^{-1}), with sample acquisition triggered on forward scatter (FSC; 488 nm) and the background threshold set using the red autofluorescence of 0.22 µm filtered unstained samples. Gating used side scatter (SSC; 488 nm) and red autofluorescence, where *Synechococcus* (SYN) were differentiated from *Eukaryotes* (EUK) using orange autofluorescence. Across all populations, abort rates were <1 % and FSC height vs. area plots confirmed no cell aggregation (R^2 = 0.99).

Abundances of microbial populations were quantified based on event counts per unit volume (cells mL^{-1}) within established gating parameters. Phytoplankton traits such as cell size (FSC), granularity (SSC), and autofluorescence of chlorophyll (red) and phycoerytherin (orange)

pigments were expressed as median single-cell values of the population. Median FSC values were converted to equivalent spherical diameter (ESD; µm) using a linear regression with size calibration beads (R^2 = 0.98). Granularity and pigments were normalised to cell size by dividing these values by ESD.

5.2.7 eDNA analysis

Bottles were gently swirled, and between 1.95 - 2.07 L of sample was vacuum-filtered through a Sterivex-GP filter unit (0.22 µm, Millipore SVGPL10RC, Merck; Australia). Filters were sealed with parafilm and stored at –80 °C until further processing by an external laboratory (enviroDNA; Brunswick, Australia). Sequencing was performed on the Illumina MiSeq platform using a paired-end 300-bp kit (Monash Health Translation Precinct; Clayton, Australia). Bacterial 16S rRNA genes were amplified using the 27F/519R primer pair targeting the V1–V3 regions (Caporaso et al., 2011; Keller et al., 1997; Lane et al., 1993), while Eukaryotic 18S rRNA genes were amplified with the V4F/V4R primer pair targeting the V4 region (Stat et al., 2017).

Amplicon sequences were processed by enviroDNA using their custom bioinformatics pipline. Cutadapt V3.0 (Martin, 2011) was employed to remove unwanted sequences, including adapters, primers, and poly-A tails. VSEARCH V2.9.0 (Rognes et al., 2016) was used to: 1) align and merge paired-end reads; 2) dereplicate identical sequences; 3) filter out sequences shorter than 20 bp or containing ambiguous bases; 4) reduce sequencing and PCR errors via clustering of variants; and 5) assign taxonomic identities to each sequence. Taxonomic classification was performed at a 50% confidence threshold using the SILVA SSU Ref NR99 database (https://www.arb-silva.de/) for prokaryotes and the NCBI GenBank database (https://www.ncbi.nlm.nih.gov/genbank/) for eukaryotes. SILVA provided more detailed resolution for prokaryotic taxa, while NCBI taxonomy yielded more consistent and stable assignments for eukaryotes.

Subsequent data processing used similar methods to Bracewell et al. (2023). Taxa unassigned at the Kingdom or Phylum levels were removed, as well as 16S taxa annotated as eukaryotic organelles (i.e., chloroplasts and mitochondria). Taxa present in only one replicate across all samples and treatments were excluded to reduce the influence of exceptionally rare taxa. To account for differences in sequencing depth, read counts were normalised within each sample

by dividing each taxon's count by the total read count for that sample (McKnight et al., 2019) and multiplying by 100 for a percentage. This normalisation method was selected as it outperformed all other methods for producing accurate Bray-Curtis dissimilarities and associated analyses (McKnight et al., 2019). Alpha diversity metrics, including Shannon diversity, Simpson diversity, and species richness, were calculated using the *vegan* package (Oksanen et al., 2022) in R software (V4.4.2; (R Core Team, 2021)). These complementary indices were selected to capture different aspects of microbial community structure: Shannon for diversity, accounting for both richness and evenness, Simpson for dominance and evenness, and species richness for the total observed taxa.

5.2.8 Physical water parameters

Bottles were carefully mixed before dispensing 500 mL into autoclaved, glass beakers. Water quality parameters were then examined for temperature, dissolved oxygen, conductivity, salinity, and pH using a calibrated multi-parameter meter (MultiLine Multi 3630 IDS; Xylem, USA). Light received within the bottles and flasks used in experimental treatments was assessed in unshaken and shaken vessels using a 4-pi light sensor (Universal Light Meter & Data Logger (ULM-500), Heinz Walz GmbH, Germany).

5.2.9 Statistical analysis

To account for the effect of the incubation over time, PAM fluorometry and flow cytometry data were standardised by subtracting the mean value of the control incubation from each raw wildfire treatment value on the same day, yielding "relative" trait values. Principal Component Analysis (PCA) was performed on relative flow cytometry-derived trait data to assess population-level responses to wildfire-enriched particle additions (correlation-based matrix). To identify thresholds for enrichment or toxicity in Clyde River microbes, we adopted an approach similar to Harper et al. (2019). Raw relative abundance data from the Dose Response Experiment were analysed using two-factor analysis of variance (ANOVA) or permutational analysis of variance (PERMANOVA, Bray–Curtis dissimilarity, 999 permutations) when assumptions of normality and homogeneity of variance were violated (as indicated by residual histograms and Levene's test). This analysis included dry deposition flux and day of incubation as fixed factors and was conducted separately for each microbial population identified by flow cytometry. Where significant results were detected, post-hoc tests (Tukey's HSD or pairwise PERMANOVA comparisons, both with Bonferroni correction) were used to assess differences between days

and/or PM doses. A similar approach was used to analyse the Scenario Experiment, in which unstandardised abundances for each microbial population were tested, with treatment (Control, Average, Maximum) and day of incubation as fixed factors.

For community composition data in the Scenario Experiment, difference in microbial community structure among treatments were assessed using non-metric multidimensional scaling (nMDS), calculated from Bray-Curtis dissimilarities of abundance data after 10 days of incubation. This was performed separately for bacterial and eukaryotic taxa (16S, 18S, respectively). Differences in alpha diversity indices and species richness between treatments were tested using PERMANOVA (Bray–Curtis dissimilarity, 999 permutations) and pairwise PERMANOVA comparisons with Bonferroni adjustment. Composition data was visualised as orders (bacteria) and classes (eukaryotes) to maximise diversity and interpretability whilst minimising unclassified or less abundant taxa. Orders and classes contributing to differences between treatments were assessed using similarity percentages (SIMPER, Bray–Curtis dissimilarity, 999 permutations).

Physical water quality parameters and PAM Fv/Fm measurements were analysed by one-factor ANOVA and Tukey's HSD with Bonferroni adjustment. All plots and analyses were performed in R v4.4.2 (R Core Team, 2021) and utilised the following packages: Bioconductor (Huber et al., 2015), BiocManager (Morgan and Ramos, 2025), car (Fox and Weisberg, 2019), dplyr (Wickham et al., 2021), ggh4x (van den Brand, 2024), ggplot2 (Wickham, 2016), ggpubr (Kassambara, 2020), grid (R Core Team, 2021), ggtext (Wilke, 2020), phyloseq (McMurdie and Holmes, 2013), tidyr (Wickham et al., 2019), scales (Wickham et al., 2011), stringr (Wickham, 2009), vegan (Oksanen et al., 2022).

5.3 Results and discussion

5.3.1 Dose response curves

Bottle incubation experiments with Clyde River microbes revealed a diversity of responses to wildfire-enriched aerosol deposition. After 24 hours of exposure, fertilisation effects were first evident in the viruses, which responded positively to small aerosol inputs up to a flux of 0.17 g m^{-}

^{2} d^{-1}, at which point relative abundances started to decline (p = 0.012). In heterotrophic and phycoerytherin-positive bacteria (excluding larger *Synechococcus*), significant concentration-dependent effects were observed, with growth at aerosol fluxes ≥0.17 g m^{-2} d^{-1} after 24 hours exposure (p < 0.01; Figure 5.2B, D; gold points). These microbial responses were rapid but transient, with cell abundances returning to baseline levels over the remainder of the incubation period (p < 0.01; Figure 5.2B, D), except for day 5 where phycoerythrin-positive bacteria showed a secondary peak at low aerosol fluxes (p = 0.009; Figure 5.2D; pink points). In contrast, *Synechococcus* exhibited a consistent dose-dependent decline in abundance at fluxes ≥0.17 g m^{-2} d^{-1}, remaining suppressed throughout the entire 5-day period (p < 0.001; Figure 5.2F). Other microbial populations showed no substantial change during the initial 24-hour period (p > 0.05; Figure 5.2). Conversely, eukaryotes and chlorophyll-positive bacteria displayed increased growth starting at a flux of 0.1 g m^{-2} d^{-1}, which accelerated significantly at concentrations ≥0.50 g m^{-2} d^{-1} (p < 0.01; Figure 5.2C, E). These effects were additive with each day of exposure (Figure 5.2C, E; pink points).

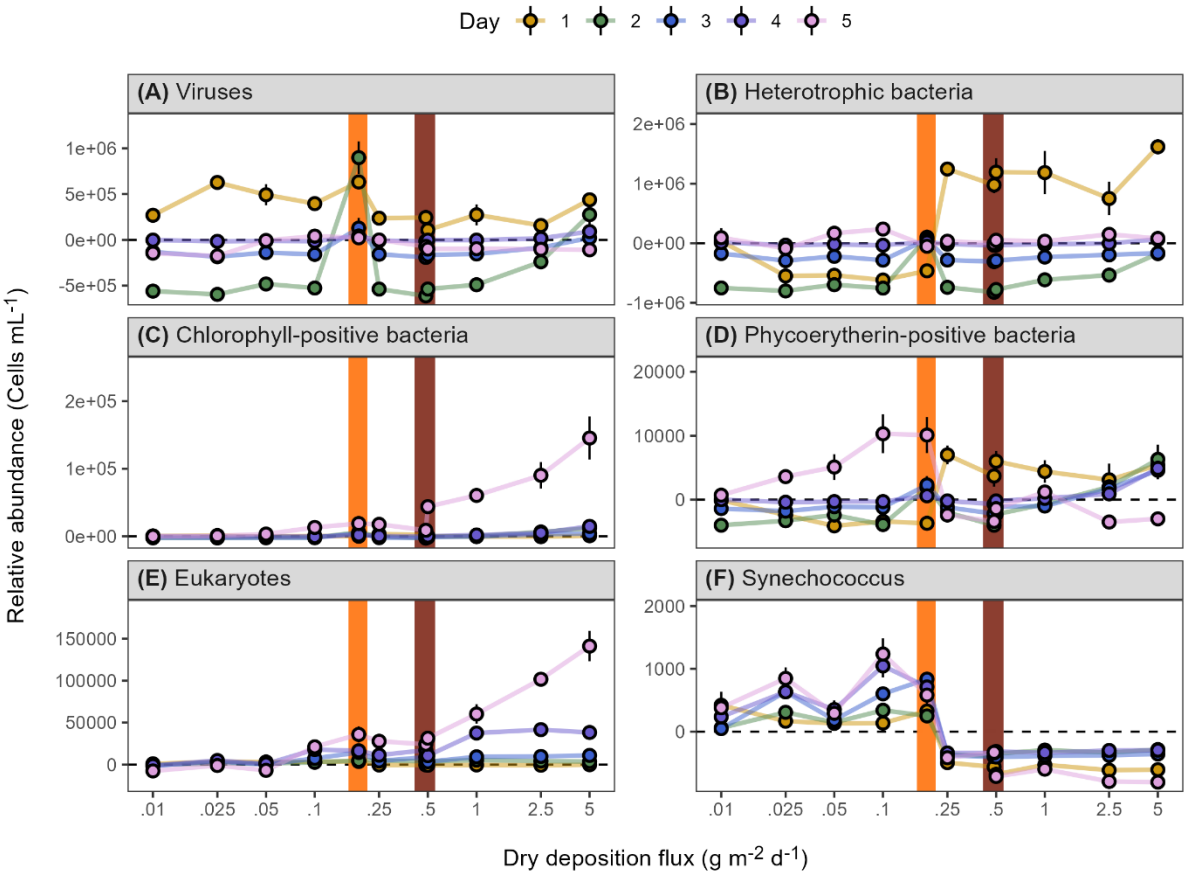


Figure 5.2 Dose response curves depicting cellular abundance (y-axis) relative to Control Incubations (dashed line) with increasing wildfire deposition flux (x-axis). Microbial populations are separated into individual facets, where duration of exposure is denoted by colour. Orange and dark red bars depict concentrations corresponding to average and maximum daily deposition during the 2019-20 Black Summer wildfires. Points and black error bars represent means and standard errors, respectively (n = 5).

These findings indicate that small, fast-growing microbes are the first responders to wildfire inputs, likely responding to an abundance of bioavailable organic carbon (Azam et al., 1983). Our results also suggest that *Synechococcus* may be particularly sensitive to wildfire smoke, especially when PM_{10} deposition exceeds 0.17 g m^{-2} d^{-1} – equivalent to an ambient air concentration of ~97 µg m^{-3} and typical of local conditions during the 2019-20 Black Summer wildfires. This may be due to the presence of potentially toxic elements in wildfire smoke, with PM treatments containing dissolved forms of the following elements: zinc > manganese > copper > mercury > nickel > antimony > cobalt > lead > cadmium (Gill et al., 2024). This is consistent with literature demonstrating the heightened sensitivity of *Synechococcus* relative to other microbial groups, even when nutrients are favourable for growth (de la Broise and Palenik, 2007; Debelius et al., 2011; Paytan et al., 2009).

5.3.2 Temporal dynamics

Microbial responses to wildfire-enriched particle additions in the Scenario experiment exhibited distinct temporal patterns and population-specific dynamics over the ten-day incubation (Figures 5.3 and 5.4), with increasing divergence from the control over time - particularly under the maximum wildfire scenario (Figure 5.3A).Heterotrophic bacteria showed a sustained increase over the entire 10-day period, with a sharp incline from day 6 that peaked on day 8 ($p = 0.008$; Figure 5.4B). Similar to its dose response curve (Figure 5.2B), this peak in relative abundance was higher in the maximum wildfire treatment than the average scenario ($p = 0.011$; Figure 5.4B). This expansion of heterotrophs is reflected in the community traitscape, where the relative abundance vector for heterotrophic bacteria aligns with the average and maximum treatment trajectories at the end of the incubation (Figure 5.3B, HET_ABUN and full pink/purple circles).

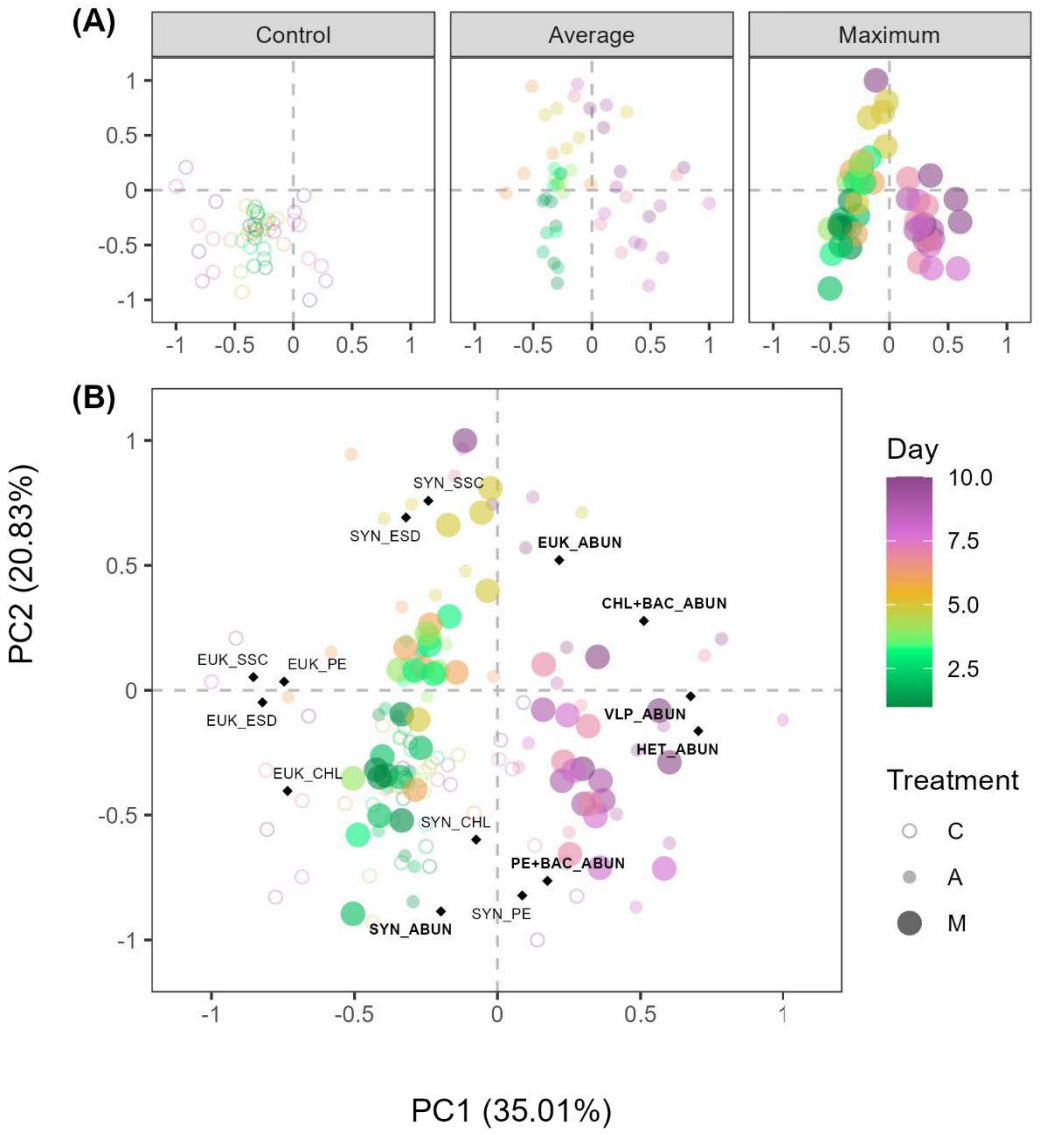


Figure 5.3 Community traitscape of Clyde River microbes in Scenario experiment following 10-day incubations with wildfire-enriched particles, as indicated by Principal Component Analysis (PCA). Data was normalised to the mean control (no aerosol) incubation and includes flow cytometry-based measurements of eukaryotes ("EUK"), Synechococcus ("SYN"), heterotrophic bacteria ("HET"), chlorophyll-positive ("CHL+BAC") and phycoerytherin-positive ("PE+BAC") bacteria, and virus-like particles ("VLP"). Points represent replicate incubation vessels, coloured by day and shaped by treatment (C = control incubation; A = average scenario; M = maximum scenario). All biplots depict the same PCA, but are separated by treatment (A) or marked with PCA loadings (B). Loadings (black diamonds and text) indicate the contribution of each trait to community variation, with bolded labels representing those relating to cellular abundance. Percentages on axes indicate the total variation explained by the first two principal components (PC1 and PC2).

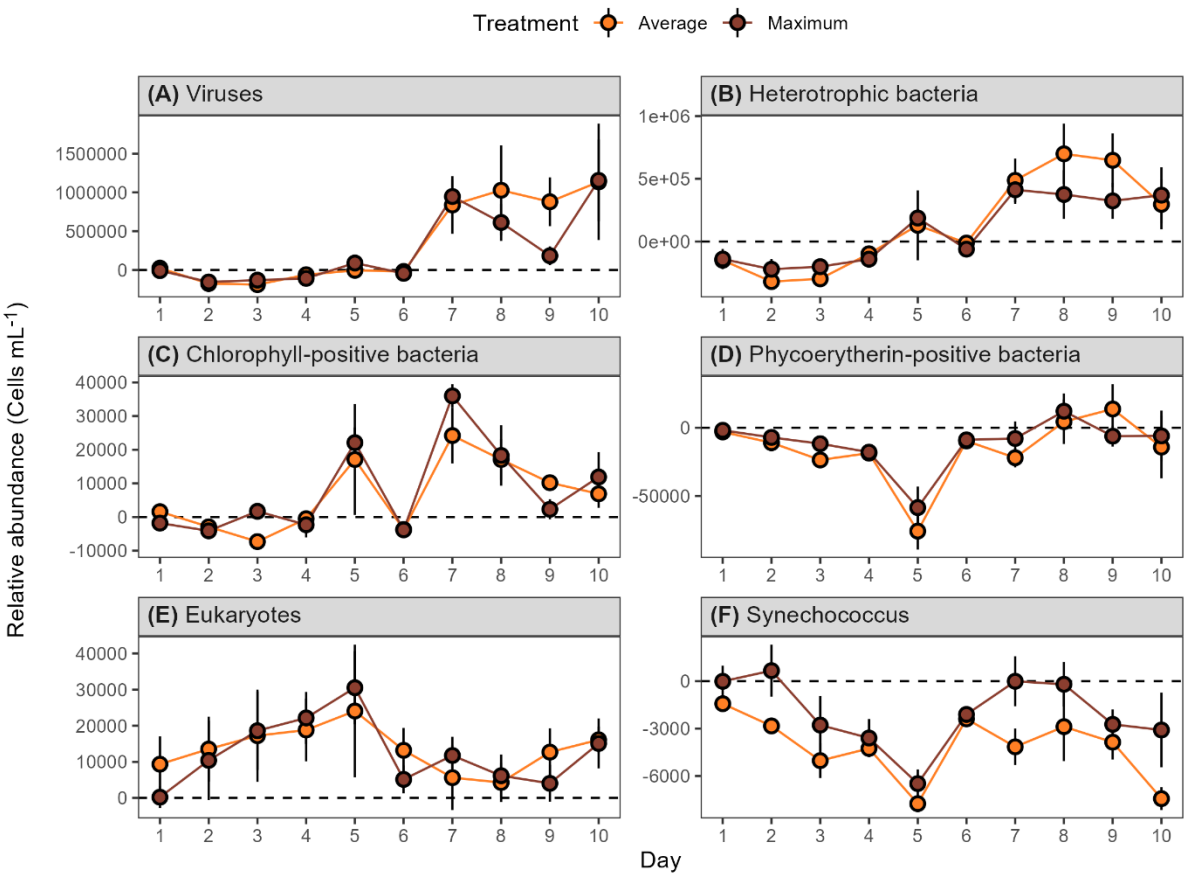


Figure 5.4 Time series displaying changes in cell abundance (y-axis) relative to Control Incubations (dashed lines) over 10 days of daily wildfire exposure in the Scenario experiment. Populations are separated into individual facets, where wildfire treatment is shown by colour: Orange and dark red points depict average and maximum daily deposition scenarios during the 2019-20 wildfires. Points and error bars indicate means and standard deviations, respectively.

In contrast, growth of eukaryotic microbes peaked at day 5, followed by a sharp drop that barely recovered over the next 5 days (p = 0.005; Figure 5.4E). Similar to above (Figure 5.2E), we did not observe a significant difference in growth between these two wildfire concentrations (p = 0.246; Figure 5.4E). This decline in eukaryotes contributed to the shifting traitscape after day 5, with reduced contributions from the eukaryotic abundance vector and smaller, less complex and less fluorescent cells (Figure 5.3B, EUK_ vectors). These results suggest that while wildfire-enriched PM provided an initial stimulus for bacterial growth – likely in the form of dissolved organic matter (DOM) - the sharp decline in eukaryotic microbes between days 5-6 likely released an additional pulse of labile, cellular DOM into the bottles, which became available to heterotrophic bacteria and fuelled further proliferation.

While the collapse of the eukaryotic population may have been triggered by multiple factors - such as nutrient limitation, toxic effects of wildfire-enriched PM, and/or inhibitory microbial interactions (Martínez-Pérez et al., 2024) - we observed a delayed rise in viral abundance from day 6 (p = 0.003; Figure 5.4A) coinciding with the decline in eukaryotic cells. As above (Figure 5.2A), this increase in abundance was not observed in the first 5 days of the incubations (p = 0.103; Figure 5.4A). This dynamic is captured in the community traitscape, where the abundance vector for viruses points towards later time points in the two wildfire treatments (Figure 5.3B, VLP_ABUN and full pink/purple circles). Given that viruses are typically released upon host cell lysis (Mojica and Brussaard, 2014), this pattern aligns with the "kill the winner" hypothesis (Winter et al., 2010). This concept posits that dominant, fast-growing taxa are preferentially targeted by viruses due to their high densities, greater encounter rates, and increased selection pressure for host-specific viral predators (Castledine and Buckling, 2024). This dynamic has been documented previously in phytoplankton communities, where viral infections can both abruptly terminate bloom events and prevent their recurrence over extended periods (Flynn et al., 2022; Pound et al., 2020).

Interestingly, *Synechococcus* rebounded after an initial five-day decline (p = 0.002), however this growth was transient, with a secondary decline observed on days 9-10 (p = 0.018; Figure 5.4F). Consistent with its dose response (Figure 5.2F), this suppression of growth was greater under the average wildfire treatment than the maximum scenario, however only at some time points (p < 0.05; Figure 5.4F). The transient recovery and subsequent decline of *Synechococcus* is reflected by its association with the PC2 axis in the community traitscape, where its abundance vector increases towards days 5-6 (Figure 5.3B, SYN_ABUN and full yellow/orange circles). Higher abundances of *Synechococcus* were also associated with larger, more complex but less pigmented cells (Figure 5.3B, SYN_ vectors). These findings suggest that the temporary alleviation of top-down pressure from the eukaryotes, such as grazing or nutrient competition, or the release of additional DOM from decaying eukaryotic cells, may have enabled a short-lived resurgence.

We observed no significant impact of wildfire-enriched particles on dark-adapted photosynthetic yield after the ten-day period (p = 0.186; Supplementary Figure 5.1), despite clear shifts in microbial abundances and traits. This indicates that the phytoplankton community was able to maintain its photosynthetic function, despite losses in cell abundances.

Collectively, these findings indicate that wildfire-enriched particles can rapidly restructure estuarine microbial communities by enhancing heterotrophic activity and stimulating viral interactions, while simultaneously suppressing more sensitive photoautotrophs. By targeting fast-growing or dominant taxa, viruses may create ecological space for less competitive community members to access limiting resources such as nutrients. Notably, these effects began to emerge within 24 hours of exposure at concentrations reflecting average dry deposition during an extreme fire season. Such rapid microbial restructuring has significant implications for estuarine biogeochemistry, including altered nutrient cycling, primary productivity, and food web structure. Enhanced heterotrophic activity and viral suppression of dominant autotrophs may decrease carbon fixation and oxygen production (Statham, 2012), while increasing organic matter remineralisation (Burkhardt et al., 2014). At the same time, viral lysis of opportunistic taxa may aid in maintaining microbial diversity by creating space and resource access for less competitive community members (Heinrichs et al., 2020). Future studies should include viral enumeration and span longer time frames to clarify how viral dynamics influence the trajectory of microbial community succession and resilience to future wildfire disturbances.

5.3.3 Overview of community composition

Community composition analysis revealed distinct microbial responses to wildfire-enriched particle exposure (Figure 5.5). For bacteria, the nMDS ordination shows minimal overlap between the control incubation and maximum wildfire scenario (Figure 5.5A, blue and dark red clusters), revealing a major shift in composition due to aerosols. The average scenario displayed high variability, overlapping substantially with both treatments, especially the control incubation (Figure 5.5A). For eukaryotes , the average scenario overlapped substantially with controls (Figure 5.5B, orange and blue clusters), while the maximum treatment was clearly separate from other treatments (Figure 5.5B). These results indicate that wildfire-enriched particle additions induced changes in both bacterial and eukaryotic community structure, with a greater magnitude of change observed among eukaryotic communities. This suggests higher sensitivity or more pronounced responses to nutrient inputs in these taxa, consistent with observations from NSW South Coast estuaries (including Clyde River) where benthic eukaryotic communities exhibited stronger responses to fire than bacterial communities (Bracewell et al., 2023).

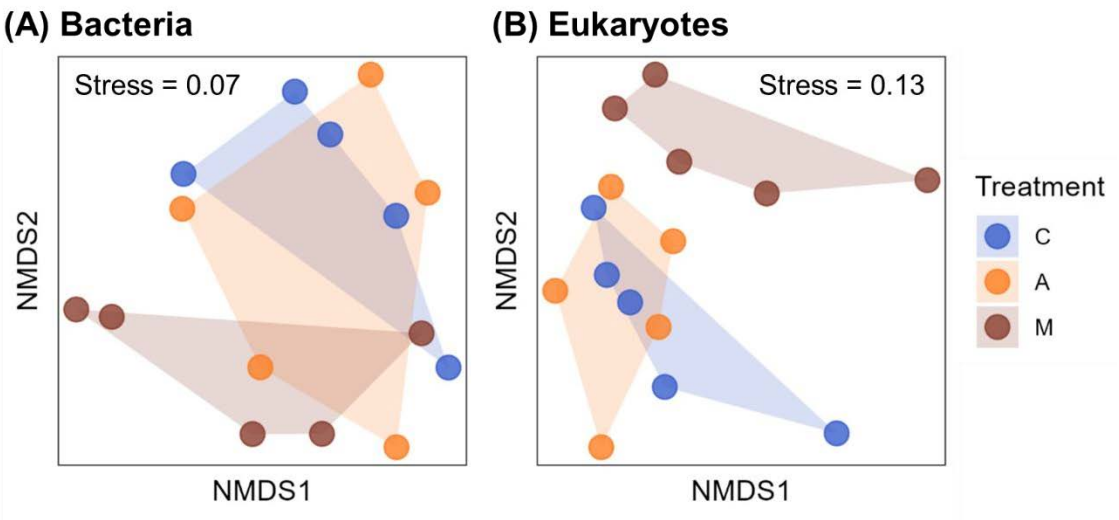


Figure 5.5 Non-metric multidimensional (nMDS) ordinations of the composition of bacteria (A) and eukaryotes (B) in the Scenario experiment based on Bray-Curtis dissimilarities. Each point represents a replicate community (n = 5) after 10-day incubations under one of three treatments: Control (C, blue); Average wildfire (A, orange); Maximum wildfire (M, dark red).

Exposure to higher doses of wildfire-enriched particles significantly enhanced the diversity of bacterial assemblages (Figure 5.6). After ten days of daily particle additions, both alpha diversity indices were significantly higher in the maximum scenario compared to the control ($p_{adj} < 0.05$), indicating greater richness and evenness under the highest exposure scenario (Figure 5.6A, B). Species richness also appeared elevated (Figure 5.6C), though variability was higher and differences were not statistically significant ($p_{adj} > 0.05$). Taxonomic resolution increased substantially in the maximum treatment (Figure 5.5D), suggesting that wildfire smoke may support the proliferation of rare taxa. This is highlighted by the relative abundances of bacteria comprising <1% of total reads, which increased substantially in the maximum wildfire treatment (excluded from SIMPER analysis; Figure 5.7).

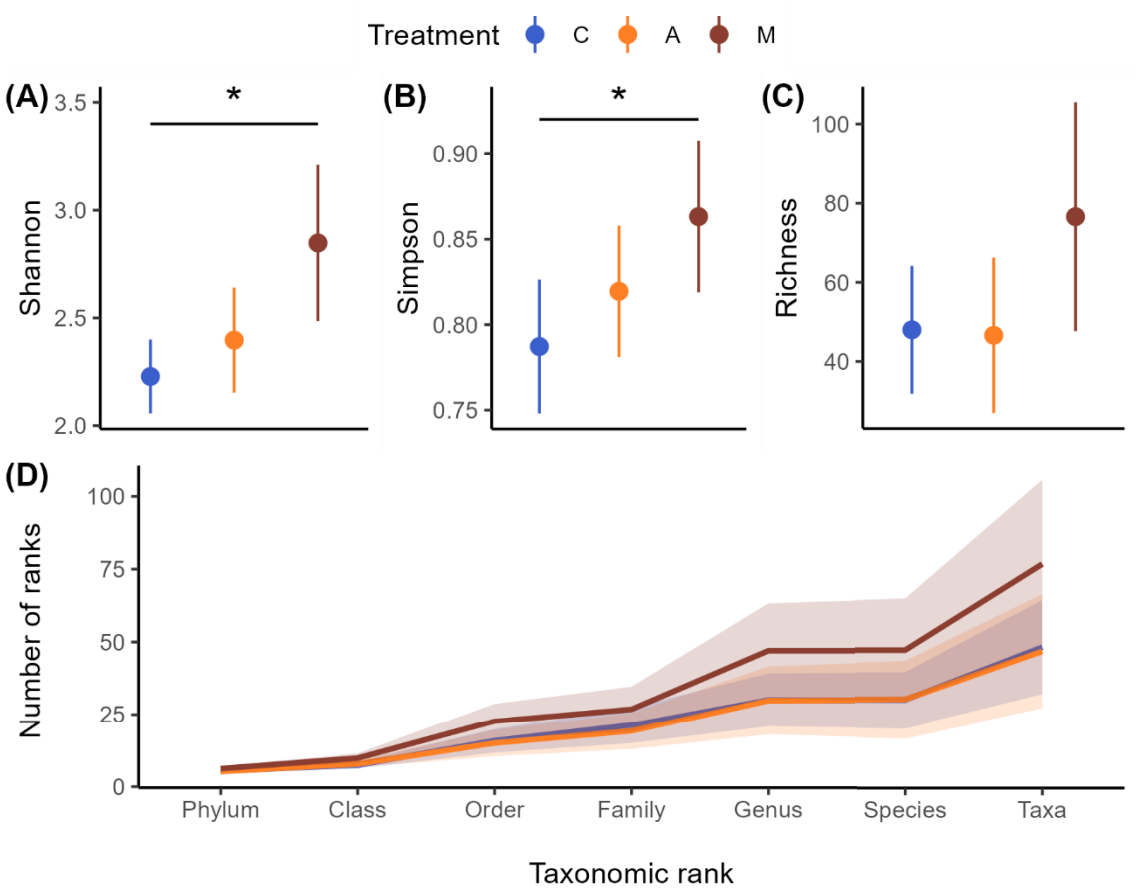


Figure 5.6 Bacterial alpha diversity indices (A, B), species richness (C) and number of unique ranks identified across various levels of taxonomy (D) - from phylum to species. Note that total taxa counts are higher than species counts because they include all distinct groupings at each taxonomic rank (i.e. phylum x class x order x family x genus x species x taxa). Plots are coloured by incubation treatment in the Scenario experiment, including Control (”C”), Average (”A”) and Maximum (”M”), respectively. Asterisks in (A) to (C) represent significant treatment comparisons (PERMANOVA, $p_{adj} < 0.05$).

In contrast to bacteria, eukaryotic diversity declined under higher particle additions (Figure 5.7). After ten days of exposure to the maximum scenario, alpha diversity indices were significantly lower compared to the control ($p_{adj} < 0.05$; Figure 5.7A, B). Species richness also appeared to decline, however higher variability rendered these comparisons non-significant ($p_{adj} > 0.05$; Figure 5.7C). Taxonomic resolution remained relatively low across all treatments, especially in the maximum wildfire treatment (Figure 5.7D).

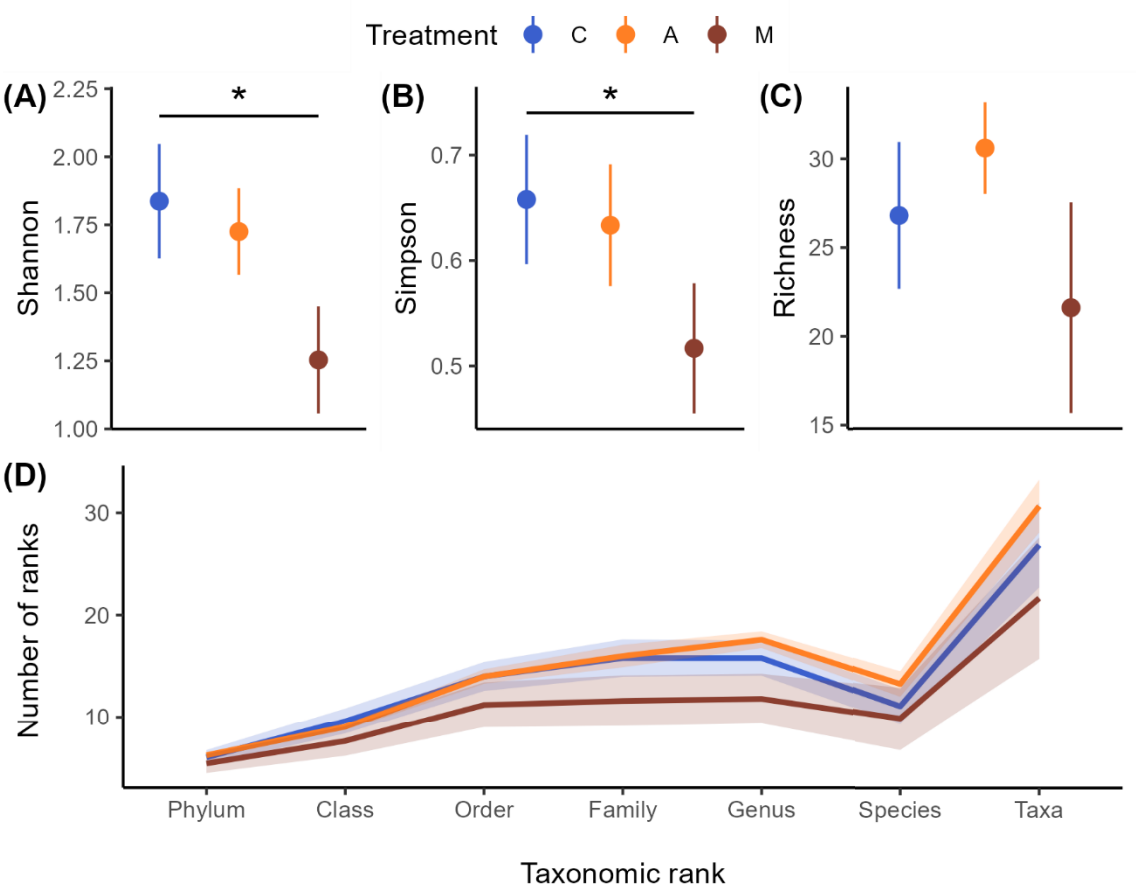


Figure 5.7 Eukaryote alpha diversity indices (A, B), species richness (C) and number of unique taxonomic ranks (D) from Phylum to Taxa. Plots are coloured by incubation treatment, including Control (”C”), Average (”A”) and Maximum (”M”), respectively. Asterisks in (A) to (C) represent significant treatment comparisons (PERMANOVA, $p_{adj} < 0.05$).

5.3.4 Bacterial community

In the control incubations, bacterial assemblages were dominated mostly by orders of *PCC-6307* (Phylum: *Cyanobacteria*) and *NS11-12g* (Phylum: *Bacteriodota*), with smaller levels of *Rhodobacterales*, *Flavobacteriales*, and *Actinomycetales* (Figure 5.8, “Control” facet). Communities sampled from maximum wildfire bottles had increased abundances of *Rhodobacterales* (contributing 6% to total Bray-Curtis dissimilarity, SIMPER) and decreased abundances of *PCC-6307* (Phylum: *Cyanobacteria*; 16%) and *Flavobacteriales* (9%), among other taxa (remaining contributions <5% each; Figure 5.8). These results support the contrasting life strategies of these bacterial orders, where *Rhodobacterales* populations tend to allocate a greater proportion of their proteome to functions associated with metabolic versatility and resource acquisition, while *Flavobacteriales* may focus on more specialised functions, including gene expression processes and uptake of complex carbohydrates like starch (Kieft et al., 2018).

As such, *Rhodobacterales* are an opportunistic, metabolically diverse group capable of degrading a wide range of compounds that may be deposited during wildfires, including organics, aromatics, and sulfur (Bryson et al., 2016; Buchan et al., 2005; Tada et al., 2011).

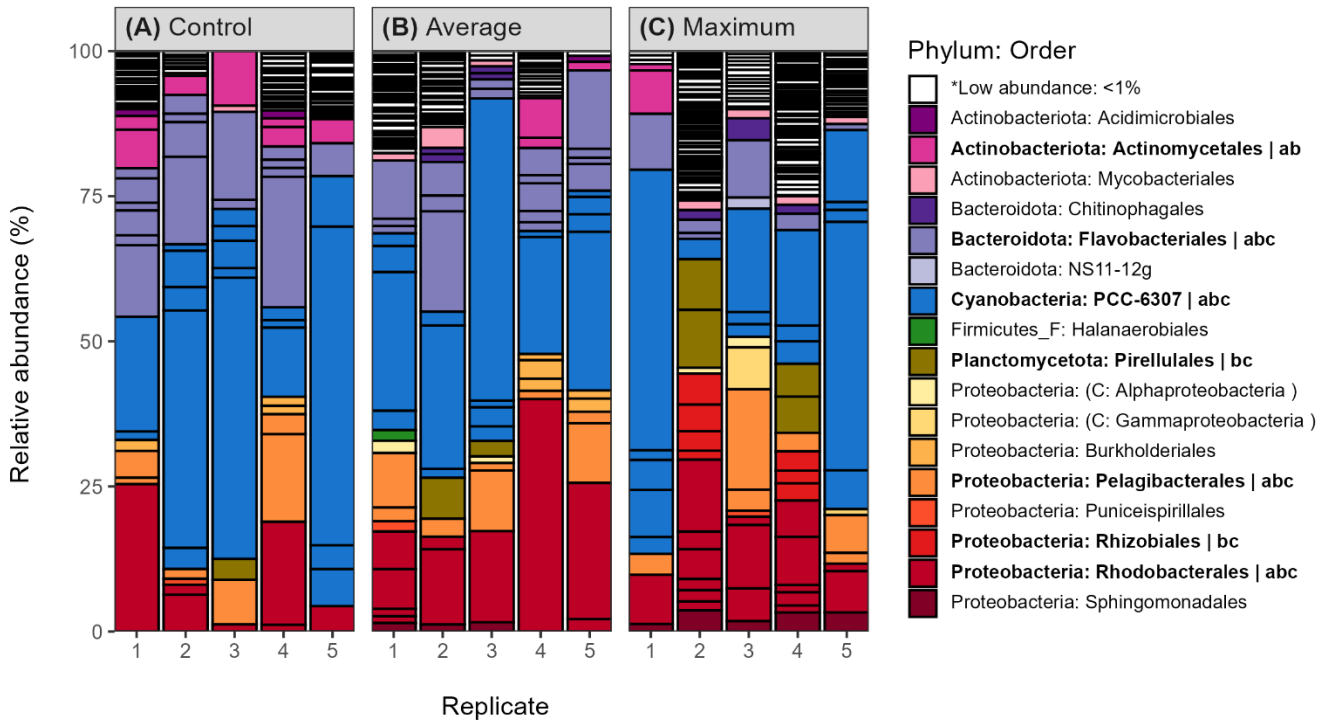


Figure 5.8 Bacterial community composition in incubation of Clyde River microbes with wildfire-enriched particles in Scenario experiment. Each bar on the x-axis represents an individual replicate bottle, while the y-axis shows the relative abundance of taxa. Bars are coloured by Phylum × Order, with individual taxa indicated by each segment. Facets represent 10-day incubation treatments. Legend labels in bold denote orders contributing >5 % to the observed dissimilarity between treatments (SIMPER), where letters listed after each taxa indicate the following treatment comparisons: Control × Average (”a”), Control × Maximum (”b”), Average × Maximum (”c”).

The average scenario displayed similar directional shifts in *PCC-6307* (P: *Cyanobacteria*; 13% contribution) and *Rhodobacterales* (+8%) but also shared many similarities to the control (Figures 5.5 and 5.8). *Cyanobacteria* exhibited high variability among replicates, but overall declines in abundance are consistent with their known sensitivity to environmental stressors such as heavy metals, which are prevalent in wildfire smoke and were present in the particles used in this study (Gill et al., 2024). This may have significant implications for estuarine productivity, given that *Cyanobacteria* can be a major source of primary production in coastal food webs (Novotny et al., 2023).

The pronounced response under the maximum deposition scenario, particularly the decline in sensitive taxa such as *Cyanobacteria* and the enrichment of opportunistic lineages like *Rhodobacterales*, suggests that wildfire-enriched aerosols may select for microbial generalists with traits for metabolic flexibility and stress tolerance. Importantly, changes in *Rhodobacterales* under the average scenario indicate that estuarine microbiomes are responsive even to more moderate particle exposures, underscoring the ecological relevance of atmospheric deposition events linked to wildfire activity.

5.3.5 Eukaryotic community

Across all incubations, eukaryotic microbes were dominated by members of the class *Coscinodiscophyceae* (aka. diatoms) except for two replicates under the average scenario which were mostly *Dinophyceae* (dinoflagellates) (Figure 5.9). Control communities also contained several rare taxa, collectively accounting for ~30% of total reads in those samples (Figure 5.9). Communities exposed to the maximum scenario were less diverse than the control, driven by an increase in diatoms (contributing 10% to total Bray-Curtis dissimilarity, SIMPER) and a loss of *Trebouxiophyceae* (3%), amongst other taxa (Figure 5.9). Besides the increase in dinoflagellates in two replicates of the average treatment, contributions to the limited dissimilarity to the control (Figure 5.5) was also driven by an increase in *Coscinodiscophyceae* (16%) (Figure 5.9). This class was comprised mostly of the genus *Skeletonema* from the order *Thalassiosirales*, with lesser but still substantial contributions from the *Chaetoceros* genus of order *Chaetocerotales*.

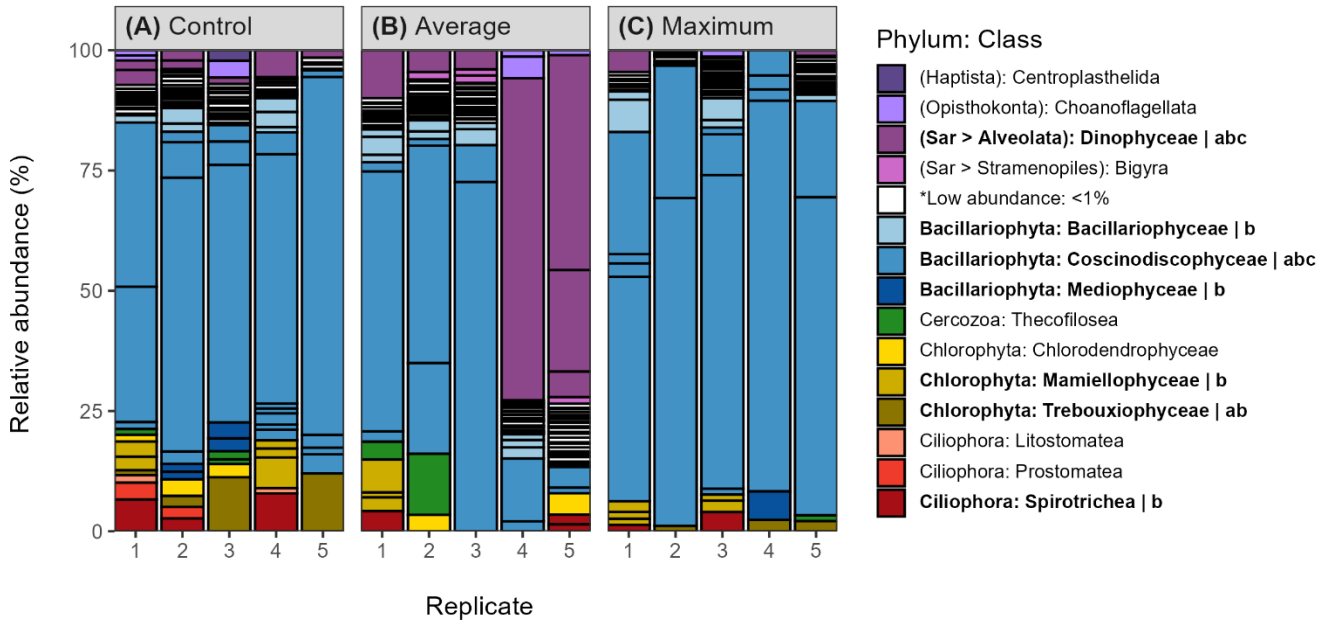


Figure 5.9 Eukaryotic community composition in incubations of Clyde River microbes with wildfire-enriched particles in Scenario experiment. Each bar on the x-axis represents an individual replicate bottle, while the y-axis shows the relative abundance of taxa. Bars are coloured by Phylum × Class, with individual taxa indicated by each segment. Facets represent 10-day incubation treatments. Legend labels in bold denote orders contributing >5 % to the observed dissimilarity between treatments (SIMPER), where letters listed after each taxa indicate the following treatment comparisons: Control × Average (”a”), Control × Maximum (”b”), Average × Maximum (”c”).

This shift reflects a transition toward a more opportunistic, diatom-dominated community, consistent with phytoplankton responses observed in urban estuaries under nutrient enrichment following stormwater inflow (Varkey et al., 2018). Diatoms are known for their rapid growth and competitive advantage in high nutrient environments, especially in the presence of dissolved silica which often limits their growth (Statham, 2012). In the presence of dissolved nutrients from wildfire particulates, its deposition can easily create conditions favourable for bloom-forming generalists like diatoms (Tang et al., 2021). Concurrently, the decline of *Trebouxiophyceae* – a group that includes small, green algal cells – may reflect the loss of more specialised or stress-sensitive taxa unable to compete under altered wildfire conditions. These taxa are typically associated with oligotrophic or stable environments and may decline under competitive exclusion (Litchman and Klausmeier, 2008). These results suggest that wildfire exposure may cause significant changes in community structure, favouring taxa with higher maximum growth rates (Litchman and Klausmeier, 2008) that enable these cells to take quick advantage of increased nutrient availability upon wildfire particle deposition.

5.3.6 Physical water parameters

Physical water parameters following 10-day incubations are presented in Figure 5.10. We observed a minor decrease in light availability within the maximum scenario incubation, from ~198 µmol m^2 s^{-1} in the control and average treatments to ~194 µmol m^2 s^{-1} in the maximum treatment (p_{adj} < 0.05; Figure 5.10, "Light" facet). Given this only represents a ~4 µmol m^2 s^{-1} decrease in irradiance, the results found in this study are likely driven by the toxic and nutritional components of wildfire-enriched particles, rather than any shading effects. We also observed a dose-dependent increase in pH with wildfire additions, increasing from ~7.75 in the control to ~7.9 and ~8.1 in the average and maximum scenario, respectively (p_{adj} < 0.002; Figure 5.10, "pH" facet). This may have an indirect effect on water quality by alkalinising receiving waters. The remaining physical parameters remained unchanged over the 10-day period.

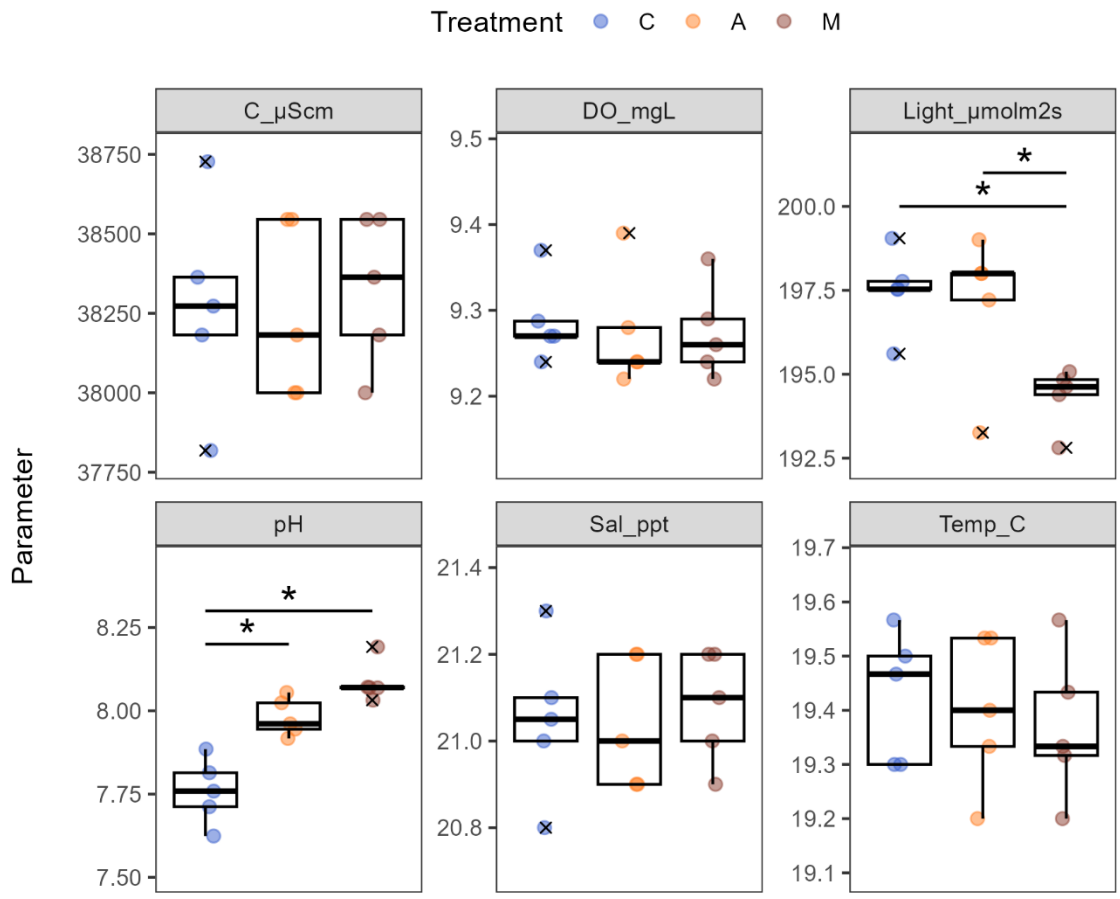


Figure 5.10 Physical water parameters of 10-day bottle incubations with wildfire-enriched particles in the Scenario experiment. Plots are coloured by incubation treatment, including Control ("C"), Average ("A") and Maximum ("M"), respectively. Asterisks represent significant treatment comparisons (Tukey HSD, p_{adj} < 0.05). Facets are labelled with parameter as follows: C_µScm = conductivity; DO_mgL = dissolved oxygen; light_µmolm2s = light received in shaken vessel; pH = pH; Sal_ppt = salinity; Temp_C = temperature.

5.4 Summary and conclusions

In this study, we document the various responses of estuarine microbial populations to wildfire-enriched particulate matter in one estuary over a longer time course than previously analysed. Dose response experiments highlighted the short-lived growth of viruses at low particles fluxes, while heterotrophic and phycoerythrin-containing bacteria required higher doses to elicit a stimulatory effect. Over a five-day period, chlorophyll-containing bacteria and eukaryotes increased in abundance with increasing wildfire dose, while viruses, heterotrophic and phycoerytherin-positive bacteria remained neutral and *Synechococcus* declined. The Scenarios experiment demonstrated a sharp decline in eukaryotes on day 6, with a population collapse persisting for the remaining four days. These cells exhibited a reduction in cell size, complexity and fluorescence. Viruses and heterotrophic bacteria resurged 24 hours later (day 7), with higher abundances observed in the Average compared to the Maximum Scenario. By day 10, substantial shifts in microbial community composition were evident, with eukaryotic alpha diversity declining under the Maximum Scenario, and communities being increasingly dominated by diatoms – particularly from the genus' *Skeletonema* and *Chaetoceros*. In contrast, bacterial diversity increased under the same treatment, including higher relative abundances of the order *Rhodobacterales*, and reductions in *PCC-6307* (Cyanobacteria) and *Flavobacteriales*, alongside changes in several rarer taxa. These findings demonstrate that wildfire-enriched aerosols can alter the abundance and structure of estuarine microbial communities in a concentration- and time-dependent manner, with effects ranging from diatom blooms to potential viral infections and suppression of cyanobacteria. As wildfire activity intensifies globally, understanding these processes will be essential for predicting and managing the consequences of future fire seasons, with significant implications for an Australian and global audience.

Funding

This work was supported by the Faculty of Science and Climate Change Cluster at the University of Technology Sydney (UTS) through provision of equipment and operation funds, as well in-kind contributions of expertise and consumables from the NSW Department of Planning and Environment (DPE). RLG was supported by an Australian Government Research Training Program Scholarship at UTS.

CRediT authorship contribution statement

RLG, PS, FRT and MAD designed the study; PS facilitated and resourced field work; CJ facilitated eDNA analyses; RLG, RF and FRT prepared wildfire-enriched particulate matter treatments; RLG performed air quality analysis; RLG, CM, and AW collected estuary samples; RLG, CM, AW and RF contributed to experimental set up/pack up; RLG and ALP processed samples; RLG analysed & interpreted PAM and flow cytometry data; RLG and KCS analysed & interpreted the eDNA data; RLG drafted the manuscript. All authors edited and reviewed the manuscript.

Declaration of competing interest

The authors declare that they have no known competing financial interests or personal relationships that could have appeared to influence the work reported in this paper.

Acknowledgements

We would like to acknowledge Dr. Michaela Larsson for her assistance with refining our protocols for gating of microbial populations in flow cytometry analysis.

6. Summary and significance

Prelude

This thesis presents the first comprehensive investigation into how extreme wildfire events influence both atmospheric chemistry and aquatic microbial ecology, using Australia's 2019–20 Black Summer fires as a focal case. By integrating atmospheric science, analytical chemistry and experimental microbial ecology, this work bridges disciplines to uncover new mechanisms by which wildfires affect downstream ecosystems.

6.1 Summary of major thesis findings

The research presented in Chapters 2 and 3 demonstrated that wildfire-enriched particulate matter (PM) is physically and chemically distinct not only from typical urban emissions, but also from mineral dust and freshly burned biomass smoke previously described in the literature. The aqueous extracts of wildfire-enriched PM resulted in finer, more spherical particles compared to urban PM samples as well as literature reports of mineral dust, which enhances their residence time in the atmosphere and potential bioavailability upon deposition. Samples taken during the 2019-20 Black Summer fires in Sydney were coarser than fresh smoke emissions reported in the literature, which likely reflect both atmospheric processes and methodological artefacts. Coagulation and condensation during atmospheric transport (Reid et al., 2005; Seinfeld and Pandis, 2016) and the entrainment of coarse mineral particles by fire-driven winds (Peterson et al., 2021; Wagner et al., 2018) are all known to increase the size of PM in wildfire plumes. However, PM collected on HVAC filters is also subject to sampling artefacts, including incomplete recovery of particles < 1 μm and particle retention within the pre-screen and filter mesh (Mahdavi et al., 2021; Mahdavi and Siegel, 2020), which likely shifts the size distribution towards coarser particles (see Supplementary Text 2.1 and 2.2 for more a detailed discussion). Despite these artefacts, the relative difference in size distributions between the 2019-20 Black Summer and 2020-21 Reference periods remain valid and indicate a significant shift towards smaller particles. Compared with urban PM, wildfire-enriched aerosols were enriched in 35% of the potentially toxic elements considered on a per mass basis (antimony, chloride, cobalt, fluoride, manganese, nitrate), only 20% of macronutrients (nitrate, sulfate), and 67% of

micronutrients (calcium, cobalt, iron, magnesium, manganese, molybdenum, and silica). All analytes were generally less soluble in wildfire-enriched PM, except for mercury (~12 vs 1%), nitrogen (~45 vs 13%) and calcium (~46 vs 27%). Source apportionment revealed a complex blend of aged biomass smoke, marine inputs, mineral dust, and legacy urban contaminants in wildfire-enriched samples - a mixture more heterogeneous than assumed in most health studies assessing impacts of wildfire aerosol exposure, which often rely on freshly combusted biomass from laboratory-based burns. These findings challenge the prevailing notion that wildfire-enriched aerosols are uniformly nutrient-rich and instead demonstrate that their composition may be highly contingent on fire history, land use, and atmospheric transport.

This complexity had cascading effects on estuarine microbial communities, as shown in Chapters 4 and 5. Through an integrated approach combining field sampling, controlled incubations, and both single-cell and community-level analytical techniques, these chapters reveal both concentration- and time-dependent effects of wildfire-enriched aerosols of estuarine microbial communities. Acute 24-hour incubations across five estuaries showed divergent responses that could be grouped into autotrophic, heterotrophic, or non-responsive categories. Groupings exhibited moderate-strong correlations with historical data or conditions at the time of sampling, including water quality, nutrients, and microbial traits pre-incubation, however further research is required to fully resolve this relationship. Interestingly, most estuaries were non-responsive to “Average” wildfire-enriched particle additions, whereas autotrophic responses were characterised by smaller, less complex, more pigmented and fast-growing phytoplankton cells. Heterotrophic responses featured growth of viruses and low-DNA containing bacteria (and vice versa). Under the “Extreme” wildfire scenario, all five estuaries responded relatively consistently, with a strong heterotrophic response. Longer (5-10 day) incubations in one pristine estuary revealed additional complexity. Phytoplankton declined in abundance and diversity due to the potential for viral suppression of eukaryotes and *Synechococcus* metal toxicity, with a shift toward diatom dominance (e.g., *Skeletonema*, *Chaetoceros*) under high particle loads, while bacterial communities became more diverse and were dominated by groups such as *Rhodobacterales*. These findings demonstrate that wildfire-enriched aerosols can restructure microbial communities through a combination of nutrient stimulation, toxicity, and competitive dynamics.

6.2 Research methodology and considerations

This research employed a multifaceted methodological design, integrating field-based estuary sampling, laboratory-based techniques for filter forensics, chemical analysis and microbial characterisation, and computational techniques for atmospheric modelling. Throughout all modes of research, errors and biases were minimised by ensuring completion of adequate training and pilot studies prior to conducting main experiments, the use of sterile techniques wherever possible, incorporating as many replicates as possible, and randomising sampling order and placement where applicable. Artefacts from incubation bottle effects and microbial acclimation to laboratory conditions were addressed by carefully considering incubation time for each vessel size in reference to the literature and discussions with senior academics and ensuring that environmental conditions were closely matched to field conditions with the use of sensors and controls.

The use of HVAC filters for aerosol capture represents a novel and scalable method to retrospectively assess urban exposure to wildfire-enriched emissions, offering new avenues for both ecological and public health research. Furthermore, it allowed the bulk-capture of an integrated, 4-month sample to collected sufficient material required for the extensive chemical analysis and subsequent experimental incubations in this thesis. The use of HVAC filters for aerosol capture represents a novel and scalable method to retrospectively assess urban exposure to wildfire-enriched emissions, offering new avenues for both ecological and public health research. Furthermore, it allowed the bulk-capture of an integrated, 4-month sample to collected sufficient material required for the extensive chemical analysis and subsequent experimental incubations in this thesis. An inherent limitation of this approach is that it captures PM from multiple emission sources rather than solely wildfire smoke. Accordingly, the collected material reflects mixed-source aerosols, consistent with other in situ aerosol sampling approaches not deployed at the emission source. Despite this, source apportionment indicates that the composition was strongly shaped by wildfire emissions and fire-mobilised material, with PMF analysis estimating that aged wildfire smoke accounted for ~44% of analysed mass and soil-related factors entrained by fire-driven winds a further ~38%, together representing ~82% of analysed sample mass. Additionally, despite the sampling location in Sydney, factors associated with anthropogenic emissions comprised only ~1% of the analysed sample mass during the 2019-20 Black Summer period. Therefore, the dataset provides a meaningful assessment of

wildfire-enriched aerosols during the 2019-20 Black Summer fires, particularly for downwind locations influenced by widespread, long-lived plumes that affected much of eastern Australia.

The filter forensics approach has two key limitations that may influence the representativeness of extracted PM when compared to suspended aerosols: 1) many building HVAC systems, including the one utilised in this thesis, are not rated highly for submicron particle capture, and 2) "caking" of particles to the filter bed over time may coagulate particles together, artificially increasing the size of the particles. These effects were assessed by checking for the presence of submicron particles by flow cytometry and verifying particle sizes using scanning electron microscopy (SEM), as well as comparing (particle) number size distributions of particulate filter extracts to air monitoring data during the 2019-20 Black Summer fires. The impact of "caking" was examined by comparing the distributions of lightly used and heavily "caked" filters using the analytical techniques described above. In both cases, submicron particles were detected in abundance by both flow cytometry and SEM pilots, and distributions were as expected compared to available monitoring data (see Supplementary Material: Chapter 2). Therefore, its impact on the results of this thesis was likely negligible, however researchers should carefully consider and examine these limitations prior to its use in research projects.

6.3 Conceptual contributions to the field

Together, the results of this thesis reveal new insight into how major wildfire events influence both atmospheric chemistry and aquatic microbial ecology. At the atmospheric scale, the compositional fingerprint of wildfire-enriched PM challenges the assumption that such aerosols are uniformly nutrient-rich or toxic. Instead, the 2019–20 Black Summer fires produced aerosols with a highly heterogeneous chemical makeup, with a mixture of potentially harmful and fertilising elements shaped by a mixture of sources - each contributing distinct chemical signatures and solubility profiles. Importantly, Chapters 2 and 3 highlight the importance of considering previous land use when assessing the risk of wildfire-enriched aerosol exposure due to potential volatilisation and/or remobilisation of legacy deposits. To this end, these chapters also challenge the assumption that real-world wildfire aerosols are similar to freshly burnt biomass, contributing to a growing body of literature demonstrating that wildfire aerosol exposure is vastly different to the aerosols produced under controlled laboratory-based burns

which are often used to infer toxicity. The 2019-2020 wildfires were exceptional not only in their scale and intensity but also in the distance and duration over which aerosols were transported – wildfire plumes cloaked not only Australia, but many locations around the Southern Hemisphere - making them a powerful vector for introducing bioactive inputs to downstream ecosystems. This complexity cascaded into estuarine incubations, where microbial responses varied markedly with aerosol concentration, exposure time, microbial population, and individual estuary characteristics.

Notably, the acute estuary experiments in Chapter 4 showed that water quality, nutrient status, and pre-existing microbial traits were moderately-strongly correlated with whether systems exhibited autotrophic, heterotrophic, or no measurable response to wildfire-enriched PM under the local Average Scenario. These results align with and extend ecological theory on microbial resilience, suggesting that planktonic estuarine communities can maintain core functions under moderate wildfire-enriched aerosol exposure. However, under high deposition scenarios - reflective of extreme fire conditions - this resilience eroded, triggering pronounced shifts in community structure and function. Longer incubations (Chapter 5) revealed how such restructuring unfolds over time in a relatively pristine system, including potential viral suppression of dominant phytoplankton groups, decline of *Synechococcus* due to heavy metal toxicity, collapse of eukaryotic diversity, and opportunistic growth of diatoms (e.g., *Skeletonema*, *Chaetoceros*) and copiotrophic bacteria (e.g., *Rhodobacterales*). Together, these findings demonstrate that extreme wildfires act as both sources of nutrition and stress, revealing thresholds beyond which microbial community stability breaks down. The results affirm that microbial communities are sensitive integrators of environmental change and underscore the importance of understanding fire-enriched aerosol pathways - especially as climate change drives longer, hotter, and more frequent fire seasons. This thesis therefore bridges atmospheric and aquatic science, reinforcing the need to consider cross-system connectivity, variability, and intensity when forecasting the ecological consequences of future wildfire events.

6.4 Broader significance of research

To explore the broader impacts and relevance of this research, the Department of Climate Change, Energy, the Environment, and Water (NSW DCCEEW) invited me to examine their

historical estuarine water quality monitoring data (2007-2022) to assess the impact of the 2019-20 Black Summer fires on intermittently open and closed lagoons (ICOLLs) and rivers across the state and contextualise the findings of this thesis. Of the 172 estuaries available, 84 are included here as they contained at least five years of data and at least one during or post-fire observation. Redundant water quality probe variables were examined using scatterplots and pearson correlations and removed if coefficients were ≥0.90. The final dataset contains two microbial indicators: chlorophyll-a fluorescence for phytoplankton ("Chl-a", ug L^{-1}) and phycoerythrin fluorescence for cyanobacteria ("PE", ug L^{-1}), as well as the following variables: salinity ("Sal.", PSU), temperature ("Temp.", °C), turbidity ("Turb.", NTU), dissolved oxygen ("DO", %), pH, and fluorescent dissolved organic matter ("fDOM", QSU).

By local government area (LGA), the proportion of estuaries during and/or after the 2019-20 Black Summer fires that differed significantly from their pre-fire condition is depicted in Figure 6.1 below. Across all relevant LGAs, at least ~40% of ICOLLs experienced one or more significant shifts in water quality (Figure 6.1, left panel). Meanwhile, the proportion of fire-impacted river systems ranged widely between 0 and 100% (Figure 6.1, right panel), likely reflecting differences in hydrology and connectivity that facilitated the export of pyrogenic material. In Chapter 4 of this thesis, differences in estuary responses to the Average Scenario did not group together by estuary type, however the degree of variation was similar in that responses to wildfire-enriched aerosol additions varied markedly depending on site-specific conditions. This highlights the importance of factors such as local water chemistry, underlying microbial community composition, and flux of PM deposition in shaping microbial responses. Southern LGAs were impacted more heavily by the fires for both estuary types, consistent with maps of burn area severity across NSW catchments (Fryirs et al., 2022) and regional air-mass trajectories from Chapter 2 which suggest predominant origins outside of Sydney along the east/south-east coastline of Australia.

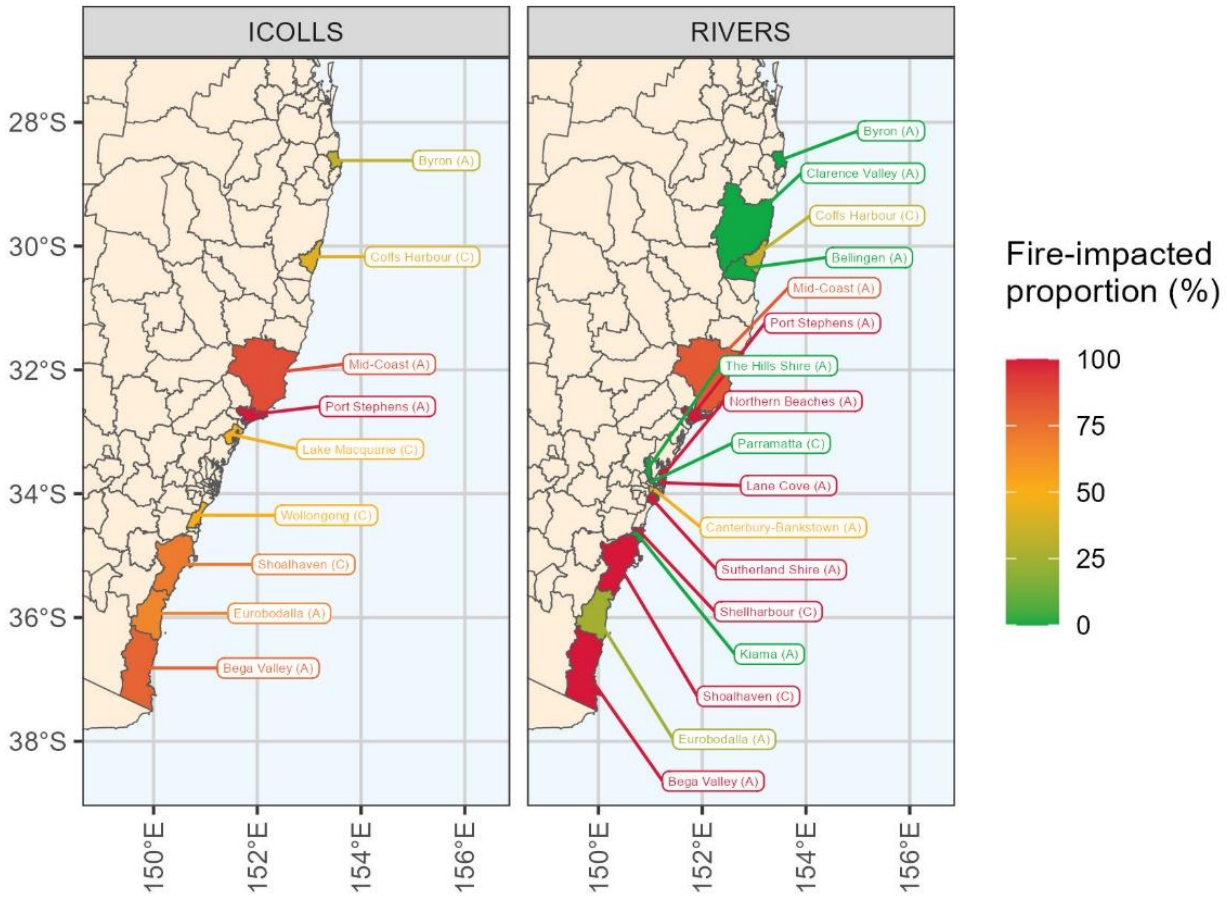


Figure 6.1 Proportion of valid ICOLLs and Rivers (n = 84) in each NSW LGA that displayed at least one significant shift in water quality during and/or after the 2019-20 Black Summer fires, relative to pre-fire conditions (PERMANOVA with Bray-Curtis distance and 999 permutations; $p < 0.05$).

The water quality parameters driving differences between pre-fire and fire-impacted phases of each estuary are shown in Figure 6.2 below. Drivers of water quality shifts remained relatively consistent across the three fire phases (Figure 6.2, see three panels), indicating that impacts were not only immediate but also persistent. Dissolved organic matter and dissolved oxygen showed the strongest fire-associated changes, followed by cyanobacteria, salinity and phytoplankton, with minimal effects on temperature, turbidity and pH (Figure 6.2). Notably, changes in dissolved organic matter and oxygen may have arisen from the deposition of fine particles enriched with redox-sensitive metals (e.g. cobalt, iron, manganese). These metals can be utilised by microbes in their energy-generating reactions, acting as electron donors or acceptors during respiration (Majzlan, 2013). By providing alternative pathways for microbial metabolism, the deposition of these metals may enhance the breakdown of organic matter, increase oxygen consumption and consequently alter dissolved oxygen levels (Zhang et al.,

2010). As described in Chapters 2 and 3 of this thesis, wildfire-enriched PM contained elevated concentrations of these metals, indicating that their deposition during the fire period could have influenced microbial respiration and productivity.

The ranking of water quality parameters partly contrasts with findings from Chapter 5 of this thesis, where microbial shifts were most pronounced in eukaryotic phytoplankton rather than bacteria. However, this discrepancy may arise from methodological differences: whereas Chapter 5 applied high-resolution flow cytometry and eDNA approaches to a single estuary under controlled exposure, the broader monitoring dataset uses in situ fluorescence of the water column as a proxy for biomass and photosynthetic activity, which may better capture cyanobacterial pigment changes than structural community shifts. The rank order of drivers remained similar between ICOLL and river systems, though contributions were generally higher and more variable in ICOLLs (Figure 6.2, green boxplots). This suggests that these partially closed systems experience more varied and intense changes in water parameters during fire events, likely due to the influence of estuary type on hydrology and flushing.

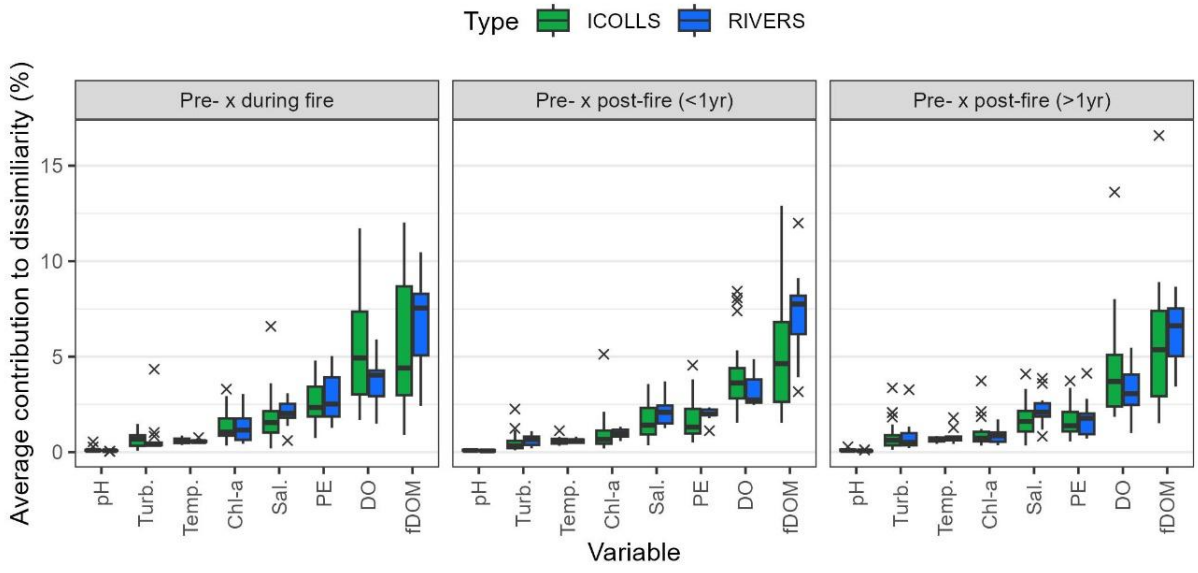


Figure 6.2 Average contributions of water quality variables to the overall dissimilarity between fire phases (top facets) for all valid fire-impacted estuaries (SIMPER with Bray-curtis distance and 999 permutations). Estuaries are grouped by type (colour).

Together, these datasets offer complementary perspectives: the long-term, state-wide monitoring reveals broad patterns of ecological disturbance, while this thesis provides mechanistic insight into the atmospheric and biological processes driving those shifts. This thesis makes a significant contribution to understanding how extreme wildfire events affect both atmospheric chemistry and aquatic microbial ecology, demonstrating that aged wildfire-enriched aerosols are capable of reshaping coastal microbial communities via the provision of potentially toxic and fertilising elements. Chapters 2 and 3 improve our understanding of fire-enriched PM by reporting on elements other than iron and highlighting how wildfire emissions differ markedly from ambient urban air, mineral dust aerosol, and fresh biomass smoke. Chapters 4 and 5 build on this by showing that estuarine microbial communities respond in concentration- and time-dependent ways to this airborne material, ranging from subtle physiological changes to complete community restructuring under high particle loads – particularly at thresholds above the Average Scenario for dry deposition in the South Coast of NSW (>0.17 g m^{-2} d^{-1}).

Collectively, these studies demonstrate that wildfire-enriched PM introduces a multi-dimensional stressor to aquatic ecosystems – simultaneously supplying nutrients, delivering toxicants, and altering microbial competition. In doing so, this thesis expands on knowledge on ecological disturbance and resilience, while offering a different lens through which to assess the broader environmental consequences of intensifying fire regimes. These findings have implications for air quality regulation, environmental management and fire preparedness. Wildfire PM is not just an air pollutant - it is a biogeochemical vector with profound ecological implications, altering nutrient cycling, food web dynamics, and ecosystem resilience in estuarine environments.

6.5 Future research directions

While existing literature has focused on the role of wildfire-enriched iron in fuelling marine productivity, the findings of this thesis highlight the need to broaden future research towards other bioactive elements such as mercury, antimony and fluoride. These elements were all found to have elevated solubility in wildfire-enriched aerosols and are known toxins. Increased reporting of these elements is essential to better understand their environmental fate and

potential impacts on aquatic systems. This body of work highlights how past and changing land use patterns contribute to the composition of wildfire plumes. Future work should also consider land-use when studying aerosol sources, such as how the remobilisation of legacy contaminants may affect environments upon atmospheric deposition. Additionally, while this thesis provides valuable insight into real-world exposures during a major wildfire event, the samples inevitably contain contributions from multiple emission sources - an inherent feature of wildfire plumes sampled downwind, as they entrain surrounding dust and legacy deposits. Experiments using PM composed exclusively of wildfire smoke – such as samples collected from controlled combustion facilities like CSIRO's Pyrotron or during prescribed hazard reduction burns – would allow the specific effects of wildfire PM on aquatic microbiota to be isolated and better understood. Furthermore, the relative influence of dry versus wet deposition on the delivery of wildfire-enriched aerosols to estuaries remains poorly constrained. Studies capturing both deposition modes during active wildfire seasons would help determine how aerosol delivery mechanisms influence bioavailability and microbial responses.

In aquatic systems, longer-term experiments and time series monitoring are needed to evaluate the extent to which wildfire impacts microbial abundances, diversity, and functions, as well as their resilience and capacity for recovery. Mesocosm or *in situ* incubations may help capture these responses over longer time frames by avoiding size-dependent bottle effects. Expanding the geographic and estuarine coverage of experimental work would also aid in verifying whether the patterns observed in this thesis - particularly the autotrophic-to-heterotrophic shift under extreme aerosol exposure and the correlations between baseline estuary conditions and microbial responses under average aerosol exposure – is consistent across various bioregions, climates, and estuary types. Understanding the thresholds at which microbial systems switch from autotrophy to heterotrophy would be of great benefit for preparedness and recovery.

Future research should aim to develop frameworks that integrate the spatial heterogeneity of wildfire emissions, atmospheric transport conditions, and the vulnerability of receiving waterways, enabling more accurate prediction and management of fire-related impacts in an increasingly fire-prone climate. In parallel, studies should broaden their scope to include overlooked microbial groups such as viruses and archaea, as well as higher trophic levels, which remain largely absent from aerosol impact research. This omission may obscure key ecological dynamics, as illustrated in Chapter 5 of this thesis where viral infection of dominant eukaryotic

taxa altered microbial succession by suppressing the most competitive population – effectively "killing the winner" – and reshaping the community trajectory.

6.6 Concluding remarks

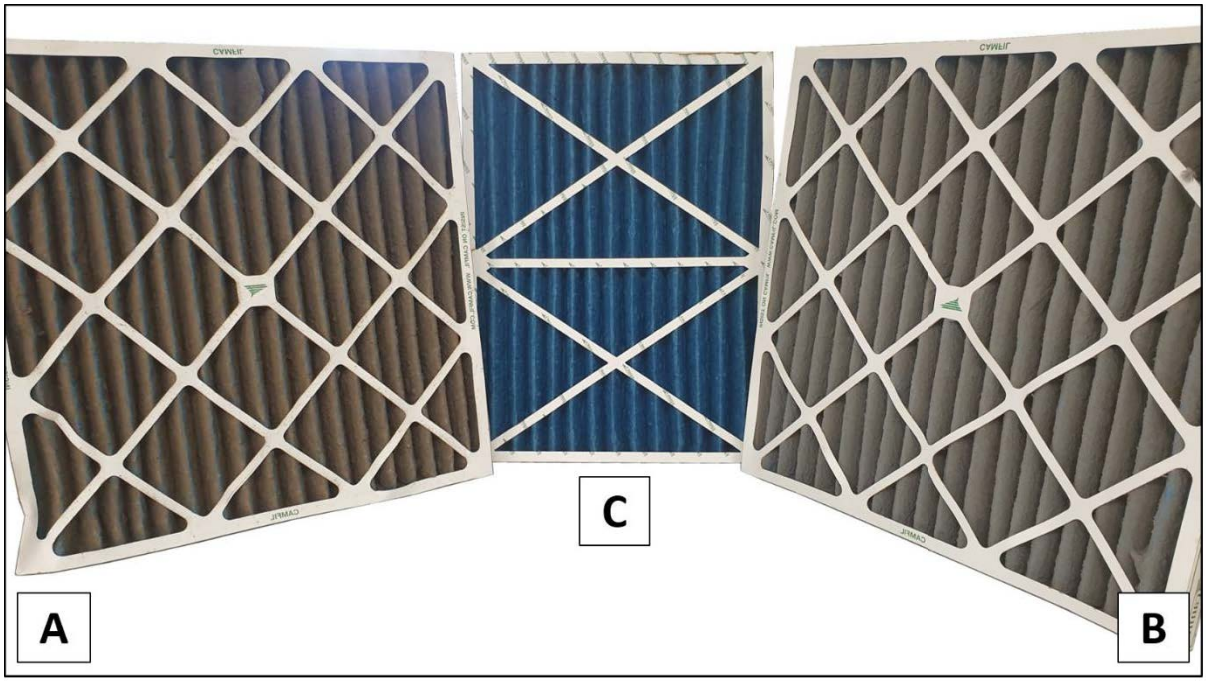
This thesis provides novel insights into how extreme wildfire events influence both the atmosphere and aquatic ecosystems, highlighting the dual role of fire-enriched aerosols as vectors of both nutrients and pollutants. Through the application of atmospheric chemistry and aquatic microbial ecology, the research presented here sheds light on the complexity of real-world wildfire emissions relating to their bioactive potential – including flux of deposition, particle size, chemical composition, fractional solubility, and source origins – as well as the variable ecological impacts that follow their dry deposition to estuarine environments. This knowledge advances our understanding of how wildfire events modify the composition of the atmosphere and receiving environments located downwind of the emission source. It then follows the impact of this mixture of bioactive materials on estuarine microbial dynamics from the community level down to a single-cell perspective and explores the ways in which microbes respond to wildfire aerosol dose across spatial and temporal scales. This work not only advances our understanding of wildfire-driven biogeochemical processes but also establishes a foundation for future research aimed at predicting, managing, and ultimately mitigating the cascading ecological effects of extreme fire events.

Given the magnitude and reach of emissions during major wildfires, the results presented here pose great significance to a global audience, especially when considering the rise in fire frequency and severity worldwide. Therefore, understanding their atmospheric and aquatic consequences has become more critical now than ever before. Governments and regulatory agencies around the world should act with urgency to understand and mitigate the consequences of increasingly severe wildfires, ensuring that impacts on both the atmosphere and biosphere are reflected in environmental policy and practice. This includes closer examination of fire-prone regions with high fuel loads, proactive assessment of current and historical land use to project future emission scenarios, and the preparation of vulnerable regions through education initiatives that promote community readiness. In addition, monitoring of post-fire impacts on sensitive ecosystems - such as estuaries - should be strengthened

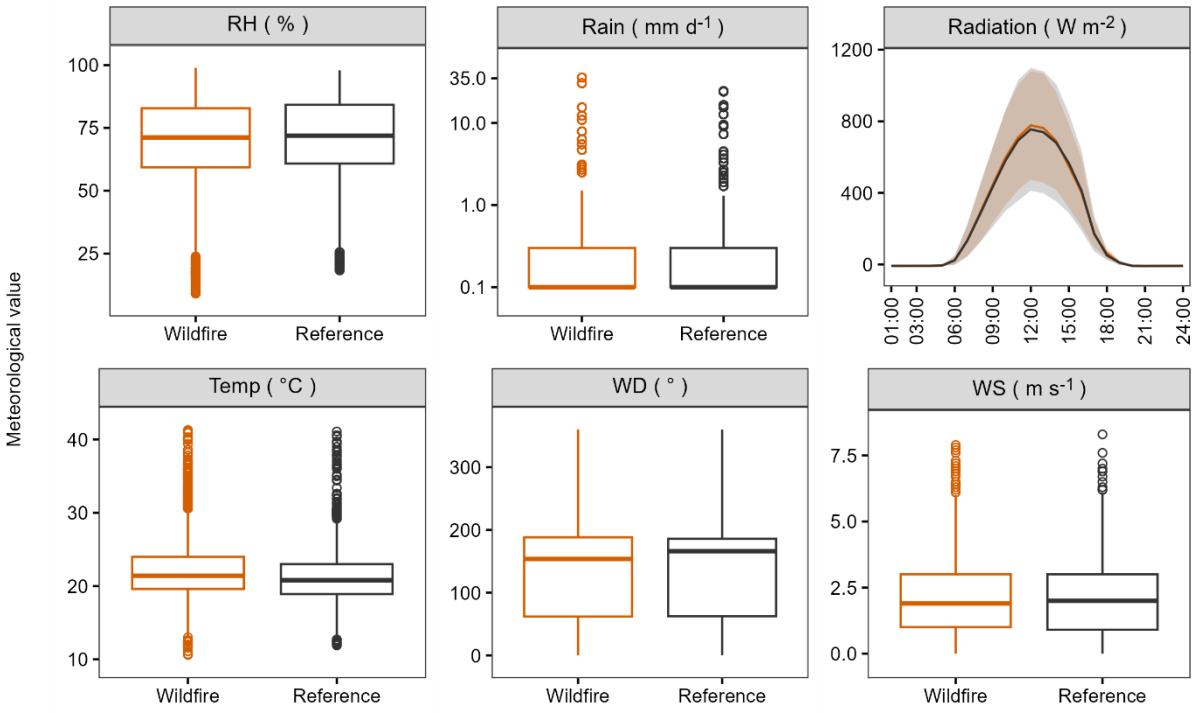
through support for local monitoring groups, targeted research funding, and the establishment and maintenance of long-term monitoring programs, which are essential for accurately determining the ecological impacts of wildfire events.

Chapter 2: Supplementary Material

Supplementary Figures



Supplementary Figure. 2.1 Building HVAC filters containing particulate matter captured in Sydney during the Black Summer Wildfires (A; November 2019 - February 2020) and the Reference period (B; November 2020 - February 2021). Procedural control is pictured in the centre (C).



Supplementary Figure. 2.2 Meteorological conditions at Rozelle monitoring station (22 m in height, 4 km from HVAC sampling) during the Black Summer Wildfire (November 2019 - February 2020) and Reference (November 2020 - February 2021) periods. Subplots RH, WD and WS refer to relative humidity, wind direction and wind speed, respectively. All variables are provided as hourly averages, except for rain (24-hourly). Meteorological conditions did not differ between the two study periods (PERMANOVA: $p > 0.05$). Boxes depict the lower and upper quartiles of the data, which contains the middle 50 % of values. Vertical whiskers and points outside this range contain the remaining lower/upper 25 % of data, with points denoting outliers (defined as those 1.5 times above/below the lower/upper whisker value). The median is indicated by the horizontal, thick line centred in each box. Curves depict the mean ± standard deviation of hourly values as lines/shaded regions.

Supplementary Tables

Supplementary Table 2.1 Flow cytometer parameters used for particle number and size analysis.

Parameter	Setting
Laser set up	
Laser	Blue, 488 nm
Threshold	6000 FSC-H
Gains	300 FSC-A
	179 SSC-A
Sample acquisition	
Mode	Tube
Flow rate	60 µL min^{-1}
Run time	1 min
Backflush time	10 s

Supplementary Table 2.2 HPIC parameters used for major anion and cation analysis.

Parameter	Anions	Cations
Detector	Dionex Conductivity AS-AP (Thermofisher, USA)	
IC column	2 x Dionex IonPac AG18, 50 mm	3 x Dionex IonPac CS16, 250 mm
Column temp.	30 °C	60 °C
Flow rate	0.25 mL min^{-1}	0.6 mL min^{-1}
Suppressor	Dionex ADRS 600, 38 mA	Dionex CDRS 600, 53 mA
Eluet generator	Dionex EGC KOH	Dionex CH4O3S
Eluent conc.	Initial (0 min): 18 mM Ramped at 9 min: 37.8 mM Stepped & held for 3 min: 60 mM Return to initial for 15 min: 18 mM	Full sequence (20 min): 36 mM
Sample injection	Full loop, 25 uL	
Compartment temp.	15 °C	
Detector temp.	35 °C	

Supplementary Table 2.3 SN-ICP-MS parameters used for trace element analysis.

Parameter	**Setting**
Sample introduction	
Tubing	Tygon, 1.02 mm internal diameter
Peristaltic pump	3-channel, 6 rpm
Flow rate	1 mL min-1
Concentric nebuliser	MicromistTM (Glass Expansion, Australia)
Spray chamber	Scott type, double pass, 2 °C
RF power (W)	1500 W
Gas	99.999 % Argon 5.0 (Coregas, Australia)
Carrier gas (Ar) flow rate	0.7 L min^{-1}
Makeup gas (Ar) flow rate	0.5 L min^{-1}
Sample depth	8 mm
Ion lenses	
Extracts 1, 2	3.8, -185 V
Omega bias, lens	-120, 18 V
Cell entrance, exit	-30, -40 V
Octopole	
RF	190 V
Bias	-8 V
Collision gas flow rate	0 mL min^{-1}

Supplementary Table 2.4 Traffic count data at nearest Parramatta Road monitoring station (#19065, 3 km from HVAC sampling and Rozelle air monitoring) during the Black Summer Wildfire (November 2019 - February 2020) and Reference (November 2020 - February 2021) periods. Daily mean counts for eastbound, westbound, and total traffic are depicted for each month. Daily mean counts across entire study periods are shown as means ± standard error. Daily mean traffic counts across all months/directions did not differ between the two study periods (ANOVA: p = 0.342).

Period	Direction	Directional daily mean traffic count		Total daily mean traffic count	
		Wildfire (2019-2020)	Reference (2020-2021)	Wildfire (2019-2020)	Reference (2020-2021)
By month					
Nov	East	30834	30114	61872	61812
	West	31038	31698		
Dec	East	29946	30150	59800	62565
	West	29903	32415		
Jan	East	28082	27696	55812	56453
	West	27730	28757		
Feb	East	30272	30753	60221	62467
	West	29949	31714		
By period					
Nov - Feb (inclusive)	East	29784 ± 596	29678 ± 677	59426 ± 2570	60824 ± 2933
	West	29655 ± 693	31146 ± 814		

Supplementary Table 2.5 Comparison of $PM_{2.5}$ / PM_{10} proportions between HVAC samples (by particle number) and in-situ airborne measurements (by PM mass) (median, q1-q3). Bold values denote higher proportions from HVAC × Airborne PERMANOVA comparisons ($P_{(p\text{-}aov)}$), where stars denote significant (***p ⩽ 0.001) and ns non-significant (p > 0.05) results. The relative change in proportion between median Wildfire and Reference conditions did not differ between measurements (PERMANOVA: p = 0.916).

Method	Wildfire	Reference	$P_{(p\text{-}aov)}$
Proportion of $PM_{2.5}$ / PM_{10} (%)			
HVAC	83.5 (80.9-86.1)	69.4 (64.6-73.6)	***
Airborne	38.1 (31.9-50.0)	32.1 (27.9-35.7)	
Relative change from median Reference condition (%)			
HVAC	20.3 (16.6-24.1)	n/a	ns
Airborne	19.9 (0.5-59.2)	n/a	

Supplementary Text

Supplementary Text 2.1 Representativeness of filter forensic approach.

Filter forensics (FF) by vacuum extraction has demonstrated satisfactory size distributions for particles spanning 1-10 μm. For instance, Mahdavi et al. (2021) performed weekly sampling of MERV-11 filters in tandem with airborne measurements over a six-week period; they found substantial underrepresentation of particles in the <1 μm fraction (0 vs 31.6 % by mass), but 1-2.5 μm and 2.5-10 μm fractions differed by only 3.3-3.4 % and the >10 μm fraction was within airborne measurement uncertainties (Mahdavi et al., 2021). Another study by Mahdavi and Siegel (2020) artificially loaded and extracted ISO Fine and ASHRAE #2 test dust from 20 HVAC filters of varying efficiencies (MERV-8, -8E, -11, -14). They found a slight overrepresentation of particles >10 μm, but closer proximity between volume distributions of particles <10 μm and negligible differences among their count-based size distributions (Mahdavi and Siegel, 2020). Furthermore, the size distribution modes of PM_{10} were preserved at 0.9 and 4.3 μm, varying only in their magnitude, while particles >10 μm exhibited significant modal displacement. Deviations from test dust distributions within the PM_{10} fraction were relatively constant among particles >1 μm, suggesting that these relative differences are largely preserved, and were even smaller in particles <1 μm where sizes down to 0.45 μm were well-represented. Interestingly, this trend was observed for all MERV-ratings regardless of differences in theoretical filtration efficiency (Mahdavi and Siegel, 2020).

Despite the apparent lack of submicron particles in Mahdavi et al. (2021), the trace element composition of HVAC samples was relatively consistent with airborne measurements; elemental concentrations were strongly correlated (Spearman's coefficient = 0.97) and most fell within a factor of two (Mahdavi et al., 2021). To this end, the authors concluded that particles <1 μm were likely present but masked/agglomerated to larger particles, and/or below instrument detection. This was supported by in-situ HVAC filter efficiency testing which showed the presence of submicron particles within the filter (Mahdavi et al., 2021). Amongst other studies, the degree to which submicron particles are captured by HVAC and/or FF techniques varies, though most demonstrate reduced recovery efficiencies (Dev et al., 2022; Stephens and Siegel, 2012). This is not unique to the FF approach, with commonly used airborne samplers such as the N6 Single Stage Andersen Cascade Impactor (Thermo Scientific, USA) and AGI-30 Air Sampling Impinger (Ace Glass Inc., USA) displaying cut-off sizes of 0.65 and 0.3 μm, respectively.

Investigations into other potential biases, such as ongoing chemical transformation on the HVAC filter surface during deployment, suggest that this effect is minimal. Observations of 30-day old MERV-7 filters deployed across 14 retail buildings have shown that the ratio of particulate phthalates and polybrominated diphenyl ethers to their gaseous forms were generally proportional to the octanol-air partition coefficient (Xu et al., 2015). Given semi-volatile organic compounds (SVOCs) are among the more susceptible elements for ongoing chemical change, this suggests that an equilibrium assumption upon deposition to the HVAC filter surface may be reasonable (Xu et al., 2015). This is supported by an analysis of 19 studies with simultaneous measurements of up to 66 SVOCs in indoor air and settled dust, displaying a strong, linear relationship (R^2 = 0.75) with near-unit slope (0.98) between the observed mass fractions and those predicted under equilibrium partitioning (Weschler and Nazaroff, 2010).

Supplementary Text 2.2 Impact of atmospheric concentration on HVAC trapping efficiency.

Prolonged exposure to heavily polluted air may have differentially enhanced the fine PM trapping efficiency of the Wildfire HVAC filters, generating a stronger clogging effect compared to the less polluted Reference filters. To investigate this potential sampling bias, we calculated the relative change in Wildfire $PM_{2.5}$ / PM_{10} particle number proportions from the median Reference condition and compared these to the in-situ airborne mass proportions in the DPE record (Table S2.5). As expected, $PM_{2.5}$ / PM_{10} proportions from HVAC sampling were higher than airborne mass, given that fine particles are numerous but contribute less mass individually than coarser particles (PERMANOVA: p = 0.001). However, despite the disparity in atmospheric concentration, the relative change in Wildfire $PM_{2.5}$ / PM_{10} proportions from the median Reference condition were of a similar magnitude for both particle number and mass measurements (PERMANOVA: p = 0.916). While stronger filter clogging during the Wildfires would serve to increase the capture of fine particles disproportionately to the Reference filters, a median 0.4 % discrepancy offers little evidence for differentially altered trapping efficiencies. Therefore, the comparisons drawn between the two study periods remain valid.

Supplementary References

Dev, S., Barnes, D., Kadir, A., Betha, R., Aggarwal, S., 2022. Outdoor and indoor concentrations of size-resolved particulate matter during a wildfire episode in interior Alaska and the impact of ventilation. Air Qual. Atmos. Heal. 15, 149-158. https://doi.org/10.1007/s11869-021-01094-8.

Mahdavi, A., Dingle, J., Chan, A.W.H., Siegel, J.A., 2021. HVAC filtration of particles and trace metals: Airborne measurements and the evaluation of quantitative filter forensics. Environ. Pollut. 271, 116388. https://doi.org/10.1016/j.envpol.2020.116388.

Mahdavi, A., Siegel, J.A., 2020. Extraction of dust collected in HVAC filters for quantitative filter forensics. Aerosol Sci. Technol. 54, 1282-1292. https://doi.org/10.1080/02786826.2020.1774492.

Stephens, B., Siegel, J.A., 2012. Comparison of test methods for determining the particle removal efficiency of filters in residential and light-commercial central HVAC systems. Aerosol Sci. Technol. 46, 504-513. https://doi.org/10.1080/02786826.2011.642825.

Weschler, C.J., Nazaroff, W.W., 2010. SVOC partitioning between the gas phase and settled dust indoors. Atmos. Environ. 44, 3609-3620. https://doi.org/10.1016/j.atmosenv.2010.06.029.

Xu, Y., Liang, Y., Urquidi, J.R., Siegel, J.A., 2015. Semi-volatile organic compounds in heating, ventilation, and air-conditioning filter dust in retail stores. Indoor Air 25, 79-92. https://doi.org/10.1111/ina.12123.

Chapter 4: Supplementary Material

Supplementary Tables

Supplementary Table 4.1 Summary of the physical characteristics of each estuary sampled in the Southern Rivers region on the South Coast of NSW, Australia. Summarised from information provided by NSW Department of Climate Change, Energy, the Environment and Water (DCCEEW) (links in refs (NSW Department of Climate Change, Energy, the Environment, 2018a, 2018b, 2018c, 2018d, 2018e)).

Estuary	Estuary code	Entrance location	Group	Type	Entrance condition	Catchment area (km^2)	Estuary area (km^2)	Estuary volume (ML)	Average depth (m)
Lake Brou	BRO	36.13°S 150.13°E	Intermittently closed	Saline coastal lagoon	Intermittent	41.6	2.5	2736.1	1.2
Lake Tabourie	TAB	35.44°S 150.41°E	Intermittently closed	Saline coastal lagoon	Intermittent	46.1	1.5	1123.8	0.8
Clyde River	CLY	35.71°S 150.18°E	Tide dominated	Drowned valley	Open to the sea	1722.9	17.5	50736.6	3
Moruya River	MOR	35.91°S 150.15°E	Wave dominated	Barrier	Open to the sea and trained	1423.7	6.1	10168	1.9
Tuross River	TUR	36.07°S 150.13°E	Wave dominated	Barrier	Open to the sea	1813.8	15.5	18208.2	1.2

Supplementary Table 4.2 Water quality probe measurements recorded at the time of sampling in each estuary in Bateman's Bay, NSW. Measurements were taken using the standard NSW DCCEEW sampling procedure and a calibrated water quality sonde (YSI EXO 2, Yellow Springs Instruments; OH, USA) at a depth of ~0.5m. Full parameter names are provided in the footnotes below.

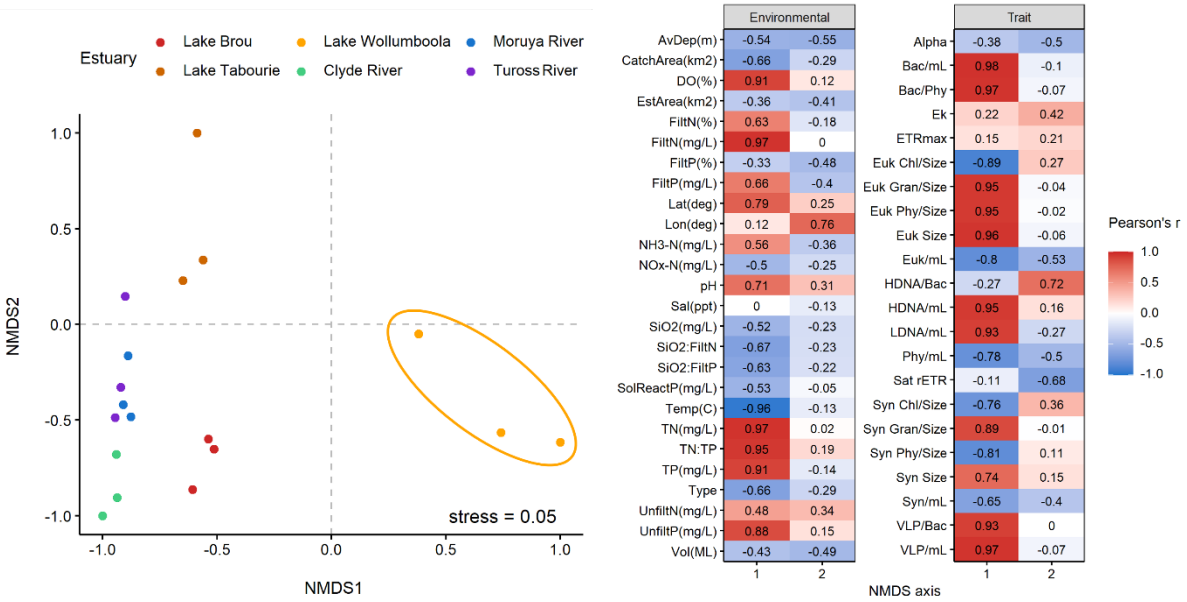
	BRO			TAB			CLY			MOR			TUR		
Date	04/21/2021			04/24/2021			04/25/2021			04/26/2021			04/22/2021		
Time	9:15AM	±	6min	10:00AM	±	6min	11:04AM	±	12min	11:23AM	±	10min	9:50AM	±	13min
Dep (m)	0.08	±	0.10	0.15	±	0.15	1.00	±	0.06	0.96	±	0.04	1.46	±	0.05
Temp (°C)	17.61	±	0.08	16.82	±	0.54	19.11	±	0.11	19.14	±	0.20	17.89	±	0.15
DO (%)	92.48	±	0.97	92.08	±	4.76	85.02	±	5.28	91.74	±	1.15	81.96	±	3.00
DO (mg/L)	7.25	±	0.07	7.56	±	0.41	6.75	±	0.33	7.27	±	0.13	6.77	±	0.24
C (µS/cm)	43015	±	103	36346	±	3036	35650	±	3445	35989	±	2736	31492	±	1590
SPC (µS/cm)	50083	±	50	43060	±	3150	40158	±	3792	40513	±	2912	36439	±	1889
Sal (ppt)	32.86	±	0.03	27.78	±	2.24	25.72	±	2.69	25.97	±	2.07	23.09	±	1.31
pH	7.72	±	0.02	8.18	±	0.06	7.99	±	0.07	8.11	±	0.03	8.05	±	0.05
Turb (NTU)	3.80	±	0.73	12.13	±	14.99	11.34	±	17.82	13.04	±	15.53	3.94	±	0.18
PE (RFU)	2.13	±	0.25	2.45	±	0.67	2.21	±	0.51	1.61	±	0.48	1.94	±	0.35
PE (µg/L)	6.00	±	0.69	6.92	±	1.89	6.23	±	1.42	4.54	±	1.35	5.48	±	1.00
CHL (RFU)	0.58	±	0.08	0.51	±	0.11	0.67	±	0.10	0.55	±	0.21	0.54	±	0.13
CHL (µg/L)	2.50	±	0.34	2.21	±	0.42	2.84	±	0.40	2.38	±	0.83	2.35	±	0.51
fDOM (RFU)	7.74	±	0.08	12.01	±	2.36	3.89	±	1.37	2.25	±	0.86	7.19	±	0.62
fDOM (QSU)	23.40	±	0.24	36.35	±	7.15	11.75	±	4.17	6.79	±	2.61	21.74	±	1.88

Abbreviated parameter names are as follows: Temp = temperature; DO = dissolved oxygen; C = conductivity; SPC = specific conductivity; Sal = salinity; pH = pH; Turb = turbidity; PE = phycoerytherin fluorescence; CHL = chlorophyll fluorescence; fDOM = fluorescent dissolved organic matter.

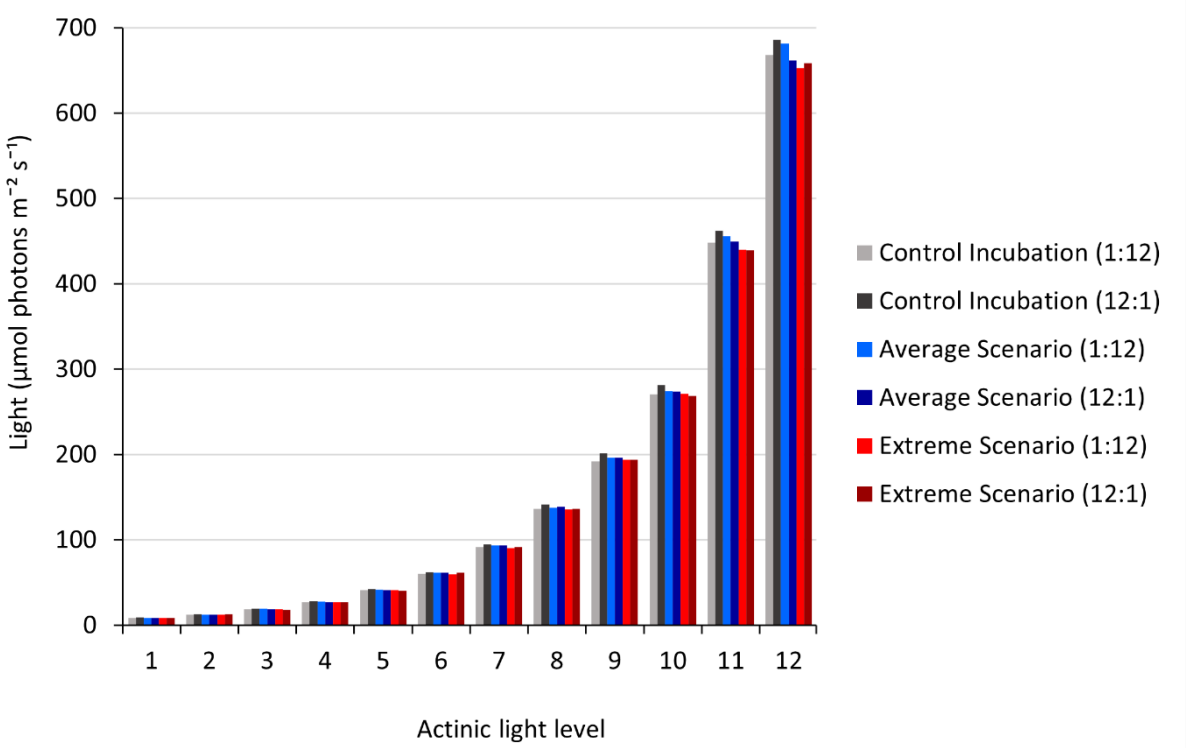
Supplementary Table 4.3 Summary of weather and tidal conditions for each estuary sampled in the Southern Rivers region on the South Coast of NSW, Australia. Data summarised from information provided by the Bureau of Meteorology (Bureau of Meteorology, 2021a, 2021b). Weather conditions taken from 9:00 AEDT measurements. RH = relative humidity.

Estuary	**Date**	**Boat dep.**	**Weather conditions**			**Tidal conditions**					
			Nearest station (distance)	Temp (°C)	RH (%)	Nearest station	Nearest high (time/height)		Nearest low (time/height)		Tide
Lake Brou	21/04/21	8:45	Narooma (9.3 km)	14.2	53	Moruya (25.6 km)	3:00	1.21 m	10:08	0.39 m	↓
Lake Tabourie	24/04/21	9:30	Ulladulla (10.7 km)	17.2	59	Ulladulla Harbour (11 km)	5:34	1.58 m	12:03	0.31 m	↓
Clyde River	25/04/21	10:33	Batemans Bay (1.6 km)	16.1	88	Princess Jetty (Batemans Bay) (0.6 km)	6:47	1.54 m	13:15	0.23 m	↓
Moruya River	26/04/21	11:05	Moruya (0.3 km)	14.2	79	Moruya (3.2 km)	7:53	1.43 m	14:08	0.14 m	↓
Tuross River	22/04/21	8:42	Narooma (16 km)	13.5	61	Moruya (18.9 km)	4:07	1.25 m	11:04	0.33 m	↓

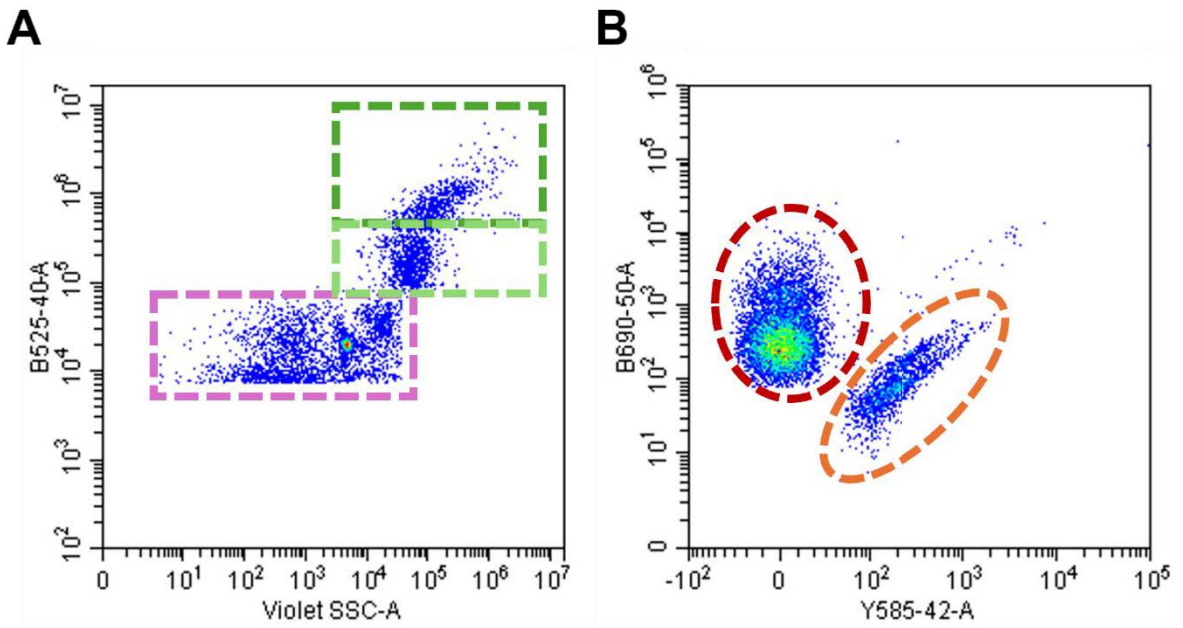
Supplementary Figures



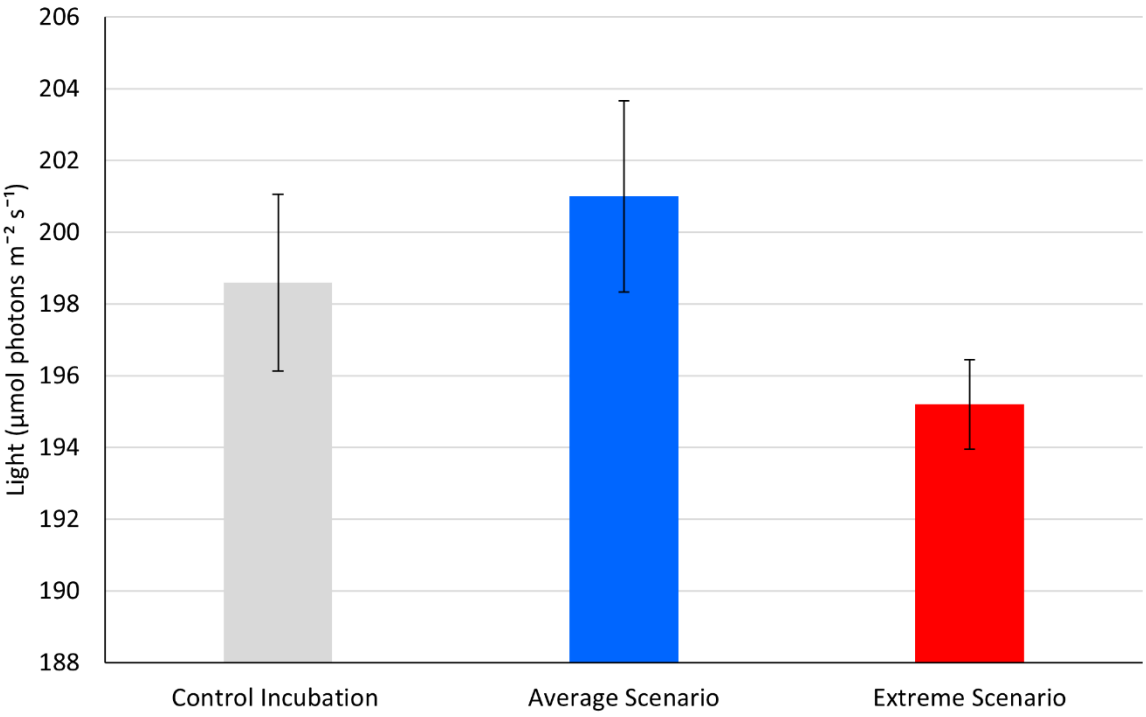
Supplementary Figure 4.1 At the time of sampling, Lake Wollumboola displayed substantial differences to all five other estuaries sampled. These differences were driven predominantly by an extremely high abundance of total bacteria (r = 0.98), including low (r = 0.93) and high (r = 0.95) DNA sub-populations, and to a lesser extent a lack of phytoplankton (r = -0.78). Nutrient analyses revealed that this estuary had significantly higher concentrations of nitrogen and phosphorus, which may have led to this result. It may be worth noting that upon sampling, Lake Wollumboola was visibly discoloured (yellowing) and presented with an unpleasant smell. As such, the sixth estuary was removed from the formal analysis in this thesis chapter.



Supplementary Figure 4.2 Light (µmol m^{-2} s^{-1}) received in the centre of the cuvette within the emitter-detector unit of a water pulse amplitude modulated fluorometer (Heinz Walz GmbH, Germany), as detected by a 4-pi light sensor fitted to an emitter-detector unit (Universal Light Meter & Data Logger (ULM-500), Heinz Walz GmbH, Germany). Wildfire ash treatments were mixed in Milli-Q water and were measured under constant actinic light starting at either light level 1 through to 12 (1:12), or 12 through to 1 (12:1) (n = 2). Overall, light levels did not differ between treatments (ANOVA with Tukey HSD: $p > 0.05$ in all cases).



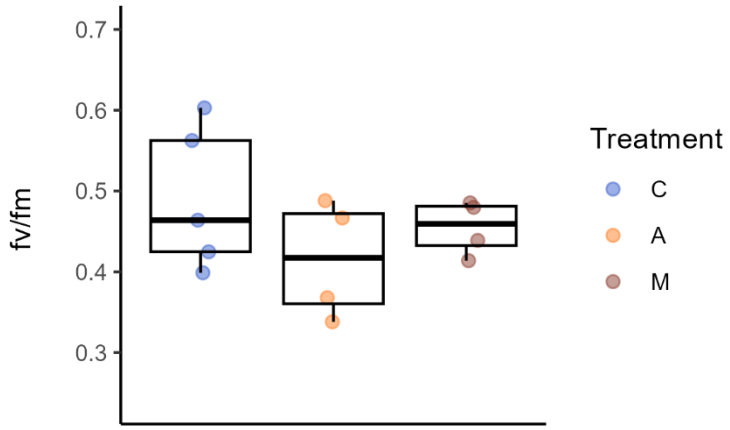
Supplementary Figure 4.3 Typical cytograms from flow cytometric enumeration of bacteria, viruses, and phytoplankton. Cytogram A depicts virus-like particles (VLP) enumerated as a single population (nucleic acid stain green fluorescence ~10^4 – 10^5; purple dashed gate), and two sub-populations of bacteria enumerated as those with low (~10^5; light-green dashed gate) and high (~10^6; dark-green dashed date) levels of DNA, respectively. Cytogram B depicts phytoplankton enumerated as Synechococcus (higher orange fluorescence, Y585-42-A; orange dashed gate) and Eukaryotes (higher red fluorescence, B690-50-A; red dashed gate). Prochlorococcus was not enumerated here as nucleic acid staining showed that it was always absent. Thresholds for background were set at ~10^4 green fluorescence for VLP, and ~10^2 red fluorescence for Eukaryotes, as indicated by controls (combination of 0.22 µm filtered sample water, TE buffer and/or nucleic acid stain for both cytograms).



Supplementary Figure 4.4 Light (µmol m^{-2} s^{-1}) received in the incubation bottles used for experimentation, as detected by a 4-pi light sensor (Universal Light Meter & Data Logger (ULM-500), Heinz Walz GmbH, Germany) sitting under the neck of the bottle. Wildfire ash treatments were mixed in Milli-Q water and were measured under a constant irradiance of 195 ± 15 µmol photons m^{-2} s^{-1} (min/max) (n = 3). Overall, there was a ~6 µmol m^{-2} s^{-1} reduction in light in the Extreme Scenario compared to the Control Incubation but this did not statistically differ (ANOVA: p = 0.112).

Chapter 5: Supplementary Material

Supplementary Figures



Supplementary Figure 5.1 Dark-adapted photosynthetic capacity (Fv/Fm) of Clyde River microbes following 10-day incubations with wildfire-enriched particles. Plots are coloured by incubation treatment, including Control (”C”), Average (”A”) and Maximum (”M”), respectively. No significant differences were detected between treatments (p = 0.33, ANOVA).

References

Abram, N.J., Gagan, M.K., McCulloch, M.T., Chappell, J., Hantoro, W.S., 2003. Coral Reef Death During the 1997 Indian Ocean Dipole Linked to Indonesian Wildfires. Science (80-.). 301, 952–955. https://doi.org/10.1126/science.1083841

Abram, N.J., Henley, B.J., Sen Gupta, A., Lippmann, T.J.R., Clarke, H., Dowdy, A.J., Sharples, J.J., Nolan, R.H., Zhang, T., Wooster, M.J., Wurtzel, J.B., Meissner, K.J., Pitman, A.J., Ukkola, A.M., Murphy, B.P., Tapper, N.J., Boer, M.M., 2021. Connections of climate change and variability to large and extreme forest fires in southeast Australia. Commun. Earth Environ. 2, 8. https://doi.org/10.1038/s43247-020-00065-8

Adachi, K., Buseck, P.R., 2015. Changes in shape and composition of sea-salt particles upon aging in an urban atmosphere. Atmos. Environ. 100, 1–9. https://doi.org/10.1016/j.atmosenv.2014.10.036

Adachi, K., Dibb, J.E., Scheuer, E., Katich, J.M., Schwarz, J.P., Perring, A.E., Mediavilla, B., Guo, H., Campuzano-Jost, P., Jimenez, J.L., Crawford, J., Soja, A.J., Oshima, N., Kajino, M., Kinase, T., Kleinman, L., Sedlacek, A.J., Yokelson, R.J., Buseck, P.R., 2022. Fine Ash-Bearing Particles as a Major Aerosol Component in Biomass Burning Smoke. J. Geophys. Res. Atmos. 127. https://doi.org/10.1029/2021JD035657

Adam, M.G., Tran, P.T.M., Bolan, N., Balasubramanian, R., 2021. Biomass burning-derived airborne particulate matter in Southeast Asia: A critical review. J. Hazard. Mater. 407, 124760. https://doi.org/10.1016/j.jhazmat.2020.124760

Aguilera, R., Corringham, T., Gershunov, A., Benmarhnia, T., 2021. Wildfire smoke impacts respiratory health more than fine particles from other sources: observational evidence from Southern California. Nat. Commun. 12. https://doi.org/10.1038/s41467-021-21708-0

Akagi, S.K., Yokelson, R.J., Wiedinmyer, C., Alvarado, M.J., Reid, J.S., Karl, T., Crounse, J.D., Wennberg, P.O., 2011. Emission factors for open and domestic biomass burning for use in atmospheric models. Atmos. Chem. Phys. 11, 4039–4072. https://doi.org/10.5194/acp-11-4039-2011

Alavy, M., Siegel, J.A., 2020. In-situ effectiveness of residential HVAC filters. Indoor Air 30, 156–166. https://doi.org/10.1111/ina.12617

Aldersley, A., Murray, S.J., Cornell, S.E., 2011. Global and regional analysis of climate and human drivers of wildfire. Sci. Total Environ. 409, 3472–3481. https://doi.org/10.1016/j.scitotenv.2011.05.032

Alexakis, D.E., 2020. Suburban areas in flames: Dispersion of potentially toxic elements from burned vegetation and buildings. Estimation of the associated ecological and human health risk. Environ. Res. 183, 109153. https://doi.org/10.1016/j.envres.2020.109153

Alonso-Blanco, E., Calvo, A.I., Fraile, R., Castro, A., 2012. The influence of wildfires on aerosol size distributions in rural areas. Sci. World J. 2012, 1–13. https://doi.org/10.1100/2012/735697

Alves, C.A., Gonçalves, C., Pio, C.A., Mirante, F., Caseiro, A., Tarelho, L., Freitas, M.C., Viegas, D.X., 2010. Smoke emissions from biomass burning in a Mediterranean shrubland. Atmos. Environ. 44, 3024–3033. https://doi.org/10.1016/j.atmosenv.2010.05.010

Andersson, S.M., Martinsson, B.G., Friberg, J., Brenninkmeijer, C.A.M., Rauthe-Schöch, A., Hermann, M., van Velthoven, P.F.J., Zahn, A., 2013. Composition and evolution of volcanic aerosol from eruptions of Kasatochi, Sarychev and Eyjafjallajökull in 2008–2010 based on CARIBIC observations. Atmos. Chem. Phys. 13, 1781–1796. https://doi.org/10.5194/acp-13-1781-2013

Andreae, M.O., 2019. Emission of trace gases and aerosols from biomass burning - An updated assessment. Atmos. Chem. Phys. 19, 8523–8546. https://doi.org/10.5194/acp-19-8523-2019

Araujo-Lima, C.A.R.M., Forsberg, B.R., Victoria, R., Martinelli, L., 1986. Energy sources for detritivorous fishes in the Amazon. Science (80-.). 234, 1256–1258. https://doi.org/10.1126/science.234.4781.1256

Ardyna, M., Hamilton, D.S., Harmel, T., Lacour, L., Bernstein, D.N., Laliberté, J., Horvat, C., Laxenaire, R., Mills, M.M., van Dijken, G., Polyakov, I., Claustre, H., Mahowald, N., Arrigo, K.R., 2022. Wildfire aerosol deposition likely amplified a summertime Arctic phytoplankton bloom. Commun. Earth Environ. 3, 1–8. https://doi.org/10.1038/s43247-022-00511-9

Arimoto, R., Ray, B.J., Lewis, N.F., Tomza, U., Duce, R.A., 1997. Mass-particle size distributions of atmospheric dust and the dry deposition of dust to the remote ocean. J. Geophys. Res. Atmos. 102, 15867–15874. https://doi.org/10.1029/97jd00796

Arnholt, A.T.A.T., Evans, B., 2021. BSDA: Basic Statistics and Data Analysis [WWW Document]. URL https://cran.r-project.org/package=BSDA (accessed 3.22.23).

Arrigo, K.R., 2005. Marine microorganisms and global nutrient cycles. Nature 437, 349–355. https://doi.org/10.1038/nature04159

Attiya, A.A., Jones, B.G., 2022. An extensive dust storm impact on air quality on 22 November 2018 in Sydney, Australia, using satellite remote sensing and ground data. Environ. Monit. Assess. 194, 432. https://doi.org/10.1007/s10661-022-10080-1

Australian Bureau of Statistics, 2023. Regional Population [WWW Document]. URL https://www.abs.gov.au/. (accessed 3.22.23).

Ayars, J., Kramer, H.A., Jones, G.M., 2023. The 2020 to 2021 California megafires and their impacts on wildlife habitat. Proc. Natl. Acad. Sci. 120. https://doi.org/10.1073/pnas.2312909120

Azam, F., Fenchel, T., Field, J., Gray, J., Meyer-Reil, L., Thingstad, F., 1983. The Ecological Role of Water-Column Microbes in the Sea. Mar. Ecol. Prog. Ser. 10, 257–263. https://doi.org/10.3354/meps010257

Baddock, M., Parsons, K., Strong, C., Leys, J., McTainsh, G., 2015. Drivers of Australian dust: a case study of frontal winds and dust dynamics in the lower lake Eyre basin. Earth Surf. Process. Landforms 40, 1982–1988. https://doi.org/10.1002/esp.3773

Baetge, N., Halsey, K.H., Hanan, E.J., Behrenfeld, M.J., Milligan, A.J., Graff, J.R., Hansen, P., Carlson, C.A., Boiteau, R.M., Arrington, E.C., Comstock, J., Halewood, E.R., Harvey, E.L., Nelson, N.B., Opalk, K., Ver Wey, B., 2025. Pre-existing phytoplankton biomass concentrations shape coastal plankton response to fire-generated ash leachate. Limnol. Oceanogr. https://doi.org/10.1002/lno.70087

Baker, A.R., Adams, C., Bell, T.G., Jickells, T.D., Ganzeveld, L., 2013. Estimation of atmospheric nutrient inputs to the Atlantic Ocean from 50°N to 50°S based on large-scale field sampling: Iron and other dust-associated elements. Global Biogeochem. Cycles.

https://doi.org/10.1002/gbc.20062

Baker, A.R., French, M., Linge, K.L., 2006a. Trends in aerosol nutrient solubility along a west–east transect of the Saharan dust plume. Geophys. Res. Lett. 33. https://doi.org/10.1029/2005GL024764

Baker, A.R., Jickells, T.D., 2006. Mineral particle size as a control on aerosol iron solubility. Geophys. Res. Lett. 33, L17608. https://doi.org/10.1029/2006GL026557

Baker, A.R., Jickells, T.D., Witt, M., Linge, K.L., 2006b. Trends in the solubility of iron, aluminium, manganese and phosphorus in aerosol collected over the Atlantic Ocean. Mar. Chem. 98, 43–58. https://doi.org/10.1016/j.marchem.2005.06.004

Balfour, V.N., Woods, S.W., 2013. The hydrological properties and the effects of hydration on vegetative ash from the Northern Rockies, USA. CATENA 111, 9–24. https://doi.org/10.1016/j.catena.2013.06.014

Banks, S.C., Knight, E.J., McBurney, L., Blair, D., Lindenmayer, D.B., 2011. The Effects of Wildfire on Mortality and Resources for an Arboreal Marsupial: Resilience to Fire Events but Susceptibility to Fire Regime Change. PLoS One 6, e22952. https://doi.org/10.1371/journal.pone.0022952

Banwart, S.A., Nikolaidis, N.P., Zhu, Y.-G., Peacock, C.L., Sparks, D.L., 2019. Soil Functions: Connecting Earth's Critical Zone. Annu. Rev. Earth Planet. Sci. 47, 333–359. https://doi.org/10.1146/annurev-earth-063016-020544

Barkley, A.E., Prospero, J.M., Mahowald, N., Hamilton, D.S., Popendorf, K.J., Oehlert, A.M., Pourmand, A., Gatineau, A., Panechou-Pulcherie, K., Blackwelder, P., Gaston, C.J., 2019. African biomass burning is a substantial source of phosphorus deposition to the Amazon, Tropical Atlantic Ocean, and Southern Ocean. Proc. Natl. Acad. Sci. U. S. A. 116, 16216–16221. https://doi.org/10.1073/pnas.1906091116

Barros, T.L., Bracewell, S.A., Mayer-Pinto, M., Dafforn, K.A., Simpson, S.L., Farrell, M., Johnston, E.L., 2022. Wildfires cause rapid changes to estuarine benthic habitat. Environ. Pollut. 308, 119571. https://doi.org/10.1016/j.envpol.2022.119571

Battles, J.J., Fahey, T.J., Driscoll, C.T., Blum, J.D., Johnson, C.E., 2014. Restoring Soil Calcium Reverses Forest Decline. Environ. Sci. Technol. Lett. 1, 15–19. https://doi.org/10.1021/ez400033d

Bearman, C., Grunwald, J.A., Brooks, B.P., Owen, C., 2015. Breakdowns in coordinated decision making at and above the incident management team level: An analysis of three large scale Australian wildfires. Appl. Ergon. 47, 16–25. https://doi.org/10.1016/j.apergo.2014.08.009

Beck, H.E., Zimmermann, N.E., McVicar, T.R., Vergopolan, N., Berg, A., Wood, E.F., 2018. Present and future köppen-geiger climate classification maps at 1-km resolution. Sci. Data 5, 1–12. https://doi.org/10.1038/sdata.2018.214

Benedict, K.B., Prenni, A.J., Carrico, C.M., Sullivan, A.P., Schichtel, B.A., Collett, J.L., 2017. Enhanced concentrations of reactive nitrogen species in wildfire smoke. Atmos. Environ. 148, 8–15. https://doi.org/10.1016/j.atmosenv.2016.10.030

Bernath, P., Boone, C., Crouse, J., 2022. Wildfire smoke destroys stratospheric ozone. Science (80-.). 375, 1292–1295. https://doi.org/10.1126/science.abm5611

Biswas, T.K., Karim, F., Kumar, A., Wilkinson, S., Guerschman, J., Rees, G., McInerney, P.,

Zampatti, B., Sullivan, A., Nyman, P., Sheridan, G.J., Joehnk, K., 2021. 2019–2020 Bushfire impacts on sediment and contaminant transport following rainfall in the Upper Murray River catchment. Integr. Environ. Assess. Manag. 17, 1203–1214. https://doi.org/10.1002/ieam.4492

Bixby, R.J., Cooper, S.D., Gresswell, R.E., Brown, L.E., Dahm, C.N., Dwire, K.A., 2015. Fire effects on aquatic ecosystems: An assessment of the current state of the science. Freshw. Sci. 34, 1340–1350. https://doi.org/10.1086/684073

Bodí, M.B., Martin, D.A., Balfour, V.N., Santín, C., Doerr, S.H., Pereira, P., Cerdà, A., Mataix-Solera, J., 2014. Wildland fire ash: Production, composition and eco-hydro-geomorphic effects. Earth-Science Rev. 130, 103–127. https://doi.org/10.1016/j.earscirev.2013.12.007

Boer, M.M., Resco de Dios, V., Bradstock, R.A., 2020. Unprecedented burn area of Australian mega forest fires. Nat. Clim. Chang. 10, 171–172. https://doi.org/10.1038/s41558-020-0716-1

Borchers Arriagada, N., Palmer, A.J., Bowman, D.M.J.S., Morgan, G.G., Jalaludin, B.B., Johnston, F.H., 2020. Unprecedented smoke-related health burden associated with the 2019–20 bushfires in eastern Australia. Med. J. Aust. 213, 282–283. https://doi.org/10.5694/mja2.50545

Bowd, E.J., Banks, S.C., Strong, C.L., Lindenmayer, D.B., 2019. Long-term impacts of wildfire and logging on forest soils. Nat. Geosci. 12, 113–118. https://doi.org/10.1038/s41561-018-0294-2

Bowman, D., Williamson, G., Yebra, M., Lizundia-Loiola, J., Pettinari, M.L., Shah, S., Bradstock, R., Chuvieco, E., 2020. Wildfires: Australia needs national monitoring agency. Nature 584, 188–191. https://doi.org/10.1038/d41586-020-02306-4

Bowman, D.M.J.S., Kolden, C.A., Abatzoglou, J.T., Johnston, F.H., van der Werf, G.R., Flannigan, M., 2020. Vegetation fires in the Anthropocene. Nat. Rev. Earth Environ. 1, 500–515. https://doi.org/10.1038/s43017-020-0085-3

Bowman, D.M.J.S., Moreira-Muñoz, A., Kolden, C.A., Chávez, R.O., Muñoz, A.A., Salinas, F., González-Reyes, Á., Rocco, R., de la Barrera, F., Williamson, G.J., Borchers, N., Cifuentes, L.A., Abatzoglou, J.T., Johnston, F.H., 2019. Human–environmental drivers and impacts of the globally extreme 2017 Chilean fires. Ambio 48, 350–362. https://doi.org/10.1007/s13280-018-1084-1

Boyd, P.W., Ellwood, M.J., Tagliabue, A., Twining, B.S., 2017. Biotic and abiotic retention, recycling and remineralization of metals in the ocean. Nat. Geosci. 10, 167–173. https://doi.org/10.1038/ngeo2876

Bracewell, S.A., Barros, T.L., Mayer-Pinto, M., Dafforn, K.A., Simpson, S.L., Johnston, E.L., 2023. Contaminant pulse following wildfire is associated with shifts in estuarine benthic communities. Environ. Pollut. 316, 120533. https://doi.org/10.1016/j.envpol.2022.120533

Bradshaw, S.D., Dixon, K.W., Lambers, H., Cross, A.T., Bailey, J., Hopper, S.D., 2018. Understanding the long-term impact of prescribed burning in mediterranean-climate biodiversity hotspots, with a focus on south-western Australia. Int. J. Wildl. Fire 27, 643–657. https://doi.org/10.1071/WF18067

Bradstock, R.A., 2010. A biogeographic model of fire regimes in Australia: current and future implications. Glob. Ecol. Biogeogr. 19, 145–158. https://doi.org/10.1111/j.1466-8238.2009.00512.x

Brahney, J., Ballantyne, A.P., Sievers, C., Neff, J.C., 2013. Increasing Ca2+ deposition in the western US: The role of mineral aerosols. Aeolian Res. 10, 77–87. https://doi.org/10.1016/j.aeolia.2013.04.003

Bratbak, G., Thingstad, F., Heldal, M., 1994. Viruses and the microbial loop. Microb. Ecol. 28, 209–221. https://doi.org/10.1007/BF00166811

Britt, A., Senior, A., 2021. Australian Resource Reviews: Antimony 2020. Canberra. https://doi.org/10.11636/9781922446534

Browning, T.J., Moore, C.M., 2023. Global analysis of ocean phytoplankton nutrient limitation reveals high prevalence of co-limitation. Nat. Commun. 14, 5014. https://doi.org/10.1038/s41467-023-40774-0

Bryson, S., Li, Z., Pett-Ridge, J., Hettich, R.L., Mayali, X., Pan, C., Mueller, R.S., 2016. Proteomic Stable Isotope Probing Reveals Taxonomically Distinct Patterns in Amino Acid Assimilation by Coastal Marine Bacterioplankton. mSystems 1. https://doi.org/10.1128/mSystems.00027-15

Buchan, A., González, J.M., Moran, M.A., 2005. Overview of the Marine Roseobacter Lineage. Appl. Environ. Microbiol. 71, 5665–5677. https://doi.org/10.1128/AEM.71.10.5665-5677.2005

Bureau of Meteorology, 2021a. Climate Data Online [WWW Document]. Aust. Gov. URL http://www.bom.gov.au/climate/data/ (accessed 10.15.21).

Bureau of Meteorology, 2021b. Tide Predictions for Australia, South Pacific and Antarctica [WWW Document]. Aust. Gov. URL http://www.bom.gov.au/australia/tides/ (accessed 10.14.21).

Bureau of Meteorology, 2019. Special Climate Statement 71—severe fire weather conditions in southeast Queensland and northeast New South Wales in September 2019 [WWW Document]. Aust. Gov. URL http://www.bom.gov.au/climate/current/statements/scs71.pdf (accessed 3.28.23).

Burkhardt, B.G., Watkins-Brandt, K.S., Defforey, D., Paytan, A., White, A.E., 2014. Remineralization of phytoplankton-derived organic matter by natural populations of heterotrophic bacteria. Mar. Chem. 163, 1–9. https://doi.org/10.1016/j.marchem.2014.03.007

Caetano, M., Madureura, M., Vale, C., 2003. Metal reombilisation during resuspension of anoxic contaminated sediment: short-term laboratory study. Water, Air Soil Pollut. 143, 23–40. https://doi.org/https://doi.org/10.1023/A:1022877120813

Campbell, L., Nolla, H.A., Vaulot, D., 1994. The importance of Prochlorococcus to community structure in the central North Pacific Ocean. Limnol. Oceanogr. 39, 954–961. https://doi.org/10.4319/lo.1994.39.4.0954

Campbell, P.C., Tong, D., Saylor, R., Li, Y., Ma, S., Zhang, X., Kondragunta, S., Li, F., 2022. Pronounced increases in nitrogen emissions and deposition due to the historic 2020 wildfires in the western U.S. Sci. Total Environ. 839, 156130. https://doi.org/10.1016/j.scitotenv.2022.156130

Canadell, J.G., Meyer, C.P. (Mick., Cook, G.D., Dowdy, A., Briggs, P.R., Knauer, J., Pepler, A., Haverd, V., 2021. Multi-decadal increase of forest burned area in Australia is linked to climate change. Nat. Commun. 12, 6921. https://doi.org/10.1038/s41467-021-27225-4

Caporaso, J.G., Lauber, C.L., Walters, W.A., Berg-Lyons, D., Lozupone, C.A., Turnbaugh, P.J., Fierer, N., Knight, R., 2011. Global patterns of 16S rRNA diversity at a depth of millions of sequences per sample. Proc. Natl. Acad. Sci. 108, 4516–4522. https://doi.org/10.1073/pnas.1000080107

Carslaw, D.C., Ropkins, K., 2012. openair — An R package for air quality data analysis. Environ. Model. Softw. 27–28, 52–61. https://doi.org/10.1016/j.envsoft.2011.09.008

Castledine, M., Buckling, A., 2024. Critically evaluating the relative importance of phage in shaping microbial community composition. Trends Microbiol. 32, 957–969. https://doi.org/10.1016/j.tim.2024.02.014

Chambers, R.M., Fourqurean, J.W., Hollibaugh, J.T., Vink, S.M., 1995. Importance of terrestrially-derived, particulate phosphorus to phosphorus dynamics in a west coast estuary. Estuaries 18, 518–526. https://doi.org/10.2307/1352369

Chapin, F.S., Matson, P.A., Vitousek, P.M., 2011. Nutrient Cycling, in: Principles of Terrestrial Ecosystem Ecology. Springer New York, New York, NY, pp. 259–296. https://doi.org/10.1007/978-1-4419-9504-9_9

Charette, T., Prepas, E.E., 2003. Wildfire impacts on phytoplankton communities of three small lakes on the Boreal Plain, Alberta, Canada: a paleolimnological study. Can. J. Fish. Aquat. Sci. 60, 584–593. https://doi.org/10.1139/F03-049

Che, Y., Yu, B., Bracco, K., 2024. Temporal and spatial variations in dust activity in Australia based on remote sensing and reanalysis datasets. Atmos. Chem. Phys. 24, 4105–4128. https://doi.org/10.5194/acp-24-4105-2024

Chen, Y., Randerson, J.T., Van der Werf, G.R., Morton, D.C., Mu, M., Kasibhatla, P.S., 2010. Nitrogen deposition in tropical forests from savanna and deforestation fires. Glob. Chang. Biol. 16, 2024–2038. https://doi.org/10.1111/j.1365-2486.2009.02156.x

Cheng, B., Alapaty, K., Shu, Q., Arunachalam, S., 2022. Dry Deposition Methods Based on Turbulence Kinetic Energy: 2. Extension to Particle Deposition Using a Single-Point Model. J. Geophys. Res. Atmos. 127. https://doi.org/10.1029/2022JD037803

Chessman, B., 1986. Impact of the 1983 wildfires on river water quality in East Gippsland, Victoria. Mar. Freshw. Res. 37, 399–420. https://doi.org/10.1071/MF9860399

Clarke, H., Gibson, R., Cirulis, B., Bradstock, R.A., Penman, T.D., 2019. Developing and testing models of the drivers of anthropogenic and lightning-caused wildfire ignitions in south-eastern Australia. J. Environ. Manage. 235, 34–41. https://doi.org/10.1016/j.jenvman.2019.01.055

Clarke, H., Pitman, A.J., Kala, J., Carouge, C., Haverd, V., Evans, J.P., 2016. An investigation of future fuel load and fire weather in Australia. Clim. Change 139, 591–605. https://doi.org/10.1007/s10584-016-1808-9

Cloern, J.E., 2007. Habitat Connectivity and Ecosystem Productivity: Implications from a Simple Model. Am. Nat. 169, E21–E33. https://doi.org/10.1086/510258

Cohen, A.J., Brauer, M., Burnett, R., Anderson, H.R., Frostad, J., Estep, K., Balakrishnan, K., Brunekreef, B., Dandona, L., Dandona, R., Feigin, V., Freedman, G., Hubbell, B., Jobling, A., Kan, H., Knibbs, L., Liu, Y., Martin, R., Morawska, L., Pope, C.A., Shin, H., Straif, K., Shaddick, G., Thomas, M., van Dingenen, R., van Donkelaar, A., Vos, T., Murray, C.J.L., Forouzanfar, M.H., 2017. Estimates and 25-year trends of the global burden of disease attributable to ambient air pollution: an analysis of data from the Global Burden of

Diseases Study 2015. Lancet 389, 1907–1918. https://doi.org/10.1016/S0140-6736(17)30505-6

Cohen, D.D., Atanacio, A.J., Stelcer, E., Garton, D., 2016a. Sydney particle characterisation study. Australian Nuclear Science and Technology Organisation, NSW, Australia.

Cohen, D.D., Atanacio, A.J., Stelcer, E., Garton, D., 2016b. Sydney particle characterisation study PM2. 5 source apportionment in the Sydney Region between 2000 and 2014. Lucas Height. NSW Aust. Nucl. Sci. Technol. Organ.

Cohen, D.D., Stelcer, E., Garton, D., Crawford, J., 2011. Fine particle characterisation, source apportionment and longrange dust transport into the Sydney Basin: A long term study between 1998 and 2009. Atmos. Pollut. Res. 2, 182–189. https://doi.org/10.5094/APR.2011.023

Collins, L., Bradstock, R.A., Clarke, H., Clarke, M.F., Nolan, R.H., Penman, T.D., 2021. The 2019/2020 mega-fires exposed Australian ecosystems to an unprecedented extent of high-severity fire. Environ. Res. Lett. 16, 044029. https://doi.org/10.1088/1748-9326/abeb9e

Cook, P.L.M., Holland, D.P., 2012. Long term nutrient loads and chlorophyll dynamics in a large temperate Australian lagoon system affected by recurring blooms of cyanobacteria. Biogeochemistry 107, 261–274. https://doi.org/10.1007/s10533-010-9551-1

Cooper, S.D., Page, H.M., Wiseman, S.W., Klose, K., Bennett, D., Even, T., Sadro, S., Nelson, C.E., Dudley, T.L., 2015. Physicochemical and biological responses of streams to wildfire severity in riparian zones. Freshw. Biol. 60, 2600–2619. https://doi.org/10.1111/fwb.12523

Costa, D.L., Dreher, K.L., 1997. Bioavailable transition metals in particulate matter mediate cardiopulmonary injury in healthy and compromised animal models. Environ. Health Perspect. 105 Suppl, 1053–1060. https://doi.org/10.1289/ehp.97105s51053

Cropp, R.A., Gabric, A.J., Levasseur, M., McTainsh, G.H., Bowie, A., Hassler, C.S., Law, C.S., McGowan, H., Tindale, N., Viscarra Rossel, R., 2013. The likelihood of observing dust-stimulated phytoplankton growth in waters proximal to the Australian continent. J. Mar. Syst. 117–118, 43–52. https://doi.org/10.1016/j.jmarsys.2013.02.013

Crump, B.C., Bowen, J.L., 2024. The Microbial Ecology of Estuarine Ecosystems. Ann. Rev. Mar. Sci. 16, 335–360. https://doi.org/10.1146/annurev-marine-022123-101845

Darcy, J.L., Schmidt, S.K., Knelman, J.E., Cleveland, C.C., Castle, S.C., Nemergut, D.R., 2018. Phosphorus, not nitrogen, limits plants and microbial primary producers following glacial retreat. Sci. Adv. 4. https://doi.org/10.1126/sciadv.aaq0942

de la Broise, D., Palenik, B., 2007. Immersed in situ microcosms: A tool for the assessment of pollution impact on phytoplankton. J. Exp. Mar. Bio. Ecol. 341, 274–281. https://doi.org/10.1016/j.jembe.2006.10.045

Debelius, B., Forja, J.M., Lubián, L.M., 2011. Toxicity of copper, nickel and zinc to Synechococcus populations from the Strait of Gibraltar. J. Mar. Syst. 88, 113–119. https://doi.org/10.1016/j.jmarsys.2011.02.009

Department of Climate Change, Energy, the E. and W. (DCCEEW), 2020. National Indicative Aggregated Fire Extent Datasets (NIAFED_20190701_20200622_v20200623) [WWW Document]. URL https://fed.dcceew.gov.au/datasets/erin::national-indicative-aggregated-fire-extent-dataset/about (accessed 3.22.23).

Department of Planning and Environment, 2023. Air quality monitoring network [WWW Document]. URL www.environment.nsw.gov.au/ (accessed 3.22.23).

Department of the Environment and Heritage, 2005. National Standards for Criteria Air Pollutants 1 in Australia [WWW Document]. URL https://webarchive.nla.gov.au/awa/20200609072119/https://www.environment.gov.au/protection/publications/factsheet-national-standards-criteria-air-pollutants-australia (accessed 3.22.23).

Desboeufs, K.V. V., Sofikitis, A., Losno, R., Colin, J.L.L., Ausset, P., 2005. Dissolution and solubility of trace metals from natural and anthropogenic aerosol particulate matter. Chemosphere 58, 195–203. https://doi.org/10.1016/j.chemosphere.2004.02.025

Descals, A., Gaveau, D.L.A., Verger, A., Sheil, D., Naito, D., Peñuelas, J., 2022. Unprecedented fire activity above the Arctic Circle linked to rising temperatures. Science (80-.). 378, 532–537. https://doi.org/10.1126/science.abn9768

Dev, S., Barnes, D., Kadir, A., Betha, R., Aggarwal, S., 2022. Outdoor and indoor concentrations of size-resolved particulate matter during a wildfire episode in interior Alaska and the impact of ventilation. Air Qual. Atmos. Heal. 15, 149–158. https://doi.org/10.1007/s11869-021-01094-8

Di Virgilio, G., Evans, J.P., Blake, S.A.P., Armstrong, M., Dowdy, A.J., Sharples, J., McRae, R., 2019. Climate Change Increases the Potential for Extreme Wildfires. Geophys. Res. Lett. 46, 8517–8526. https://doi.org/10.1029/2019GL083699

Ding, C., Chen, J., Zhu, F., Chai, L., Lin, Z., Zhang, K., Shi, Y., 2022. Biological Toxicity of Heavy Metal(loid)s in Natural Environments: From Microbes to Humans. Front. Environ. Sci. 10, 1–23. https://doi.org/10.3389/fenvs.2022.920957

Doblin, M.A., Petrou, K., Sinutok, S., Seymour, J.R., Messer, L.F., Brown, M. V., Norman, L., Everett, J.D., McInnes, A.S., Ralph, P.J., Thompson, P.A., Hassler, C.S., 2016. Nutrient uplift in a cyclonic eddy increases diversity, primary productivity and iron demand of microbial communities relative to a western boundary current. PeerJ 4, e1973. https://doi.org/10.7717/peerj.1973

Dong, T.T.T., Hinwood, A.L., Callan, A.C., Zosky, G., Stock, W.D., 2017. In vitro assessment of the toxicity of bushfire emissions: A review. Sci. Total Environ. 603–604, 268–278. https://doi.org/10.1016/j.scitotenv.2017.06.062

Douglas, E.J., Bulmer, R.H., MacDonald, I.T., Lohrer, A.M., 2022. Estuaries as coastal reactors: importance of shallow seafloor habitats for primary productivity and nutrient transformation, and impacts of sea level rise. New Zeal. J. Mar. Freshw. Res. 56, 553–569. https://doi.org/10.1080/00288330.2022.2107027

Dragulescu, A., Arendt, C., 2020. xlsx: Read, Write, Format Excel 2007 and Excel 97/2000/XP/2003 Files.

Du, E., Terrer, C., Pellegrini, A.F.A., Ahlström, A., van Lissa, C.J., Zhao, X., Xia, N., Wu, X., Jackson, R.B., 2020. Global patterns of terrestrial nitrogen and phosphorus limitation. Nat. Geosci. 13, 221–226. https://doi.org/10.1038/s41561-019-0530-4

Du Laing, G., Rinklebe, J., Vandecasteele, B., Meers, E., Tack, F.M.G., 2009. Trace metal behaviour in estuarine and riverine floodplain soils and sediments: A review. Sci. Total Environ. 407, 3972–3985. https://doi.org/10.1016/j.scitotenv.2008.07.025

Duarte, C.M., Dachs, J., Llabrés, M., Alonso-Laita, P., Gasol, J.M., Tovar-Sánchez, A., Sañudo-

Wilhemy, S., Agustí, S., 2006. Aerosol inputs enhance new production in the subtropical northeast Atlantic. J. Geophys. Res. Biogeosciences 111, 1–8. https://doi.org/10.1029/2005JG000140

Duce, R.A., Liss, P.S., Merrill, J.T., Atlas, E.L., Buat-Menard, P., Hicks, B.B., Miller, J.M., Prospero, J.M., Arimoto, R., Church, T.M., Ellis, W., Galloway, J.N., Hansen, L., Jickells, T.D., Knap, A.H., Reinhardt, K.H., Schneider, B., Soudine, A., Tokos, J.J., Tsunogai, S., Wollast, R., Zhou, M., 1991. The atmospheric input of trace species to the world ocean. Global Biogeochem. Cycles 5, 193–259. https://doi.org/10.1029/91GB01778

Dunnington, D., 2023. ggspatial: Spatial Data Framework for ggplot2 [WWW Document]. URL https://cran.r-project.org (accessed 3.22.23).

Elser, J.J., Bracken, M.E.S., Cleland, E.E., Gruner, D.S., Harpole, W.S., Hillebrand, H., Ngai, J.T., Seabloom, E.W., Shurin, J.B., Smith, J.E., 2007. Global analysis of nitrogen and phosphorus limitation of primary producers in freshwater, marine and terrestrial ecosystems. Ecol. Lett. 10, 1135–1142. https://doi.org/10.1111/j.1461-0248.2007.01113.x

Enright, N.J., Fontaine, J.B., 2014. Climate Change and the Management of Fire-Prone Vegetation in Southwest and Southeast Australia. Geogr. Res. 52, 34–44. https://doi.org/10.1111/1745-5871.12026

Environmental Protection Agency, 2020. Particulate Matter (PM) Basics [WWW Document]. United States Gov. URL https://www.epa.gov/pm-pollution/particulate-matter-pm-basics (accessed 10.20.20).

Farmer, D.K., Boedicker, E.K., DeBolt, H.M., 2021. Dry Deposition of Atmospheric Aerosols: Approaches, Observations, and Mechanisms. Annu. Rev. Phys. Chem. 72, 375–397. https://doi.org/10.1146/annurev-physchem-090519-034936

Feikema, P.M., Sheridan, G.J., Argent, R.M., Lane, P.N.J., Grayson, R.B., 2011. Estimating catchment-scale impacts of wildfire on sediment and nutrient loads using the E2 catchment modelling framework. Environ. Model. Softw. 26, 913–928. https://doi.org/10.1016/j.envsoft.2011.02.002

Fiedler, V., Arnold, F., Ludmann, S., Minikin, A., Hamburger, T., Pirjola, L., Dörnbrack, A., Schlager, H., 2011. African biomass burning plumes over the Atlantic: aircraft based measurements and implications for H 2 SO 4 and HNO 3 mediated smoke particle activation. Atmos. Chem. Phys. 11, 3211–3225. https://doi.org/10.5194/acp-11-3211-2011

Filkov, A.I., Ngo, T., Matthews, S., Telfer, S., Penman, T.D., 2020. Impact of Australia's catastrophic 2019/20 bushfire season on communities and environment. Retrospective analysis and current trends. J. Saf. Sci. Resil. 1, 44–56. https://doi.org/10.1016/j.jnlssr.2020.06.009

Fletcher, M.-S., Romano, A., Connor, S., Mariani, M., Maezumi, S.Y., 2021. Catastrophic Bushfires, Indigenous Fire Knowledge and Reframing Science in Southeast Australia. Fire 4, 61. https://doi.org/10.3390/fire4030061

Flynn, K.J., Mitra, A., Wilson, W.H., Kimmance, S.A., Clark, D.R., Pelusi, A., Polimene, L., 2022. 'Boom-and-busted' dynamics of phytoplankton–virus interactions explain the paradox of the plankton. New Phytol. 234, 990–1002. https://doi.org/10.1111/nph.18042

Fornasiero, R.B., 2001. Phytotoxic effects of fluorides. Plant Sci. 161, 979–985. https://doi.org/10.1016/S0168-9452(01)00499-X

Fox, J., Weisberg, S., 2019. An {R} Companion to Applied Regression. Sage, Thousand Oaks.

Franklin, N.M., Stauber, J.L., Lim, R.P., 2001. Development of flow cytometry-based algal bioassays for assessing toxicity of copper in natural waters. Environ. Toxicol. Chem. 20, 160–170. https://doi.org/10.1002/etc.5620200118

Franzi, L.M., Bratt, J.M., Williams, K.M., Last, J.A., 2011. Why is particulate matter produced by wildfires toxic to lung macrophages? Toxicol. Appl. Pharmacol. 257, 182–188. https://doi.org/10.1016/j.taap.2011.09.003

Fryirs, K.A., Zhang, N., Duxbury, E., Ralph, T., 2022. Rivers up in smoke: impacts of Australia's 2019–2020 megafires on riparian systems. Int. J. Wildl. Fire 31, 720–727. https://doi.org/10.1071/WF22046

Fujitani, Y., Furuyama, A., Tanabe, K., Hirano, S., 2017. Comparison of oxidative abilities of PM2.5 collected at traffic and residential sites in Japan. contribution of transition metals and primary and secondary aerosols. Aerosol Air Qual. Res. 17, 574–587. https://doi.org/10.4209/aaqr.2016.07.0291

Fung, I.Y., Meyn, S.K., Tegen, I., Doney, S.C., John, J.G., Bishop, J.K.B., 2000. Iron supply and demand in the upper ocean. Global Biogeochem. Cycles 14, 281–295. https://doi.org/10.1002/(ISSN)1944-9224

Gabric, A.J., Cropp, R., McTainsh, G., Butler, H., Johnston, B.M., O'Loingsigh, T., Van Tran, D., 2016. Tasman Sea biological response to dust storm events during the austral spring of 2009. Mar. Freshw. Res. 67, 1090–1102. https://doi.org/10.1071/MF14321

Gabric, A.J., Cropp, R.A., McTainsh, G.H., Johnston, B.M., Butler, H., Tilbrook, B., Keywood, M., 2010. Australian dust storms in 2002-2003 and their impact on Southern Ocean biogeochemistry. Global Biogeochem. Cycles 24, 1–17. https://doi.org/10.1029/2009GB003541

Gall, J.E., Boyd, R.S., Rajakaruna, N., 2015. Transfer of heavy metals through terrestrial food webs: a review. Environ. Monit. Assess. 187, 201. https://doi.org/10.1007/s10661-015-4436-3

Gao, Q., Zhu, S., Zhou, K., Zhai, J., Chen, S., Wang, Q., Wang, S., Han, J., Lu, X., Chen, H., Zhang, L., Wang, L., Wang, Z., Yang, X., Ying, Q., Zhang, H., Chen, J., Wang, X., 2023. High enrichment of heavy metals in fine particulate matter through dust aerosol generation. Atmos. Chem. Phys. 23, 13049–13060. https://doi.org/10.5194/acp-23-13049-2023

Gaudichet, A., Echalar, F., Chatenet, B., Quisefit, J.P., Malingre, G., Cachier, H., Buat-Menard, P., Artaxo, P., Maenhaut, W., 1995. Trace elements in tropical African savanna biomass burning aerosols. J. Atmos. Chem. 22, 19–39. https://doi.org/10.1007/BF00708179

Geng, H., Park, Y., Hwang, H., Kang, S., Ro, C.-U., 2009. Elevated nitrogen-containing particles observed in Asian dust aerosol samples collected at the marine boundary layer of the Bohai Sea and the Yellow Sea. Atmos. Chem. Phys. 9, 6933–6947. https://doi.org/10.5194/acp-9-6933-2009

Genty, B., Briantais, J.M., Baker, N.R., 1989. The relationship between the quantum yield of photosynthetic electron transport and quenching of chlorophyll fluorescence. Biochim. Biophys. Acta - Gen. Subj. 990, 87–92. https://doi.org/10.1016/S0304-4165(89)80016-9

Gill, R.L., Fleck, R., Chau, K., Westerhausen, M.T., Lockwood, T.E., Violi, J.P., Irga, P.J., Doblin, M.A., Torpy, F.R., 2024. Fine particle pollution during megafires contains potentially toxic elements. Environ. Pollut. 344, 123306. https://doi.org/10.1016/j.envpol.2024.123306

Gillanders, B.M., Elsdon, T.S., Halliday, I.A., Jenkins, G.P., Robins, J.B., Valesini, F.J., 2011. Potential effects of climate change on Australian estuaries and fish utilising estuaries: a review. Mar. Freshw. Res. 62, 1115. https://doi.org/10.1071/MF11047

Giordano, M., Espinoza, C., Asa-Awuku, A., 2015. Experimentally measured morphology of biomass burning aerosol and its impacts on CCN ability. Atmos. Chem. Phys. 15, 1807–1821. https://doi.org/10.5194/acp-15-1807-2015

Golding, L.A., Binet, M.T., Adams, M.S., Hochen, J., Humphrey, C.A., Price, G.A.V., Reichelt-Brushett, A.J., Salmon, M., Stauber, J.L., 2023. Acute and chronic toxicity of manganese to tropical adult coral (Acropora millepora) to support the derivation of marine manganese water quality guideline values. Mar. Pollut. Bull. 194, 115242. https://doi.org/10.1016/j.marpolbul.2023.115242

Gomez Isaza, D.F., Cramp, R.L., Franklin, C.E., 2022. Fire and rain: A systematic review of the impacts of wildfire and associated runoff on aquatic fauna. Glob. Chang. Biol. 28, 2578–2595. https://doi.org/10.1111/gcb.16088

Grigoratos, T., Martini, G., 2015. Brake wear particle emissions: a review. Environ. Sci. Pollut. Res. 22, 2491–2504. https://doi.org/10.1007/s11356-014-3696-8

Guieu, C., Aumont, O., Paytan, A., Bopp, L., Law, C.S., Mahowald, N., Achterberg, E.P., Marañón, E., Salihoglu, B., Crise, A., Wagener, T., Herut, B., Desboeufs, K., Kanakidou, M., Olgun, N., Peters, F., Pulido-Villena, E., Tovar-Sanchez, A., Völker, C., Aumont, O., Paytan, A., Bopp, L., Law, C.S., Mahowald, N., Achterberg, E.P., Marañón, E., Salihoglu, B., Crise, A., Wagener, T., Herut, B., Desboeufs, K., Kanakidou, M., Olgun, N., Peters, F., Völker, C., 2014. The significance of the episodic nature of atmospheric deposition to Low Nutrient Low Chlorophyll regions. Global Biogeochem. Cycles 28, 1–20. https://doi.org/10.1002/2014GB004852.Received

Guo, C., Zhou, Y., Zhou, H., Su, C., Kong, L., 2022. Aerosol Nutrients and Their Biological Influence on the Northwest Pacific Ocean (NWPO) and Its Marginal Seas. Biology (Basel). 11, 842. https://doi.org/10.3390/biology11060842

Gutiérrez-Barral, A., Teira, E., Díaz-Alonso, A., Justel-Díez, M., Kaal, J., Fernández, E., 2024. Impact of wildfire ash on bacterioplankton abundance and community composition in a coastal embayment (Ría de Vigo, NW Spain). Mar. Environ. Res. 194, 106317. https://doi.org/10.1016/j.marenvres.2023.106317

Hallegraeff, G.M., Anderson, D.M., Belin, C., Bottein, M.-Y.D., Bresnan, E., Chinain, M., Enevoldsen, H., Iwataki, M., Karlson, B., McKenzie, C.H., Sunesen, I., Pitcher, G.C., Provoost, P., Richardson, A., Schweibold, L., Tester, P.A., Trainer, V.L., Yñiguez, A.T., Zingone, A., 2021. Perceived global increase in algal blooms is attributable to intensified monitoring and emerging bloom impacts. Commun. Earth Environ. 2, 117. https://doi.org/10.1038/s43247-021-00178-8

Hallett, C.S., Valesini, F., Elliott, M., 2016. A review of Australian approaches for monitoring, assessing and reporting estuarine condition: III. Evaluation against international best practice and recommendations for the future. Environ. Sci. Policy 66, 282–291. https://doi.org/10.1016/j.envsci.2016.07.015

Hallquist, M., Wenger, J.C., Baltensperger, U., Rudich, Y., Simpson, D., Claeys, M., Dommen, J., Donahue, N.M., George, C., Goldstein, A.H., Hamilton, J.F., Herrmann, H., Hoffmann, T., Iinuma, Y., Jang, M., Jenkin, M.E., Jimenez, J.L., Kiendler-Scharr, A., Maenhaut, W., McFiggans, G., Mentel, T.F., Monod, A., Prévôt, A.S.H., Seinfeld, J.H., Surratt, J.D., Szmigielski, R., Wildt, J., 2009. The formation, properties and impact of secondary organic

aerosol: current and emerging issues. Atmos. Chem. Phys. 9, 5155–5236. https://doi.org/10.5194/acp-9-5155-2009

Hamilton, D.S., Moore, J.K., Arneth, A., Bond, T.C., Carslaw, K.S., Hantson, S., Ito, A., Kaplan, J.O., Lindsay, K., Nieradzik, L., Rathod, S.D., Scanza, R.A., Mahowald, N.M., 2020. Impact of Changes to the Atmospheric Soluble Iron Deposition Flux on Ocean Biogeochemical Cycles in the Anthropocene. Global Biogeochem. Cycles 34, 1–22. https://doi.org/10.1029/2019GB006448

Hamilton, D.S., Perron, M.M.G., Bond, T.C., Bowie, A.R., Buchholz, R.R., Guieu, C., Ito, A., Maenhaut, W., Myriokefalitakis, S., Olgun, N.N., Rathod, S.D., Schepanski, K., Tagliabue, A., Wagner, R., Mahowald, N.M., 2022. Earth, Wind, Fire, and Pollution: Aerosol Nutrient Sources and Impacts on Ocean Biogeochemistry. Ann. Rev. Mar. Sci. 14, 303–330. https://doi.org/10.1146/annurev-marine-031921-013612

Hanley, J.T., Ensor, D.S., Smith, D.D., Sparks, L.E., 1994. Fractional Aerosol Filtration Efficiency of In-Duct Ventilation Air Cleaners. Indoor Air 4, 169–178. https://doi.org/10.1111/j.1600-0668.1994.t01-1-00005.x

Harper, A.R., Santin, C., Doerr, S.H., Froyd, C.A., Albini, D., Otero, X.L., Viñas, L., Pérez-Fernández, B., 2019. Chemical composition of wildfire ash produced in contrasting ecosystems and its toxicity to Daphnia magna. Int. J. Wildl. Fire 28, 726. https://doi.org/10.1071/WF18200

Harrison, E.T., Dyer, F., Wright, D.W., Levings, C., 2014. Historical Land-Use Influences the Long-Term Stream Turbidity Response to a Wildfire. Environ. Manage. 53, 393–400. https://doi.org/10.1007/s00267-013-0193-7

He, C., Miljevic, B., Crilley, L.R., Surawski, N.C., Bartsch, J., Salimi, F., Uhde, E., Schnelle-Kreis, J., Orasche, J., Ristovski, Z., Ayoko, G.A., Zimmermann, R., Morawska, L., 2016. Characterisation of the impact of open biomass burning on urban air quality in Brisbane, Australia. Environ. Int. 91, 230–242. https://doi.org/10.1016/j.envint.2016.02.030

Heath, J.T., Chafer, C.J., van Ogtrop, F.F., Bishop, T.F.A., 2014. Post-wildfire recovery of water yield in the Sydney Basin water supply catchments: An assessment of the 2001/2002 wildfires. J. Hydrol. 519, 1428–1440. https://doi.org/10.1016/j.jhydrol.2014.09.033

Heinrichs, M.E., Tebbe, D.A., Wemheuer, B., Niggemann, J., Engelen, B., 2020. Impact of Viral Lysis on the Composition of Bacterial Communities and Dissolved Organic Matter in Deep-Sea Sediments. Viruses 12, 922. https://doi.org/10.3390/v12090922

Hird, C., Perron, M.M.G., Holmes, T.M., Meyerink, S., Nielsen, C., Townsend, A.T., de Caritat, P., Strzelec, M., Bowie, A.R., 2024. On the use of lithogenic tracer measurements in aerosols to constrain dust deposition fluxes to the ocean southeast of Australia. Aerosol Res. 2, 315–327. https://doi.org/10.5194/ar-2-315-2024

Hirsch, E., Koren, I., 2021. Record-breaking aerosol levels explained by smoke injection into the stratosphere. Science (80-.). 371, 1269–1274. https://doi.org/10.1126/science.abe1415

Hou, R., Chen, X., Li, K., Gao, H., Zhao, Y., 2019. Microcosm Experiments Reveal Asian Dust Deposition Stimulates Growth and Reduces Diversity in Bacterioplankton of the China Seas. Ecoscience 27, 1–10. https://doi.org/10.1080/11956860.2019.1681090

Howard, D., Macsween, K., Edwards, G.C., Desservettaz, M., Guérette, E.A., Paton-Walsh, C., Surawski, N.C., Sullivan, A.L., Weston, C., Volkova, L., Powell, J., Keywood, M.D., Reisen, F., (Mick) Meyer, C.P., 2019. Investigation of mercury emissions from burning of Australian

eucalypt forest surface fuels using a combustion wind tunnel and field observations. Atmos. Environ. 202, 17–27. https://doi.org/10.1016/j.atmosenv.2018.12.015

Hsu, S.-C.C., Wong, G.T.F., Gong, G.-C.C., Shiah, F.-K.K., Huang, Y.-T.T., Kao, S.-J.J., Tsai, F., Candice Lung, S.-C.C., Lin, F.-J.J., Lin, I.-I.I., Hung, C.-C.C., Tseng, C.-M.M., 2010. Sources, solubility, and dry deposition of aerosol trace elements over the East China Sea. Mar. Chem. 120, 116–127. https://doi.org/10.1016/j.marchem.2008.10.003

Huang, R., Nicholas, S., Wei, Z., 2024. Thermochemical Transformation of Calcium during Biomass Burning and the Effects on Postfire Aqueous Dissolution of Macronutrients. Environ. Sci. Technol. 58, 17304–17312. https://doi.org/10.1021/acs.est.4c04820

Huang, Y., Wu, S., Kaplan, J.O., 2015. Sensitivity of global wildfire occurrences to various factors in the context of global change. Atmos. Environ. 121, 86–92. https://doi.org/10.1016/j.atmosenv.2015.06.002

Huber, W., Carey, V.J., Gentleman, R., Anders, S., Carlson, M., Carvalho, B.S., Bravo, H.C., Davis, S., Gatto, L., Girke, T., Gottardo, R., Hahne, F., Hansen, K.D., Irizarry, R.A., Lawrence, M., Love, M.I., MacDonald, J., Obenchain, V., Oleś, A.K., Pagès, H., Reyes, A., Shannon, P., Smyth, G.K., Tenenbaum, D., Waldron, L., Morgan, M., 2015. Orchestrating high-throughput genomic analysis with Bioconductor. Nat. Methods 12, 115–121. https://doi.org/10.1038/nmeth.3252

IPCC, 2021. Weather and Climate Extreme Events in a Changing Climate, Climate Change 2021: The Physical Science Basis. Contribution of Working Group I to the Sixth Assessment Report of the Intergovernmental Panel on Climate Change. Cambridge University Press.

Isley, C.F., Taylor, M.P., 2020. Atmospheric remobilization of natural and anthropogenic contaminants during wildfires. Environ. Pollut. 267, 115400. https://doi.org/10.1016/j.envpol.2020.115400

Ito, A., 2015. Atmospheric Processing of Combustion Aerosols as a Source of Bioavailable Iron. Environ. Sci. Technol. Lett. 2, 70–75. https://doi.org/10.1021/acs.estlett.5b00007

Ito, A., Penner, J.E., 2004. Global estimates of biomass burning emissions based on satellite imagery for the year 2000. J. Geophys. Res. D Atmos. 109, D14S05. https://doi.org/10.1029/2003JD004423

Ito, A., Ye, Y., Yamamoto, A., Watanabe, M., Aita, M.N., 2020. Responses of ocean biogeochemistry to atmospheric supply of lithogenic and pyrogenic iron-containing aerosols. Geol. Mag. 157, 741–756. https://doi.org/10.1017/S0016756819001080

Jayarathne, T., Stockwell, C.E., Yokelson, R.J., Nakao, S., Stone, E.A., 2014. Emissions of fine particle fluoride from biomass burning. Environ. Sci. Technol. 48, 12636–12644. https://doi.org/10.1021/es502933j

Jellett, J., Li, W., Dickie, P., Boraie, A., Kepkay, P., 1996. Metabolic activity of bacterioplankton communities assessed by flow cytometry and single carbon substrate utilization. Mar. Ecol. Prog. Ser. 136, 213–225. https://doi.org/10.3354/meps136213

Jia, Z., Li, S., Liu, Q., Jiang, F., Hu, J., 2021. Distribution and partitioning of heavy metals in water and sediments of a typical estuary (Modaomen, South China): The effect of water density stratification associated with salinity. Environ. Pollut. 287, 117277. https://doi.org/10.1016/j.envpol.2021.117277

Jickells, T.D., An, Z., Andersen, K., Baker, A., Bergametti, G., Brooks, N., Cao, J., Boyd, P., Duce,

R., Hunter, K., Kawahata, H., Kubilay, N., LaRoche, J., Liss, P., Mahowald, N., Prospero, J., Ridgwell, A., Tegen, I., Torres, R., 2005. Global Iron Connections Between Desert Dust, Ocean Biogeochemistry, and Climate. Science (80-.). 308, 67–71. https://doi.org/10.1126/science.1105959

Johnson, M.S., Meskhidze, N., 2013. Atmospheric dissolved iron deposition to the global oceans: effects of oxalate-promoted Fe dissolution, photochemical redox cycling, and dust mineralogy. Geosci. Model Dev. 6, 1137–1155. https://doi.org/10.5194/gmd-6-1137-2013

Johnston, F.H., Borchers-Arriagada, N., Morgan, G.G., Jalaludin, B., Palmer, A.J., Williamson, G.J., Bowman, D.M.J.S., 2021. Unprecedented health costs of smoke-related PM2.5 from the 2019–20 Australian megafires. Nat. Sustain. 4, 42–47. https://doi.org/10.1038/s41893-020-00610-5

Jordi, A., Basterretxea, G., Tovar-Sánchez, A., Alastuey, A., Querol, X., 2012. Copper aerosols inhibit phytoplankton growth in the Mediterranean Sea. Proc. Natl. Acad. Sci. 109, 21246–21249. https://doi.org/10.1073/pnas.1207567110

Journet, E., Desboeufs, K. V., Caquineau, S., Colin, J.-L.J., 2008. Mineralogy as a critical factor of dust iron solubility. Geophys. Res. Lett. 35, n/a-n/a. https://doi.org/10.1029/2007GL031589

Jurado, E., Dachs, J., Duarte, C.M., Simó, R., 2008. Atmospheric deposition of organic and black carbon to the global oceans. Atmos. Environ. 42, 7931–7939. https://doi.org/10.1016/j.atmosenv.2008.07.029

Kanakidou, M., Duce, R.A., Prospero, J.M., Baker, A.R., Benitez-Nelson, C., Dentener, F.J., Hunter, K.A., Liss, P.S., Mahowald, N., Okin, G.S., Sarin, M., Tsigaridis, K., Uematsu, M., Zamora, L.M., Zhu, T., Benitez-Nelson, C., Dentener, F.J., Hunter, K.A., Liss, P.S., Mahowald, N., Okin, G.S., Sarin, M., Tsigaridis, K., Uematsu, M., Zamora, L.M., Zhu, T., 2012. Atmospheric fluxes of organic N and P to the global ocean. Global Biogeochem. Cycles 26, 2011GB004277. https://doi.org/10.1029/2011GB004277

Kanakidou, M., Seinfeld, J.H., Pandis, S.N., Barnes, I., Dentener, F.J., Facchini, M.C., Van Dingenen, R., Ervens, B., Nenes, A., Nielsen, C.J., Swietlicki, E., Putaud, J.P., Balkanski, Y., Fuzzi, S., Horth, J., Moortgat, G.K., Winterhalter, R., Myhre, C.E.L., Tsigaridis, K., Vignati, E., Stephanou, E.G., Wilson, J., 2005. Organic aerosol and global climate modelling: A review. Atmos. Chem. Phys. 5, 1053–1123. https://doi.org/10.5194/acp-5-1053-2005

Kanowski, P.J., Whelan, R.J., Ellis, S., 2005. Inquiries following the 2002–2003 Australian bushfires: common themes and future directions for Australian bushfire mitigation and management. Aust. For. 68, 76–86. https://doi.org/10.1080/00049158.2005.10674950

Kasischke, E.S., Turetsky, M.R., 2006. Recent changes in the fire regime across the North American boreal region - Spatial and temporal patterns of burning across Canada and Alaska. Geophys. Res. Lett. 33. https://doi.org/10.1029/2006GL025677

Kassambara, A., 2020. ggpubr: 'ggplot2' Based Publication Ready Plots [WWW Document]. URL cran.r-project.org (accessed 3.22.23).

Keene, W.C., Pszenny, A.A.P., Galloway, J.N., Hawley, M.E., 1986. Sea-salt corrections and interpretation of constituent ratios in marine precipitation. J. Geophys. Res. Atmos. 91, 6647–6658. https://doi.org/https://doi.org/10.1029/JD091iD06p06647

Keith, H., Lindenmayer, D.B., Mackey, B.G., Blair, D., Carter, L., McBurney, L., Okada, S.,

Konishi-Nagano, T., 2014. Accounting for Biomass Carbon Stock Change Due to Wildfire in Temperate Forest Landscapes in Australia. PLoS One 9, e107126. https://doi.org/10.1371/journal.pone.0107126

Keller, E.A., Valentine, D.W., Gibbs, D.R., 1997. Hydrological response of small watersheds following the Southern California Painted Cave Fire of June 1990. Hydrol. Process. 11, 401–414. https://doi.org/10.1002/(SICI)1099-1085(19970330)11:4<401::AID-HYP447>3.0.CO;2-P

Kelly, L.T., Giljohann, K.M., Duane, A., Aquilué, N., Archibald, S., Batllori, E., Bennett, A.F., Buckland, S.T., Canelles, Q., Clarke, M.F., Fortin, M.-J., Hermoso, V., Herrando, S., Keane, R.E., Lake, F.K., McCarthy, M.A., Morán-Ordóñez, A., Parr, C.L., Pausas, J.G., Penman, T.D., Regos, A., Rumpff, L., Santos, J.L., Smith, A.L., Syphard, A.D., Tingley, M.W., Brotons, L., 2020. Fire and biodiversity in the Anthropocene. Science (80-.). 370. https://doi.org/10.1126/science.abb0355

Kelly, R.L., Bian, X., Feakins, S.J., Fornace, K.L., Gunderson, T., Hawco, N.J., Liang, H., Niggemann, J., Paulson, S.E., Pinedo-Gonzalez, P., West, A.J., Yang, S., John, S.G., 2021. Delivery of Metals and Dissolved Black Carbon to the Southern California Coastal Ocean via Aerosols and Floodwaters Following the 2017 Thomas Fire. J. Geophys. Res. Biogeosciences 126. https://doi.org/10.1029/2020JG006117

Khaykin, S., Legras, B., Bucci, S., Sellitto, P., Isaksen, L., Tencé, F., Bekki, S., Bourassa, A., Rieger, L., Zawada, D., Jumelet, J., Godin-Beekmann, S., 2020. The 2019/20 Australian wildfires generated a persistent smoke-charged vortex rising up to 35 km altitude. Commun. Earth Environ. 1, 1–12. https://doi.org/10.1038/s43247-020-00022-5

Kieft, B., Li, Z., Bryson, S., Crump, B.C., Hettich, R., Pan, C., Mayali, X., Mueller, R.S., 2018. Microbial Community Structure–Function Relationships in Yaquina Bay Estuary Reveal Spatially Distinct Carbon and Nitrogen Cycling Capacities. Front. Microbiol. 9. https://doi.org/10.3389/fmicb.2018.01282

Kolarova, N., Napiórkowski, P., 2021. Trace elements in aquatic environment. Origin, distribution, assessment and toxicity effect for the aquatic biota. Ecohydrol. Hydrobiol. 143–160. https://doi.org/10.1016/j.ecohyd.2021.02.002

Koplitz, S.N., Nolte, C.G., Sabo, R.D., Clark, C.M., Horn, K.J., Thomas, R.Q., Newcomer-Johnson, T.A., 2021. The contribution of wildland fire emissions to deposition in the U S: implications for tree growth and survival in the Northwest. Environ. Res. Lett. 16, 024028. https://doi.org/10.1088/1748-9326/abd26e

Kopriva, S., Malagoli, M., Takahashi, H., 2019. Sulfur nutrition: Impacts on plant development, metabolism, and stress responses. J. Exp. Bot. 70, 4069–4073. https://doi.org/10.1093/jxb/erz319

Kramer, S.J., Bisson, K.M., Fischer, A.D., 2020. Observations of Phytoplankton Community Composition in the Santa Barbara Channel During the Thomas Fire. J. Geophys. Res. Ocean. 125, 1–16. https://doi.org/10.1029/2020JC016851

Kristensen, L.J., Taylor, M.P., Odigie, K.O., Hibdon, S.A., Flegal, A.R., 2014. Lead isotopic compositions of ash sourced from Australian bushfires. Environ. Pollut. 190, 159–165. https://doi.org/10.1016/j.envpol.2014.03.025

Kubier, A., Wilkin, R.T., Pichler, T., 2019. Cadmium in soils and groundwater: A review. Appl. Geochemistry 108, 104388. https://doi.org/10.1016/j.apgeochem.2019.104388

Ladd, T.M., Catlett, D., Maniscalco, M.A., Kim, S.M., Kelly, R.L., John, S.G., Carlson, C.A., Iglesias-Rodríguez, M.D., 2023. Food for all? Wildfire ash fuels growth of diverse eukaryotic plankton. Proc. R. Soc. B Biol. Sci. 290. https://doi.org/10.1098/rspb.2023.1817

Lafferty, K.D., Porter, J.W., Ford, S.E., 2004. Are Diseases Increasing in the Ocean? Annu. Rev. Ecol. Evol. Syst. 35, 31–54. https://doi.org/10.1146/annurev.ecolsys.35.021103.105704

Lane, P., Brocker, T., Hubele, S., Padovan, E., Lanzavecchia, A., McConnell, F., 1993. Soluble CD40 ligand can replace the normal T cell-derived CD40 ligand signal to B cells in T cell-dependent activation. J. Exp. Med. 177, 1209–1213. https://doi.org/10.1084/jem.177.4.1209

Lane, P.N.J., Sheridan, G.J., Noske, P.J., Sherwin, C.B., 2008. Phosphorus and nitrogen exports from SE Australian forests following wildfire. J. Hydrol. 361, 186–198. https://doi.org/10.1016/j.jhydrol.2008.07.041

Lawrence, G.B., David, M.B., Shortle, W.C., 1995. A new mechanism for calcium loss in forest-floor soils. Nature 378, 162–165. https://doi.org/10.1038/378162a0

Leduc, A.O.H.C., Munday, P.L., Brown, G.E., Ferrari, M.C.O., 2013. Effects of acidification on olfactorymediated behaviour in freshwater and marine ecosystems: A synthesis. Philos. Trans. R. Soc. B Biol. Sci. 368, 20120447. https://doi.org/10.1098/rstb.2012.0447

Leigh, R.A., Wyn Jones, R.G., 1984. A hypothesis relating critical potassium concentrations for growth to the distribution and function of this ion in the plant cell. New Phytol. 97, 1–13.

Levin, N., Yebra, M., Phinn, S., 2021. Unveiling the Factors Responsible for Australia's Black Summer Fires of 2019/2020. Fire 4, 58. https://doi.org/10.3390/fire4030058

Lewandowska, A., Falkowska, L., Jóźwik, J., 2013. Factors determining the fluctuation of fluoride concentrations in PM10 aerosols in the urbanized coastal area of the Baltic Sea (Gdynia, Poland). Environ. Sci. Pollut. Res. 20, 6109–6118. https://doi.org/10.1007/s11356-013-1592-2

Li, C., Ma, Z., Chen, J., Wang, X., Ye, X., Wang, L., Yang, X., Kan, H., Donaldson, D.J., Mellouki, A., 2015. Evolution of biomass burning smoke particles in the dark. Atmos. Environ. 120, 244–252. https://doi.org/10.1016/j.atmosenv.2015.09.003

Li, J., Pósfai, M., Hobbs, P. V., Buseck, P.R., 2003. Individual aerosol particles from biomass burning in southern Africa: 2, Compositions and aging of inorganic particles. J. Geophys. Res. Atmos. 108. https://doi.org/10.1029/2002JD002310

Li, J., Reardon, P., McKinley, J.P., Joshi, S.R., Bai, Y., Bear, K., Jaisi, D.P., 2017. Water column particulate matter: A key contributor to phosphorus regeneration in a coastal eutrophic environment, the chesapeake bay. J. Geophys. Res. Biogeosciences 122, 737–752. https://doi.org/10.1002/2016JG003572

Li, M., Shen, F., Sun, X., 2021. 2019–2020 Australian bushfire air particulate pollution and impact on the South Pacific Ocean. Sci. Rep. 11, 12288. https://doi.org/10.1038/s41598-021-91547-y

Li, R., Zhang, H., Wang, F., Ren, Y., Jia, S., Jiang, B., Jia, X., Tang, Y., Tang, M., 2022. Abundance and fractional solubility of phosphorus and trace metals in combustion ash and desert dust: Implications for bioavailability and reactivity. Sci. Total Environ. 816, 151495. https://doi.org/10.1016/j.scitotenv.2021.151495

Li, W.K.W., Dickie, P.M., 2001. Monitoring phytoplankton, bacterioplankton, and virioplankton

in a coastal inlet (Bedford Basin) by flow cytometry. Cytometry 44, 236–246. https://doi.org/10.1002/1097-0320(20010701)44:3<236::AID-CYTO1116>3.0.CO;2-5

Li, W.K.W., Jellett, J.F., Dickie, P.M., 1995. DNA distributions in planktonic bacteria stained with TOTO or TO-PRO. Limnol. Oceanogr. 40, 1485–1495. https://doi.org/10.4319/lo.1995.40.8.1485

Lim, C.C., Yoon, J., Reynolds, K., Gerald, L.B., Ault, A.P., Heo, S., Bell, M.L., 2023. Harmful algal bloom aerosols and human health. eBioMedicine 93, 104604. https://doi.org/10.1016/j.ebiom.2023.104604

Lindaas, J., Pollack, I.B., Calahorrano, J.J., O'Dell, K., Garofalo, L.A., Pothier, M.A., Farmer, D.K., Kreidenweis, S.M., Campos, T., Flocke, F., Weinheimer, A.J., Montzka, D.D., Tyndall, G.S., Apel, E.C., Hills, A.J., Hornbrook, R.S., Palm, B.B., Peng, Q., Thornton, J.A., Permar, W., Wielgasz, C., Hu, L., Pierce, J.R., Collett, J.L., Sullivan, A.P., Fischer, E. V., 2021a. Empirical Insights Into the Fate of Ammonia in Western U.S. Wildfire Smoke Plumes. J. Geophys. Res. Atmos. 126. https://doi.org/10.1029/2020JD033730

Lindaas, J., Pollack, I.B., Garofalo, L.A., Pothier, M.A., Farmer, D.K., Kreidenweis, S.M., Campos, T.L., Flocke, F., Weinheimer, A.J., Montzka, D.D., Tyndall, G.S., Palm, B.B., Peng, Q., Thornton, J.A., Permar, W., Wielgasz, C., Hu, L., Ottmar, R.D., Restaino, J.C., Hudak, A.T., Ku, I., Zhou, Y., Sive, B.C., Sullivan, A., Collett, J.L., Fischer, E. V., 2021b. Emissions of Reactive Nitrogen From Western U.S. Wildfires During Summer 2018. J. Geophys. Res. Atmos. 126. https://doi.org/10.1029/2020JD032657

Litchman, E., Klausmeier, C.A., 2008. Trait-Based Community Ecology of Phytoplankton. Annu. Rev. Ecol. Evol. Syst. 39, 615–639. https://doi.org/10.1146/annurev.ecolsys.39.110707.173549

Liu, D., Zhou, C., Keesing, J.K., Serrano, O., Werner, A., Fang, Y., Chen, Y., Masque, P., Kinloch, J., Sadekov, A., Du, Y., 2022. Wildfires enhance phytoplankton production in tropical oceans. Nat. Commun. 13, 1348. https://doi.org/10.1038/s41467-022-29013-0

Liu, L., Li, W., Lin, Q., Wang, Y., Zhang, J., Zhu, Y., Yuan, Q., Zhou, S., Zhang, D., Baldo, C., Shi, Z., 2022. Size-dependent aerosol iron solubility in an urban atmosphere. npj Clim. Atmos. Sci. 5, 53. https://doi.org/10.1038/s41612-022-00277-z

Liu, W., Wang, W., 2025. The Impact of Anomalous Biomass Burning on Phytoplankton and Surface Ocean Carbon Pool in the Indo-China Peninsula. J. Geophys. Res. Ocean. 130. https://doi.org/10.1029/2024JC022070

Longo, A.F., Feng, Y., Lai, B., Landing, W.M., Shelley, R.U., Nenes, A., Mihalopoulos, N., Violaki, K., Ingall, E.D., 2016. Influence of Atmospheric Processes on the Solubility and Composition of Iron in Saharan Dust. Environ. Sci. Technol. 50, 6912–6920. https://doi.org/10.1021/acs.est.6b02605

Lund, K., Refsnes, M., Sandstrom, T., Søstrand, P., Schwarze, P., Boe, J., Kongerud, J., 1999. Increased CD3 positive cells in bronchoalveolar lavage fluid after hydrogen fluoride inhalation. Scand. J. Work. Environ. Heal. 25, 326–334. https://doi.org/10.5271/sjweh.442

Lunn, T.J., Gerwin, M., Buettel, J.C., Brook, B.W., 2018. Impact of intense disturbance on the structure and composition of wet-eucalypt forests: A case study from the Tasmanian 2016 wildfires. PLoS One 13, e0200905. https://doi.org/10.1371/journal.pone.0200905

Lydersen, E., Høgberget, R., Moreno, C.E., Garmo, Ø.A., Hagen, P.C., 2014. The effects of wildfire on the water chemistry of dilute, acidic lakes in southern Norway.

Biogeochemistry 119, 109–124. https://doi.org/10.1007/s10533-014-9951-8

Mackey, K.R.M., Hunter, D., Fischer, E. V., Jiang, Y., Allen, B., Chen, Y., Liston, A., Reuter, J., Schladow, G., Paytan, A., 2013. Aerosol-nutrient-induced picoplankton growth in Lake Tahoe. J. Geophys. Res. Biogeosciences 118, 1054–1067. https://doi.org/10.1002/jgrg.20084

Mackie, D.S., Boyd, P.W., McTainsh, G.H., Tindale, N.W., Westberry, T.K., Hunter, K.A., 2008. Biogeochemistry of iron in Australian dust: From eolian uplift to marine uptake. Geochemistry, Geophys. Geosystems 9. https://doi.org/10.1029/2007GC001813

Mahdavi, A., Dingle, J., Chan, A.W.H., Siegel, J.A., 2021. HVAC filtration of particles and trace metals: Airborne measurements and the evaluation of quantitative filter forensics. Environ. Pollut. 271, 116388. https://doi.org/10.1016/j.envpol.2020.116388

Mahdavi, A., Siegel, J.A., 2020. Extraction of dust collected in HVAC filters for quantitative filter forensics. Aerosol Sci. Technol. 54, 1282–1292. https://doi.org/10.1080/02786826.2020.1774492

Mahowald, N., 2011. Aerosol Indirect Effect on Biogeochemical Cycles and Climate. Science (80-.). 334, 794–796. https://doi.org/10.1126/science.1207374

Mahowald, N., Jickells, T.D., Baker, A.R., Artaxo, P., Benitez-Nelson, C.R., Bergametti, G., Bond, T.C., Chen, Y., Cohen, D.D., Herut, B., Kubilay, N., Losno, R., Luo, C., Maenhaut, W., McGee, K.A., Okin, G.S., Siefert, R.L., Tsukuda, S., 2008. Global distribution of atmospheric phosphorus sources, concentrations and deposition rates, and anthropogenic impacts. Global Biogeochem. Cycles 22, 1–19. https://doi.org/10.1029/2008GB003240

Mahowald, N., Ward, D.S., Kloster, S., Flanner, M.G., Heald, C.L., Heavens, N.G., Hess, P.G., Lamarque, J.-F.F., Chuang, P.Y., 2011. Aerosol impacts on climate and biogeochemistry. Annu. Rev. Environ. Resour. 36, 45–74. https://doi.org/10.1146/annurev-environ-042009-094507

Mahowald, N.M., Baker, A.R., Bergametti, G., Brooks, N., Duce, R.A., Jickells, T.D., Kubilay, N., Prospero, J.M., Tegen, I., 2005. Atmospheric global dust cycle and iron inputs to the ocean. Global Biogeochem. Cycles 19, n/a-n/a. https://doi.org/10.1029/2004GB002402

Mahowald, N.M., Engelstaedter, S., Luo, C., Sealy, A., Artaxo, P., Benitez-Nelson, C., Bonnet, S., Chen, Y., Chuang, P.Y., Cohen, D.D., Dulac, F., Herut, B., Johansen, A.M., Kubilay, N., Losno, R., Maenhaut, W., Paytan, A., Prospero, J.M., Shank, L.M., Siefert, R.L., 2009. Atmospheric Iron Deposition: Global Distribution, Variability, and Human Perturbations. Ann. Rev. Mar. Sci. 1, 245–278. https://doi.org/10.1146/annurev.marine.010908.163727

Mahowald, N.M., Hamilton, D.S., Mackey, K.R.M.M., Moore, J.K., Baker, A.R., Scanza, R.A., Zhang, Y., 2018. Aerosol trace metal leaching and impacts on marine microorganisms. Nat. Commun. 9, 2614. https://doi.org/10.1038/s41467-018-04970-7

Mahowald, N.M., Scanza, R., Brahney, J., Goodale, C.L., Hess, P.G., Moore, J.K., Neff, J., 2017. Aerosol Deposition Impacts on Land and Ocean Carbon Cycles. Curr. Clim. Chang. Reports 3, 16–31. https://doi.org/10.1007/s40641-017-0056-z

Majzlan, J., 2013. Minerals and Aqueous Species of Iron and Manganese as Reactants and Products of Microbial Metal Respiration, in: Microbial Metal Respiration. Springer Berlin Heidelberg, Berlin, Heidelberg, pp. 1–28. https://doi.org/10.1007/978-3-642-32867-1_1

Marcotte, A.R., Anbar, A.D., Majestic, B.J., Herckes, P., 2020. Mineral Dust and Iron Solubility:

Effects of Composition, Particle Size, and Surface Area. Atmosphere (Basel). 11, 533. https://doi.org/10.3390/atmos11050533

Marie, D., Brussaard, C.P.D., Thyrhaug, R., Bratbak, G., Vaulot, D., 1999a. Enumeration of Marine Viruses in Culture and Natural Samples by Flow Cytometry. Appl. Environ. Microbiol. 65, 45–52. https://doi.org/10.1128/AEM.65.1.45-52.1999

Marie, D., Partensky, F., Vaulot, D., Brussaard, C., 1999b. Enumeration of Phytoplankton, Bacteria, and Viruses in Marine Samples. Curr. Protoc. Cytom. 10. https://doi.org/10.1002/0471142956.cy1111s10

Martin, J.H., Gordon, M., Fitzwater, S.E., 1991. The case for iron. Limnol. Oceanogr. 36, 1793–1802. https://doi.org/10.4319/lo.1991.36.8.1793

Martin, M., 2011. Cutadapt removes adapter sequences from high-throughput sequencing reads. EMBnet.journal 17, 10. https://doi.org/10.14806/ej.17.1.200

Martínez-Pérez, C., Zweifel, S.T., Pioli, R., Stocker, R., 2024. Space, the final frontier: The spatial component of phytoplankton–bacterial interactions. Mol. Microbiol. 122, 331–346. https://doi.org/10.1111/mmi.15293

McFarlane, A.C., Van Hooff, M., 2009. Impact of childhood exposure to a natural disaster on adult mental health: 20-year longitudinal follow-up study. Br. J. Psychiatry 195, 142–148. https://doi.org/10.1192/bjp.bp.108.054270

McKenzie, E.R., Money, J.E., Green, P.G., Young, T.M., 2009. Metals associated with stormwater-relevant brake and tire samples. Sci. Total Environ. 407, 5855–5860. https://doi.org/10.1016/j.scitotenv.2009.07.018

McKnight, D.T., Huerlimann, R., Bower, D.S., Schwarzkopf, L., Alford, R.A., Zenger, K.R., 2019. Methods for normalizing microbiome data: An ecological perspective. Methods Ecol. Evol. 10, 389–400. https://doi.org/10.1111/2041-210X.13115

McMurdie, P.J., Holmes, S., 2013. phyloseq: An R package for reproducible interactive analysis and graphics of microbiome census data. PLoS One 8, e61217.

McNeill, J., Snider, G., Weagle, C.L., Walsh, B., Bissonnette, P., Stone, E., Abboud, I., Akoshile, C., Anh, N.X., Balasubramanian, R., Brook, J.R., Coburn, C., Cohen, A., Dong, J., Gagnon, G., Garland, R.M., He, K., Holben, B.N., Kahn, R., Kim, J.S., Lagrosas, N., Lestari, P., Liu, Y., Jeba, F., Joy, K.S., Martins, J.V., Misra, A., Norford, L.K., Quel, E.J., Salam, A., Schichtel, B., Tripathi, S.N., Wang, C., Zhang, Q., Brauer, M., Gibson, M.D., Rudich, Y., Martin, R. V., 2020. Large global variations in measured airborne metal concentrations driven by anthropogenic sources. Sci. Rep. 10, 21817. https://doi.org/10.1038/s41598-020-78789-y

McNulty, I.B., Newman, D.W., 1961. Mechanism(s) of fluoride induced chlorosis. Plant Physiol. 36, 385–388. https://doi.org/10.1104/pp.36.4.385

McTainsh, G.H., Pitblado, J.R., 1987. Dust storms and related phenomena measured from meteorological records in Australia. Earth Surf. Process. Landforms 12, 415–424. https://doi.org/10.1002/esp.3290120407

Mendez, J., Guieu, C., Adkins, J., 2010. Atmospheric input of manganese and iron to the ocean: Seawater dissolution experiments with Saharan and North American dusts. Mar. Chem. 120, 34–43. https://doi.org/10.1016/j.marchem.2008.08.006

Meng, X., Chen, Y., Wang, B., Ma, Q.W., Wang, F.J., 2016. Responses of phytoplankton community to the input of different aerosols in the East China Sea. Geophys. Res. Lett. 43,

7081–7088. https://doi.org/10.1002/2016GL069068

Merchant, S.S., Helmann, J.D., 2012. Elemental Economy. Microbial Strategies for Optimizing Growth in the Face of Nutrient Limitation, Advances in Microbial Physiology. https://doi.org/10.1016/B978-0-12-398264-3.00002-4

Miller, F.J., Gardner, D.E., Graham, J.A., Lee, R.E., Wilson, W.E., Bachmann, J.D., 1979. Size Considerations for Establishing a Standard for Inhalable Particles. J. Air Pollut. Control Assoc. 29, 610–615. https://doi.org/10.1080/00022470.1979.10470831

Mojica, K.D.A., Brussaard, C.P.D., 2014. Factors affecting virus dynamics and microbial host - virus interactions in marine environments. FEMS Microbiol. Ecol. 89, 495–515. https://doi.org/10.1111/1574-6941.12343

Monger, B.C., Landry, M.R., 1993. Flow cytometric analysis of marine bacteria with Hoechst 33342. Appl. Environ. Microbiol. 59, 905–911. https://doi.org/10.1128/aem.59.3.905-911.1993

Monteith, D.T., Stoddard, J.L., Evans, C.D., De Wit, H.A., Forsius, M., Høgåsen, T., Wilander, A., Skjelkvåle, B.L., Jeffries, D.S., Vuorenmaa, J., Keller, B., Kopécek, J., Vesely, J., 2007. Dissolved organic carbon trends resulting from changes in atmospheric deposition chemistry. Nature 450, 537–540. https://doi.org/10.1038/nature06316

Morgan, M., Ramos, M., 2025. BiocManager: Access the Bioconductor Project Package Repository.

Müller, C., Eickhout, B., Zaehle, S., Bondeau, A., Cramer, W., Lucht, W., 2007. Effects of changes in CO 2 , climate, and land use on the carbon balance of the land biosphere during the 21st century. J. Geophys. Res. Biogeosciences 112. https://doi.org/10.1029/2006JG000388

Muniz, I.P., 1990. Freshwater acidification: its effects on species and communities of freshwater microbes, plants and animals. Proc. - R. Soc. Edinburgh, B 97, 227–254. https://doi.org/10.1017/S0269727000005364

Muñoz-Rojas, M., Erickson, T.E., Martini, D., Dixon, K.W., Merritt, D.J., 2016. Soil physicochemical and microbiological indicators of short, medium and long term post-fire recovery in semi-arid ecosystems. Ecol. Indic. 63, 14–22. https://doi.org/10.1016/j.ecolind.2015.11.038

Myriokefalitakis, S., Nenes, A., Baker, A.R., Mihalopoulos, N., Kanakidou, M., 2016. Bioavailable atmospheric phosphorous supply to the global ocean: a 3-D global modeling study. Biogeosciences 13, 6519–6543. https://doi.org/10.5194/bg-13-6519-2016

Nagata, T., 2000. Production of dissolved organic matter. Microb. Ecol. Ocean. 121–152.

National Oceans Office, 2002. Sea Country – an Indigenous perspective The South-east Regional Marine Plan Assessment Reports.

Nayar, S., Goh, B.P.L., Chou, L.M., 2004. Environmental impact of heavy metals from dredged and resuspended sediments on phytoplankton and bacteria assessed in in situ mesocosms. Ecotoxicol. Environ. Saf. 59, 349–369. https://doi.org/10.1016/j.ecoenv.2003.08.015

Nellemann, C., Corcoran, E., Duarte, C.M., Valdés, L., De Young, C., Fonseca, L., Grimsditch, G., 2009. Blue carbon: The Role of Healthy Oceans in Binding Carbon.

Nemmar, A., Hoet, P.H.M., Vanquickenborne, B., Dinsdale, D., Thomeer, M., Hoylaerts, M.F.,

Vanbilloen, H., Mortelmans, L., Nemery, B., 2002. Passage of inhaled particles into the blood circulation in humans. Circulation 105, 411–414. https://doi.org/10.1161/hc0402.104118

Netzer, F., Mueller, C.W., Scheerer, U., Grüner, J., Kögel-Knabner, I., Herschbach, C., Rennenberg, H., 2018. Phosphorus nutrition of Populus × canescens reflects adaptation to high P-availability in the soil. Tree Physiol. 38, 6–24. https://doi.org/10.1093/treephys/tpx126

Ng, N.L., Brown, S.S., Archibald, A.T., Atlas, E., Cohen, R.C., Crowley, J.N., Day, D.A., Donahue, N.M., Fry, J.L., Fuchs, H., Griffin, R.J., Guzman, M.I., Herrmann, H., Hodzic, A., Iinuma, Y., Jimenez, J.L., Kiendler-Scharr, A., Lee, B.H., Luecken, D.J., Mao, J., McLaren, R., Mutzel, A., Osthoff, H.D., Ouyang, B., Picquet-Varrault, B., Platt, U., Pye, H.O.T., Rudich, Y., Schwantes, R.H., Shiraiwa, M., Stutz, J., Thornton, J.A., Tilgner, A., Williams, B.J., Zaveri, R.A., 2017. Nitrate radicals and biogenic volatile organic compounds: oxidation, mechanisms, and organic aerosol. Atmos. Chem. Phys. 17, 2103–2162. https://doi.org/10.5194/acp-17-2103-2017

Nho-Kim, E., 2004. Parameterization of size-dependent particle dry deposition velocities for global modeling. Atmos. Environ. 38, 1933–1942. https://doi.org/10.1016/j.atmosenv.2004.01.002

Nolan, R.H., Boer, M.M., Resco de Dios, V., Caccamo, G., Bradstock, R.A., 2016. Large-scale, dynamic transformations in fuel moisture drive wildfire activity across southeastern Australia. Geophys. Res. Lett. 43, 4229–4238. https://doi.org/10.1002/2016GL068614

Norris, G., Duvall, R., Brown, S., Bai, S., 2014. EPA Positive Matrix Factorization (PMF) 5.0 Fundamentals and User Guide.

Novotny, A., Serandour, B., Kortsch, S., Gauzens, B., Jan, K.M.G., Winder, M., 2023. DNA metabarcoding highlights cyanobacteria as the main source of primary production in a pelagic food web model. Sci. Adv. 9. https://doi.org/10.1126/sciadv.adg1096

NPI Australia, 2015. National Pollutant Inventory Guide (NPI) 2003/2015 53.

NSW Department of Climate Change, Energy, the Environment, and W. (DCCEEW), 2025. National Pollution Inventory [WWW Document]. URL https://www.dcceew.gov.au/environment/protection/npi

NSW Department of Climate Change, Energy, the Environment, and W. (DCCEEW), 2021a. Rural air quality network - Live air quality data [WWW Document]. NSW Gov. URL https://www.dpie.nsw.gov.au/air-quality/rural-air-quality-network-live-data (accessed 4.1.21).

NSW Department of Climate Change, Energy, the Environment, and W. (DCCEEW), 2021b. Air Quality Data API [WWW Document]. NSW Gov. URL https://data.airquality.nsw.gov.au/docs/index.html (accessed 4.1.21).

NSW Department of Climate Change, Energy, the Environment, and W. (DCCEEW), 2018a. Estuaries of NSW: Lake Brou [WWW Document]. NSW Gov. URL https://www.environment.nsw.gov.au/topics/water/estuaries/estuaries-of-nsw/lake-brou (accessed 10.13.21).

NSW Department of Climate Change, Energy, the Environment, and W. (DCCEEW), 2018b. Estuaries of NSW: Clyde River [WWW Document]. NSW Gov. URL https://www.environment.nsw.gov.au/topics/water/estuaries/estuaries-of-nsw/clyde-

river%0A (accessed 10.13.21).

NSW Department of Climate Change, Energy, the Environment, and W. (DCCEEW), 2018c. Estuaries of NSW: Moruya River [WWW Document]. NSW Gov. URL https://www.environment.nsw.gov.au/topics/water/estuaries/estuaries-of-nsw/moruya-river%0A (accessed 10.13.21).

NSW Department of Climate Change, Energy, the Environment, and W. (DCCEEW), 2018d. Estuaries of NSW: Tuross River [WWW Document]. NSW Gov. URL https://www.environment.nsw.gov.au/topics/water/estuaries/estuaries-of-nsw/tuross-river%0A (accessed 10.13.21).

NSW Department of Climate Change, Energy, the Environment, and W. (DCCEEW), 2018e. Estuaries of NSW: Tabourie Lake [WWW Document]. NSW Gov. URL https://www.environment.nsw.gov.au/topics/water/estuaries/estuaries-of-nsw/tabourie-lake%0A (accessed 10.13.21).

Nyman, P., Sheridan, G.J., Smith, H.G., Lane, P.N.J., 2011. Evidence of debris flow occurrence after wildfire in upland catchments of south-east Australia. Geomorphology 125, 383–401. https://doi.org/10.1016/j.geomorph.2010.10.016

O'Donnell, A.J., Boer, M.M., McCaw, W.L., Grierson, P.F., 2011. Climatic anomalies drive wildfire occurrence and extent in semi-arid shrublands and woodlands of southwest Australia. Ecosphere 2, art127. https://doi.org/10.1890/ES11-00189.1

Office of Environment and Heritage (OEH), 2016. Assessing Estuary Ecosystem Health: Sampling, Data Analysis and Reporting Protocols. Sydney, Australia. https://doi.org/doi.org/10.13140/RG.2.2.22492.90242

Okoshi, R., Rasheed, A., Chen Reddy, G., McCrowey, C.P., Curtis, D.B., 2014. Size and mass distributions of ground-level sub-micrometer biomass burning aerosol from small wildfires. Atmos. Environ. 89, 392–402. https://doi.org/10.1016/j.atmosenv.2014.01.024

Oksanen, J., Blanchet, G.F., Friendly, M., Kindt, R., Legendre, P., McGlinn, D., Minchin, P.R., O'Hara, R.B., Simpson, G.L., Solymos, P., Stevens, M.H.H., Szoecs, E., Wagner, H., 2022. vegan: Community Ecology Package [WWW Document]. URL https://cran.r-project.org/package=vegan (accessed 3.22.23).

Olson, N.E., Boaggio, K.L., Rice, R.B., Foley, K.M., LeDuc, S.D., 2023. Wildfires in the western United States are mobilizing PM 2.5 -associated nutrients and may be contributing to downwind cyanobacteria blooms. Environ. Sci. Process. Impacts 25, 1049–1066. https://doi.org/10.1039/D3EM00042G

Ooms, J., 2014. The jsonlite Package: A Practical and Consistent Mapping Between JSON Data and R Objects. arXiv:1403.2805 [stat.CO]. https://doi.org/arXiv:1403.2805

Owens, D., O'Kane, M., 2020. Final report of the NSW Bushfire Inquiry.

Pacyna, E.G., Pacyna, J.M., Steenhuisen, F., Wilson, S., 2006. Global anthropogenic mercury emission inventory for 2000. Atmos. Environ. 40, 4048–4063. https://doi.org/10.1016/j.atmosenv.2006.03.041

Pacyna, J.M., Pacyna, E.G., 2001. An assessment of global and regional emissions of trace metals to the atmosphere from anthropogenic sources worldwide. Environ. Rev. 9, 269–298. https://doi.org/10.1139/a01-012

Paris, R., Desboeufs, K. V., Formenti, P., Nava, S., Chou, C., 2010. Chemical characterisation of

iron in dust and biomass burning aerosols during AMMA-SOP0/DABEX: implication for iron solubility. Atmos. Chem. Phys. 10, 4273–4282. https://doi.org/10.5194/acp-10-4273-2010

Park, J.D., Zheng, W., 2012. Human exposure and health effects of inorganic and elemental mercury. J. Prev. Med. Public Heal. 45, 344–352. https://doi.org/10.3961/jpmph.2012.45.6.344

Park, S.S., Sim, S.Y., Bae, M.S., Schauer, J.J., 2013. Size distribution of water-soluble components in particulate matter emitted from biomass burning. Atmos. Environ. 73, 62–72. https://doi.org/10.1016/j.atmosenv.2013.03.025

Parslow, R.A., Jorm, A.F., Christensen, H., 2006. Associations of pre-trauma attributes and trauma exposure with screening positive for PTSD: analysis of a community-based study of 2085 young adults. Psychol. Med. 36, 387–395. https://doi.org/10.1017/S0033291705006306

Paul, M.J., LeDuc, S.D., Lassiter, M.G., Moorhead, L.C., Noyes, P.D., Leibowitz, S.G., 2022. Wildfire Induces Changes in Receiving Waters: A Review With Considerations for Water Quality Management. Water Resour. Res. 58. https://doi.org/10.1029/2021WR030699

Paytan, A., Mackey, K.R.M.M., Chen, Y., Lima, I.D., Doney, S.C., Mahowald, N., Labiosa, R., Post, A.F., 2009. Toxicity of atmospheric aerosols on marine phytoplankton. Proc. Natl. Acad. Sci. 106, 4601–4605. https://doi.org/10.1073/pnas.0811486106

Pebesma, E., 2018. Simple Features for R: Standardized Support for Spatial Vector Data. R J. 10, 439–446. https://doi.org/10.32614/RJ-2018-009

Pechony, O., Shindell, D.T., 2010. Driving forces of global wildfires over the past millennium and the forthcoming century. Proc. Natl. Acad. Sci. U. S. A. 107, 19167–19170. https://doi.org/10.1073/pnas.1003669107

Perron, M.M.G., Meyerink, S., Corkill, M., Strzelec, M., Proemse, B.C., Gault-Ringold, M., Sanz Rodriguez, E., Chase, Z., Bowie, A.R., 2022. Trace elements and nutrients in wildfire plumes to the southeast of Australia. Atmos. Res. 270, 106084. https://doi.org/10.1016/j.atmosres.2022.106084

Perron, M.M.G., Proemse, B.C., Strzelec, M., Gault-Ringold, M., Boyd, P.W., Rodriguez, E.S., Paull, B., Bowie, A.R., 2020a. Origin, transport and deposition of aerosol iron to Australian coastal waters. Atmos. Environ. 228, 117432. https://doi.org/10.1016/j.atmosenv.2020.117432

Perron, M.M.G., Strzelec, M., Gault-Ringold, M., Proemse, B.C., Boyd, P.W., Bowie, A.R., 2020b. Assessment of leaching protocols to determine the solubility of trace metals in aerosols. Talanta 208, 120377. https://doi.org/10.1016/j.talanta.2019.120377

Peterson, D.A., Campbell, J.R., Hyer, E.J., Fromm, M.D., Kablick, G.P., Cossuth, J.H., DeLand, M.T., 2018. Wildfire-driven thunderstorms cause a volcano-like stratospheric injection of smoke. npj Clim. Atmos. Sci. 1, 30. https://doi.org/10.1038/s41612-018-0039-3

Peterson, D.A., Fromm, M.D., McRae, R.H.D.D., Campbell, J.R., Hyer, E.J., Taha, G., Camacho, C.P., Kablick, G.P., Schmidt, C.C., DeLand, M.T., 2021. Australia's Black Summer pyrocumulonimbus super outbreak reveals potential for increasingly extreme stratospheric smoke events. npj Clim. Atmos. Sci. 4, 1–16. https://doi.org/10.1038/s41612-021-00192-9

Pinkerton, K.E., Green, F.H.Y., Saiki, C., Vallyathan, V., Plopper, C.G., Gopal, V., Hung, D., Bahne, E.B., Lin, S.S., Ménache, M.G., Schenker, M.B., 2000. Distribution of particulate

matter and tissue remodeling in the human lung. Environ. Health Perspect. 108, 1063–1069. https://doi.org/10.1289/ehp.001081063

Platt, T., Gallegos, C.L., Harrison, W.G., 1980. Photoinhibition of Photosynthesis in Natural Assemblages of Marine Phytoplankton. J. Mar. Res.

Pósfai, M., Simonics, R., Li, J., Hobbs, P. V., Buseck, P.R., 2003. Individual aerosol particles from biomass burning in southern Africa: 1. Compositions and size distributions of carbonaceous particles. J. Geophys. Res. Atmos. 108, n/a-n/a. https://doi.org/10.1029/2002JD002291

Pound, H.L., Gann, E.R., Tang, X., Krausfeldt, L.E., Huff, M., Staton, M.E., Talmy, D., Wilhelm, S.W., 2020. The "Neglected Viruses" of Taihu: Abundant Transcripts for Viruses Infecting Eukaryotes and Their Potential Role in Phytoplankton Succession. Front. Microbiol. 11. https://doi.org/10.3389/fmicb.2020.00338

Price, O., Bradstock, R., 2013. Landscape Scale Influences of Forest Area and Housing Density on House Loss in the 2009 Victorian Bushfires. PLoS One 8, e73421. https://doi.org/10.1371/journal.pone.0073421

Qin, Y.M., Tan, H.B., Li, Y.J., Schurman, M.I., Li, F., Canonaco, F., Prévôt, A.S.H., Chan, C.K., 2017. Impacts of traffic emissions on atmospheric particulate nitrate and organics at a downwind site on the periphery of Guangzhou, China. Atmos. Chem. Phys. 17, 10245–10258. https://doi.org/10.5194/acp-17-10245-2017

R Core Team, 2021. R: A Language and Environment for Statistical Computing.

Radhi, M., Box, M.A., Box, G.P., Keywood, M.D., Cohen, D.D., Stelcer, E., Mitchell, R.M., 2011. Size-resolved chemical composition of Australian dust aerosol during winter. Environ. Chem. 8, 248. https://doi.org/10.1071/EN10134

Ralph, P.J., Gademann, R., 2005. Rapid light curves: A powerful tool to assess photosynthetic activity. Aquat. Bot. 82, 222–237. https://doi.org/10.1016/j.aquabot.2005.02.006

Ralph, P.J., Gademann, R., Larkum, A.W.D., Kühl, M., 2002. Spatial heterogeneity in active chlorophyll fluorescence and PSII activity of coral tissues. Mar. Biol. 141, 639–646. https://doi.org/10.1007/s00227-002-0866-x

Rasch, P.J., Feichter, J., Law, K., Mahowald, N., Penner, J., Benkovitz, C., Genthon, C., Giannakopoulos, C., Kasibhatla, P., Koch, D., Levy, H., Maki, T., Prather, M., Roberts, D.L., Roelofs, G.-J., Stevenson, D., Stockwell, Z., Taguchi, S., Kritz, M., Chipperfield, M., Baldocchi, D., McMurry, P., Barrie, L., Balkanski, Y., Chatfield, R., Kjellstrom, E., Lawrence, M., Lee, H.N., Lelieveld, J., Noone, K.J., Seinfield, J., Stenchikov, G., Schwartz, S., Walcek, C., Williamson, D., 2000. A comparison of scavenging and deposition processes in global models: results from the WCRP Cambridge Workshop of 1995. Tellus B 52, 1025–1056. https://doi.org/10.1034/j.1600-0889.2000.00980.x

Rau, J.A., 1989. Composition and Size Distribution of Residential Wood Smoke Particles. Aerosol Sci. Technol. 10, 181–192. https://doi.org/10.1080/02786828908959233

Reche, I., Ortega-Retuerta, E., Romera, O., Villena, E.P., Baquero, R.M., Casamayor, E.O., 2009. Effect of Saharan dust inputs on bacterial activity and community composition in Mediterranean lakes and reservoirs. Limnol. Oceanogr. 54, 869–879. https://doi.org/10.4319/lo.2009.54.3.0869

Refsnes, M., Schwarze, P.E., Holme, J.A., Låg, M., 2003. Fluoride-induced apoptosis in human epithelial lung cells (A549 cells): Role of different G protein-linked signal systems. Hum.

Exp. Toxicol. 22, 111–123. https://doi.org/10.1191/0960327103ht322oa

Reid, C.E., Brauer, M., Johnston, F.H., Jerrett, M., Balmes, J.R., Elliott, C.T., 2016. Critical review of health impacts of wildfire smoke exposure. Environ. Health Perspect. 124, 1334–1343. https://doi.org/10.1289/ehp.1409277

Reid, J.S., Koppmann, R., Eck, T.F., Eleuterio, D.P., 2005. A review of biomass burning emissions part II: Intensive physical properties of biomass burning particles. Atmos. Chem. Phys. 5, 799–825. https://doi.org/10.5194/acp-5-799-2005

Reinl, K.L., Brookes, J.D., Carey, C.C., Harris, T.D., Ibelings, B.W., Morales-Williams, A.M., De Senerpont Domis, L.N., Atkins, K.S., Isles, P.D.F., Mesman, J.P., North, R.L., Rudstam, L.G., Stelzer, J.A.A., Venkiteswaran, J.J., Yokota, K., Zhan, Q., 2021. Cyanobacterial blooms in oligotrophic lakes: Shifting the high-nutrient paradigm. Freshw. Biol. 66, 1846–1859. https://doi.org/10.1111/fwb.13791

Riemer, N., Ault, A.P., West, M., Craig, R.L., Curtis, J.H., 2019. Aerosol Mixing State: Measurements, Modeling, and Impacts. Rev. Geophys. 57, 187–249. https://doi.org/10.1029/2018RG000615

Riley, M.L., Kirkwood, J., Jiang, N., Ross, G., Scorgie, Y., 2020. Air quality monitoring in NSW: From long term trend monitoring to integrated urban services, in: Air Qual. Clim. Change. https://doi.org/10.3316/informit.078202598997117

Robson, B.J., Chester, E.T., Matthews, T.G., Johnston, K., 2018. Post-wildfire recovery of invertebrate diversity in drought-affected headwater streams. Aquat. Sci. 80, 21. https://doi.org/10.1007/s00027-018-0570-7

Rognes, T., Flouri, T., Nichols, B., Quince, C., Mahé, F., 2016. VSEARCH: a versatile open source tool for metagenomics. PeerJ 4, e2584. https://doi.org/10.7717/peerj.2584

Rolph, G., Stein, A., Stunder, B., 2017. Real-time Environmental Applications and Display sYstem: READY. Environ. Model. Softw. 95, 210–228. https://doi.org/10.1016/j.envsoft.2017.06.025

Rönnbäck, P., 1999. The ecological basis for economic value of seafood production supported by mangrove ecosystems. Ecol. Econ. 29, 235–252. https://doi.org/10.1016/S0921-8009(99)00016-6

Roper, T., Creese, B., Scanes, P., Stephens, K., Williams, R., Dela-Cruz, J., Coade, G., Coates, B., Fraser, M., 2011. Assessing the condition of estuaries and coastal lake ecosystems in NSW.

Roy, P.., Williams, R.., Jones, A.., Yassini, I., Gibbs, P.., Coates, B., West, R.., Scanes, P.., Hudson, J.., Nichol, S., 2001. Structure and Function of South-east Australian Estuaries. Estuar. Coast. Shelf Sci. 53, 351–384. https://doi.org/10.1006/ecss.2001.0796

Ruellan, S., 1999. Airborne aerosols over central Africa during the Experiment for Regional Sources and Sinks of Oxidants (EXPRESSO). J. Geophys. Res. Atmos. 104, 30673–30690. https://doi.org/10.1029/1999JD900804

Russell, S., Sullivan, C.A., Reichelt-Brushett, A.J., 2015. Aboriginal Consumption of Estuarine Food Resources and Potential Implications for Health through Trace Metal Exposure; A Study in Gumbaynggirr Country, Australia. PLoS One 10, e0130689. https://doi.org/10.1371/journal.pone.0130689

Saito, M.A., Goepfert, T.J., Ritt, J.T., 2008. Some thoughts on the concept of colimitation: Three

definitions and the importance of bioavailability. Limnol. Oceanogr. 53, 276–290. https://doi.org/10.4319/lo.2008.53.1.0276

Samsonov, Y.N., Ivanov, V.A., Mcrae, D.J., Baker, S.P., 2012. Chemical and dispersal characteristics of particulate emissions from forest fires in Siberia. Int. J. Wildl. Fire 21, 818–827. https://doi.org/10.1071/WF11038

Sánchez-García, C., Santín, C., Neris, J., Sigmund, G., Otero, X.L., Manley, J., González-Rodríguez, G., Belcher, C.M., Cerdà, A., Marcotte, A.L., Murphy, S.F., Rhoades, C.C., Sheridan, G., Strydom, T., Robichaud, P.R., Doerr, S.H., 2023. Chemical characteristics of wildfire ash across the globe and their environmental and socio-economic implications. Environ. Int. 178, 108065. https://doi.org/10.1016/j.envint.2023.108065

Sanderson, P., Naidu, R., Bolan, N., 2014. Ecotoxicity of chemically stabilised metal(loid)s in shooting range soils. Ecotoxicol. Environ. Saf. 100, 201–208. https://doi.org/10.1016/j.ecoenv.2013.11.003

Santín, C., Doerr, S.H., Otero, X.L., Chafer, C.J., 2015. Quantity, composition and water contamination potential of ash produced under different wildfire severities. Environ. Res. 142, 297–308. https://doi.org/10.1016/j.envres.2015.06.041

Sardans, J., Alonso, R., Janssens, I.A., Carnicer, J., Vereseglou, S., Rillig, M.C., Fernández-Martínez, M., Sanders, T.G.M., Peñuelas, J., 2016. Foliar and soil concentrations and stoichiometry of nitrogen and phosphorous across <scp>E</scp> uropean *<scp>P</scp> inus sylvestris* forests: relationships with climate, <scp>N</scp> deposition and tree growth. Funct. Ecol. 30, 676–689. https://doi.org/10.1111/1365-2435.12541

Sarkar, S., Ahmed, T., Swami, K., Judd, C.D., Bari, A., Dutkiewicz, V.A., Husain, L., 2015. History of atmospheric deposition of trace elements in lake sediments, ~1880 to 2007. J. Geophys. Res. Atmos. 120, 5658–5669. https://doi.org/10.1002/2015JD023202

Schäfer, R.B., Hearn, L., Kefford, B.J., Mueller, J.F., Nugegoda, D., 2010. Using silicone passive samplers to detect polycyclic aromatic hydrocarbons from wildfires in streams and potential acute effects for invertebrate communities. Water Res. 44, 4590–4600. https://doi.org/10.1016/j.watres.2010.05.044

Schroth, A.W., Crusius, J., Sholkovitz, E.R., Bostick, B.C., 2009. Iron solubility driven by speciation in dust sources to the ocean. Nat. Geosci. 2, 337–340. https://doi.org/10.1038/ngeo501

Scordo, F., Chandra, S., Suenaga, E., Kelson, S.J., Culpepper, J., Scaff, L., Tromboni, F., Caldwell, T.J., Seitz, C., Fiorenza, J.E., Williamson, C.E., Sadro, S., Rose, K.C., Poulson, S.R., 2021. Smoke from regional wildfires alters lake ecology. Sci. Rep. 11. https://doi.org/10.1038/s41598-021-89926-6

Seinfeld, J.H., Pandis, S.N., 2016. Atmospheric Chemistry and Physics: From Air Pollution to Climate Change.

Seinfeld, J.H., Pandis, S.N., 1998. Atmospheric Chemistry and Physics. Wiley, New York.

Sheridan, G.J., Lane, P.N.J., Noske, P.J., 2007. Quantification of hillslope runoff and erosion processes before and after wildfire in a wet Eucalyptus forest. J. Hydrol. 343, 12–28. https://doi.org/10.1016/j.jhydrol.2007.06.005

Sherry, N.L., Padiglione, A.A., Spelman, D.W., Cleland, H., 2013. Microbiology of wildfire victims differs significantly from routine burns patients: Data from an Australian wildfire disaster. Burns 39, 331–334. https://doi.org/10.1016/j.burns.2012.07.017

Shi, Z., Bonneville, S., Krom, M.D., Carslaw, K.S., Jickells, T.D., Baker, A.R., Benning, L.G., 2011. Iron dissolution kinetics of mineral dust at low pH during simulated atmospheric processing. Atmos. Chem. Phys. 11, 995–1007. https://doi.org/10.5194/acp-11-995-2011

Shoalhaven City Council, 2020. Currowan & Comberton Fires 2019/2020 - Statistics Snapshot. South Coast, Australia.

Sholkovitz, E.R., Sedwick, P.N., Church, T.M., 2010. On the fractional solubility of copper in marine aerosols: Toxicity of aeolian copper revisited. Geophys. Res. Lett. 37. https://doi.org/10.1029/2010GL044817

Shoman, N., Solomonova, E., Akimov, A., Rylkova, O., 2025. Toxic and protective mechanisms of cyanobacteria Synechococcus sp. in response to zinc oxide nanoparticles. Ecotoxicology 34, 565–576. https://doi.org/10.1007/s10646-025-02860-5

Silsbe, G.M., Malkin, S.Y., 2015. phytotools: Phytoplankton Production Tools.

Simkin, S.M., Allen, E.B., Bowman, W.D., Clark, C.M., Belnap, J., Brooks, M.L., Cade, B.S., Collins, S.L., Geiser, L.H., Gilliam, F.S., Jovan, S.E., Pardo, L.H., Schulz, B.K., Stevens, C.J., Suding, K.N., Throop, H.L., Waller, D.M., 2016. Conditional vulnerability of plant diversity to atmospheric nitrogen deposition across the United States. Proc. Natl. Acad. Sci. 113, 4086–4091. https://doi.org/10.1073/pnas.1515241113

Simmons, J.B., Paton-Walsh, C., Mouat, A.P., Kaiser, J., Humphries, R.S., Keywood, M., Griffith, D.W.T.T., Sutresna, A., Naylor, T., Ramirez-Gamboa, J., 2022. Bushfire smoke plume composition and toxicological assessment from the 2019–2020 Australian Black Summer. Air Qual. Atmos. Heal. 15, 2067–2089. https://doi.org/10.1007/s11869-022-01237-5

Sinha, P., Hobbs, P. V., Yokelson, R.J., Bertschi, I.T., Blake, D.R., Simpson, I.J., Gao, S., Kirchstetter, T.W., Novakov, T., 2003. Emissions of trace gases and particles from savanna fires in southern Africa. J. Geophys. Res. Atmos. 108. https://doi.org/10.1029/2002JD002325

Smith, H.G., Hopmans, P., Sheridan, G.J., Lane, P.N.J., Noske, P.J., Bren, L.J., 2012. Impacts of wildfire and salvage harvesting on water quality and nutrient exports from radiata pine and eucalypt forest catchments in south-eastern Australia. For. Ecol. Manage. 263, 160–169. https://doi.org/10.1016/j.foreco.2011.09.002

Smith, V.H., Schindler, D.W., 2009. Eutrophication science: where do we go from here? Trends Ecol. Evol. 24, 201–207. https://doi.org/10.1016/j.tree.2008.11.009

Smits, A.P., Scordo, F., Tang, M., Cortés, A., Farruggia, M.J., Culpepper, J., Chandra, S., Jin, Y., Valbuena, S.A., Watanabe, S., Schladow, G., Sadro, S., 2024. Wildfire smoke reduces lake ecosystem metabolic rates unequally across a trophic gradient. Commun. Earth Environ. 5, 265. https://doi.org/10.1038/s43247-024-01404-9

Sokolik, I.N., Soja, A.J., DeMott, P.J., Winker, D., 2019. Progress and Challenges in Quantifying Wildfire Smoke Emissions, Their Properties, Transport, and Atmospheric Impacts. J. Geophys. Res. Atmos. 124, 13005–13025. https://doi.org/10.1029/2018JD029878

Solomon, S., Stone, K., Yu, P., Murphy, D.M., Kinnison, D., Ravishankara, A.R., Wang, P., 2023. Chlorine activation and enhanced ozone depletion induced by wildfire aerosol. Nature 615, 259–264. https://doi.org/10.1038/s41586-022-05683-0

Song, Y., Zhang, Y., Xie, S., Zeng, L., Zheng, M., Salmon, L.G., Shao, M., Slanina, S., 2006. Source apportionment of PM2.5 in Beijing by positive matrix factorization. Atmos. Environ. 40, 1526–1537. https://doi.org/10.1016/j.atmosenv.2005.10.039

Sparks, T.L., Wagner, J., 2021. Composition of particulate matter during a wildfire smoke episode in an urban area. Aerosol Sci. Technol. 55, 734–747. https://doi.org/10.1080/02786826.2021.1895429

Spencer, M.T., Shields, L.G., Sodeman, D.A., Toner, S.M., Prather, K.A., 2006. Comparison of oil and fuel particle chemical signatures with particle emissions from heavy and light duty vehicles. Atmos. Environ. 40, 5224–5235. https://doi.org/10.1016/j.atmosenv.2006.04.011

Spokes, L.J., Jickells, T.D., 1996. Factors controlling the solubility of aerosol trace metals in the atmosphere and on mixing into seawater. Aquat. Geochemistry 1, 355–374. https://doi.org/10.1007/BF00702739

Stabler, B., 2022. shapefiles: Read and Write ESRI Shapefiles [WWW Document]. URL cran.r-project.org (accessed 3.22.23).

Stat, M., Huggett, M.J., Bernasconi, R., DiBattista, J.D., Berry, T.E., Newman, S.J., Harvey, E.S., Bunce, M., 2017. Ecosystem biomonitoring with eDNA: metabarcoding across the tree of life in a tropical marine environment. Sci. Rep. 7, 12240. https://doi.org/10.1038/s41598-017-12501-5

Statham, P.J., 2012. Nutrients in estuaries — An overview and the potential impacts of climate change. Sci. Total Environ. 434, 213–227. https://doi.org/10.1016/j.scitotenv.2011.09.088

Stein, A.F., Draxler, R.R., Rolph, G.D., Stunder, B.J.B., Cohen, M.D., Ngan, F., 2015. Noaa's hysplit atmospheric transport and dispersion modeling system. Bull. Am. Meteorol. Soc. 96, 2059–2077. https://doi.org/10.1175/BAMS-D-14-00110.1

Stephens, B., Siegel, J.A., 2012. Comparison of test methods for determining the particle removal efficiency of filters in residential and light-commercial central HVAC systems. Aerosol Sci. Technol. 46, 504–513. https://doi.org/10.1080/02786826.2011.642825

Stephenson, C., Handmer, J., Betts, R., 2013. Estimating the economic, social and environmental impacts of wildfires in Australia. Environ. Hazards 12, 93–111. https://doi.org/10.1080/17477891.2012.703490

Stockdale, A., Krom, M.D., Mortimer, R.J.G., Benning, L.G., Carslaw, K.S., Herbert, R.J., Shi, Z., Myriokefalitakis, S., Kanakidou, M., Nenes, A., 2016. Understanding the nature of atmospheric acid processing of mineral dusts in supplying bioavailable phosphorus to the oceans. Proc. Natl. Acad. Sci. 113, 14639–14644. https://doi.org/10.1073/pnas.1608136113

Stoessel, D.J., Ayres, R.M., Raadik, T.A., 2012. Improving spawning success for Barred Galaxias (Galaxias fuscus) in streams affected by bushfire – an aid to recovery: Black Saturday Victoria 2009 – Natural values fire recovery program. Heidelberg, Victoria.

Strzelec, M., Proemse, B.C., Barmuta, L.A., Gault-Ringold, M., Desservettaz, M., Boyd, P.W., Perron, M.M.G.G., Schofield, R., Bowie, A.R., 2020a. Atmospheric Trace Metal Deposition from Natural and Anthropogenic Sources in Western Australia. Atmosphere (Basel). 11, 474. https://doi.org/10.3390/atmos11050474

Strzelec, M., Proemse, B.C., Gault-Ringold, M., Boyd, P.W., Perron, M.M.G., Schofield, R., Ryan, R.G., Ristovski, Z.D., Alroe, J., Humphries, R.S., Keywood, M.D., Ward, J., Bowie, A.R., 2020b. Atmospheric Trace Metal Deposition near the Great Barrier Reef, Australia. Atmosphere (Basel). 11, 390. https://doi.org/10.3390/atmos11040390

Sturman, Tapper, 1996. Weather and Climate.

Sumner, M., 2021. ozmaps: Australia Maps [WWW Document]. URL https://cran.r-project.org/package=ozmaps (accessed 3.22.23).

Surawski, N.C., Sullivan, A.L., Roxburgh, S.H., Polglase, P.J., 2016. Estimates of greenhouse gas and black carbon emissions from a major Australian wildfire with high spatiotemporal resolution. J. Geophys. Res. Atmos. 121, 9892–9907. https://doi.org/10.1002/2016JD025087

Tada, Y., Taniguchi, A., Nagao, I., Miki, T., Uematsu, M., Tsuda, A., Hamasaki, K., 2011. Differing Growth Responses of Major Phylogenetic Groups of Marine Bacteria to Natural Phytoplankton Blooms in the Western North Pacific Ocean. Appl. Environ. Microbiol. 77, 4055–4065. https://doi.org/10.1128/AEM.02952-10

Tanaka, T.Y., Chiba, M., 2006. A numerical study of the contributions of dust source regions to the global dust budget. Glob. Planet. Change 52, 88–104. https://doi.org/10.1016/j.gloplacha.2006.02.002

Tang, W., Llort, J., Weis, J., Perron, M.M.G., Basart, S., Li, Z., Sathyendranath, S., Jackson, T., Sanz Rodriguez, E., Proemse, B.C., Bowie, A.R., Schallenberg, C., Strutton, P.G., Matear, R., Cassar, N., 2021. Widespread phytoplankton blooms triggered by 2019–2020 Australian wildfires. Nature 597, 370–375. https://doi.org/10.1038/s41586-021-03805-8

Telford, K., Maher, W., Krikowa, F., Foster, S., Ellwood, M.J., Ashley, P.M., Lockwood, P. V., Wilson, S.C., 2009. Bioaccumulation of antimony and arsenic in a highly contaminated stream adjacent to the Hillgrove Mine, NSW, Australia. Environ. Chem. 6, 133–143. https://doi.org/10.1071/EN08097

Textor, C., Schulz, M., Guibert, S., Kinne, S., Balkanski, Y., Bauer, S., Berntsen, T., Berglen, T., Boucher, O., Chin, M., Dentener, F., Diehl, T., Easter, R., Feichter, H., Fillmore, D., Ghan, S., Ginoux, P., Gong, S., Grini, A., Hendricks, J., Horowitz, L., Huang, P., Isaksen, I., Iversen, T., Kloster, S., Koch, D., Kirkevåg, A., Kristjansson, J.E., Krol, M., Lauer, A., Lamarque, J.F., Liu, X., Montanaro, V., Myhre, G., Penner, J., Pitari, G., Reddy, S., Seland, Stier, P., Takemura, T., Tie, X., 2006. Analysis and quantification of the diversities of aerosol life cycles within AeroCom. Atmos. Chem. Phys. 6, 1777–1813. https://doi.org/10.5194/acp-6-1777-2006

Townsend, S.A., Douglas, M.M., 2000. The effect of three fire regimes on stream water quality, water yield and export coefficients in a tropical savanna (northern Australia). J. Hydrol. 229, 118–137. https://doi.org/10.1016/S0022-1694(00)00165-7

Tsagaraki, T.M., Herut, B., Rahav, E., Berman Frank, I.R., Tsiola, A., Tsapakis, M., Giannakourou, A., Gogou, A., Panagiotopoulos, C., Violaki, K., Psarra, S., Lagaria, A., Christou, E.D., Papageorgiou, N., Zervoudaki, S., de Puelles, M.L.F., Nikolioudakis, N., Meador, T.B., Tanaka, T., Pedrotti, M.L., Krom, M.D., Pitta, P., 2017. Atmospheric deposition effects on plankton communities in the Eastern Mediterranean: A mesocosm experimental approach. Front. Mar. Sci. 4, 1–17. https://doi.org/10.3389/fmars.2017.00210

Tsiola, A., Tsagaraki, T.M., Giannakourou, A., Nikolioudakis, N., Yücel, N., Herut, B., Pitta, P., 2017. Bacterial growth and mortality after deposition of saharan dust and mixed aerosols in the eastern mediterranean sea: A mesocosm experiment. Front. Mar. Sci. 3, 1–13. https://doi.org/10.3389/FMARS.2016.00281

Uria-Tellaetxe, I., Carslaw, D.C., 2014. Conditional bivariate probability function for source identification. Environ. Model. Softw. 59, 1–9. https://doi.org/10.1016/j.envsoft.2014.05.002

van den Brand, T., 2024. ggh4x: Hacks for “ggplot2.”

van der Velde, I.R., van der Werf, G.R., Houweling, S., Maasakkers, J.D., Borsdorff, T., Landgraf, J., Tol, P., van Kempen, T.A., van Hees, R., Hoogeveen, R., Veefkind, J.P., Aben, I., 2021. Vast CO2 release from Australian fires in 2019–2020 constrained by satellite. Nature 597, 366–369. https://doi.org/10.1038/s41586-021-03712-y

Van Der Werf, G.R., Randerson, J.T., Giglio, L., Collatz, G.J., Kasibhatla, P.S., Arellano, A.F., 2006. Interannual variability in global biomass burning emissions from 1997 to 2004. Atmos. Chem. Phys. 6, 3423–3441. https://doi.org/10.5194/acp-6-3423-2006

Varkey, D., Mazard, S., Jeffries, T.C., Hughes, D.J., Seymour, J., Paulsen, I.T., Ostrowski, M., 2018. Stormwater influences phytoplankton assemblages within the diverse, but impacted Sydney Harbour estuary. PLoS One 13, e0209857. https://doi.org/10.1371/journal.pone.0209857

Visviki, I., Rachlin, J.W., 1994. Acute and chronic exposure of Dunaliella salina and Chlamydomonas bullosa to copper and cadmium: Effects on ultrastructure. Arch. Environ. Contam. Toxicol. 26. https://doi.org/10.1007/BF00224799

Volkova, L., Weston, C.J., 2019. Effect of thinning and burning fuel reduction treatments on forest carbon and bushfire fuel hazard in Eucalyptus sieberi forests of South-Eastern Australia. Sci. Total Environ. 694, 133708. https://doi.org/10.1016/j.scitotenv.2019.133708

Wagner, R., Jähn, M., Schepanski, K., 2018. Wildfires as a source of airborne mineral dust - Revisiting a conceptual model using large-eddy simulation (LES). Atmos. Chem. Phys. 18, 11863–11884. https://doi.org/10.5194/acp-18-11863-2018

Wang, F.J., Chen, Y., Guo, Z.G., Gao, H.W., Mackey, K.R., Yao, X.H., Zhuang, G.S., Paytan, A., 2017. Combined effects of iron and copper from atmospheric dry deposition on ocean productivity. Geophys. Res. Lett. 44, 2546–2555. https://doi.org/10.1002/2016GL072349

Wang, R., Balkanski, Y., Boucher, O., Ciais, P., Peñuelas, J., Tao, S., 2015. Significant contribution of combustion-related emissions to the atmospheric phosphorus budget. Nat. Geosci. 8, 48–54. https://doi.org/10.1038/ngeo2324

Wang, Y., Chen, H.-H.H., Tang, R., He, D., Lee, Z., Xue, H., Wells, M., Boss, E., Chai, F., 2022. Australian fire nourishes ocean phytoplankton bloom. Sci. Total Environ. 807, 150775. https://doi.org/10.1016/j.scitotenv.2021.150775

Wang, Y., Zhuang, G., Chen, S., An, Z., Zheng, A., 2007. Characteristics and sources of formic, acetic and oxalic acids in PM2.5 and PM10 aerosols in Beijing, China. Atmos. Res. 84, 169–181. https://doi.org/10.1016/j.atmosres.2006.07.001

Ward, M., Tulloch, A.I.T.T., Radford, J.Q., Williams, B.A., Reside, A.E., Macdonald, S.L., Mayfield, H.J., Maron, M., Possingham, H.P., Vine, S.J., O’Connor, J.L., Massingham, E.J., Greenville, A.C., Woinarski, J.C.Z.Z., Garnett, S.T., Lintermans, M., Scheele, B.C., Carwardine, J., Nimmo, D.G., Lindenmayer, D.B., Kooyman, R.M., Simmonds, J.S., Sonter, L.J., Watson, J.E.M.M., 2020. Impact of 2019–2020 mega-fires on Australian fauna habitat. Nat. Ecol. Evol. 4, 1321–1326. https://doi.org/10.1038/s41559-020-1251-1

Waters, M.N., Smoak, J.M., Vachula, R.S., 2023. Linking prescribed fire, nutrient deposition and cyanobacteria dominance through pyroeutrophication in a subtropical lake ecosystem from the mid Holocene to present. Anthropocene 44, 100420. https://doi.org/10.1016/j.ancene.2023.100420

Wegesser, T.C., Pinkerton, K.E., Last, J.A., 2009. California wildfires of 2008: Coarse and fine

particulate matter toxicity. Environ. Health Perspect. 117, 893–897. https://doi.org/10.1289/ehp.0800166

Weis, J., Chase, Z., Schallenberg, C., Strutton, P.G., Bowie, A.R., Fiddes, S.L., 2024. One-third of Southern Ocean productivity is supported by dust deposition. Nature 629, 603–608. https://doi.org/10.1038/s41586-024-07366-4

Weis, J., Schallenberg, C., Chase, Z., Bowie, A.R., Wojtasiewicz, B., Perron, M.M.G., Mallet, M.D., Strutton, P.G., 2022. Southern Ocean Phytoplankton Stimulated by Wildfire Emissions and Sustained by Iron Recycling. Geophys. Res. Lett. 49. https://doi.org/10.1029/2021GL097538

Weschler, C.J., Nazaroff, W.W., 2010. SVOC partitioning between the gas phase and settled dust indoors. Atmos. Environ. 44, 3609–3620. https://doi.org/10.1016/j.atmosenv.2010.06.029

Westerling, A.L.R., 2016. Increasing western US forest wildfire activity: Sensitivity to changes in the timing of spring. Philos. Trans. R. Soc. B Biol. Sci. 371. https://doi.org/10.1098/rstb.2015.0178

Wickham, H., 2020. httr: Tools for Working with URLs and HTTP.

Wickham, H., 2016. ggplot2: Elegant Graphics for Data Analysis. Springer-Verlag, New York.

Wickham, H., 2009. stringr: Simple, Consistent Wrappers for Common String Operations. CRAN Contrib. Packag. https://doi.org/10.32614/CRAN.package.stringr

Wickham, H., Averick, M., Bryan, J., Chang, W., McGowan, L., François, R., Grolemund, G., Hayes, A., Henry, L., Hester, J., Kuhn, M., Pedersen, T., Miller, E., Bache, S., Müller, K., Ooms, J., Robinson, D., Seidel, D., Spinu, V., Takahashi, K., Vaughan, D., Wilke, C., Woo, K., Yutani, H., 2019. Welcome to the Tidyverse. J. Open Source Softw. 4, 1686. https://doi.org/10.21105/joss.01686

Wickham, H., Francois, R., Henry, L., Muller, K., 2021. dplyr: A Grammar of Data Manipulation.

Wickham, H., Pedersen, T.L., Seidel, D., 2011. scales: Scale Functions for Visualization. CRAN Contrib. Packag. https://doi.org/10.32614/CRAN.package.scales

Wilhelm, S.M., Liang, L., Kirchgessner, D., 2006. Identification and Properties of Mercury Species in Crude Oil. Energy & Fuels 20, 180–186. https://doi.org/10.1021/ef0501391

Wilke, C.O., 2020. ggtext: Improved Text Rendering Support for 'ggplot2.

Williams, J., de Reus, M., Krejci, R., Fischer, H., Ström, J., 2002. Application of the variability-size relationship to atmospheric aerosol studies: estimating aerosol lifetimes and ages. Atmos. Chem. Phys. 2, 133–145. https://doi.org/10.5194/acp-2-133-2002

Williams, R.J., Gill, A.M., Bradstock, R.A., 2012. Flammable Australia : Fire Regimes, Biodiversity and Ecosystems in a Changing World. CSIRO Publishing, Collingwood, AUSTRALIA.

Wilson, S.C., Tighe, M., Paterson, E., Ashley, P.M., 2014. Food crop accumulation and bioavailability assessment for antimony (Sb) compared with arsenic (As) in contaminated soils. Environ. Sci. Pollut. Res. 21, 11671–11681. https://doi.org/10.1007/s11356-014-2577-5

Wilson, W.H., Carr, N.G., Mann, N.H., 1996. THE EFFECT OF PHOSPHATE STATUS ON THE KINETICS OF CYANOPHAGE INFECTION IN THE OCEANIC CYANOBACTERIUM

SYNECHOCOCCUS SP. WH7803 1. J. Phycol. 32, 506–516. https://doi.org/10.1111/j.0022-3646.1996.00506.x

Winter, C., Bouvier, T., Weinbauer, M.G., Thingstad, T.F., 2010. Trade-Offs between Competition and Defense Specialists among Unicellular Planktonic Organisms: the "Killing the Winner" Hypothesis Revisited. Microbiol. Mol. Biol. Rev. 74, 42–57. https://doi.org/10.1128/MMBR.00034-09

Winton, V.H.L., Edwards, R., Bowie, A.R., Keywood, M., Williams, A.G., Chambers, S.D., Selleck, P.W., Desservettaz, M., Mallet, M.D., Paton-Walsh, C., 2016. Dry season aerosol iron solubility in tropical northern Australia. Atmos. Chem. Phys. 16, 12829–12848. https://doi.org/10.5194/acp-16-12829-2016

Wu, L., Taylor, M.P., Handley, H.K., 2017. Remobilisation of industrial lead depositions in ash during Australian wildfires. Sci. Total Environ. 599–600, 1233–1240. https://doi.org/10.1016/j.scitotenv.2017.05.044

Wu, T., Boor, B.E., 2021. Urban aerosol size distributions: A global perspective. Atmos. Chem. Phys. 21, 8883–8914. https://doi.org/10.5194/acp-21-8883-2021

Wu, Z., Li, M., Qu, L., Zhang, C., Xie, W., 2024. Metagenomic insights into microbial adaptation to the salinity gradient of a typical short residence-time estuary. Microbiome 12, 115. https://doi.org/10.1186/s40168-024-01817-w

WWF Australia, 2020. Impacts of the unprecedented 2019-20 Bushfires on Australian animals.

Xu, Y., Liang, Y., Urquidi, J.R., Siegel, J.A., 2015. Semi-volatile organic compounds in heating, ventilation, and air-conditioning filter dust in retail stores. Indoor Air 25, 79–92. https://doi.org/10.1111/ina.12123

Yamasoe, M.A., Artaxo, P., Miguel, A.H., Allen, A.G., 2000. Chemical composition of aerosol particles from direct emissions of vegetation fires in the Amazon Basin: Water-soluble species and trace elements. Atmos. Environ. 34, 1641–1653. https://doi.org/10.1016/S1352-2310(99)00329-5

Yang, J., Ma, L., He, X., Au, W.C., Miao, Y., Wang, W.X., Nah, T., 2023. Measurement report: Abundance and fractional solubilities of aerosol metals in urban Hong Kong - insights into factors that control aerosol metal dissolution in an urban site in South China. Atmos. Chem. Phys. 23, 1403–1419. https://doi.org/10.5194/acp-23-1403-2023

Yu, W., Xu, R., Ye, T., Abramson, M.J., Morawska, L., Jalaludin, B., Johnston, F.H., Henderson, S.B., Knibbs, L.D., Morgan, G.G., Lavigne, E., Heyworth, J., Hales, S., Marks, G.B., Woodward, A., Bell, M.L., Samet, J.M., Song, J., Li, S., Guo, Y., 2024. Estimates of global mortality burden associated with short-term exposure to fine particulate matter (PM2·5). Lancet Planet. Heal. 8, e146–e155. https://doi.org/10.1016/S2542-5196(24)00003-2

Zhan, X., Huang, Z., Tigabu, M., Zhao, P., He, Y., Guo, F., 2025. Plants can directly absorb carbon derived from deposition of wildfire smoke. Plant Soil. https://doi.org/10.1007/s11104-025-07213-z

Zhang, C., Ito, A., Shi, Z., Aita, M.N., Yao, X., Chu, Q., Shi, J., Gong, X., Gao, H., 2019. Fertilization of the Northwest Pacific Ocean by East Asia Air Pollutants. Global Biogeochem. Cycles 33, 690–702. https://doi.org/10.1029/2018GB006146

Zhang, C., Yu, Z., Zeng, G., Jiang, M., Yang, Z., Cui, F., Zhu, M., Shen, L., Hu, L., 2014. Effects of sediment geochemical properties on heavy metal bioavailability. Environ. Int. 73, 270–281. https://doi.org/10.1016/j.envint.2014.08.010

Zhang, G., Lin, Q., Peng, L., Yang, Y., Fu, Y., Bi, X., Li, M., Chen, D., Chen, J., Cai, Z., Wang, X., Peng, P., Sheng, G., Zhou, Z., 2017. Insight into the in-cloud formation of oxalate based on in situ measurement by single particle mass spectrometry. Atmos. Chem. Phys. 17, 13891–13901. https://doi.org/10.5194/acp-17-13891-2017

Zhang, J., Gilbert, D., Gooday, A.J., Levin, L., Naqvi, S.W.A., Middelburg, J.J., Scranton, M., Ekau, W., Peña, A., Dewitte, B., Oguz, T., Monteiro, P.M.S., Urban, E., Rabalais, N.N., Ittekkot, V., Kemp, W.M., Ulloa, O., Elmgren, R., Escobar-Briones, E., Van der Plas, A.K., 2010. Natural and human-induced hypoxia and consequences for coastal areas: synthesis and future development. Biogeosciences 7, 1443–1467. https://doi.org/10.5194/bg-7-1443-2010

Zhang, R., Chan, C.K., 2023. Simultaneous formation of sulfate and nitrate via co-uptake of SO2 and NO2 by aqueous NaCl droplets: combined effect of nitrate photolysis and chlorine chemistry. Atmos. Chem. Phys. 23, 6113–6126. https://doi.org/10.5194/acp-23-6113-2023

Zhang, Y., Li, J., Tan, J., Li, W., Singh, B.P., Yang, X., Bolan, N., Chen, X., Xu, S., Bao, Y., Lv, D., Peng, A., Zhou, Y., Wang, H., 2023. An overview of the direct and indirect effects of acid rain on plants: Relationships among acid rain, soil, microorganisms, and plants. Sci. Total Environ. 873, 162388. https://doi.org/10.1016/j.scitotenv.2023.162388

Zhang, Y., Lim, S., Sharples, J.J., 2017. Effects of climate on the size of wildfires in the Eucalyptus camaldulensis forests and the dry lands of the Riverina Bioregion, Australia. For. Ecol. Manage. 401, 330–340. https://doi.org/10.1016/j.foreco.2017.07.009

Zhang, Y., Mahowald, N., Scanza, R.A., Journet, E., Desboeufs, K., Albani, S., Kok, J.F., Zhuang, G., Chen, Y., Cohen, D.D., Paytan, A., Patey, M.D., Achterberg, E.P., Engelbrecht, J.P., Fomba, K.W., 2015. Modeling the global emission, transport and deposition of trace elements associated with mineral dust. Biogeosciences 12, 5771–5792. https://doi.org/10.5194/bg-12-5771-2015

Zhao, S., Feng, C., Wang, D., Liu, Y., Shen, Z., 2013. Salinity increases the mobility of Cd, Cu, Mn, and Pb in the sediments of Yangtze Estuary: Relative role of sediments' properties and metal speciation. Chemosphere 91, 977–984. https://doi.org/10.1016/j.chemosphere.2013.02.001